Characterization of Thin Films for Polymer Solar Cells

Stability and Response to Concentrated Light

Tromholt, Thomas; Krebs, Frederik C

Publication date:
2012

Document Version
Publisher's PDF, also known as Version of record

Technical University of Denmark

Characterization of Thin Films for Polymer Solar Cells:

Stability and Response to Concentrated Light

Ph.D Thesis

Thomas Tromholt - June 2012

Author	**Thomas Tromholt**
Instititution	Functional Organic Materials, Department of Energy Conversion and Storage, Technical University of Denmark
Title	Characterization of Thin Films for Polymer Solar Cells: Stability and Response to Concentrated Light
Academic advisor	Professor Frederik Christian Krebs, Department of Energy Conversion and Storage, Technical University of Denmark
Publication date	June 2012
ISBN:	

Preface

This PhD thesis presents the main results of the work carried at during my PhD at the Technical University of Denmark in the period from July 1, 2009 until June 30 2012 in the Functional Organic Materials programme in the Department of Energy Conversion and Storage. My work was funded by the Danish Strategic Research Council (2104-07-0022) and supervised by Professor Frederik C. Krebs. The discusses my published work, as can be found in the appendix, within the field of polymer and solar cell stability and concentrated light in a broader context. A number of articles are not discussed in this thesis since they do not strictly relate to the polymer and cell stability, and were thus omitted to increase the focus on the main goals of this work.

During this PhD I have been in contact with a very broad spectrum of scientific fields on the interface between physics and chemistry. Hereby I have had the change to work on physics, solar cell processing, electronics, programming, polymer chemistry, material characterization, and mechanical design. Combining all these different fields and skills has been highly stimulating to me, and for that I am very thankful

I want to thank my supervisor Frederik C. Krebs for the support of this work and for providing the freedom that allows for generation of truly innovative solutions. While not being practically involved in my work, you have always had exceptional ability to supervise and provide valuable contributions to my work.

Special thanks go to Morten M. Madsen with whom I spend more or less two years in symbiotic collaboration. With your high level of technical insight, you always find a workaround to any problem. I really appreciate our constant discussions about everything from cooking to religion, all of it seen from a physicist's perspective. Additionally, I thank Kristian Larsen and Kristian Sylvester Hvid for their important contribution to my work.

I would like to thank the entire Functional Organic Material group. I really enjoyed working in the friendly and open atmosphere. For comments on the thesis, I would like to thanks Frederik and Jens.

During all three years, I have worked in close collaboration with Dr. Eugene A. Katz and his student Assaf Manor at the Ben Gurion University of the Negev, Israel. This has resulted in two interesting visits at his groups, and 5 published articles. I am thankful for the both scientific and personal aspects of this fruitful collaboration.

Finally I would like to thank my family and girlfriend Pamela for their support and forced interest in my work.

Abstract

The field of polymer solar cells has undergone an extensive development in recent years after the invention of semiconducting polymers in 1991. Efficiencies have gradually increased to above 10 %, and high throughput processing methods such as roll-to-roll coating allow for production of thousands of solar cells with low embedded time, material, and energy consumption as compared to silicon solar cells. Consequently, different demonstration products of small mobile gadgets based on polymer solar cells have been produced, which are fully competitive with conventional energy technologies, illustrating the maturity of the technology.

However, a limiting factor in terms of full commercialization is the stability of polymer solar cells. While is has been estimated that 10 years lifetime is needed, existing technologies only provide stabilities up to 1 year. Degradation of polymer solar cell is a multi facetted process where oxygen and water diffusion from the atmosphere, morphology evolution, and photo-bleaching of the polymer are some of the dominant processes. Encapsulation by foils consisting of multi-layer polymer stacks is a conventional way to reduce the diffusion into the solar cell, by which the life time of the cell is highly increased. An alternative approach is to increase the photo stability of the cell components, and especially the light absorbing conjugated polymer has been subject to extensive attention. The photo stability of conjugated polymers varies by orders of magnitude from type to type depending on the chemical structure of the material and consequently, the lifetime is highly influenced by the polymer stability.

Photochemical degradation of polymers, i.e. degradation of thin films of polymer in the ambient under light exposure, is a technique normally applied to evaluate polymer stabilities. Hereby, an extensive list of stabilities of different materials has been established providing an understanding of the stability of the individual building blocks of polymer. While being a highly practical tool, no rigorous reports on the photochemical degradation as a technique exist where the technique is validated and different pit-falls identified. Consequently, a rigorous study on the validation and maturing of this technique was performed during this PhD work **(Chapter 2).**

Furthermore, as research gradually increases the lifetime of polymers to months or years, stability evaluations at standard degradation conditions become impractical. Accelerated degradation has been performed with heat and different gases by which the timeframe of stability evaluations have been reduced by up to a factor of 20. However, light, which appears at the most intuitive acceleration condition to conjugated polymers, has until this PhD work not been applied as an acceleration condition to polymer degradation. Light can be concentrated up to thousand of solar intensities by optical components, which has the potential to significantly accelerate polymer degradation. Concentration of light was one of the main topics during this PhD, where the construction and development of light concentrators, both by sun light as well as artificial light, was given extensive attention. This resulted in three different light concentrators, a lens based solar concentrator, a mirror based solar concentrator, and an artificial light concentrator for indoor use **(Chapter 3).**

With these concentration setups, acceleration factors of up to 1200 were obtained for degradation of typical conjugated polymers thus significantly reducing the timeframe of stability evaluations. The potential of this approach is that stability evaluation can become a routine characterization technique for novel conjugated polymers, when these are applied to polymer solar cells and their efficiencies are reported. By making the polymer stability practically accessible, development of polymer stability can become significantly more transparent and focused **(Chapter 4).**

A direct alternative application of concentrated light is the application to polymer solar cells. Stabilities of polymer solar cells is within the same order of magnitude of photo chemical stabilities of polymers as the oxidation rate of the polymer in the solar cell is lower, but a large number of additional degradation mechanisms are introduced. Consequently, research in the stability of polymer solar cells is impractical since the extensive timeframe of stability testing reduces the pace of the research. This thesis reports the first results on the response of polymer solar cells to concentrated light, both in terms of performance as well as stability. Additionally, concentrated light was used to study some of the mechanisms governing solar cells operation, which are dominant when currents are very high as a consequence of high photon flux. The response in terms of stability of the cells was found to be highly complex and effects not dominant at 1 sun were observed. Thus, specific knowledge of the response of the different layers to concentrated light is needed to use concentrated light as a valid acceleration parameter **(Chapter 5).**

Resumé

Polymere solceller er et område som har gennemgået en omfattende udvikling siden opfindelsen af halvledende polymerer i 1991. Celleeffektiviteter er gradvist steget op til 10 %, og produktionsteknikker såsom rulle-til-rulle processering muliggør produktion af tusindvis af solceller hvorved det indlejrede energi, materiale- og tidsforbrug holdes lavt sammenlignet med silicium baserede solceller. Som følge af dette er flere forskellige demonstrationsprodukter baseret på polymere solceller blevet lancerede, som er fuldt konkurrencedygtige med eksisterende energiteknologier. Dette viser at polymere solceller som teknologi nærmer sig et kommercielt potentiale.

En begrænsende faktor i forhold til kommercialisering er den begrænsede stabilitet for polymer solceller. Hvor det forventes at 10 års levetid er nødvendigt for fuld konkurrencedygtighed med eksisterende teknologier ligger den maksimale, praktiske levetid for polymer solceller på 1 år. Nedbrydning af polymere solceller er en multifacceteret proces hvor ilt og vand diffusion, udvikling af morfologi, og fotoblegning af polymererne er dominerende processer. En konventionel metode til at forøge levetid er ved indkapsling af solcellerne med folier bestående af multilags polymer strukturer for at begrænse diffusionen ind i cellen hvorved levetiden øges betragteligt. En alternativ fremgangsmåde går ud på at øge fotostabiliteten af solcellens komponenter og med specielt fokus på den lysabsorberende halvledende polymer. Stabiliteten varierer med flere størrelsesordener for forskellige polymerer afhængigt af den kemiske struktur, hvilket derved også påvirker hele solcellens stabilitet betragteligt.

Fotokemisk nedbrydning af polymerer, hvor polymere tynd film nedbrydes i atmosfærisk luft, anvendes normalt til bestemmelse af polymer stabiliteter. Herigennem er en lang liste af materialer blevet stabilitetstestede hvilket giver en forståelse for stabiliteten af de enkelte byggesten for polymererne. Selvom denne teknik er yderst praktisk, findes intet større studie af teknikken som metode, hvor denne valideres og faldgruber identificeres. Dette blev derfor studeret nærmere i denne afhandling **(Kapitel 2)**.

Validering og modning af fotokemisk stabilitetstest har derfor været et af målene for denne afhandling. Fotostabiliteten af polymerer øges som følge af den omfattende forskning. Med levetider på måneder

og år ved standard nedbrydningsbetingelser opstår en flaskehals i forskningen hvor bestemmelsen af fotostabiliteten tidsmæssigt overstiger udviklingen af materialet. Accelereret nedbrydning er en løsning på dette problem, hvorved et aggressivt nedbrydningsmiljø betyder at tidsrammen for bestemmelse af stabilitet begrænses markant. Accelereret nedbrydning af polymer er allerede blevet foretaget med varme og forskellige aggressive gasser hvorved den observerede stabilitet er blevet reduceret med op til en faktor 20. Imidlertid er lys en mere oplagt accelerationsbetingelse i forbindelse med solceller, hvilket før dette PhD studie ikke havde været demonstreret for polymerer. Lys kan koncentreres op til tusinder af solintensiteter af optiske komponenter, hvilket har potentiale til at accelerere nedbrydninger betydeligt. Koncentration af lys var et af hovedmålene med dette PhD arbejde, hvor konstruktion og kalibrering af 3 forskellige solkoncentratorer udførtes, både baseret på sollys såvel som kunstigt lys. En koncentrator var baseret på en linse som fokuserede sollys, og en anden fokuserede sollys med et konkavt spejl. Den tredje opstilling fokuserede en kraftig lampe med en elliptisk reflektor, og kunne derfor anvendes til indendørs brug **(Kapitel 3)**.

Ved anvendelse af disse lys koncentratorer opnåedes accelerationsfaktorer på 1200 ved nedbrydning af konventionelle polymerer hvorved tidsrammen for stabilitetsbestemmelsen reduceredes markant. Denne fremgangsmåde har et stort potentiale, da stabilitetsbestemmelse kan blive et rutineværktøj for nye halvledende polymerer, på linje med effektivitetsmålinger af polymer anvendt i solceller. Ved at gøre polymerstabiliteten praktisk tilgængelig kan udviklingen af fotostabile polymerer gøres langt mere transparent og fokuseret **(Kapitel 4)**.

En alternativ oplagt anvendelse af koncentreret lys er i forbindelse med polymere solceller. Stabiliteter er inden for samme størrelsesorden som fotostabiliteten af polymerer, da oxidationsraten er signifikant lavere, men et stort antal nye nedbrydningsmekanismer opstår ved introduktionen af de nye lag. Generelt hersker der derfor samme flaskehals mellem materialeudvikling og test. Denne afhandling beskriver de første studier af polymer solcellerespons ved koncentreret lys, både i forbindelse med ydelse og stabilitet. Desuden kan koncentreret lys med fordel anvendes til karakterisering af solceller idet nye effekter opstår ved de høje strømtætheder ved koncentreret lys. Solcellestabiliteten under koncentreret lys var kompleks at forstå, og en forståelse for responsen for hvert lag kræves hvis koncentreret lys skal kunne anvendes som en valid accelerationsparameter **(Kapitel 5)**.

Table of Contents

1 Introduction to Polymer Solar Cells

With the increasing world population and the continuous development of technological societies, the worldwide power consumption increases day by day. Only from 2009 to 2010 the world consumption increased by 5.5 % from 12186 to 12852 million tons of oil equivalent (Mtoe)[1]. At the time of writing, the vast majority of the energy sources are based on fossil fuels, primarily gas, oil, and coal. However, the scarcity of the reserves of these fuels has been realized by both the industrial and the scientific communities. Calculations based on a constant consumption of fossil fuels leave the planet with 126 years of coal, 60 year of natural gas[2], and 54[5] years of oil as estimated from the world-wide reserves-to-production ratio. However considering the expected population growth and increased power consumption, the resources are expected to fully deplete even earlier and thus the development of alternative energy sources is urgent[4]. Additionally, within recent years the discussion about CO_2 emission has been a major issue that has caught the interest of scientists, the medias, as well as the world population. Combustion of fossil fuels releases huge amounts of CO_2 and other gases into the atmosphere. These absorb the incident light from the sun and the back-radiated infra red light from the earth and consequently the surface temperature is increased. It is generally acknowledged that due to this increased green house effect, climate changes occur. Before irreparable fatal changes are undergone by the climate, the worldwide energy policy has to be debated and alternatives to the fossil fuels need to be discussed.

1.1 Renewable energy sources

Due to the scarcity and environmentally problematic fossil fuels, renewable energy sources have experienced strong growth, both in terms of public and private investment (Table 1), but also in terms of installed power capacity of the existing renewable energy technologies[5]. Several different renewable energy sources have been discussed internationally as a successor of the fossil fuels. A few technologies are already well exploited worldwide such as hydro-power and biomass energy. Other energy sources, e.g. solar energy and wind energy, have not yet exploited the worldwide potential to the same extent

and their rate of development is expected to increase significantly. The share of renewable energy of the total final energy consumption is 16 % of which traditional biomass (combustion of biomass for heating etc.) accounts for 10 %[5]. The share of renewable energy in the global electricity production in 2010 was however 19.4 %, where hydro-power dominated with a share of 16.1 %[5]. Generally, a strong growth of renewable energy is needed to be able to cover the world energy demand once fossil fuel reserves have been depleted.

Energy technology	Unit	2008	2010	Two year increase
Global renewable energy investment	*Billion USD*	200	312	56%
Hydropower	*GW*	950	1010	6%
Windpower	*GW*	121	198	64%
Solar PV	*GW*	16	40	150%
Biomass	*GW*		62	

Table 1.1. Power capacity of selected renewable energy technologies in 2008 and 2010 and the increase during this period[5]

Hydro power is the most widely implemented renewable energy source with a power capacity of 1010 GW[5]. Electricity is generated when large masses of water are guided from higher to lower altitudes. The potential energy is transferred to electric energy by turbines and thus large amounts of energy are produced. In some countries such as Sweden, the largest source of energy is hydro power[5]. However, this energy resource is reserved to specific areas of the world, and is only available at certain periods of the year. A certain level of storage is intrinsic to this energy source since the water reservoirs can be kept on a high altitude until energy is needed. However, due to e.g. weather limits, the energy cannot be stored during indefinitely long time and thus storage only works within some constraints. Additionally, the technology suffers from certain drawbacks in terms of the cultural and ecological consequences of establishing large hydro power plans for which large areas of land mass are flooded implying that many people have to move and the local fauna and flora are lost. Hydro power provides a means of obtaining large quantities of energy, but still has drawbacks, which imply that hydro-power does not solve the energy problem.

Wind power is the second most widely applied renewable energy source with a power capacity of 198 GW. However, the potential has not been fully exploited in all countries, and the capacity is still growing as reflected in the two-year increase of 64 %[5]. In Denmark political and economical incitements have resulted in 20% of the total electricity consumption being covered by wind energy by 2011[5]. The technology thus provides a feasible alternative to fossil energy under the right economical and regional

conditions. Wind power suffers from the drawbacks: energy is only produced at certain attractive locations and storage of the energy in periods of peak production is not intrinsic to the technology. The energy is only produced at certain times of the day and year and is thus highly unpredictable within a small time scale. Investments both in construction of wind mill parks as well as continued research are believed to drive this technology further to reach a more dominant role in the world wide energy supply[5,6].

Biomass constitutes the third renewable energy source worldwide with a power capacity of 62 GW. This technology utilizes that energy stored in biological material, e.g. plants and trees, during combustion is freed and transformed into electric energy by turbines. Plants are grown specifically for the purpose of biomass in which the energy from the sun is converted by photosynthesis into chemical energy in the plants to allow for growth of the organic material. Only little energy is needed to sustain the growth of these plants and thus the solar energy is continuously harvested and stored in the plants. This implies a certain level of storage since the material can be grown until the point where the biomass energy is needed. Additionally, only little geographical constraint hinders this energy source from being utilized worldwide as long as the climate allows for growth of the organic materials. These conditions provide good possibilities for the use of biomass as an alternative energy source. Generally biomass avoids the use of fossil fuels and thus deals with the problem regarding fossil fuel shortage. However in terms of CO_2 energy savings, biomass does not introduce a significant improvement as compared to fossil fuels since the combustion of fossil carbon and biomass carbon emit largely the same amounts of CO_2 during combustion[6].

Solar power has, while still being a smaller player on the renewable energy scene, seen a massive increase of power capacity from 16 to 40 GW from 2008 to 2010. Two forms of solar power are widely used, solar thermal energy and photovoltaics. Solar thermal energy utilizes the effect of heating when the solar radiation impinges on a surface. This energy is used either directly as heating of e.g. water for household consumption, or indirectly for heat engines where the thermal energy is converted into electric energy. Photovoltaics is a technology where electricity is generated directly by panels of solar cells. A problem in relation to solar power is that the energy is supplied only during periods of sunshine. No intrinsic storage is possible for this technology and thus external storage technologies have to be applied. However, PV is a versatile technology in the sense that there is no need for large installations. Small scale setups can provide remotely located areas instant access to electricity during sunshine, which is a unique feature of this technology. However, solar power is still not well-exploited

commercially even though the technology has reached a level of development where the price per watt is attractive for a worldwide economically feasible everyday use in certain countries[5]. Political initiatives and further development are needed to make the investment of solar energy e.g. in housing more attractive before this technology becomes a preferred energy source for everyday use.

The solution to future shortage of fossil energy supply will be based on a combination of different renewable energies while the combustion of fossil fuels will gradually attain a secondary role. The renewable energy technologies will complement each other thus benefiting from the individual advantages while the drawbacks are minimized by the interplay between the technologies. However, extensive research is needed within the above described fields in order to increase the economical and technological feasibility of making renewable energy a serious alternative to fossil fuels.

1.2 Solar power

In the discussion of PV, the development of the technology is typically divided into three major groups referred to as *generations* of solar cells[7]. Certain characteristics pertain to each generation based on the basic principles of operation.

1st Generation Solar Cells

This designation refers to the technology of the first commercial solar cells made by bulk high-purity mono-crystalline Si. These cells are all based on single junctions with low defect concentrations for which 25% efficiency has been achieved[8]. This technology has been exploited both within niche application such as satellite power supply and power supply for remotely located areas with no connection to the electric grid, as well as for large-scale power plants. The major drawback of this technology is the high processing temperatures and the need for high purity Si that increases the cost of the end product. However since the technology has matured, material costs have developed into being by far the biggest cost for the end product, partly due to the shortage of mono-crystalline Si. Research is conducted in optimizing the cell performance and increasing the commercial feasibility for the consumer by development of external devices such as solar concentrators etc. While 1st generation solar cells have reached a level of technological maturity, scientific attention gradually moves in the direction of 2nd and 3nd generation solar cells due to the potential of these technologies. Presently, 1st generation solar cells

still constitute the most significant contribution to installed PV power capacity, since future generations are not economically competitive.

2nd Generation Solar Cells

With the intention of decreasing material costs, a novel generation of solar cells has been developed. This technology is based on the deposition of a thin semiconducting layer on a low cost substrate. The most common material used for thin film cells is amorphous Si while other material combinations, e.g. cadmium telluride (CdTe) and copper indium gallium selenide (CIGS) have been introduced due to their potential of achieving higher efficiencies. The layer thickness is in the range of a few microns for the costly semiconducting material, which is a decrease by a factor of 100 compared to 1st generation Si cells. This decreases the material use without severely renouncing the energy conversion properties. Additionally, the processing of the cells avoids high temperature steps. An example of this is the use of chemical vapor deposition of SiH_4 at approximately 250°C used for the Si deposition of these cells. With such low energy consuming processing steps, the cost of the end product is reduced. Efficiencies of Si thin film cells are confined to below 10% for commercially sized cells. However with the ongoing present research it is believed that the price per watt can be decreased to a level below the one of bulk Si solar cells clearing the path for a commercial breakthrough for this technology[8].

3rd Generation Solar Cells

Within recent years, alternative approaches have been followed in the pursuit of higher efficiency and lower cost cells. These are referred to as 3rd generation cells, which is the common label for the novel cell structures based on 2nd generation technologies as well as the application of new materials and cell compositions. Sophisticated inorganic thin film cell structures are being subjected to scientific interest in order to enhance the photovoltaic properties. Tandem cells is one approach where a double junction is created with a high band gap material positioned above a low band gap material. This creates a filtering of the light increasing the overall absorption while decreasing the thermalisation loss. Other approaches are directed at introducing an impurity level in the photoactive layer enabling two-photon excitation with the impurity level as an intermediate level. These cells are still under development since control of

the production parameters and further optimization and cost reduction is needed before a feasible commercialization is possible[9].

A novel approach to the field of photovoltaics has evolved for which the electric properties of organic materials are utilized. The dye synthesized solar cells (DSSC) being reported in 1991 introduced a new cell structure based on a photo-electrochemical system. An organic dye coating of TiO_2 nanoparticles in an electrolyte is used for the absorption of photons. The electrons are injected into the conduction band of the nanoparticles while the dye is reduced by the surrounding electrolyte. This produces an electric circuit purely based on low cost materials. Efficiencies exceeding 11 % have been reported for DSSC, which is higher than the practical efficiencies of Si based thin film cells. However, drawbacks in terms of stability, toxicity and cost of the cell hinder the technology at the present stage from reaching full commercialization[10].

An alternative approach to the field of photovoltaics is based on organic materials. The term *organic solar cells* covers both solar cells based on small organic molecules and cells based on semiconducting polymers, referred to as *polymer solar cells* (PSC). In both cases a photoactive layer is processed in which photon absorption occurs. Hereby, charges are generated, separated and electrons are driven through an external circuit. Small organic molecule solar cells are processed by vacuum deposition of single molecules creating a photoactive layer with a high thickness control[11]. For PSC the photoactive layer is processed from solution. This layer is comprised of semiconducting polymers and electron acceptors. PSC performances have developed rapidly during recent years, and now efficiencies of 9.1 % have been demonstrated[12]. The major advantage of polymer based solar cells is that the entire cell can be processed completely by solution, which eases processing. Production of PSC can be done on flexible substrates onto which the layers are deposited successively using standard printing techniques, referred to as roll-to-roll coating (R2R). This allows for up-scaling the production and thus the potential of this is to bring the scientific field of PSC from the lab and into the everyday life where a large part of the daily consumption can be covered by solar energy. However, many processes still need to be optimized before a commercial breakthrough can be reached by this technology[13,14].

1.3 Polymer solar cells

PSC are solar cells based on conjugated polymers, which combine high absorptivity with good mobility. The cells are constructed of polymer thin films sandwiched between two electrodes. The polymers offer

a major versatility in terms of different physical and chemical properties, as the molecular structure can be rationally engineered. The field of PSC is currently subject to extensive scientific attention since this technology holds a promising potential as a future renewable energy source on a commercial scale. PSC provide an alternative approach to photovoltaics in which the costly Si is avoided and instead semiconducting polymers are used.

The existing PSC technology suffers from severe drawbacks that presently inhibit the commercial large scale production of R2R processed cells. Generally these can be summarized as dealing with efficiency, stability and processability of the cells. No single PSC combines high performance in these three parameters, and focus is thus on developing materials that fulfill all three criteria, referred to as the *unification challenge* (Figure 1.1).

Efficiency is an issue for PSC, which generally attain significantly lower values than for of inorganic cells [8]. While efficiencies approaching 10 % have been achieved for PSC, these performances are based on small lab scale cells, which have no direct practical applicability. The PSCs produced on a lab scale normally attain nominal areas between 0.01 and 1 cm^2.Since the electric properties are affected by the entire nominal area, smaller cells tend to attain higher quality and thus higher efficiencies. A material combination can be studied at near ideal conditions on small area lab scale cells.

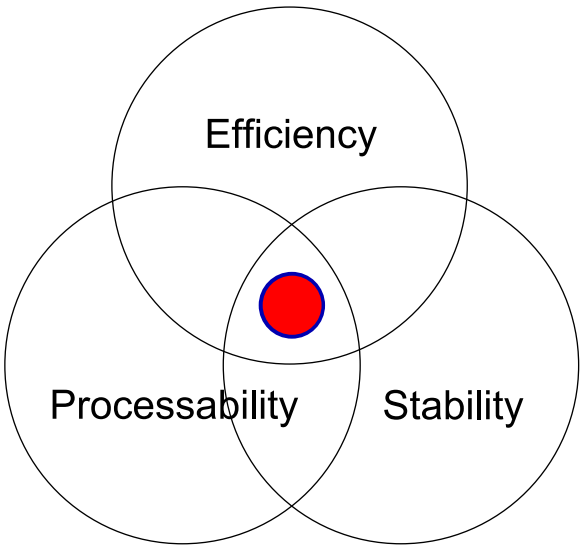

Figure 1.1. The unification challenge, which describes the goal of PSC research by the development of an efficient and stable cell that can be easily processed

Stability is the second issue regarding the conjugated polymers and PSC [15,16]. The general tendency is that immediately after the processing of the PSC the cell starts to degrade. All cells are intrinsically metastable, which results in a comparatively short lifetime of the cell. The conventional polymers, electron acceptors and electrodes are highly sensitive to O_2 and H_2O and degrade heavily when exposed to these species. Furthermore, the rate of degradation is known to increase with irradiance and temperature and thus the operational environment is naturally harsh for PSC. One approach to decrease the rate of degradation is to develop more stable materials that can operate in air. Both the shelf time as well as the operational lifetime have been reported to exceed one 1 year for certain material combinations, which suffices for selected practical applications[16]. Development of instrumentation for assessment of stability of polymers has been one of the goals of this PhD work. A second approach to extend the lifetime of PSCs is by encapsulation. A physical barrier around the PSC separates the photoactive layer from the atmosphere, which decreases the rate of diffusion of O_2 and water into the cell. This has shown to increase the lifetime of the cell thus enabling the use of higher efficiency yielding polymers on a practical time scale. However, instability is still a major issue that has to be dealt with in future research.

Processing is a third issue that addresses the complications of transferring the PSC technology from a lab to a large production scale. To obtain a lower price per area of the cells, a large up-scaling of the production is needed. This is done by the above described R2R technique for which large areas can be produced with high through-put and with a minimum of manual handling. However, this is a new field research within PSC and thus extensive R&D is needed to obtain satisfying photovoltaic properties of the produced cells. The cost can be significantly decreased if the polymer allows for a successful transfer from the lab scale to the R2R scale. However, the effect of this technology transfer is generally lower stability and efficiency, and the best materials exhibit efficiencies up to 4.2 % for R2R coated cells. New materials are needed to further decrease the cost of the R2R cells while the stability and efficiency known from the lab scale cells are conserved. However, not much information is obtained about the large scale potential of the material from these lab scale tests. Both the lab scale and the R2R scale efficiencies have to be improved before a commercial breakthrough can be envisaged. However for niche purposes the existing efficiencies would suffice if no other drawbacks were associated with the material.

1.4 Operation principle of organic solar cells

The physics behind the conversion of photons to free electrons in a PSC is intricate and demands for sophisticated models to account for a full description of the processes taking place within the cells. This is not within the scope of this work and a more qualitative description of the working principle behind the photovoltaic processes is presented. Additionally, the practical steps for the processing of PSCs are discussed as well as the materials used for the PSC.

The PSC can be characterized as a stack of thin films on a substrate, with different optical properties, thicknesses and meso-scopic structures. Between the layers, interfaces exist where the material composition gradually changes from one layer to another. Within this stack the photovoltaic processes occur, and the charges are traveling across the stack. The physical and chemical properties of each layer thus affect the photovoltaic properties of the entire cell. A PSC of the normal geometry consists of a number of thin films deposited on a substrate with a transparent conductor, typically a glass substrate with indium tin oxide (ITO) (Figure 1.2).

The first layer is Poly3,4-ethylenedioxythiophene (PEDOT) : polystyrene sulfonate (PSS), which is typically spin coated from water. It is a hole-conducting layer that blocks the passage of electrons as a function of the energy levels of the material. On top of this layer, the photoactive layer is deposited. Within the photoactive layer the impinging photons are ideally absorbed resulting in electron excitation generating an electron-hole pair. Finally a back electrode is deposited by thermal evaporation of Al to finish the construction of the cell. During illumination of the cell, photons are transmitted through the glass substrate, the ITO and the PEDOT:PSS layer with an overall transmission around 80 % above 300 nm. Consequently, a relatively high intensity impinges on the photoactive layer. With a band gap around 600 nm for most semiconducting polymers the photons are thus absorbed in the spectral range of 300 nm to 600 nm. In the photoactive layer electrons and holes are generated and driven toward the electrodes. The light that is not absorbed in the photoactive layer is reflected at the back electrode and thus traverses the photoactive layer twice allowing for an increased absorption.

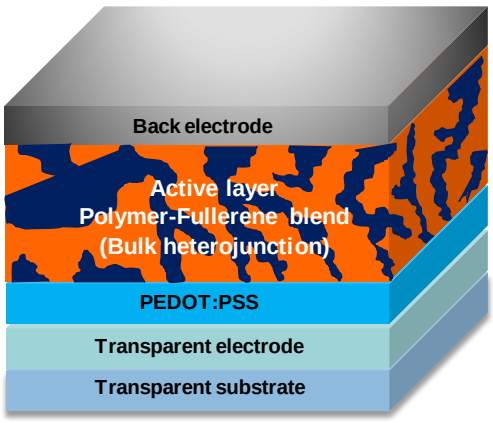

Figure 1.2. The layer stack of a normal geometry PSC comprising a BHJ

Conjugated polymers exhibit a high mobility compared to other organic molecules due to delocalization of π-electrons throughout the polymer chain and possibly across chains as well[17]. Combined with high extinction coefficients in the visible range and their solubility in organic solvents, conjugated polymers are the preferred choice for electron donors in PSC. Electrons within these polymers are excited promoting electrons to excited states while leaving behind holes. Between these oppositely charged particles, a strong Coulomb attraction pertains. This attraction can be considered as a bond between the charges, and consequently the electron-hole pair behaves as an imaginary particle referred to as an *exciton*[17]. If the Coulomb attraction between these oppositely charged forces is not overcome, the exciton will recombine. Physical separation of the charges is needed to avoid this, which is achieved through the introduction of an electron accepting species to which the excited electron is physically transferred. This creates an electron acceptor-donor structure, and thus the active layer always consists of two materials. The charge transfer is shown in Figure 1.3a where a photon is absorbed by a conjugated polymer. The excited electron is transferred to an electronegative electron acceptor thus providing a physical separation between the charges. This lowers the Coulomb attraction and thus minimizes the possibility of exciton recombination[17].

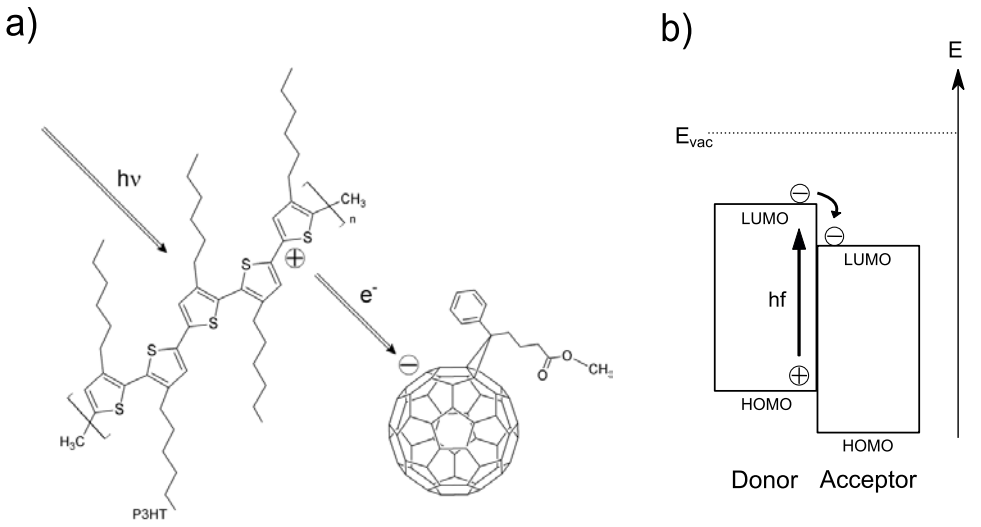

Figure 1.3. a) The charge transfer between the electron donor (P3HT) and acceptor (PCBM) which provides the essential step of charge separation in the photoactive layer. b) The energy levels associated with the charge transfer for a simplified donor-acceptor system

The choice of material for electron and donor materials for a functional cell can be theoretically predicted by the energy level of the highest occupied molecular orbital (HOMO) and the lowest unoccupied molecular orbital (LUMO) for the electron donor and acceptor material. Figure 1.3b shows a simplified illustration of the energy levels for the donor-acceptor system. During the excitation the electron is transferred from the HOMO to the LUMO of the donor molecule. This leaves behind a hole in the donor, which is not transferred due to the lower LUMO level of the electron acceptor. For efficient charge transfer to occur, the electron energy loss of the transfer should exceed the exciton binding energy. A minimum LUMO difference of 0.3 eV has been reported to be the minimum value for obtaining significant photocurrents[18–20].

Extensive research effort has been directed at optimizing the structure of the photoactive layer to obtain optimal conditions for extraction of the charges. The diffusion length of excitons in semiconducting polymers has been found to be in the range of 4-20 nm[21,22]. This means that all excitons generated more than 20 nm from an interface between a donor and an acceptor material are lost to recombination. The bulk hetero junction (BHJ) is the present state-of-the-art structure in which electron donor and acceptor materials are mixed in solution and spin coated on a substrate creating an intermixing structure of donor and acceptor domains. This creates a large interfacial area between the two materials within which the charge separation occurs. An impinging photon is transmitted by the glass substrate and the ITO and absorbed in the photoactive layer close to a donor-acceptor domain.

Due to the energy levels of the materials, the electron is transferred to the n-type material. If the acceptor domain has a direct percolation path from the charge transfer location to an electrode, the charge migrates to the electrode. If the electron is located in an isolated domain with no contact to the Al electrode, the electron is lost to recombination. The force driving the charges towards the electrodes is an effect of two phenomena. First of all, a charge carrier gradient throughout the cell is built up as soon as electron-hole pairs start to be generated at each side of a domain interface. This results in the diffusion of the charges due to the charge carrier gradient from the donor-acceptor interface to the electrode. A second reason for the driving force is the energy gradient due to the difference in work function of the two electrodes. Figure 1.4 shows the prediction of the HOMO-LUMO levels using a metal-insulator-metal (MIM) model, which can be used to describe the PSC. Two extreme cases are illustrated, which can be used to understand the driving force of the electrons.

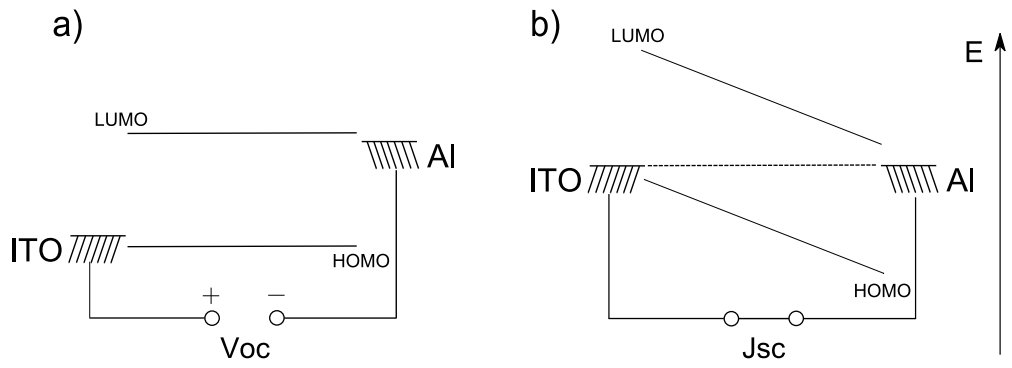

Figure 1.4. Illustration of the energy distribution throughout a PSC comprising ITO and Al electrodes using a MIM model of a) the HOMO-LUMO levels under band conditions and b) under short circuit conditions.

Figure 1.4a shows a situation where the two electrodes are not connected for a simplified cell in darkness. In this case the energy levels of the electrodes are not of the same material, their work functions differ. If a p-n junction is located between the electrodes, the HOMO and the LUMO levels behave as if they were in vacuum. If the cell is illuminated, electrons are excited to the LUMO level while holes are generated. The electrons will flow to the Al electrode and the holes to the ITO. This will increase respectively decrease the energies of the electrodes until the work functions reach the HOMO LUMO levels of the junction. The potential difference is the maximum extractable voltage for the charge carrier, referred to as the open circuit voltage, V_{oc}. If the two electrodes are connected, the energy difference will be minimized by highest energy electrons flowing into lower energy states. For the Al and ITO electrodes this implies that the energies of the highest energy from the Al flow to the ITO electrode until a new equilibrium is established. The consequence of this is polarization of the two electrodes with

the ITO being slightly negative and the Al being slightly positive. This forces the electrons away from the ITO toward the Al and *vice versa* for the holes, with the overall effect of an internal electric field (Figure 1.4b). The current attains its maximum for no external load when the resistance is zero. This current is referred to as the short circuit current, J_{sc}. If there is a resistance between the electrodes the electrons cannot flow freely and the work functions cannot level totally. As the external resistance increases fewer electrons are allowed to flow until the V_{oc} is reached where no electrons flow between the electrodes. The operation of the PSC can now be described based on both the donor-acceptor concept and the MIM model as described above. A 2-dimensional illustration of the energy levels in a bi-layer hetero junction is used to describe the concept of operation of the cell in general. illustrates the short circuit condition for a donor-acceptor interface under illumination where both the charge carrier gradient as well as the internal electric field are illustrated. Within the active zone confined by the exciton diffusion length, excited electrons are transferred from donor to acceptor molecules. The built-in electric field combined with the charge carrier gradient force the electrons toward the cathode while the holes move towards the anode.

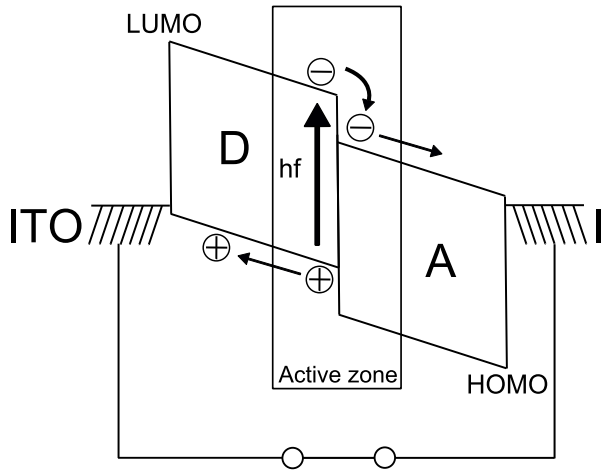

Figure 1.5. A cell diagram under short circuit conditions where free charges generated within the active zone can be extracted from the cell

The morphology of the BHJ is a key factor within the field of PSC. The morphology determines to a large extent the final properties since this is the starting point in every conversion of a photon to an electron. The theoretical efficiency limit for solar cells being subjected to AM1.5 illumination has been calculated by Schockley and Queisser. This simple calculation describes the maximum thermodynamical efficiency of solar cells when only considering two effects: Firstly, all impinging photons exceeding the material band gap are absorbed resulting in generation of free charge carriers. Secondly, all excited electrons

relax to the conduction band by thermalisation. This calculation yields 30% for an optimum band gap of 1.1 eV. For higher band gaps, efficiency is lost due to fewer photons being absorbed while lower band gaps suffer from a lower voltage of the extracted photons[23]. For PSC the concept of charge transfer further reduces the theoretical efficiency. An energy difference between the donor-acceptor LUMO levels of 0.3 V is needed to overcome the exciton binding energy and separate the charge carriers. For a realistic value of the potential of PSC, additional considerations have to be made. In addition to this, not all photons impinging on the PSC are absorbed and only a ratio of these generates free charge carriers that are extracted by the electrodes. Additionally, the charge carriers are subjected to transport losses, which further reduce the efficiency. Inclusion of these considerations into the calculation of the upper, theoretical efficiency yielded 11 % for a band gap of 1.5 eV for single junction cells. This limit can be seen as the efficiency that can be obtained from pure optimization of cell structure, layer morphology etc. However, with recent development of better performing materials, at present time efficiencies approaching 10 % have been reached[12].

1.5 Electrical characterization

Evaluation of the performance of PSCs is made by electrical characterization, which provides the cell efficiency and other central electric parameters. Hereby, all the components in the PSC, their interfaces etc. are probed providing the overall cell performance. The measurement is conducted as a voltage sweep across the PSC while the current is being measured. This measurement can be conducted in darkness to study the diode properties of the PSC, which yields information about the predominant effects in the PSC. This determines its overall rectification properties. The same measurement conducted during illumination of the PSC provides information about the properties in terms of light-to-power conversion properties. The irradiance from the sun outside the atmosphere can be approximated by a Planck distribution for a black body radiating at 5778 K as

$$I(\lambda, T) = \frac{2hc^2}{\lambda^5} \frac{1}{\exp\left(\frac{hc}{\lambda k_B T}\right) - 1},$$

where *h* is Planck's constant, *c* is the speed of light, k_B is Boltzmann's constant, λ is the wavelength and T is the absolute temperature of the black body. This spectrum ranges from the deep UV into the infrared peaking at the green part of the visible part of the spectrum. Passing the atmosphere, intensity is lost due to scattering and Frauenhofer lines from the molecular components of the atmosphere, e.g.

N_2, O_2 and H_2O. Thus the general irradiance decreases as the path length increases. The general reference spectrum used for PSC electric characterization is Air Mass 1.5 Global (AM1.5G), which indicates that the spectrum is based on the sun spectrum passing through 1.5 times the vertical thickness of the atmosphere. This corresponds to an illumination angle of 37° from zenith solar position. Integration of the energy flux from the entire spectrum results in a total irradiance of 1000 W/m_2.

Based on the IV curve obtained from each PSC a number of electric quantities can be extracted and from these the cell efficiency is determined. The *JV*-curves can be measured for samples in darkness and under illumination, referred to as dark and light curve, respectively. In the darkness, the PSC works as a diode with a *JV*-characteristic as shown in Figure 1.6. For an ideal diode, the dark current as a function of the voltage *V* can be described as

$$J_{dark}(V) = J_0\left(\exp\left[\frac{eV}{k_B T}\right] - 1\right),$$

where *e* is the elementary charge, J_o is the reverse saturation current, k_B is Boltzmann's constant and *T* is the temperature. During illumination the curve is approximately parallel-shifted with respect to the dark curve due to the current generation. Examples of *JV* curves obtained for a PSC under illumination and in the darkness are shown in Figure 1.6.. It can be seen that the light curve is not perfectly parallel-shifted relative to the dark curve, but rather has another curvature. This is due to losses within the cell as further described below. The voltage sweep is normally confined to between -1 and 1 V since only in the fourth quadrant the solar cell is physically operational in terms of power generation.

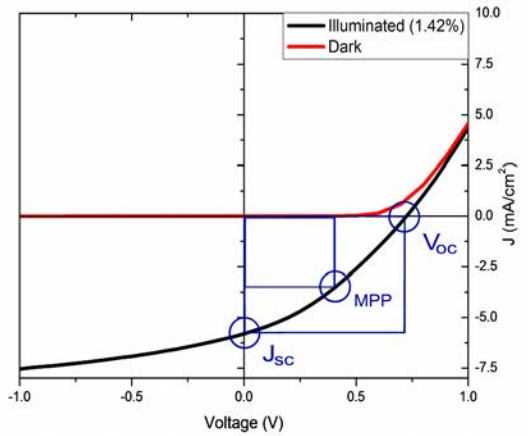

Figure 1.6. *JV* characterization of a PSC under illumination and in darkness with the key cell parameters being indicated

The current density at zero applied bias is referred to as the short circuit current density (J_{sc}). The current flows through the system when the electric contacts are connected and the electrode work functions are leveled (Figure 1.4). The current density is affected by many different parameters within the cell such as charge carrier density, charge mobility, the internal electric field, and the charge carrier gradient. The voltage applied to counteract the current during illumination is referred to as the V_{oc} as indicated on Figure 1.6. Ideally this quantity is the difference in HOMO-LUMO levels of the two types of charge carriers, and thus the V_{oc} depends on the choice of donor and acceptor material. Although being an intrinsic parameter to the PSC e.g. losses at the contacts, the morphology of the organic layers, and their interfaces influence the magnitude of the V_{oc}. *JV* curves generally attain different shapes due to variations in the physical properties of the PSC. This plays a role in terms of the maximum power that the PSC can produce. The power of the PSC under operation is described by $P = J \cdot V$. Consequently, the cell attains its maximum output power at a given point on the *JV* curve, referred to as the maximum power point (*MPP*). For this point the current and the voltage are lower than for the J_{sc} and the V_{oc} as illustrated in Figure 1.6. The fill factor is used to quantify the ratio between the cell *MPP* power to the theoretical output power for a current of J_{sc} and a voltage of V_{oc} and can be expressed by

$$FF = \frac{J_{MPP}V_{MPP}}{J_{sc}V_{oc}},$$

where J_{MMP} and V_{MPP} correspond to the current and voltage at the *MMP*. The *FF* can thus be regarded as a factor describing the percentage to which the cell exhibits an ideal diode behavior. To get a better understanding of the losses within the cell, which are also reflected by the *FF*, a circuit description as depicted in Figure 1.7 can be used. This is based on individual electronic components for which the overall property resembles the one observed for *JV* curve. When a solar cell is subjected to an external load, the current decreases with increasing load until the current cancels at which the V_{oc} is reached. This system can be described as an electrical circuit by a current generator connected in parallel to a diode. The current generator drives a current in the direction of the arrow. As the external load increases, the dark current J_{dark} leaking through the diode increases[24].

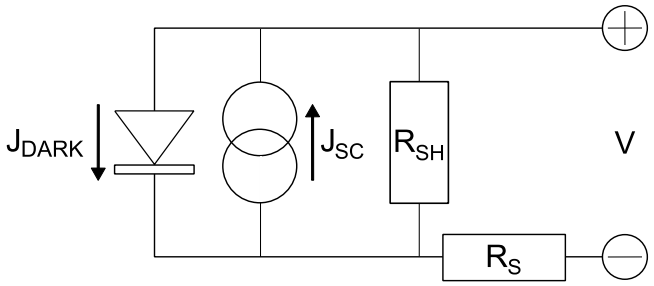

Figure 1.7. An equivalent circuit description of a solar cell based on individual electric components. The solar cell generates the current J_{sc} while a current J_{Dark} runs through the diode.

Real PSCs suffer from series resistance meaning that the overall resistance increases due to e.g. contacting to the electrodes and the introduction of barrier layers. Schematically this is modeled as a series resistance (r_{s}). Additionally, current is known to leak between the two electrodes due to a finite resistance of layers and pin holes etc. within the cell. This effect is modeled by a shunt resistance (r_{sh}), which for an ideal cell is infinite. The obtained current from the cell thus equals the photocurrent subtracted by the diode current and the current drop due to the series resistance as can be expressed using Kirchhoff's law by

$$J(V) = J_0\left(\exp\left[\frac{e(V_d + Jr_s)}{k_B T}\right] - 1\right) - J_{\mathrm{sc}} + \frac{V_d + Jr_{\mathrm{s}}}{r_{\mathrm{sh}}},$$

where $V_d + Jr_{\mathrm{s}}$ is the voltage drop across diode and the series resistor and the specific serial and shunt resistances r_{s} and r_{sh}have been introduced. The last term describes the ohmic current loss due to the shunt resistor. The *FF* describes the losses relative to an ideal diode and is affected by the r_{s} and r_{sh}. The power conversion efficiency relates the power output to the power input. With the above defined quantities it can be defined as

$$\eta = \frac{P_{out}}{P_{in}} = \frac{J_{MPP}V_{MPP}}{P_{in}} = \frac{V_{oc}J_{sc}FF}{P_{in}},$$

where P_{in} is the input power and the numerator corresponds to the power[24,25].

1.6 Conclusion

PSCs provide an attractive renewable energy source as an alternative to fossil fuel, where the vast amount of light impinging on the earth is converted into electricity. While conventional silicon based

solar cells suffer from high material costs and high energy processing steps, PSC provides a low-cost alternative. The field of PSC has been subjected to extensive funding and research recently, which has brought by a rapid increase of the PCE to a present level around 10 %. However, on a R2R scale, efficiencies are still inferior and more work has to be directed at optimizing this. Large scale processing of R2R PSC have has been demonstrated for which a high throughput and a low material cost significantly reduce the material and energy input into each PSC. 10 % efficiency and 10 years stability have been established as two goals that are to be fulfilled for PSC to be competitive with existing energy technologies[26]. While single demonstrations of both high PCE and stability have been made, extensive research is still needed before these so-called 10-10 targets are reached.

References

1. Enerdata *World energy use in 2010 : over 5 % growth*. (2011).at <http://www.enerdata.net/enerdatauk/press-and-publication/publications/g-20-2010-strongly-energy-demand-increase.php>

2. Administration, U.S.E.I. *International Energy Outlook 2011*. (2011).at <http://www.eia.gov/forecasts/ieo/index.cfm>

3. Bp Oil reserves: Global oil reserves rose by 6.6 billion barrels to 1,383 billion barrels in 2010. at <http://www.bp.com/sectiongenericarticle800.do?categoryId=9037157&contentId=7068604>

4. *Polymer Photovoltaics - A Practical Approach*. (SPIE, Bellingham: 2008).

5. REN21 *Renewables 2011 - Global Status Report*. (2011).

6. Edenhofer, O., Ramón, P.-M., Youba, S. & Kristin, S. *Renewable Energy Sources and Climate Change Mitigation*. (Cambridge University Press: 2012).

7. Bagnall, D. & Boreland, M. Photovoltaic technologies. *Energy Policy* **36**, 4390-4396 (2008).

8. Green, M.A., Emery, K., Hishikawa, Y., Warta, W. & Dunlop, E.D. Solar cell efficiency tables (version 39). *Progdd. Photovoltaics: Res. Appl.* **20**, 12-20 (2012).

9. Gaudiana, R. Third-Generation Photovoltaic Technology − The Potential for Low-Cost Solar Energy Conversion. *J. Phys. Chem. Lett.* **1**, 1288-1289 (2010).

10. Hagfeldt, A., Boschloo, G., Sun, L., Kloo, L. & Pettersson, H. Dye-sensitized solar cells. *Chem. Rev.* **110**, 6595-6663 (2003).

11. Riede, M., Mueller, T., Tress, W., Schueppel, R. & Leo, K. Small-molecule solar cells-status and perspectives. *Nanotechnology* **19**, 424001 (2008).

12. Polyera Achieves World-Record Organic Solar Cell Performance. (2012).at <www.polyera.com>

13. Krebs, F.C., Tromholt, T. & Jørgensen, M. Upscaling of polymer solar cell fabrication using full roll-to-roll processing. *Nanoscale* **2**, 873-86 (2010).

14. Krebs, F.C. *et al.* A complete process for production of flexible large area polymer solar cells entirely using screen printing—First public demonstration. *Sol. Energy Mater. Sol. Cells* **93**, 422-441 (2009).

15. Jørgensen, M., Norrman, K. & Krebs, F.C. Stability/degradation of polymer solar cells. *Sol. Energy Mater. Sol. Cells* **92**, 686-714 (2008).

16. Jørgensen, M. *et al.* Stability of Polymer Solar Cells. *Adv. Mater.* **24**, 580-612 (2011).

17. Gregg, B. a. & Hanna, M.C. Comparing organic to inorganic photovoltaic cells: Theory, experiment, and simulation. *J. Appl. Phys.* **93**, 3605 (2003).

18. Brabec, C.J. *et al.* Origin of the Open Circuit Voltage of Plastic Solar Cells. *Adv. Funct. Mater.* **11**, 374-380 (2001).

19. Vandewal, K., Tvingstedt, K., Gadisa, A., Inganäs, O. & Manca, J.V. On the origin of the open-circuit voltage of polymer-fullerene solar cells. *Nature Mater.* **8**, 904-9 (2009).

20. Scharber, M.C. *et al.* Design Rules for Donors in Bulk-Heterojunction Solar Cells—Towards 10 % Energy-Conversion Efficiency. *Adv. Mater.* **18**, 789-794 (2006).

21. Halls, J.J.M., Pichler, K., Friend, R.H., Moratti, S.C. & Holmes, a. B. Exciton diffusion and dissociation in a poly(p-phenylenevinylene)/C60 heterojunction photovoltaic cell. *Appl. Phys. Lett.* **68**, 3120 (1996).

22. Shaw, P.E., Ruseckas, A. & Samuel, I.D.W. Exciton Diffusion Measurements in Poly(3-hexylthiophene). *Adv. Mater.* **20**, 3516-3520 (2008).

23. Shockley, W. & Queisser, H.J. Detailed Balance Limit of Efficiency of p-n Junction Solar Cells. *J. Appl. Phys.* **32**, 510-519 (1961).

24. Günes, S., Neugebauer, H. & Sariciftci, N.S. Conjugated polymer-based organic solar cells. *Chem. Rev.* **107**, 1324-38 (2007).

25. Dennler, G., Scharber, M.C. & Brabec, C.J. Polymer-Fullerene Bulk-Heterojunction Solar Cells. *Adv. Mater.* **21**, 1323-1338 (2009).

26. Søndergaard, R., Hösel, M., Angmo, D., Larsen-olsen, T.T. & Krebs, F.C. Roll-to-roll fabrication of polymer solar cells As the performance in terms of power conversion efficiency and operational. *Mater. Today* **15**, 36-49 (2012).

2 Polymer stability

The instability of the polymer in PSC is an important contributor to the overall degradation of solar cell as a macroscopic device. This chapter discusses the origin of the instability of polymers and the effect of different polymer-related as well as degradation-environment related effects on stability. Characterization techniques used to evaluate material stabilities are presented as well as the applicability of the techniques as in-situ degradation monitoring tools. Finally, the work performed in this PhD in terms of polymer stability studies is presented.

As an almost general feature to organic materials, polymers are not inert materials with infinite lifetimes, but chemically reactive materials that are susceptible to attack by a wide range of agents[1]. For conjugated polymers, the direct consequence is normally observed as a loss and/or shift in the UV-vis absorption, which in turn implies reduced solar cell performance. Through rational engineering, the stability of polymers can be controlled by orders of magnitudes to suit the given application. Different types of polymers are known to be stable in certain environments, while others are highly susceptible to attack. Some applications require highly stable materials (e.g. car tires), while other applications are intentionally designed to be unstable (e.g. plastic bottles, food encapsulation with the intention of bio-degradability). Being kept in complete darkness after synthesis, they still degrade since they are exposed to the thermal energy of the surrounding as well as the gases in the atmosphere. Environmental factors that generally induce polymer degradation in most polymer materials can be divided into chemical and physical mechanisms depending on the nature of the attack. Physical stresses that generally induce material degradation are e.g. shear action, tensile stress, and elevated temperatures. Chemical stresses include, irradiation, moisture and oxygen. Chemical stresses are parameters central to PSC technology since these are the conditions in which the PSC is expected to operate. In this work, the resistance toward irradiation has been the main focus, while the remaining parameters are more loosely discussed since they are all prone to vary with ambient conditions by which they affect the polymer stability.

Being sandwiched between different transport layers and electrodes, the location of the active layer in the PSC is shielded spectrally and in terms of gas penetration. Major contributors to the overall electrical

degradation of solar cells are morphology evolutions, electrode degradation, generation of insulating interfaces, and the actual degradation of the polymer[2]. The contribution to the degradation by each of these degradation mechanisms depend on several different cell-specific parameters as well as the environment for the degradation studies.

When novel conjugated polymers are presented in the literature, the chemical structure is typically validated through NMR studies. Additionally, the molecular weight and the polydispersity are normally obtained by HPLC tests, which are important to estimate the success of the polymerization. Finally, solar cells are processed based on the polymer and the electrical cell performance is obtained, which is considered the most central results to the polymer. Actual stability assessment of the cells is not considered as standard characterization and is thus not given much attention. Additionally, quite a large number of solar cells are needed to conclude anything about cell stability since PSC suffer from significant stability variation for the same material combination[3]. However, comparative studies of solar cell stabilities have documented effects of changes of different parameters. These results are convoluted since they do not reflect the actual effect of the polymer, but a complex system in which the polymer plays a role.

An obvious step is to focus on the polymer or photoactive layer to estimate its intrinsic material stability. In this context, only a limited number of stability studies have been made explicitly on isolated polymers. The reason for this is that neither standardized stability assessment techniques nor commercial setups are available. Different approaches are followed to assess the degradation state of the polymer or blend layer, which all probe different aspects of the degradation. Common to most of these approaches, the polymer is generally not studied in its original environment within an operating solar cell. Instead, the material is normally deposited on glass substrates as thin films and exposed directly to the air and illumination. This deviation of degradation environment thus implies that conclusions on material stabilities from these studies do not reflect the actual material stabilities within the solar cell, but the results may be used relatively to establish expected rankings of PSC stabilities based on different polymers.

2.1 Polymer stability monitoring techniques

A key parameter to understanding the degradation and stability of polymers is material characterization, where physical and chemical analysis provides information of the phenomena taking place on the molecular level. Characterization techniques can be divided into destructive and non-destructive tests depending on the nature of the technique. While destructive tests do not render the sample usable for further studies after testing, non-destructive techniques do not introduce any changes to the samples under study. A multitude of techniques can be applied to polymer characterization to get insight into the physics and chemistry of the polymers[2]. Certain non-destructive techniques do not require the sample to be removed from the experimental setup during material studies (i.e. no need for vacuum, certain temperatures etc.). Consequently, with such techniques, the material can be followed in-situ during experiments. Two such techniques that probe properties that are prone to change with degradation are UV-vis spectroscopy and Infra-red spectroscopy, which have been widely used to monitor the stability of polymers.

2.1.1 Ultraviolet-Visible spectroscopy

Ultraviolet-Visible (UV-vis) Spectroscopy is a widely used spectroscopic technique by which the absorption in the UV-visible part of the electromagnetic spectrum relevant to solar cells is studied. The UV-vis absorption is central to the polymer in the context of PSC since the absorption of UV-vis photons is the first step toward generating a current from a solar cell. UV-vis photons do not interact with the molecular bonds, but instead with features on a larger scale such as aromatic rings and molecular structures. Small molecules and oligomers do typically not exhibit visible light absorption, while conjugated polymers generally do. While the chemical structure of the polymers under study cannot be directly elucidated from the spectra, the photochemical stability of the polymers can be accurately assessed. However, different chemical properties such as conjugation length and crystallinity can be qualitatively discussed and used in conjunction with observations from other techniques. The technique is non-destructive, which allows for monitoring polymers during degradations.

A typical setup consists of a broad-band light source, which illuminates the semi-transparent sample. A spectrometer detects the transmitted light and assuming negligible scattering in the system, the absorption at normal light incidence can be expressed by

$$A = 1 - R - T,$$

where *R* is the intensity of the reflected light from the sample and *T* is the transmitted light intensity. Polymers are often studied as deposited on transparent glass substrates. Using a clean glass substrate as a reference sample, the absorption of a single layer deposited on the substrate can be expressed by

$$A = 1 - \frac{I_{ref} - I_D}{I - I_D},$$

where I is the intensity with polymer sample, I_{ref} is the intensity with the glass reference, and I_D is the dark intensity (when the light source is turned off). The absorption of a polymer film is typically given in units of *absorbance Abs*, which is defined by $Abs = -\log(A)$. Absorbance is a unit-less quantity, which scales with the thickness of the polymer film.

An example of a UV-vis absorption spectrum is shown in Figure 2.1a, where the degradation of a poly[3-hexyl-thiophene] (P3HT) is monitored during a degradation at 150 suns. Initially, the absorbance is observed in the range of 350 – 630 nm, where the higher boundary can be regarded as a crude approximation to the optical band gap. A shoulder is observed at approx. 600 nm, which has been associated with inter-chain absorption of crystalline domains[4]. The peak position is observed to blue-shift during the degradation, which has been related to backbone scission implying a reduction of the conjugation length[5].

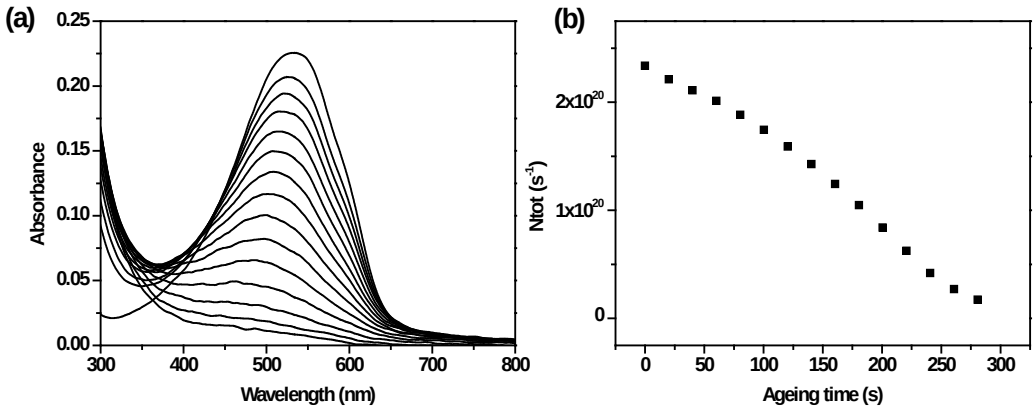

Figure 2.1. (a) UV-vis absorption spectrum of a P3HT during a degradation at 150 suns AM1.5G. (b) The evolution of N_{tot} with ageing time

UV-vis spectroscopy has been widely used to monitor the stability of polymers and blends. A simple approach to quantifying the stability is by observation of the decrease of the absorbance of the initial peak absorbance wavelength over time, which is widely reported in the literature[6]. Using this approach, a linear decrease is normally observed during degradation, from which the slope is taken as the degradation rate. However, during a degradation experiment, the absorbance peak may change over time, which is not handled by the above described method. The actual photoactive properties of the polymer are related to the overall absorption of the material and thus a better solution is to include the entire absorption spectrum into the quantification of the state of the polymer. Finally, since the polymer is meant to absorb sunlight, the impact on the photoactive material properties varies with the wavelength. Thus, to fully allow for quantification to the photo activity, *the total number of photons* N_{Tot} absorbed when the polymer absorption spectrum is exposed to a AM1.5G light spectrum is a more generally applicable quantity to monitor. This quantity is obtained by integration of the product of the absorption and the AM1.5 photonic flux and can be numerically expressed as

$$N_{Tot}(t) = \sum_{\lambda_1}^{\lambda_2} N_0(\lambda) \times (1 - 10^{-Abs(\lambda,t)}),$$

where $Abs(\lambda, t)$ is the recorded absorbance, $N_0(\lambda)$ is the photonic flux of the AM1.5G spectrum and λ_1 and λ_2 are the limits of the integration. N_{Tot} is typically observed to decrease linearly with the ageing time and thus the slope of this evolution is referred to as the degradation rate[7]. The evolution of N_{Tot} of

the P3HT degradation depicted in Figure 2.1a is shown in Figure 2.1b. This is a typical evolution where an approximately constant slope is observed until the degradation has completed and N_{Tot} reaches effectively zero. During the degradation, small monomers, oligomers and other degradation products are accumulated in the film, which contribute to the increased degradation at 300-350nm. This may imply that N_{Tot} only ends on a final value of a few percent, since the degradation products contribute to the evaluated N_{Tot}.

2.1.2 Infra-Red spectroscopy

Infra-Red (IR) spectroscopy relies on the interaction of intra-red radiation with molecules by which the chemical composition can be identified and chemical transformations followed. The mid-infrared region from 400 – 4000 cm^{-1} is relevant to polymeric materials for PSC since this region probes the vibrational modes in the bonds of the molecules, which are markers for different chemical structures. With a classic mechanic explanation, if the frequency of IR radiation matches the frequency at which a chemical bond vibrates, a resonance is the result. By detecting the ratio of the absorbed to the incoming light, a spectral absorption is obtained. The frequency of the atomic vibration can be considered as a harmonic oscillator and can thus be expressed by

$$\nu = \frac{1}{2\pi c}\sqrt{k\frac{(m_1+m_2)}{(m_1 m_2)}},$$

where m_1 and m_2 are the masses of the two atoms, c is the speed of light and k is the force constant (bond strength). Consequently, the atomic masses and the bond strength govern the oscillation frequency. Several different vibrational modes are found in polymers, which are descriptively named after the type of vibration. Table 2.1 shows the vibrational modes observed for pristine P3HT for the carbon bonds. Generally, bending and rocking modes are of lower energy than stretching modes, and thus of higher wave number.

IR mode	wavenumber (cm^{-1})
= C-H stretching	3055
CH_3, asymmetrical streching	1954
CH_3, asymmetrical streching	2924
CH_3, symmetrical streching	2870
CH_3, symmetrical streching	2855
Out of phase C=C streching	1510
In-phase C=C streching	1675
CH_2 bending	1454
CH_3, asymmetrical streching	1715
CH_3, symmetrical streching	1377
= C-H in-plane bending	820
$(CH_2)_n$ in-phase rocking	725

Table 2.1. Vibrational modes of pristine P3HT[8]

Figure 2.2 shows an example of the evolution of IR absorption spectra as a function of ageing time of P3HT for (a) 1600 – 1850 cm^{-1}, which is associated with carbonyl groups, and for (b) 700 – 1500 cm^{-1}, which are features associated with sulfur-containing molecules[8]. During degradation, the intensities of the features are found to increase, and thus these spectra identify degradation products.

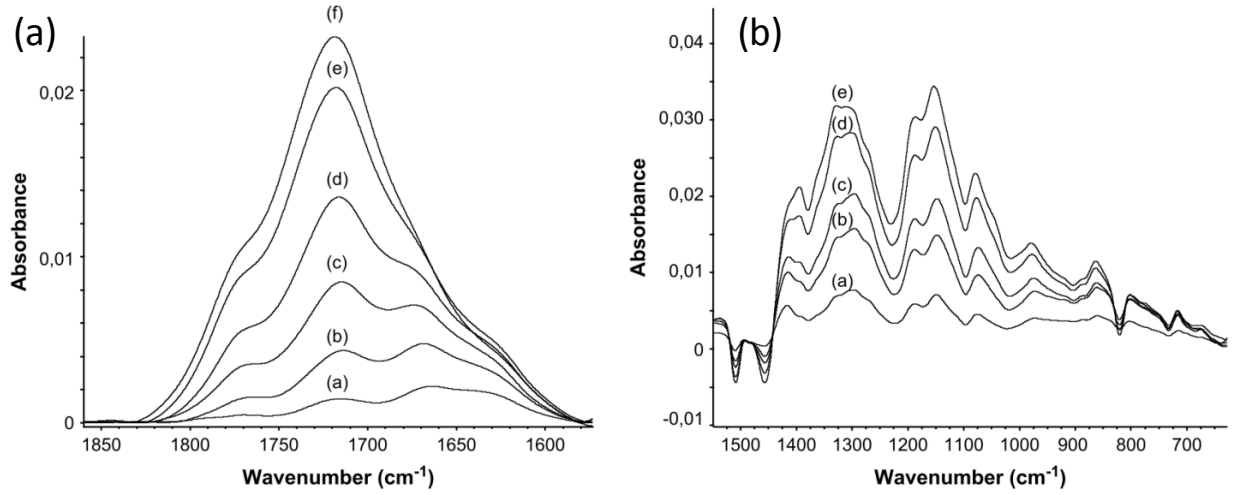

Figure 2.2. IR absorption spectra of P3HT during photooxidation. (Left) Carbonyl range for (a) 5 h; (b) 20 h; (c) 40 h; (d) 60 h; (e) 80 h; and (f) 100 h. (Right) Region for CH_3 (symmetrical bending) at times (a) 5 h; (b) 20 h; (c) 30 h; (d) 50 h; and (e) 60 h[8]

The technique is quantitative implying that the area below a given absorption peak scales with the concentration of the associated chemical group. Additionally, the technique is non-destructive implying

that a sample can be studied with IR spectroscopy at regular intervals during an experiment. Consequently, IR spectroscopy allows for monitoring chemical reactions in the polymers, by which e.g. degradation mechanisms can be elucidated. Figure 2.3 shows the evolution of different chemical species during photooxidation of P3HT[8]. The decrease of the concentration of general UV-vis absorption at 520 nm (open squares) was found to correlate with the decrease of both thiophene and alkyl groups. This correlation thus demonstrates that the absorption of the polymer is strongly dependent on these thiophene and alkyl groups. Additionally, the evolution of degradation products are observed with different on-set times, where carbonyl moieties are immediately formed, while thioesters only start forming when the polymer is in a highly degraded state. This example demonstrates how the evolution of multiple moieties can be followed as a function of the ageing time. This is important in relation to understanding the mechanisms responsible for the observed degradation.

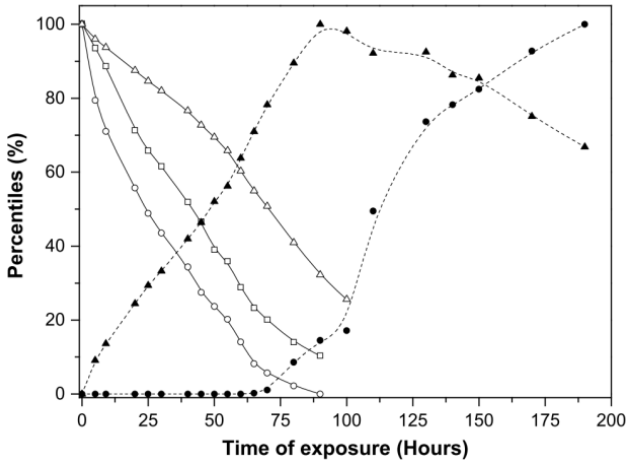

Figure 2.3. Evolutions of relative IR peak absorptions during photooxidation of P3HT. Evolution of UV-vis absorption at 520 nm (open squares), thiophene rings (1510 cm^{-1}), alkyl groups (3000-2850 cm^{-1}), carbonyl moieties (1800-1650 cm^{-1}) and thioesters (620 cm^{-1})[8].

Several chemical bonds and groups can be identified by IR spectroscopy. Some groups are only observed after photolysis, while thermolysis gives rise to other products. Table 2.2 shows some of the dominant IR features observed for degradation of P3HT. Often, spectral features are found to consist of IR features from several chemical groups and thus resolving and quantifying the relative evolution of all features over time can be cumbersome. A solution to this is to treat the material with a *derivatization treatment*. By allowing different gases to pass the oxidized polymer, specific oxidation products can be converted into products with a different spectral IR absorption feature by which the former features consisting of

several peaks can be simplified. Typically used gases are SF_4 which can turn acids into acyl fluorides, and NH_3 which transforms alcohols and hydroperoxides into nitrites and nitrates, respectively.

Degradation products Structure	**Wavenumber** v (cm^{-1})	**Identification** Derivatization reaction
-S(0)-OR	620	SF_4,NH_3
	1115	
-S(O)-	1050	
-SO2-	1125	
	1335	
Th-CO2H	1670	SF_4,NH_3
Th-CO2-R	1675	Photolysis
R-CO2h	1710	SF_4,NH_3
R-CO-R'	1715	Photolysis
-CO-O-CO-	1785	NH_3
-OOH	880	Thermolysis
	3450	
-CO2H	2340	SF_4
-OH	2450	SF_4

Table 2.2. Summary of P3HT degradation products and their derivatization reaction[9]

On a practical level, normal SiO_x based glass cannot be used for standard absorption measurements of polymers since they absorb heavily in the IR range. Consequently, alternative salt-based substrates such as KBR, KCl, and NaCl are needed, which complicates the experimental work. With IR spectroscopy, widely used polymers such as poly[2-methoxy-5-(3'-7'-dimethyloctyloxy)-1,4-phenylenevinylene] (MDMO-PPV) and P3HT were extensively studied, and their major degradation mechanisms were elucidated, both in terms of photo oxidation, thermolysis and thermooxidation[8,10].

2.2 Engineering photochemical stability

The stability of polymers when exposed to UVvis illumination as a thin film in the presence of oxygen, referred to as *photochemical stability*, is known to depend highly on several different degradation parameters. Extensive work has been directed at understanding and handling these degradation phenomena. However, the quantification of the photochemical stability of conjugated polymers has until recently been relatively unstudied and thus there was only a vague impression of the relation between polymer structure and stability. Early reports of the photochemical stability of MDMO-PPV observed photo-degradation of the polymer in the operating cell as evaluated by the increased cell reflectivity[11]. However, these results were never obtained in-situ and thus only few degradation states

over time were documented for a given degradation. A break-through was when focus was directed to the photochemical degradation of the isolated polymer spin coated on glass. Such samples were exposed to different degradation conditions and over time, they were manually studied with IR and UV-vis spectroscopy to follow the degradation. The technique of monitoring the gradual absorbance loss was first presented by Holdcroft in 1991, who studied the photochemical stability of P3HT[5]. Further work was reported in 1998 on different non-conjugated polymers, where the evolution of both UV-vis and IR absorption features were followed over time to deduce the chemical degradation mechanisms[12–14].. Additionally, the evolution of the UV-vis absorbance, which closely relates to the potential of absorbing photons in a solar cell, was studied for the different polymers and blends. This allows for direct comparisons between the photochemical stability of different polymers and is thus a highly useful technique to study the structure-stability relationship. Photochemical stability studies have consequently established an empiric relation between the molecular structure and the stability of a given polymer.

2.2.1 Stability of functional groups

Presently, photochemical stability as a technique is still in its infancy, since many of the factors influencing on material stabilities have not been explored. Additionally, the technique has been demonstrated to be highly sensitive to the effect of the film thickness under study. Finally, aspects such as the relationship between polymer stability and its associated stability when blended with an acceptor have not been studied. Since the BHJ is the context in which the polymer is intended to operate, this kind of knowledge is important to establish for photochemical stability testing to become a mature, generally accepted technique. The stability of P3HT:$PC_{60}BM$ BHJ has been briefly discussed, where the focus has been on elucidating the degradation mechanisms, while a strict quantification of the stability was omitted. Reese *et al.* observed that stabilization by a factor of 5-10 was observed by blending P3HT with $PC_{60}BM$ in a 1:1 ratio[15]. However, as the effect of film thickness was not considered, the specific factor of stabilization cannot be ascribed high validity. Rivaton *et al.* performed degradation of P3HT and P3HT:$PC_{60}BM$ as well as MDMO-PPV and MDMO-PPV:$PC_{60}BM$ in ratios of 1:1. The P3HT was found to stabilize by a factor of 5 while the value for MDMO-PPV exceeded 25. Consequently, the extent of the $PC_{60}BM$ stabilization seems to vary with the polymer. Further studies of this effect are needed to

establish whether the $PC_{60}BM$ stabilization correlates with the stability of the polymer or some other factor.

Even though several important aspects of photochemical degradation studies have to be established, interesting applications of the approach have been demonstrated. Specifically, a stability screening of more than 25 different polymers was carried out for films of optical densities of 0.6[16]. The fact that all optical densities were identical allowed for qualitatively comparing the stabilities, however, with the effect of film thickness still not being understood. Polymers comprising highly different chemical moieties were studies, which allowed for establishing a relative stability ranking of these moieties. Additional effects such as film density, crystallinity, regio-regularity, polymer purity, molecular weight, and polydispersity were not considered. While the observed trends should be considered with some conservatism, the results are still important as a guideline for organic chemists to direct their work in the direction of photochemically stable materials. A comparison of several polymers consisting of identical acceptor units and varying donor unit established a ranking of these donors (Figure 2.4). This showed that fluorene groups were highly unstable, while thiophene groups exhibited higher stability. The highest stability was observed for dithienothiophene groups. The general conclusion to be drawn from this ranking was that side chains generally destabilize the donor groups. Additionally, the presence of a quaternary carbon atom and a seemingly low energy-bond such as ethers or carbonyl bonds also destabilize the donor groups.

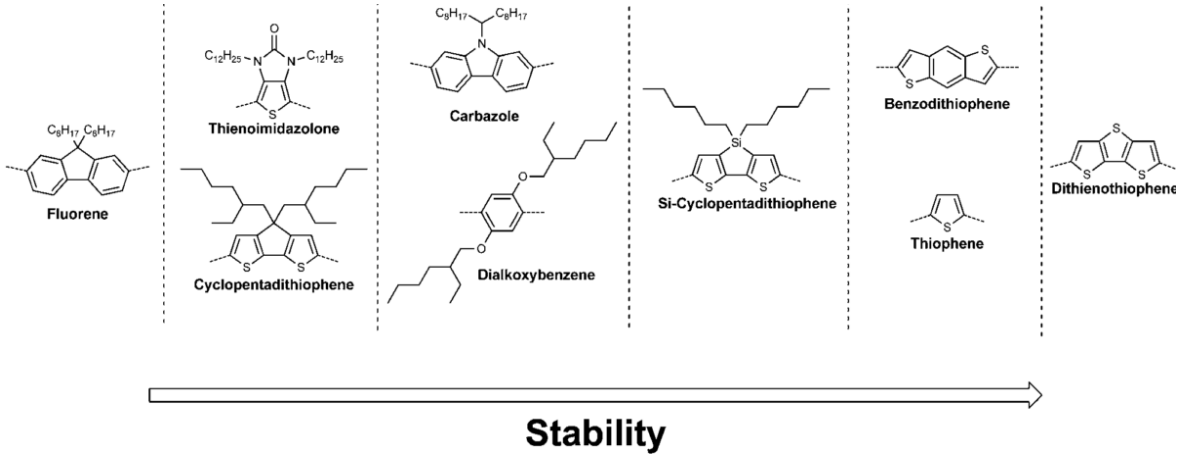

Figure 2.4. Relative stability ranking of different electron donating groups as determined by photochemical stability studies[16]

2.2.2 Novel approaches to polymer stability

Bjerring *et al.* demonstrated the complete thermal cleavage of a tertiary ester at 300°C (Figure 2.5). The polymer poly-(3-(2-methylhexyloxycarbonyl) dithiophene) (P3MHOCT) was found to lose its tertiary ester to form poly-3-carboxydithiophene (P3CT) by thermal annealing at 210°C. Further annealing at 300°C induced a further de-carboxylation by which native PT was formed. The function of the alkyl side chains of most solution processed polymers is to make the polymer soluble in common solvents. After the polymer has been processed from solution, this function is in practice not needed anymore. By removing the alkyl chain a much denser structure is obtained, and the diffusion of aggressive O_2 into the matrix is hindered. Furthermore, the alkyl chains tend to be highly reactive to photo-chemistry and thus by removing these, only the conjugated photo-active highly stable backbone remains.

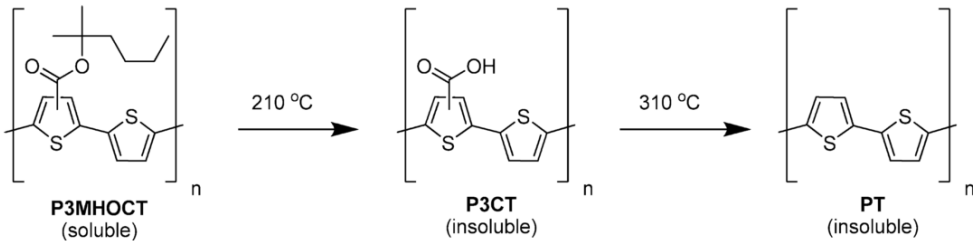

Figure 2.5. The thermocleavable polymer is cleaved at 210 °C to P3CT and at 300 °C to PT[3]

Manceau *et al.* studied the photochemical stability of these materials as well as two different thermo-cleavable dithienyltienopyrazine-based donor-acceptor polymers[17]. Even though the thickness of the studied samples are not specified in the paper, it can be assumed that these are constant for all samples. The photochemical stability of P3MHOCT was found to closely resemble the one observed for regio-regular P3HT. However, the first thermo-cleaving step to P3CT highly stabilized the system by a factor of 5, since the bulky ester was lost. The stability of PT was found to be approximately 20% higher, and thus the photo-stabilization is found already after the de-esterfication. In the case of the two other donor-acceptor polymers, a similar de-esterfication induced a stability improvement of 7 and 4, respectively. This demonstrates that thermocleaving polymers generally induces a photochemical stabilization, and thus this approach has a potential to increase PSC lifetimes. Another aspect is that the side-chain removal renders the layer insoluble in common organic solvents, which alliviates the need for orthogonal solvents for multilayer processing. Finally, the structure of the thermocleaved layers is very

dense and rigid. Consequently, the timescale for the common degradation mechanims of evolving morphology in BHJs is decreased, and consequently PSC based on e.g. P3CT have demonstrated very high cell stabilities[18].

An alternative solution to increasing the stability of BHJ is by cross-linking either the different chains of polymers[19], and even cross-linking the polymer to the $PC_{60}BM$[20]. These approaches were mediated by funcitonalization of the alkyl side chain of P3HT with either Br, N_3, azide or oxetane. By UV-illumination, if two N_3 atoms are in close physical contact, they react to form a covalent bond between the two alkyl chains (Figure 2.6). Otherwise, if the BHJ is thermally annealed to 150°C, the azide group reacts with the C_{60} part of $PC_{60}BM$ to form two single covalent bonds. The advantage of this is that both the polymer matrix and the donor-acceptor interfaces can be physically stabilized, which introduces morphological stability. PSC based on this technology indeed demonstrate high thermal stability, which is the condition where the evolution of the morphology is clearly observed.

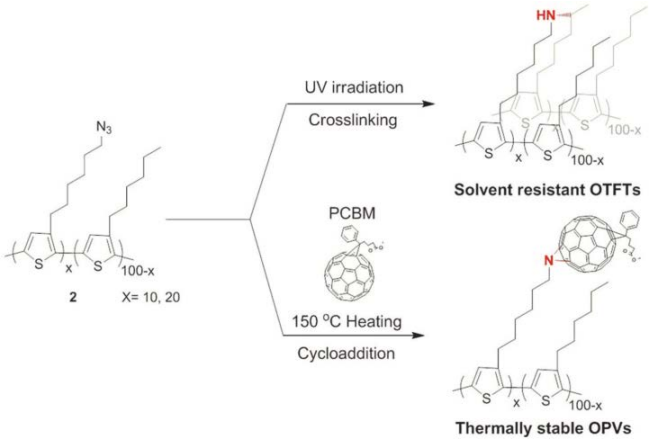

Figure 2.6. The chemical cross-binding reaction of an azide terminated side chains on P3HT that selectively, through either UV-illumination or thermal annealing, binds to other polymers or neighboring PCBM molecules[20]

However, since the monomer is kept intact during the cross-linking, the reactive side chains are still present in the cells. During this PhD work, photochemical degradation studies of both P3HT and an alternative benzo-thiadiazole based polymer functionalized with Br, N_3 and oxetan were performed. These demonstrated that all materials both before and after cross-linking did not deviate in terms of photochemical stability when compared to their un-functionalized counterparts (Results submitted as Carlé, J., Andreassen, B., Tromholt, T., Madsen, M., Jørgensen, M., & Krebs, F. C. Comparative Studies of

Photo Chemical Cross-linking Methods for Stabilizing the Bulk Hetero-Junction Morphology in Polymer Solar Cells. *Submitted to Journal of Materials Chemistry*). This result shows that while the degradation as a function of photobleaching may be unchanged, the degradation induced by morphology changes can be minimized.

2.3 Central parameters to polymer degradation

As discussed above, the photochemical stability of polymers depends on several parameters relating to the polymer external to the monomer itself. To precisely assess the stability of a given material, great care must be taken to control the degradation environment to allow for comparisons of stabilities between different polymers. Parameters such as oxygen concentration, humidity, temperature, light intensity, film optical density (thickness), UV content, ozone concentration, and molecular weight are all known to influence photochemical stabilities[6,21]. Since stability studies of polymers in the ambient have only been reported recently, no standard degradation conditions have been established. Thus, to allow for comparisons of stabilities between different laboratories, great care has to be taken to keep all parameters within the control of the experimenter constant, as well as to report all of these in scientific reports. When planning and setting up comparative polymer stability studies, knowledge about the influence of each parameter is important. In the following the influence of the most important parameters are discussed.

2.3.1 Light source

While no systematic studies on the effect of different light sources on photochemical stability are reported, several different light sources have been used for performing stability studies of PSC. These results showed significant variations in the cell stabilities. Gevorgyan *et al.* conducted a broad comparison of the stability of R2R coated solar cells as measured in 24 different laboratories[22]. In this study, cell stabilities under halogen, metal halide, Xe arc and sulphur plasma lamps were studied and compared to outdoor degradation. Ideally, the degradation of the artificial light sources should closely resemble the one observed outdoor for the same light intensity, if the effect of variation in parameters such as temperature and humidity between the laboratory and outdoor are handled. However, with the spectral differences between the light sources, variations are expected. The study demonstrated highly

different stabilities with the different light sources. The sulfur-plasma and the halogen lamps induced a much less degradation than the remaining light sources during 1000 hours illumination. After this time, cells degraded by these light sources had degraded to 30-80 % of their initial PCE, while in the case of the metal halide and Xe lamp, only 10 – 30 % of the initial performance remained. The degradation rate for the cells degraded outdoor in the sun was comparable to the metal halide and the Xe lamp, and thus these light types are obvious choices for degradation studies with artificial light.

2.3.2 UV-cutoff

The application of different light spectra naturally induces different cell stabilities. The primary reason is the high UV content in the metal halide and Xe light sources. The photochemical degradation induced by approximately monochromatic light at different wavelengths of P3HT deposited on glass substrates was demonstrated by Hintz *et al*, where the effect of several different environmental factors were studied[6]. They defined the *photon effectiveness* by

$$\gamma = \frac{dN_{tr}}{dt}\frac{1}{I_{incident}(\lambda)} = \frac{dE}{dt}\frac{N_A}{\epsilon_{tr} I_{incident}(\lambda)},$$

where dN_{tr}/dt is the number of thiophene rings lost pr time, $I_{incident}$ is the photon flux, dE/dt is the loss in peak absorbance, N_A is Avogadro's number and ϵ_{tr} is the thiophene ring molar absorption coefficient $\epsilon_{tr} = 10^4 \mathrm{M}^{-1}\mathrm{cm}^{-1}$. They thus monitored the decrease of the UV-vis absorption peak with the photon flux at different wavelength. The results showed that at 500 nm, γ was 10^{-7} in increased exponentially with decreasing wavelength to $\gamma = 5 \cdot 10^{-5}$ at 335 nm. This 20 fold increase clearly demonstrates the importance of the UV content in the degradation spectra.

2.3.3 Temperature

The operation of PSC involves degradation mechanisms with different thermal activation energies. Consequently, increasing the degradation temperatures accelerates the cell degradation. Only few studies of the influence of the ambient degradation temperature have studied the effect of the photochemical polymer stability. However, for PSC, several studies have been made, and temperature has often been used to accelerate degradations for highly stable materials[21]. Associated with this approach is the risk that the relative stabilities observed between different materials at augmented

temperatures do not necessarily hold at conventional degradation temperatures. Recently, a consensus on PSC stability testing has been established[23]. With this work, the intention is to fulfill certain requirements in terms of testing equipment and the environmental parameters during degradation. Hereby, comparisons of stability results between different laboratories will be clearer, which will benefit the entire scientific field. In terms of indoor weathering testing, three different levels of testing protocols were established with increasing complexity and control, referred to as ISOS-L-1, ISOS-L-2, and ISOS-L-3. One of the parameters that vary between the protocols is the temperature during the degradation, where the ISOS-L-1 imply the general ambient temperature of the setup and thus no direct control, while the ISOS-L-2 and ISOS-L-3 protocols dictate a temperature in the range of 65 – 85°C. This value is considered comparable to what a commercial outdoor solar panels experience on sunny days in relatively hot regions. Additionally, this range is the typical equilibrium temperature for degradation of samples in a Steuernagel solar simulator fitted with a 1200 W HMI lamp.

Due to the complex nature of the degradation of PSC, several different processes are accelerated to different extents by increasing temperature. Thus no general rules can be established to give a general description of the response of PSC to increased temperature. However, thermal acceleration is still used to decrease the timeframe of stability assessments and the results are still qualitatively valid[18]. Contrary to this, photochemical studies of polymers are not as sensitive to the degradation temperature since this is a much simpler system. Where typical activation energies for PSC are in the range of 300-350 meV[21], pure polymer activation energies have been reported in the range of 100 – 276 meV[6,24]. On a practical level, activation energies of 276 and 350 meV correspond to acceleration by a factor of 8.1 and 14.2 at 100°C compared to a reference temperature of 27°C. Several papers report photochemical degradations at 60-85°C[10,17,25]. Additionally, a single study compared different degradation temperatures with the same degradation setup. They varied the temperature from 25 to 120°C during degradation of 100 nm P3HT films deposited on glass[6] (Figure 2.7a). They observed a clear exponential increase of reaction rate with temperature, where an acceleration factor of 10 was observed between 25 and 120°C. The data was fitted with an Arrhenius model, which describes first order kinetics. The reaction rate can be expressed by:

$$k_{deg} = A\, e^{\left(\frac{-E_a}{k_B T}\right)},$$

with E_a being the activation energy, k_B the Boltzmann constant 8.62·10^{-5} eV/K, T is the absolute temperature, and *A* is constant depending on the experimental conditions. With this series of measurements, E_a was determined to 276 meV.

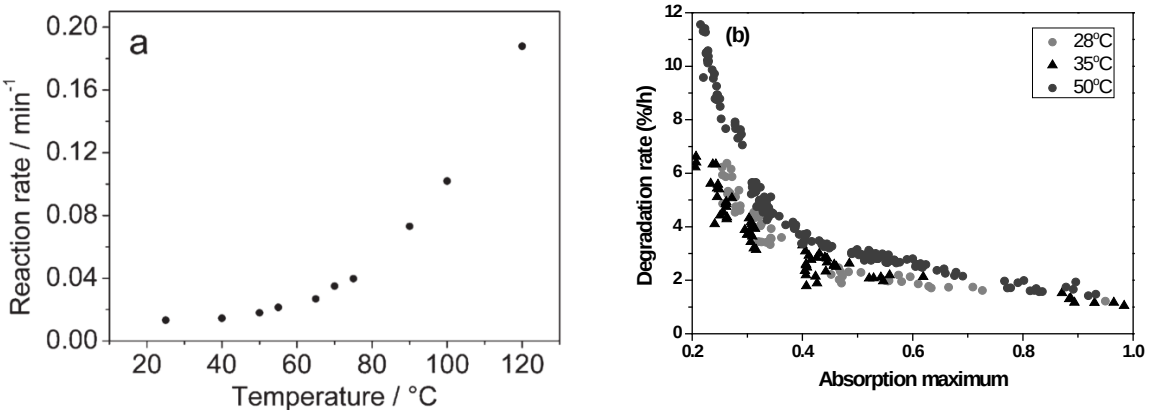

Figure 2.7. a) Reaction rates with increasing temperature for P3HT[6]. b) Degradation rates of P3HT at three different degradation temperatures

As one of the initial experiments in polymer degradation in this PhD work, the influence of the degradation temperature was studied as a function of the film thickness. Hintz *et al.* only studied a single film thickness (100 nm corresponds to peak absorption of 0.59) from which the thermal activation was observed. Thicker films absorb more light and thus reach a higher equilibrium temperature during degradation. Degradation of regio-regular P3HT was carried out for 3 different ambient temperatures of 28, 35, and 50°C (Figure 2.7b). While the two lower temperatures were typical temperatures observed in the automated degradation setup described in Section 2.6, the higher temperature was only obtained when directly heating the setup. Within this temperature range, thermal acceleration by approximately 50 % to 100 % was observed with decreasing thickness when comparing 50°C to 28°C, while no variation between 28°C and 35°C was observed. The sample temperature is expected to be higher than the ambient due to significant light absorption. Additionally, sample temperature is expected to increase with thickness and the observed influence of thermal acceleration is thus sensible. Consequently, acceleration is observed and thus care has to be taken to keep the temperature on a fixed level during all degradation. Furthermore, the thermal activation energy varies with different types of polymers and consequently, relative polymer stabilities may vary with temperature. Thus, for comparative stability

studies, it is emphasized that the degradation temperature be reported to allow for reproduction of experimental results.

2.3.4 Atmospheric conditions

It is well-known that the molecular oxygen and water are the major culprits of PSC degradation, which has been demonstrated in numerous studies[2,26]. Few studies have been carried out on single polymers in different atmospheres. A study demonstrated the degradation of P3HT in three different atmospheres, dry O_2, wet O_2 and wet N_2 (Figure 2.8a)[6]. The results showed that in the case of the dry O_2, the film bleached completely in 200 min, and thus O_2 alone can be responsible for complete degradation. The introduction of 100% relative humidity into the O_2 accelerated the degradation by a factor of 2. Finally, the polymer was very stable in humidified N_2, and a complete degradation was anticipated to happen over the range of 2000 min. In dry N_2 only negligible degradation was expected to happen within 2000 min as has been demonstrated in other studies[25]. Consequently, O_2 was found to contribute much more than humidity to the polymer degradation.

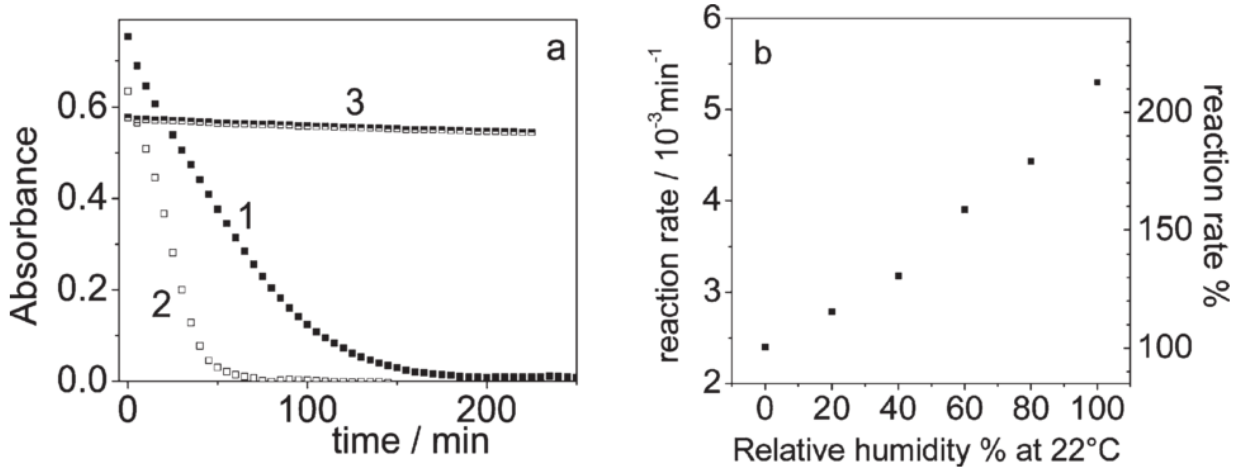

Figure 2.8. a) Degradations of P3HT at 1) dry O_2, 2) humidified O_2 and 3) humidified N_2. b) Reaction rates of P3HT with increasing relative humidity[6]

In the same study, the relative humidity was varied between 0 and 100 % in steps of 20 % to understand the impact on the reaction rate (Figure 2.8b). The rate was found to increase exponentially with a relative increase of 2.2 from 0 to 100 % relative humidity. The practical implication of this observation is

that comparative studies have to be performed under controlled humidity conditions to obtain high precision data. Furthermore, the relative humidity has to be reported in conjunction with stability data to allow for experiment reproduction.

Another parameter that is prone to vary not only within a single comparative polymer stability study, but especially between different laboratories is the concentration of ozone. Light sources that generate UV light below 300 nm also synthesize ozone by absorption of a high energy photon of O_2. Hereby O_2 is split into two O^{2-} which quickly attack other O_2 molecules to generate O_3. Ozone is highly reactive, and is known to aggressively degrade not only polymers, but organic materials in general. Another study by Hintz *et al.* studied the influence of the concentration of O_3 in the atmosphere during degradation of P3HT (Figure 2.9).

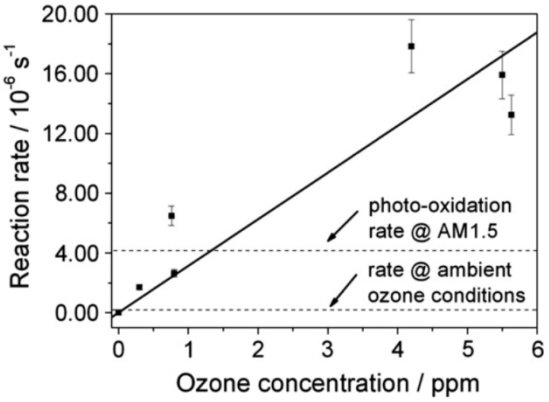

Figure 2.9. Reaction rate of P3HT evaluated as a function of ozone concentration. Dots represent measurements, solid line a linear fit to these while the dashed lines represent ozone levels at ambient and during standard degradation with an AM1.5 spectrum[6]

The reaction rate was found to increase highly when concentrations went from 0.5 to 6 ppm, and thus only small concentrations severely affect the material. When the samples are degraded in an enclosed degradation setup, a high concentration of O_3 is expected to be present in the ambient air and hereby degradations are accelerated. O_3 is not a problem for outdoor applications of commercial panels, and thus including the ozone-stability into the envelope of mechanisms only removes focus from the more valid mechanisms to handle. Consequently, it is recommended that the O_3 generated by the lamp is handled by either active removal by ventilation or mixed with the ambient air in the room to avoid direct exposures to the O_3 peak concentrations.

2.3.5 Challenges in photo chemical stability testing

The field of photochemical stability studies has demonstrated highly interesting results and a good understanding of the stability of different chemical moieties has been established. However, some basic aspects still have to be understood and handled before a high validity can be ascribed to the photochemical stabilities reported. Among these are the most central:

Film thickness is a parameter that has not been studied systematically and therefore the uncertainty introduced by thickness variation was unknown. The majority of the above mentioned parameters are normally approximately constant during a comparative degradation study using the same degradation setup if not actively changed. Contrary to this, the optical density (thickness) is more prone to variation and great attention must be given to keep this parameter constant for all samples. Furthermore, the effect of varying optical density (thickness) on material stability has not been studied systematically and therefore the uncertainty introduced by thickness variation is unknown. Degradation of conjugated polymers in the ambient is highly dominated by the concentration of light and oxygen[2]. In general, due to the higher number of monomers, a thick film is expected to be more stable than a thin film. In the literature, examples of this effect can be found by comparison of different P3HT stabilities, where the time frame for a complete degradation with the same light source was found to increase ten-fold when the film absorbance was increased from 0.2 to 0.6[16,27] Additionally, when performing comparative stability studies between different materials, the effect of the optical density (thickness) on the stability for different materials is unknown. The overall effect is that the photochemical stabilities obtained for thin films are not necessarily consistent with the stabilities obtained for thick films.

Statistical validity of photo chemical stability testing has not been established. Conventionally, few samples are degraded and UVvis absorbance is manually measured during their degradation. By this, an anticipated maximum of 15-20 samples can be degraded in parallel. Since many effects of photochemical stability testing is still to be understood, no systematic validity study has been reported where e.g. the reproducibility of a given polymer in terms of stability has studied.

PCBM stabilization by blending a polymer with $PC_{60}BM$ has only been briefly discussed in the literature. It is important since polymers operate in a BHJ with $PC_{60}BM$ and consequently, the relationship between polymer stability and the associated BHJ stability is central. Rivaton et al. reported the stabilization of P3HT:$PC_{60}BM$ relative to the P3HT of a factor of 8 for 200 nm thick films. No other polymers have been

studied in conjunction with their $PC_{60}BM$ blends, and thus no knowledge exists whether a stable polymer also implies a stable $PC_{60}BM$ blend. Finally, several different C60 derivatives have been used as electron acceptors to increase primarily V_{oc} of PSC by decreasing the LUMO-LUMO band gap between the electron donor and acceptor. While the effect on the cell performance may be clear, the effect on the photochemical stability remains unclear.

As a part of this PhD work, the above described aspects of photochemical stability testing were studied. The intention was to bring photochemical stability testing as a method to a level of maturity where it was highly trust-worthy and where data between different laboratories could be compared. To achieve this, a strong validation study of multiple samples had to be carried out to allow for a discussion of the intrinsic variations of stability observed for identical samples. Furthermore, the effect of thickness had to be described and clear guidelines as to how to handle this effect should be proposed. To accomplish these two goals, it was clear that a high number of samples had to be degraded. The most ambitious approach was considered to invest significant time into the development of a fully automated degradation setup where the manual handling was kept to a minimum. By this, the otherwise labor-intense technique would also become a tool that could be routinely used in the analysis of novel materials. Finally, a high capacity degradation setup would allow for an extensive material screening where effect of e.g. $PC_{60}BM$ stabilization would be thoroughly studied. In the following, a detailed description of the degradation setup developed during this PhD work is given.

2.4 A fully automated photochemical stability assessment setup

The degradation setup consisted of a fully automated sample exchanger mounted on an optical table (Figure 2.10). The exchanger was a circular aluminum disc of outer diameter of 40 cm into which 12 sample slots of 50.5 x 50.5 mm had been milled. The rotation of the sample exchanger was performed by a HIWIN TMS32 motor with a motor driver (Galil MDC4030). The degradation of the samples was monitored by an UV-vis spectroscopic probe mounted on a fork that sandwiched the sample slots. An optical fiber-based CCD spectrometer (Avantes AvaSpec 1024 with a 400 µm quartz fiber) and a halogen/deuterium light source (Avantes AvaLight-DHc) were used to record the absorption spectra in transmission geometry in the range of 300 to 900 nm at set intervals. The spectroscopy light source was fixed in the bottom part of the fork and light was collected from the top part of the fork. The probe into

which the optical fibers were fixed was mounted on a XY stage consisting of two motors (MCG, model 2383). Collimating lenses (Avantes - COL-UV/VIS, www.avantes.com) were used to mount both fibers to the fork as well to ensure a parallel light beam through the sample with a circular area of Ø 3 mm.

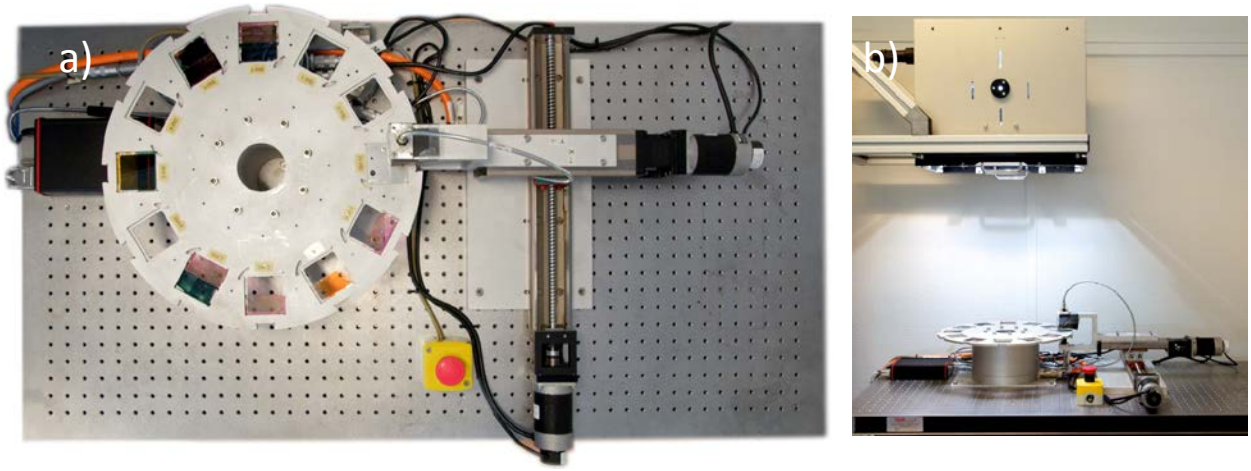

Figure 2.10. a) Top view and b) side view of a fully automated degradation setup consisting of a circular sample exchanger and a solar simulator above the setup[28]

To degrade the samples, a Steuernagel SolarConstant solar simulator with an Osram 1200 W hydrargyrum medium-arc iodide lamp providing an AM1.5G spectrum was used for all degradations (Figure 2.10b). A power meter was used to adjust the solar intensity to 1 kW m^{-2}. The light was not filtered and therefore a UV rich spectrum was obtained with a cut-off at 280 nm (Figure 3.15). The temperature during all degradation experiments was kept at 30°C. All degradations were performed in a lab with humidity and thermal control to ensure a constant degradation environment.

The glass substrates used for the polymer spin coating and degradation were microscope slides obtained in the customized dimensions of 25.0 x 50.0 x 1.0 mm from Menzel Glass (www.menzel.de). During this PhD work, in excess of 5000 glass slides were used for degradations. With this sample size, two samples fitted into each sample slot of the exchanger. One slot was used for white measurements with a clean glass slide taking up the space. This left 11 full slots with the capacity of 22 substrates for degradation samples. Prior to degradation experiments, the sample exchanger was loaded with samples with the polymer facing up the solar simulator. During degradation, the entire area of the samples were degraded, and thus multiple areas of the samples could advantageously be monitored by which more

data was recorded for the same sample. Different numbers of points of degradation on the samples were used, referred to as *degradation points*.

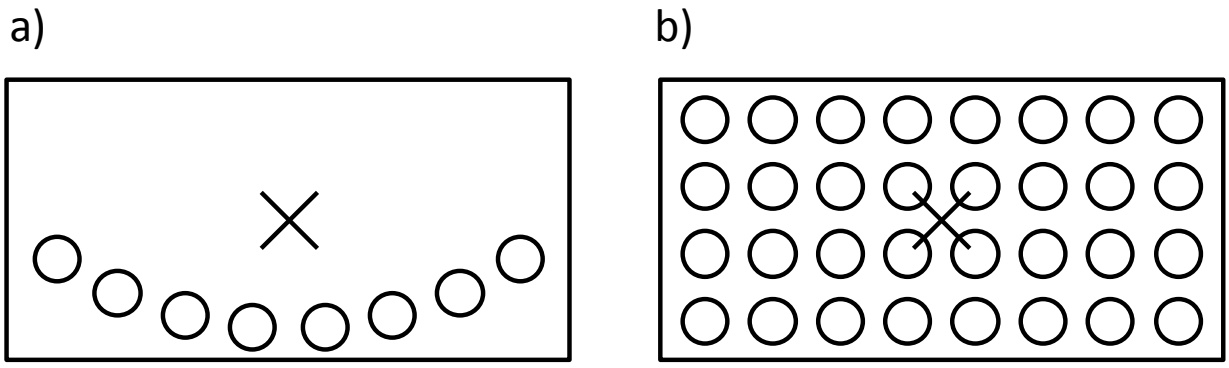

Figure 2.11. Degradation point layouts on the samples. Degradation points are represented by circles while the spin coating center is indicated by a cross. a) circular pattern b) grid pattern

The degradation points were distributed differently throughout the samples depending on the specific application: if a constant thickness were needed for all degradations, the degradation points were distributed evenly on an arc with a radius resembling the radius to the center of rotation in the sample exchanger (Figure 2.11a). The polymers were spin coated with the 25 x 50 mm glass slide being centered on the vacuum chuck of the spin coater. By this, a relatively constant film thickness was obtained for on the arc around the spin coating center. For experiments where an entire thickness range was needed, a grid pattern was used, where 28 points where distributed in a 7 x 4 pattern. In the spin coating center, thicker film was obtained, while further away from the center, the thickness decreased. The combination of the high number of degradation points on a sample and the variations in the thickness within a sample implied that only few samples were needed for a full characterization of degradation rate – thickness relationship for the given material.

The program *HektoSun* was developed in the programming language C-sharp to interact with the degradation setup (Figure 2.12). This software was used to operate all other setups described this in this PhD work, and thus a brief introduction is given. Different instruments were initialized by pressing the check boxes in the *Instrument Controls* group box in the left side of the window. For each instrument, a C-sharp class was made with standard functions, which provided easy communication from the main program. For the degradation setup discussed here, the *Spectrometer* and the *Robot* were initialized,

which referred to the Avantes AvaSpec 1024 spectrometer and the Galil motor driver and the motors. The software was used to perform photochemical studies at 1 sun, photochemical studies by concentrated light by the indoor concentrator (Section 3.4), solar cell tests at concentrated light (Chapter 5), as well as various less routinely performed tasks. The tabs in the top of the window allowed the user to navigate between the different modes of operation. In the case of 1 sun degradation studies, the *UVvis* tab was selected, since this referred to monitoring polymer degradation by an UVvis probe.

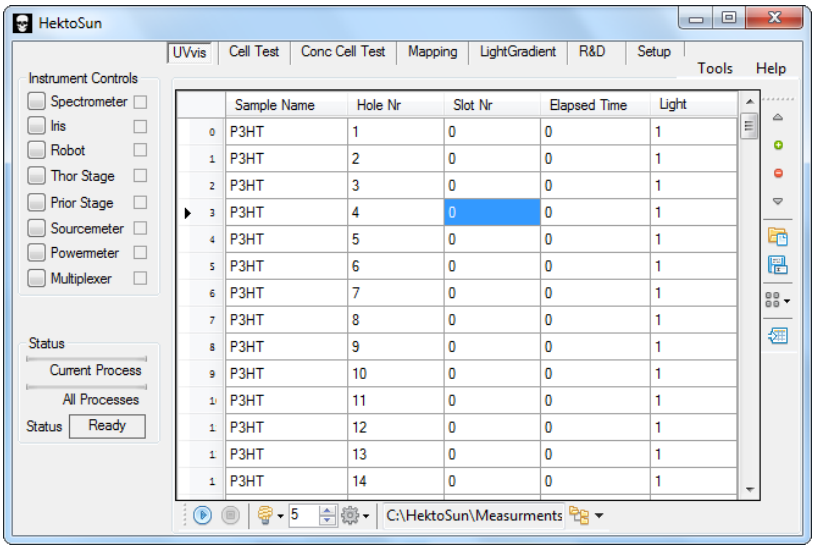

Figure 2.12. The software "HektoSun" used to control the degradation performed at 1 sun

A data grid view was used to handle the information for the high number of degradation points. Each row represented a single degradation point, for which a *sample name*, a *hole number*, a *slot number*, and a *light intensity* were stated. The buttons on the right side allowed for moving entries and down, saving and loading a serialized data grid object, and selecting degradation point layout (Figure 2.11). Finally, a button filled out a default data grid based on the selected degradation point layout. Below the data grid, the export folder for the generated data could be specified. For a given degradation experiment, a main folder is chosen to hold all data. In this folder, a folder for each degradation point is generated with the name *SampleName_HoleNr_SlotNr*. The maximum time between two rounds of measurements of all degradation points was set by the numericUpDown control. Since recording data from a fully loaded sample exchanger with 600 degradation points lasted in excess of 5 min, any maximum time below 5 min would introduce no delay, and thus measurements were continuously

obtained. A spacing of approximately 5 min between each measurement for each degradation points was sensible for most polymers, and consequently, continuous measurements were typically applied. The experiments were started by the *play* button, which changed into a *pause* button during experiments, while the experiment was stopped on the *stop* button.

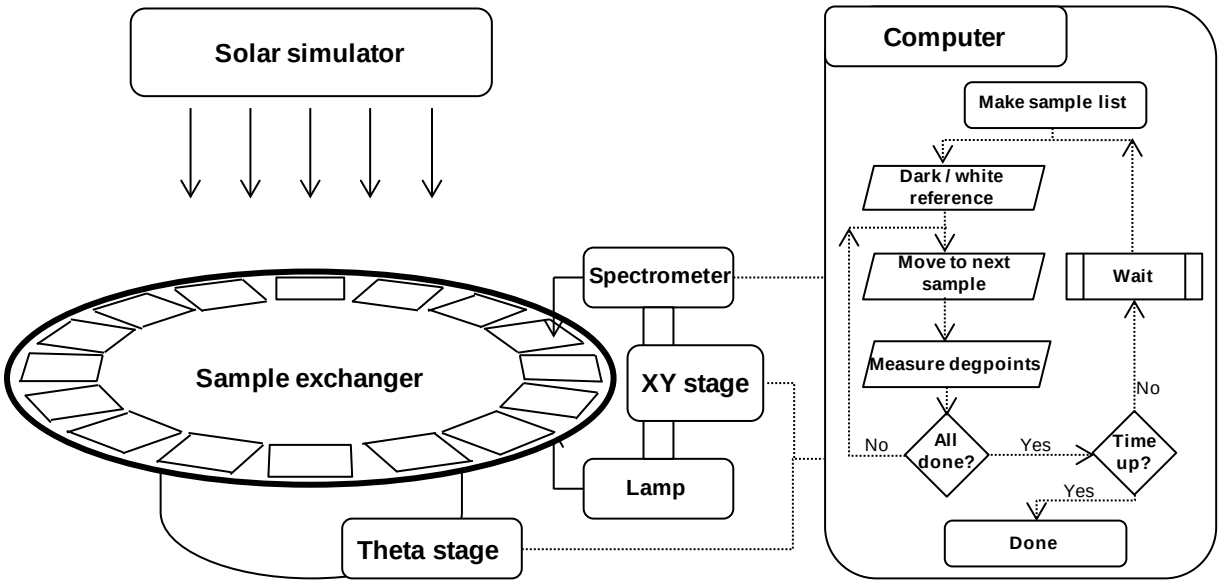

Figure 2.13. Schematic illustration of setup and the associated flow chart governing the measurement routine[28]

The operation of the degradation setup followed the flow chart as described in Figure 2.13. The exchanger was loaded with samples and the information about samples, the degradation point grid, the delay time and the export folder were setup (*Make sample list).* The UV-vis spectrometer was setup by recording both a dark and a white measurement in accordance with the principles described in Section 2.1(*Dark/white reference)*. The dark measurement was made by shutting the light source with a TTL signal from the spectrometer, while the white measurement was made by measuring the light signal through a clean glass substrate. The exchanger and the probe now moved to the first sample to be measured (*Move to next sample)*. The setup started to record absorption spectra from the sample, by which all degradation points were recorded serially and each data file was saved in their respective folders (*Measure deg points)*. When the measurements of the sample were done, the system checked whether more samples were to be measured (*All done?)*. If this was the case, the exchanger moved to the next sample and recorded the degradation points, and this process was repeated until the point where all samples had been recorded. A rarely used parameter was the *maximum time* that the

degradation should run. Some experiments ran during weekends, while only data was needed for a single day. In such a case, a maximum time could advantageously be set to decrease the number of generated data files. If this maximum time parameter was set, after all absorption spectra were recorded, the system either ended the experiment if the time limit was reached, or otherwise continued (*Time up?)*. Finally, a timer monitored the delay time between the previous measurement cycle was started and the present time to ensure that the preset delay time was fulfilled (*Wait*). With a standard setting of 5 min delay time, the delay time had always passed at this point in the flow chart, and thus a new measurement cycle was started with no delay.

2.4.1 Stability evaluation

The quantification of the degradation was done by studying the *number of photons absorbed* N_{Tot} during the degradation over the UV-visible spectrum when exposed to the theoretical AM1.5 as described in Section 2.1. A strictly linear decrease of N_{photon} was observed for all polymers during the entire degradation. The slope of the decrease of N_{photon} over time allowed for the evaluation of the degradation rate. Only few percent of degradation allowed for a precise estimation of the degradation rate due to the high density of recorded absorption spectra.

Another C-sharp based automated software infrastructure was established to handle the high number of data files generated, referred to as *Degradation Monitor* (Figure 2.14). Degradation files were dropped into the left data grid. Each of the entries in this data grid represented a degradation spot. When a degradation entry was selected, each absorption spectrum recorded during the degradation was represented in the right data grid view by its ageing time and the N_{Tot}. The limits for the integration were controlled with the control "*Int Range"* located above the left data grid. All absorption spectra for the selected degradation point were shown in the right plot window. The example in Figure 2.14 shows the typical evolution of P3HT during degradation, where the overall absorption is observed to decrease, while a new peak at 300-350 nm evolves from the generation of smaller oxidation products. For each degradation point, a series of ageing times and associated N_{Tot} described the degradation of the material. All degradation points imported into the left data grid (15 in the example shown) were represented by solid lineplots in the lower left plot window. The selected lineplot was indicated by a dashed lineplot. For each line, a linear regression was performed within reasonable limits to obtain an

expression of the evolution of N_{Tot} over time, which was referred to as the *degradation rate*. The controls for this regression are located above the right data grid under the menu "Reg range." The degradation rates as well as the peak values of the pristine absorption spectrum of each degradation point are shown at the second and third column in the left data grid.

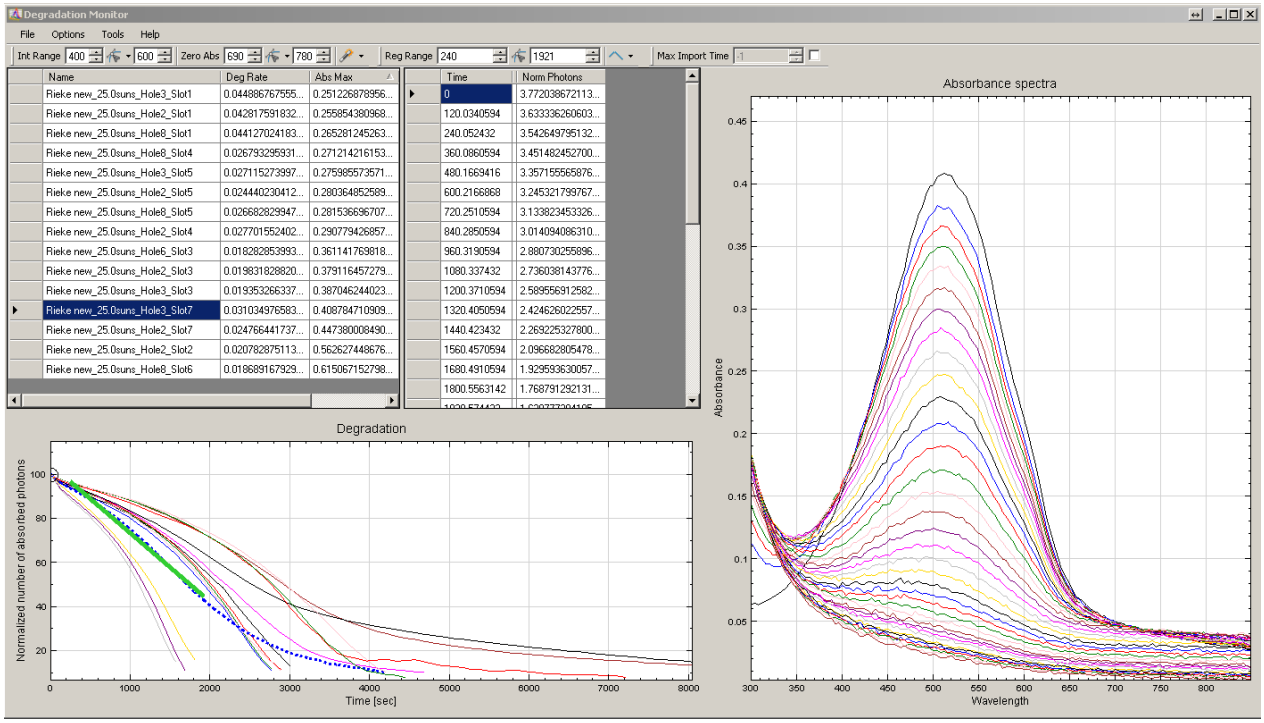

Figure 2.14. The software "Degradation Monitor" developed to allow for an automated evaluation of degradation rates.

The measurement position on each sample was only precise down to the precision of the stages. The high sensitivity of the absorbance scale to such minor variations induced variations in the baseline in the entire spectrum. If these fluctuations in the range of 700 – 800 nm shifted by more than 0.05, all absorption spectra were adjusted to attain an average value of zero in the selected *abs zero* region. The control of the limits of this feature is located above the left data grid. If an erroneous absorption spectrum was recorded, this was clearly observed when processing the data and the data point could thus be dismissed. To allow for studying correlations between different parameters, several different standard correlations are available in the *Options* menu. These were plotted in the left plot window, and the standard N_{Tot} view was obtained when another degradation point was selected. To get a good overview of the experiments, the left plot window thus changed into a correlation plot with degradation

rates as a function of peak absorption. When studying polymer degradation rates as a function of stabilities, it was important to cover the entire absorption range with sufficient data. Additionally, quickly observing tendencies was important to observe tendencies in the data as they evolve. Both aspects were handled by the software, which generally proved an indispensable tool for data evaluation.

When neglecting the significant time invested in setting up the instrument and the time required for its validation, the total operator workload for the all the 1 sun degradation data reported in this PhD is estimated to roughly 6 hours, while a manually operated setup was estimated to a work load of roughly 600 hours, clearly indicating the gain in operator efficiency. Additionally, the precision of the automated setup outperforms any manual handling since measurements were performed with higher frequency, non interrupted illumination, and with a fixed geometry during the entire degradation as opposite to the manual handling where samples are removed from the degradation setup and transported to and from the spectrometer. Finally, in terms of the reliability of the automated setup the timing of the data point acquisition was computer controlled (data is stored with millisecond accuracy), while manual handling involves an attentive operator keeping track of time, introducing a multitude of risks to the data acquisition.

2.4.2 Validation of the degradation setup

Initial studies of regio-regular P3HT films were conducted by spin coating a number of samples at different spin-coating speeds and degrading these. As the degradation rates in units of %/s were evaluated for all samples, each sample (indicated by different colors) with its associated spin-coating speed was found to group with only minor variations in degradation rates (Figure 2.15a). Additionally, a higher spin-coating speed was found to decrease the film stability, and thus relative stability variations exceeding 30 were observed for different spin coating speeds.

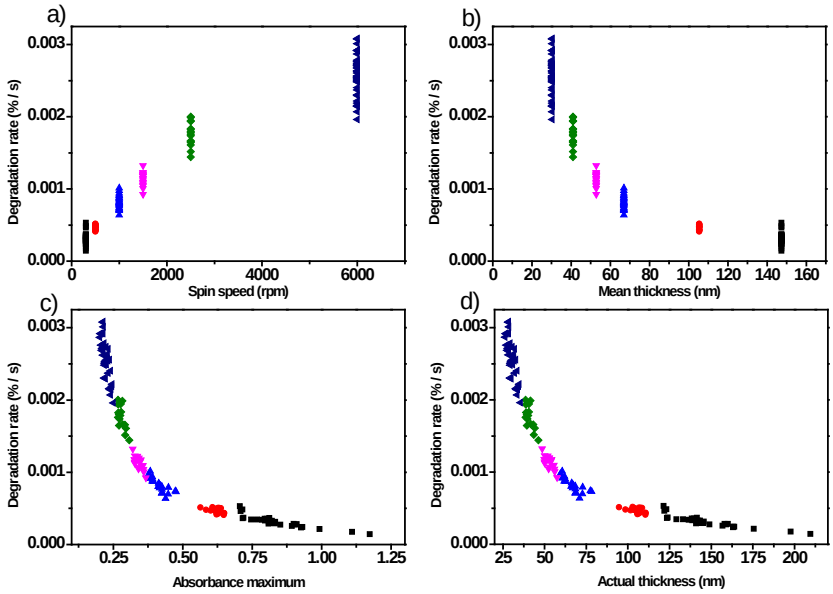

Figure 2.15. Degradation rates resolved in terms of a) spin coating speed, b) average film thickness, c) UV-vis absorbance and d) actual film thickness

AFM correlation curves between the spin coating speed and the average thickness of the samples allowed for converting the spin-coating speed into a thickness (Figure 2.15b). The degradation rates were found to follow an exponential decrease with increasing thickness. This clearly demonstrated the importance of stating the thickness of a polymer when a polymer material is reported in the literature, and explains the large stability variations for the same polymer reported in the literature. The origin of the spread of stabilities within each sample was studied further by looking at their distribution. The degradation rates were found to follow an approximate normal distribution around the average value. Thus, the observed variation could be an intrinsic variation of the polymer stability when all other parameters were fixed. With the AFM calibration curve, a typical thickness had been assigned to the sample by using the peak absorbance. However, the actual peak absorption of each degradation point on the sample was found to vary slightly, even though great care was taken to ensure homogenous film thicknesses on each sample. The peak absorbance of all degradation points and the associated degradation rates were studied, and a clear tendency emerged: the spread of stabilities within each sample did not reflect an intrinsic variation in material stability, but rather local thickness variation (Figure 2.15c). All samples were spread out nicely to make up a clear exponential decrease of stability with peak absorption. Consequently, the absolute spin coating speed did not influence the points, where

only the actual peak absorption mattered. With the clear correlation between degradation rate and peak absorbance being established, the actual thicknesses of each sample became interesting. Instead of only correlating the spin coating speed with the film thickness, now the peak absorption was also coupled to the thickness. Lambert-Beer's law expresses a linear correlation of absorbance with thickness by

$$Abs = \sigma N l = \alpha l,$$

where σ is the number density of absorbers, N is the number of absorbers, α is the linear attenuation coefficient and l is the sample thickness. An empirical validation of this was done by AFM studies of 5 samples covering a wide thickness range to obtain a thickness conversion curve for regio-regular Rieke P3HT. A clear linear thickness evolution with absorbance was found (Figure 2.16) and consequently, the thickness could be expressed by

$$t = 185.25Abs - 9.765,$$

where *Abs* is the peak absorption (Figure 2.16).

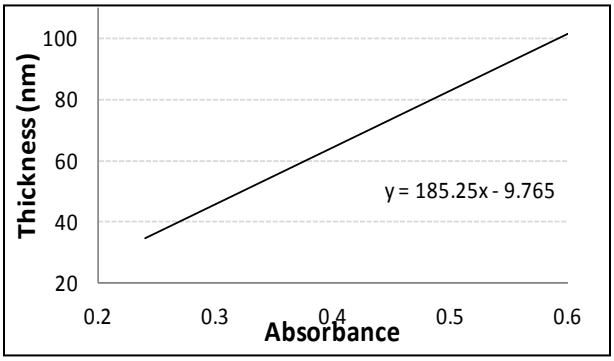

Figure 2.16. AFM thickness calibration curve between peak absorption and film thickness

Using the AFM calibration curve, all peak absorption values were converted into film thicknesses (Figure 2.15d). This alleviated the need for extensive AFM studies of all films, since thickness was extracted directly from the experimental data.

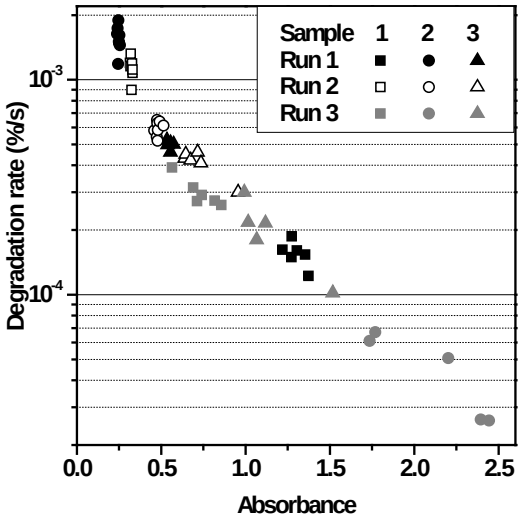

Figure 2.17. Validation test of the degradation setup where three degradation tests were performed with three P3HT samples each

As a final validation of the setup, three different degradation experiments were performed on three different days, where minor changes of humidity, temperature, and ozone levels might be expected. Each experiment comprised three samples of P3HT of different thicknesses with eight degradation points on each sample. Plotting all degradation points together the general exponential evolution of degradation rate with absorption was observed (Figure 2.17). No grouping between the samples or between the degradation experiments was observed. Consequently, the precision of the evaluated degradation rates was considered high, and degradation data recorded at different degradation experiments was clearly comparable. The uncertainty of photochemical degradation as a stability evaluation tool is thus estimated to lie within ±50 % for a single point, as estimated from the vertical width of the band in Figure 2.17. With the entire thickness range covered, this uncertainty is reduced to less than 5 %, emphasizing the need of degradation points to increase data validity.

2.5 Photochemical stability of polymers, acceptors and blends

As a part of this PhD work, a rigorous analysis was carried out on the influence of the optical density (thickness) on the photochemical stability of different materials and material combinations relevant to

PSCs[28]. This work was published in *Journal of Materials Chemistry* (2012), 22, p 7592 – 7601 with the title: *Tromholt et al.: Photochemical stability of conjugated polymers, electron acceptors and blends for polymer solar cells resolved in terms of film thickness and absorbance* and can be found in Appendix 1[28]. The intention was to bring photochemical stability testing to a level of maturity where the technique was generally accepted as valid and reliable. To achieve this goal, the issues described in Section 2.5.5 pertaining to especially reliability and thickness had to be handled.

2.5.1 Establishing guidelines for comparing stabilities between different polymers

With the strong dependence of polymer stability on film thickness, the question arises how to compare stabilities between two different polymers. Typically, the samples are adjusted in thickness to obtain resembling optical densities and compared hereby, referred to as an *absorption basis*. Numerous examples of this is given in the literature[16,17,27]. However, a constant thickness has also been applied as a comparison for different polymers, referred to as a *thickness basis*[10]. Different polymers attain highly different linear attenuation coefficients, and thus to obtain the same optical density for two different samples, their thickness may e.g. deviate by a factor of 3. Vice versa, the same thickness for two different polymers will introduce a deviation in absorbance by a factor of 3. Consequently, much more light is absorbed in one polymer than the other. The study comprised 6 different polymers with highly different linear attenuation coefficients (Figure 1 in Appendix 1). The most extreme were poly[(4,40-bis(2-ethylhexyl)dithieno [3,2-b:20,30-d]silole)-2,6-diyl-alt-(2,1,3-benzothiadiazole)-4,7-diyl] (PSBTBT) and poly-thiophene (PT).

The stabilities of all 6 polymers were found to increase exponentially with film thickness, however, with highly different absolute stabilities. As discussed in Section 2.5, the absolute degradation rates of polymers depend highly on the environmental parameters for the degradation. As there are not standards in terms of photochemical degradation, many different conditions are prone to vary. Consequently, the absolute polymer stabilities will vary between different laboratories and degradation setups. An obvious approach to allow for comparisons of stabilities between different laboratories with different degradation setups is by expressing *relative stabilities* between a given polymer and a well-described reference material, which is normally P3HT. This assumes that the response in terms of stability by a given parameter is the identical for the material under study and the reference material

within the relatively narrow limits of laboratory variations in humidity, light intensity etc. While this is not necessarily true, this assumption is needed to allow for comparisons between different laboratories. As an extreme case, accelerated studies of polymer degradation by high light intensities was made during this PhD[7] (See Chapter 4 for further discussion). In this paper, a relative variation in light-induced acceleration of 2.5 was observed between different polymers. This demonstrates that the polymer stability response not is constant for all polymers. Overall, the need for development of standards within photochemical stability testing is highly needed, with which the absolute degradation rates could be directly compared between laboratories.

The relative stabilities in units of regio-regular P3HT stability were evaluated both applying an absorption basis (Figure 5 in Appendix 1) as well as a thickness basis (Figure 6 in Appendix 1). Thus, for the absorption basis, degradation rates were expressed as a function of peak absorption of each degradation point, while for the thickness basis, degradation rates were expressed relative to the actual thickness of each degradation point. Thicknesses were evaluated by thickness calibration curves as the one shown in Figure 2.16. With a perfect basis of comparison, relative stabilities of the five different polymers should be flat lines independent of the absorption / thickness of the degradation points. However, for the thickness basis, large variations of relative stabilities were found, where especially the highly dense PT was found to vary from a 3 to 80 when film thickness increased from 20 to 100 nm. The absorption basis was found to handle the different polymers better and all polymers generally attains more constant relative stabilities. The relative stability of PT increased from 4 to 9 when absorbance increased from 0.15 to 1.2 demonstrating the much better handling of the highly different polymers. Similar comparisons were made for the 6 respective polymer:$PC_{60}BM$ blends and blends of P3HT and 5 different electron acceptors, as the conclusion was in all cases that the absorption basis provided the best basis of comparison.

2.5.2 Evaluation of stabilities of common polymers

With the effect of stability variation with thickness and a successful basis of comparison being identified, actual relative stabilities of different polymers can now be evaluated. The relative stabilities of the five different polymers could thus be evaluated from the average values of the stability curves (Figure 5 in Appendix 1). This showed that regio-random P3HT was unstable by a factor of 2.5, while MEH-PPV was

unstable by a factor of approximately 60 compared to regio-regular P3HT. PT was found to attain a relative stability of 6, which intuitively can be understood from its chemical structure, where the reactive side chain is avoided relative to P3HT. These results constitute the first reported photochemical stabilities for which the important effect of material thickness and basis of comparison have been handled.

2.5.3 Stability of electron acceptors and P3HT:acceptor blends

The stability of the four different electron acceptors were studied (Figure 2 in Appendix 1) and their degradation rates evaluated (Figure 7 in Appendix 1). The acceptors were found to be highly stable compared to regio-regular P3HT while generally exhibiting similar stabilities. The most stable acceptor was $PC_{70}BM$ followed by $PC_{60}BM$, bis$PC_{60}BM$ and ICBA. Stabilization of P3HT by blending with $PC_{60}BM$ has been reported in the literature by photochemical stability studies[10]. To a first approximation, this can be understood simply by the mere addition of a highly stable material to P3HT by which the overall stability increases. The stability ranking is in correspondence with the HOMO levels of the acceptors, where a high HOMO level implied a low stability[29]. A material with a higher HOMO level requires less energy to be excited and is thus more reactive and less stable. The LUMO level is not important in this context, since this level is much less populated than the HOMO level.

The stability of the blends of P3HT and the five different acceptors showed a significant stability variation with the acceptor type (Figure 9 in Appendix 1). While $PC_{60}BM$ blends of ratios 1:1, 1:2 and 2:1 all displayed relative stabilities (relative to pure P3HT) around 6, the C_{60} blend was 15 times more stable, while bis$PC_{60}BM$ and $PC_{70}BM$ attained values around 2. Surprisingly, the ICBA blend was destabilized by a factor of 2, and was thus less stable than the isolated cases of P3HT and ICBA. The reason for the variation in stabilization of P3HT by blending with acceptors was explained by the LUMO-LUMO gap between two materials. Charge transfer from the excited P3HT to the electron acceptor is an ultra-fast process by which the highly reactive excited electron is transferred from the relatively unstable P3HT to the normally stable acceptor on a time scale quicker than the time scale of the degradation events in the material. However, the strategy behind the design on new highly performing acceptors has been to decrease the LUMO-LUMO gap between the donor and the acceptor by which the V_{oc} of the PSC is increased. The consequence of this is that the charger transfer is mediated by a smaller energy gradient

implying a longer time scale for the transfer. This increased time of excitation of the P3HT is clearly reflected in the stabilities, which is a great disadvantage to these otherwise highly performing acceptors.

2.5.4 Stability of polymer:$PC_{60}BM$ blends

A central question to photochemical stability testing is whether, on a relative scale, a stable polymer implies a stable blend with $PC_{60}BM$, which is the natural context of the polymer in the PSC. No systematic studies have discussed this issue, and only stability of single polymers is conventionally reported. All polymers were blended with PC60BM in 1:1 ratios and compared with an absorption basis (Figure 10 in Appendix 1). The most stable blends were PT:$PC_{60}BM$ and TQ1:$PC_{60}BM$ which attained relative stabilities (in units of P3HT:$PC_{60}BM$) around 3, while the most unstable was MEH-PPV:$PC_{60}BM$ which was less stable by a factor of 30. The overall ranking of the six polymers was in accordance with the ranking of the individual polymers. While the relative stability variations of 1000 were found between the extremes of the single polymers, this quantity was only 200 for the blends. Thus, the strong stability variations observed between single polymers are slightly reduced for the blends. The overall important conclusion is that a stable polymer implies that the associated $PC_{60}BM$ is also stable. Hereby, existing photochemical stabilities reported in the literature are valid as indicators of the expected blend stabilities and the final overall PSC stability.

2.6 Influence of regio-regularity on P3HT stability

The above shown results comparing stabilities of different polymers assume that a given polymer is associated with an unambiguous stability. However, for a given polymer, many different parameters are prone to variations as a function of synthesis route, purity of reactants, polymerization time etc. Additionally, processing the thin films for degradation studies can be done from different solvents, with solvent and thermal annealing at different temperatures. Consequently, intrinsic variations in the stability of a polymer may affect the stability whereby the precision of comparative stability studies is reduced. In the case of P3HT, this knowledge is highly useful since this material is used as the reference material against which the stability of other conjugated polymers is compared. Only few reports discuss the effect of these parameters since a high precision of the evaluation of degradation rate is needed to observe variations within a polymer, whereas differences between different polymers may be on the

order of magnitudes in stability variations, which are easily resolvable. However, with the automated degradation setup presented here, an improved resolution of the stabilities allows for detecting even very small changes in stability. The dominant degradation mechanisms of P3HT have been proposed to be initiated by UV induced abstraction of the alpha hydrogen atom on the side chain of terminal P3HT by which a radical mechanism is introduced leading to decrease of absorption[8]. Hintz et al. reported a higher stability of regio-regular (r-reg) P3HT than regio-random (r-ran) P3HT. They proposed that a higher triplet yield of r-ran P3HT was the origin of this stability variation, while not taking into account the actual degradation mechanism. In another recent study, Dupuis et al. observed a linear increase of stability with regio-regularity for 4 different r-reg P3HT of 93-97% regio-regularity[31]. We studied this effect further by evaluating the photochemical stability of 18 different P3HT batches of different molecular weight, polydispersity and regio-regularity (76 – 97 %) to get a sound statistical foundation. The result of this work has been submitted to Journal of polymer degradation and stability as M. Madsen, T. Tromholt, K. Norrman & F. Krebs*: Influence of intrinsic polymer and processing parameters on photochemical stability of polymer thin films – a comparative P3HT study* and can be found in Appendix 2[30].

Commercial P3HT was obtained from Rieke Metals, Plextronics, BASF, Merck and in-house synthesized batches of both r-reg and r-ran P3HT were studied. ^{1}H NMR was used to quantify the regio-regularity as the ratio between the head-to-tail signal at 2.8 ppm and the head-to-head signal at 2.6 ppm. In accordance with expectation, degradation rates of r-ran P3HT was found to be higher than in the case of the r-reg P3HT by a factor of 2 – 2.5 (Figure 2 in Appendix 2). Furthermore, within the r-reg P3HT, an approximate linear correlation was observed between higher regio-regularity and higher stability. This is in correspondence with earlier results on stability and regio-regularity of P3HT[31]. The theory of the low stability of r-ran P3HT being a result of triplet yield did not seem convincing since our data in that case suggested that triplet yield decreases linearly with increasing regio-regularity. To study the dynamics during the degradation of different polymers of different regio-regularity, the peak position of the UVvis absorption was studied (Figure 3 in Appendix 2). The peak-shift dynamics hold information about the nature of the degradation mechanism where expected vary for different regio-regularity. The highly r-reg P3HT attained an almost constant peak position at approximately 530 nm until a degradation state of 20 % after which a steep fall was observed. For the r-ran P3HT, the peak position started at 490 nm and linearly decreased during the entire degradation. The lower peak position indicates that the

conjugation length is shorter than the r-reg P3HT, even for the r-reg in a highly degraded state. When a degradation event occurs in the r-reg P3HT at the terminal P3HT, the conjugation length is still above the critical value where the band gap changes (<10 monomers). In contradiction to this, r-ran P3HT conjugation length changes along with the degradation. 0^{th} order degradation kinetics has been observed for r-random P3HT by Hintz et al[6]. They suggested that the origin of this is that only terminal monomers on the polymer strands are attacked. In that case, each lost monomer only contributes to absorption while the peak position is expected to be constant until very late in the degradation. However, this model does not account for the increase of stability with regio-regularity. Additionally, it does not explain the linear decrease of peak absorption during degradation of r-ran P3HT. Our data indicated that terminal degradation does not only apply to physical ends of the entire polymer strand, since these exceed the number of monomers below which the band gap changes by order of magnitudes. Alternative high-energy regions in the polymer strand outside the physical terminals are out-of-plane monomer bonds induced by either lack of relaxation of the strand or possibly by head-to-head monomer bonds, where the regio-regularity symmetry is lost. While it proves complicated to control the exact number of out-of-plane monomer bonds, the concentration of head-to-head monomer bonds varies with P3HT of different regularity. If a break of regularity induces two terminals that can are prone to degradation, referred to as *attack points*, the relative number of attack points for a P3HT polymer relative to a P3HT reference can be expressed as

$$N_{ap} = \frac{2(1 - RR_x)}{2\left(1 - RR_{ref}\right)},$$

where *RR* is the regio-regularity. We chose one of the studied r-reg P3HT as a reference and evaluated the relative number of attack points for the remaining polymers. If this number affects the stability, it is expected to correlate with the degradation rate. Using a P3HT of 92 % regio-regularity, the normalized degradation rate was plotted as a function of the relative number of attack points (Dotted line in Figure 4 in Appendix 2). The simple model was found to successfully account for the linear evolution with degradation rate observed for the r-reg P3HT from 92 % to 97% as well as for the r-ran P3HT batches of 76 % regio-regularity. This shows that the instability of r-ran P3HT can be explained by only considering the breaks of symmetry in the conjugation as points of attack for UV photons.

While the model explains the stability correlation with regio-regularity, some P3HT batches were found to deviate slightly from the model. When the thin films were processed by spin coating, this was done at high speed by which the solvent evaporates abruptly and leaves the material in a relatively stressed state. It is anticipated that not only breaks of symmetry in the conjugation can generate high energy bonds that are prone to degradation. The free rotation of the single bond connecting the thiophene rings in P3HT may not align in energetically favorable angles during the film processing, which decrease the bond energy and increases the tendency of degradation. Annealing the samples is expected to increase the mobility of the polymer strands by which a better organization can be obtained. We evaluated the stability of annealed P3HT films and compared to the pristine film stability for both r-reg and r-ran P3HT (Figure 5 in Appendix 2). For both types of P3HT, stabilization by 30 % was observed at 120 °C annealing. When P3HT films are annealed, they are known to crystallize, which may affect the material stability. X-ray diffraction showed that both r-reg and r-ran P3HT on a relatively scale increase their crystallinity to the same extent. To out-rule the effect of crystallization, amorphous PPV was subjected to the same annealing by which stabilization by a factor of 3.5 was observed. Consequently, crystallinity does not play a central role in terms of stability. To study whether annealing at increased temperatures increased the conjugation length, the blue-shift as observed during degradation of r-reg P3HT samples annealed at 80 and 120°C were compared to a pristine sample. The degradation state for which the absorption peak position had shifted to 480 nm was found to be 20.85, 18.85, and 17.5 % for the pristine, 80 and 120°C degraded samples, respectively. Consequently, annealing the samples postpones the peak shift during the degradation, which indicates an increased effective conjugation length. Since the number of symmetry breaks is constant, what is changed during annealing is the number of high energy kink on the polymer backbone, which supports the hypothesis that these kinks are responsible of the stabilization by annealing.

2.7 Conclusion

Photochemical stability testing has previously been used to assess stabilities of different polymers. By this, knowledge of the intrinsic stabilities of the different functional groups has been useful in the design of novel polymers with high stability. However, no systematic study validating the technique had been reported, and thus the validity of the results was doubtful. This PhD work comprises a highly systematic study of the effects that had so far not been studied. To obtain a good statistical foundation for the

conclusions, a fully automated degradation setup was constructed, which minimized the manual work and increased the precision of the evaluated stabilities. The influence of the thickness on the stability was found to be very strong, but this could be handled by using an absorption basis for comparison of different materials. With this knowledge, comparisons of stabilities between different polymers and blends were now fully possible. Quantification of the stabilities of typical polymers such as P3HT, PT and MEH-PPV was now performed with high precision. Furthermore, it was found that a stable polymer also implies a stable $PC_{60}BM$ blend, which alleviates the need for stability studies of $PC_{60}BM$ if the polymer stability is known. Finally, P3HT blended with different electron acceptors demonstrated that a decreasing LUMO-LUMO gap implied less stabilization by the acceptor and even destabilization was observed in the case of ICBA. These results demonstrate that highly interesting conclusions can be drawn from photochemical stability testing, which will prove important for development of future photo-stable polymers for PSC. Finally, the stabilization of P3HT with increasing regio-regularity was explained by the increased number of symmetry breaks in the conjugation. The fully automated setup allowed for precisely determining the effect of thermal annealing on film stability, where stabilization by a factor of 30 % was observed. This effect was ascribed to relaxation of the film during annealing by which the lowest energy conformation was reached by the polymer strand thus decreasing the number of attack points on the polymer thus increasing material stability. In conclusion, photochemical stability testing holds a large potential to provide the information about polymers needed to develop commercial PSC with years of lifetime. As the technique gets adapted by the scientific community, material stabilities are expected to increase significantly in the years to come.

References

1. Fried, J.R. *Polymer Science & Technology*. (Prentice Hall: 2003).

2. Jørgensen, M., Norrman, K. & Krebs, F.C. Stability/degradation of polymer solar cells. *Sol. Energy Mater. Sol. Cells* **92**, 686-714 (2008).

3. Tromholt, T., Gevorgyan, S. a, Jørgensen, M., Krebs, F.C. & Sylvester-Hvid, K.O. Thermocleavable materials for polymer solar cells with high open circuit voltage-a comparative study. *ACS Appl. Mater. Interfaces* **1**, 2768-77 (2009).

4. Brown, P. *et al.* Effect of interchain interactions on the absorption and emission of poly(3-hexylthiophene). *Phys. Rev. B* **67**, 1-16 (2003).

5. Holdcroft, S. A photochemical study of poly(3-hexylthiophene). *Macromolecules* **24**, 4834-4838 (1991).

6. Hintz, H. *et al.* Photodegradation of P3HT–A Systematic Study of Environmental Factors. *Chem. Mater.* 145-154 (2010).doi:10.1021/cm102373k

7. Tromholt, T., Manceau, M., Helgesen, M., Carlé, J.E. & Krebs, F.C. Degradation of semiconducting polymers by concentrated sunlight. *Sol. Energy Mater. Sol. Cells* **95**, 1308-1314 (2010).

8. Manceau, M., Rivaton, A., Gardette, J.-L., Guillerez, S. & Lemaître, N. The mechanism of photo- and thermooxidation of poly(3-hexylthiophene) (P3HT) reconsidered. *Polym. Degrad. Stab.* **94**, 898-907 (2009).

9. Manceau, M., Gaume, J., Rivaton, A. & Gardette, J.-luc Further insights into the photodegradation of poly (3-hexylthiophene) by means of X-ray photoelectron spectroscopy. *Thin Solid Films* **518**, 7113-7118 (2010).

10. Rivaton, A. *et al.* Light-induced degradation of the active layer of polymer-based solar cells. *Polym. Degrad. Stab.* **95**, 278-284 (2010).

11. Kroon, J.M., Wienk, M.M. & Hummelen, J.C. Accurate efficiency determination and stability studies of conjugated polymeryfullerene solar cells. *Thin Solid Films* **404**, 223-228 (2002).

12. Giancaterina, S., Rossi, a, Rivaton, a & Gardette, J.. Photochemical evolution of poly(ether ether ketone). *Polym. Degrad. Stab.* **68**, 133-144 (2000).

13. Rivaton, A. & Gardette, J.. Photodegradation of polyethersulfone and polysulfone. *Polym. Degrad. Stab.* **66**, 385-403 (1999).

14. Rivaton, A. & Gardette, J.-luc Photo-oxidation of aromatic polymers. *Angew. Makromol. Chem.* **262**, 173-188 (1998).

15. Reese, M.O. *et al.* Photoinduced Degradation of Polymer and Polymer-Fullerene Active Layers: Experiment and Theory. *Adv. Funct. Mater.* **20**, 3476-3483 (2010).

16. Manceau, M. *et al.* Photochemical stability of π-conjugated polymers for polymer solar cells: a rule of thumb. *J. Mater. Chem.* **21**, 4132-4141 (2011).

17. Manceau, M., Helgesen, M. & Krebs, F.C. Thermo-cleavable polymers: Materials with enhanced photochemical stability. *Polym. Degrad. Stab.* **95**, 2666-2669 (2010).

18. Krebs, F.C. & Spanggaard, H. Significant Improvement of Polymer Solar Cell Stability. *Chem. Mater.* **17**, 5235-5237 (2005).

19. Nam, C.-yong *et al.* Photo-Cross-Linkable Azide-Functionalized Polythiophene for Thermally Stable Bulk Heterojunction Solar Cells. *Cond. Mat. Phys.* (2012).

20. Kim, H.J. *et al.* Solvent-Resistant Organic Transistors and Thermally Stable Organic Photovoltaics Based on Cross-linkable Conjugated Polymers. *Chem. Mater.* (2011).

21. Schuller, S., Schilinsky, P., Hauch, J. & Brabec, C.J. Determination of the degradation constant of bulk heterojunction solar cells by accelerated lifetime measurements. *Appl. Phys. A-Mater.* **79**, 37-40 (2004).

22. Gevorgyan, S.A. *et al.* An inter-laboratory stability study of roll-to-roll coated flexible polymer solar modules. *Sol. Energy Mater. Sol. Cells* **95**, 1398-1416 (2011).

23. Reese, M.O. *et al.* Consensus stability testing protocols for organic photovoltaic materials and devices. *Sol. Energy Mater. Sol. Cells* **95**, 1253-1267 (2011).

24. Otero, T. & Santos, F. Polythiophene oxidation: Rate coefficients, activation energy and conformational energies. *Electrochimica Acta* **53**, 3166-3174 (2008).

25. Manceau, M. *et al.* Effects of long-term UV–visible light irradiation in the absence of oxygen on P3HT and P3HT:PCBM blend. *Sol. Energy Mater. Sol. Cells* **94**, 1572-1577 (2010).

26. Jørgensen, M. *et al.* Stability of Polymer Solar Cells. *Adv. Mater.* **24**, 580-612 (2011).

27. Carlé, J.E. *et al.* Fused thiophene/quinoxaline low band gap polymers for photovoltaic's with increased photochemical stability. *Sol. Energy Mater. Sol. Cells* **95**, 3222-3226 (2011).

28. Tromholt, T., Madsen, M.V., Carlé, J.E., Helgesen, M. & Krebs, F.C. Photochemical stability of conjugated polymers , electron acceptors and blends for polymer solar cells resolved in terms of film thickness and absorbance. *J. Mater. Chem.* (2012).

29. He, Y., Zhao, G., Peng, B. & Li, Y. High-Yield Synthesis and Electrochemical and Photovoltaic Properties of Indene-C70 Bisadduct. *Adv. Funct. Mater.* **20**, 3383-3389 (2010).

30. Madsen, M.V. *et al.* Influence of processing and intrinsic polymer parameters on photochemical stability of polythiophene thin films. *Submitted to Journal of Polymer Degradation and Stability* (2012).

31. Dupuis, A., Wong-Wah-Chung, P., Rivaton, A. & Gardette, J.-L. Influence of the microstructure on the photooxidative degradation of poly(3-hexylthiophene). *Polym. Degrad. Stab.* **97**, 366-374 (2012).

3 Concentration of Light

Concentration of light has a long history, since light concentrating objects can be relatively easily processed from materials found in nature. The earliest record of light concentrating objects is the Nimrud lens, which was found in an ancient Assyrian city in 1850[1]. Dating back to 700 BC, it consists of a piece of quartz that has been carved to a plano-convex lens. This first attempt to refractive light concentration thus dates almost than 3000 years back. The precision of the carving is too low to allow for using the lens to observe distant features such as planets and starts. An alternative explanation is that the lens was used to focus light onto wood to light a fire, which would have had tremendous applications in the contemporary society. Additionally, highly reflective metallic materials or polished stones have been used to concentrate light by which high temperatures could be achieved. Light concentration by reflective materials can be obtained by polishing metals to a high reflectivity. A medieval myth describes how Archimedes used bronze shields to focus light to set fire to the Roman ships that were besieging his home town in 212 BC[2]; a principle referred to as Archimedes' heat ray. However, modern experimental work has demonstrated that while wood can be set on fire with a large number of concave mirrors over a distance, it proved highly impractical even under the best conditions compared to alternative military technologies[3]. However, the myth demonstrates that the technique of reflective light concentration has been known for centuries.

Refractive light concentration developed as the physical understanding behind optics as well as lens processing techniques were developed. A breakthrough was when three famous Dutch spectacle makers in 1590 developed the refractive telescope by placing two lenses in a sliding tube. This suddenly allowed for observations of the sky with a resolution and brightness superior to the human eye. It was quickly realized that the light collecting object could be replaced by a mirror to reduce the effect of spherical aberration and completely avoid chromatic aberrations. In 1668 Newton developed the first reflective telescope with the intention to prove his theory of light that implied that white light consisted of a spectrum of colors; this was indeed demonstrated by this *Newtonian telescope* by which chromatic

aberrations were indeed removed. This kind of telescope is nowadays a highly popular telescope type both for DIY and professional applications [4].

3.1 Concentrated light and polymer solar cells

Concentrated light within the field of PSC has only recently been studied and therefore the entire field is relatively undiscovered. However, the first demonstrations of this technique have shown a large potential. A wide range of applications have already been studied ranging from using concentrated light as a practical tool to accelerate PSC degradation to using it as a new physical environment for solar cell analysis and characterization.

Conventionally, concentrated light was developed in relation to concentrated photovoltaics (CPV). The concept behind this technology is to focus sunlight from a large area through optical components, *the collector*, down to a small area, the *absorber*. Ideally, this makes the solar cell area correspond to the area, *e.g.*, of the lens or mirror focusing the light, which is typically much cheaper than a solar cell of similar size. Normally, the *geometric concentration ratio* is used to quantify the concentration ratio, which for an ideal collector can be described by

$$C = \frac{A_c}{A_a},$$

where A_c is the collector area and A_a is the absorber area. The concentration ratio depends, *e.g.*, on the type of the collector, the quality of the components and size and position of the absorber in the concentrating system. CPV prototypes have been developed since the 1970s and nowadays many commercial setups are on the market[5]. These setups constitute the simplest type of concentration systems of which a multitude of methods for concentration have been developed. The simplest approach is the flat-plate collector, which is a construction of reflective plates placed around the solar cell making up a V-through. This increases the effective cell area by reflecting the sunlight hitting the plates onto the solar cell[6]. Flat-plate collectors can thereby provide concentration up to 3 suns (1 sun = 0.1 W/cm^2)[7]. Another more sophisticated method is based on using parabolic compound concentrators. These are optical components shaped as tapered tubes made up by a parabola rotated around the center axis. A mirror is applied on the inside and thus the light enters the large entrance, reflects on the inside of the mirror and exits the small opening. This allows for very high light concentration on small

areas, however, with a low spatial homogeneity. The parabolic compound concentrators are placed on top of the solar cell and increase both light intensity as well as the collection angle for the solar cell[5]. An alternative approach is the concept of bifacial solar cells. These are specially designed solar cells, which are able to operate with illumination from both the top and the bottom side. Special reflectors have been designed, which allow light outside the solar cell to be reflected to the back to the cell. Different setups have been demonstrated by which light concentrations > 2 suns have been achieved [3, 4].

Higher solar concentrations can be obtained by tracking the sun with a one-axis solar tracker by which concentrations from 10 to 100 suns can be achieved. Such medium concentration systems are typically based on parabolic troughs or Fresnel lenses and reflectors. For parabolic troughs the entire concentration system and the solar cells is tracking the sun around its linear axis. For the trough-based collectors, the angle between the linear axis and the sun does not affect the system considerable and therefore single-axis tracking suffices. Very high temperatures can be reached on the solar cells, leading to decreased performance and operation stability. Thus, active heat dissipation is normally needed by circulation of heat conducting fluids[10].

Two-axis tracking allows for a constant normal incidence of the sunlight. This enables very high solar concentration exceeding 500 suns. Concentration is obtained with, *e.g.*, Fresnel lenses and mirrors. However, a high precision (tolerance < 0.2°) of the tracking system is needed to ensure a constant power input on the solar cell[5]. Extensive descriptions of two-axis solar tracking systems are given below.

An alternative use of sunlight concentrating system is *concentrated solar power.* This technology uses lenses or mirrors that concentrate light onto a receiver by which heat is generated, which drives a heat engine. While the concentrating optics of this technology is similar to CPV, this technology will not be discussed in this thesis.

As a part of this PhD work, instrumentation to obtain concentrated light was developed. The motivation for this was that extensive work has been performed on IPV in terms of material characterization with concentrated light[11,12]. At the initial stage of this PhD, no studies of either PSC or semiconducting polymers had been reported in relation to concentrated light, and thus this field was completely unstudied. Commercial solar concentrating setups were discarded as a possibility since these are typically customized for the specific application of CPV. For research, a large versatility and flexibility of the setup is needed to allow for a study of many different parameters such as light intensity, light spectrum, absorber type, and absorber temperature. Two light concentrating setups were constructed applying the principle of either refractive or reflective concentration. They can be seen as evolutions of

the classical telescopes, where light from the sun instead of faint remote objects is concentrated. They can be seen as enhanced versions of commercial two-axis tracking concentrators providing increased flexibility. The third setup is based on concentrated solar simulation and thus provides an alternative solution to concentrated light where simulated sunlight from a light bulb is concentrated.

3.2 Refractive light concentration

Refractive light concentration is a simple technique by which sunlight is focused at normal incidence by a lens onto the solar cell. The majority of commercial CPV panels are based on this type of concentration where each cell typically comprises a multi-junction inorganic solar cell positioned in the focal point of a polymer Fresnel lens[5]. Since the light is transmitted through the lens, the light transmissivity of the lens material is of high importance. The UV cut-off varies for the different materials as well as the spectral transmission. BK7 Fresnel lenses are commonly used due to low price while suffering from a UV cut-off at 320 nm. Alternatively, fused silica lenses allow transmission down to 180 nm by which the high-energy part of the solar spectrum is used. While not being paramount to commercial CPV setups, the UV part of the solar spectrum is interesting in terms of solar cell research. When using concentrating optics, ideally a point source is needed as the light source to obtain the highest light concentration in the focal point. In this context the sun constitutes a highly suitable light source since it only extends 9.4 mrad / 0.5° on the sky and thus provides an almost parallel light beam as observed from the earth[13]. The diameter of the focus of a lens from a non-perfect point source cannot be focused to a perfect point source. The effect of this is that the focal point is never a point, but rather a disc. For commercial refractive concentration systems, the solar cell is positioned in the focal point on a cooling element. However, for research applications this is impractical since the changing of the solar cells is cumbersome. Additionally, the environment of the cell is not properly controlled outdoor where temperature, humidity, etc. vary over time. A solution to this is to guide the focused light indoor into a laboratory where the environment is highly controlled[14]. This is normally done using optical fibers, where a single fiber or a fiber bundle is placed in the focal point and guided indoor. The drawback to this solution is that the diameter of the focal point of the concentrator has to exceed the fiber diameter to ensure that a constant light intensity is coupled during tracking. Additionally, due to imperfect packing of the optical fibers in the focal point, further loss of intensity is introduced.

The alignment of the entire setup as well as the solar tracking has to be performed at a high precision to ensure a constant outgoing light intensity during tracking. However, the observed intensity distribution across the solar radius is almost constant[13]. This implies that within the focal point / disc of a lens, the spatial intensity is expected to be very uniform. This alleviates the need for very precise positioning of the absorber within the focal point since the absorber is allowed to move within the focal point, while still maintaining a constant coupled light intensity.

As a part of this PhD, a refractive solar concentrator was constructed. The intension was to construct a simple solar concentrating unit that could be mounted directly on the existing solar tracker at DTU. Hereby, initial studies on concentrated light could be performed, and thus no demands in terms of power output nor light stability were attributed significant importance. However, control of the output power was important since the response of solar cells and polymers to varying light intensities were one of the experimental goals with the setup. An illustration of the concept is shown in Figure 3.1, where a lens focuses light into an optical fiber. The intensity of light impinging on the lens is controlled by an adjustable iris.

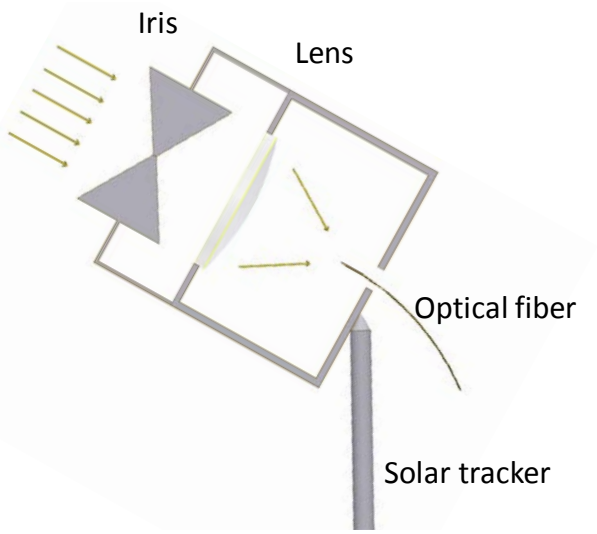

Figure 3.1. Schematic illustration of the concept behind the lens based solar concentrator

The focusing element in the setup was selected to be a BK7 planoconvex lens with a diameter of 32 cm and a focal length of 50 cm. This was an off-the-shelf product and could thus be immediately obtained at a low cost. The intention was to track the lens to get solar irradiation at normal incidence. In the focal point of the lens, an optical fiber should be placed by which light could be coupled into a controlled environment in a laboratory. An appropriate choice of optical fiber had to fulfill several requirements.

The light had to be transmitted 15 m from the concentrator to the lab and thus only high transmissivity fibers could be used. Additionally, the numerical aperture of the fiber had to exceed the one of the lens, which was 0.3. Furthermore, the material should be able to withstand the high temperatures generated in the focal point. A low cost type of optical fiber type is based on polymers. However, they do suffer from significant attenuation as well as low thermal stability, and thus this type of fiber is not suitable for the setup. An alternative solution is liquid light guides, where typically oil is confined in a tube with quartz windows in each end. The diameter is not limited to 1 mm as in the case of quartz based optical fibers. Furthermore, the transmission is highly constant during the UV-vis spectrum. However, as in the case of the polymer optical fibers, they suffer from significant attenuation. A maximum of 80% transmission can be expected per meter, and thus a 15 mm liquid light guide would almost completely attenuate the signal. The only obvious choice for optical fibers is quartz based fibers. These consist of a core of quartz and cladding of a polymer of lower refractive index. By this, light coupled into the fiber will bounce between the sides due to total internal reflectance. Attenuation as low as 0.1%/m is achievable in the UV-vis spectra and thus quartz based optical fibers are highly suited for the application. However, they do not come in diameters exceeding 1 mm as standard fibers and are a costly solution in comparison with the alternative fiber optical solutions. Additionally, quartz fibers are highly fragile and thus great take must be taken during handling and design of the concentrator to ensure that the fibers do not brake during operation.

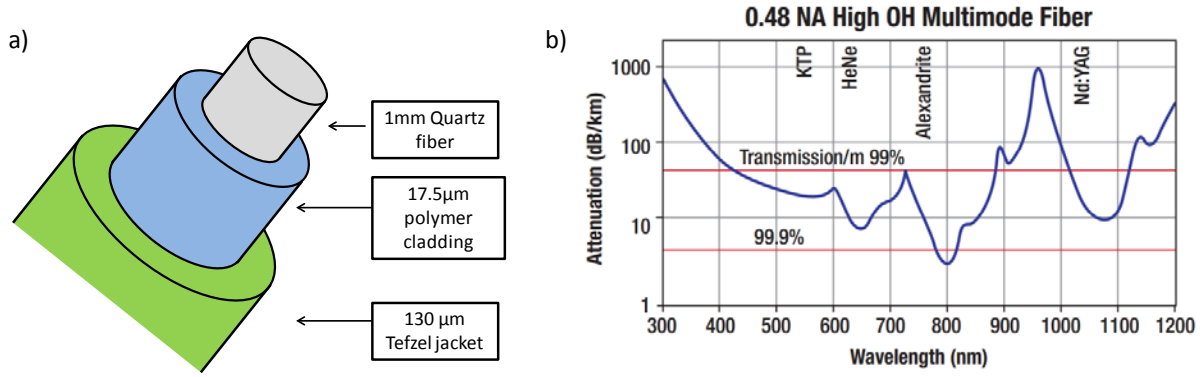

Figure 3.2. a) Schematic of the quartz core optical fiber used for the outdoor concentrator. b) Attenuation diagram for the fiber for the UV-vis and NIR range (www.thorlabs.com)

For a focusing optical element such as a lens, the diameter of the focal point of an object of angular width θ_{object} by focusing can be described by $d_{fp} = f \sin(\theta_{object})$. From the earth, the angular width of the sun is approx. 9.4 mrad[13]. Consequently, the focal point of the lens has a diameter of 4.7 mm.

Several fibers are thus needed to absorb a larger part of the light in the focal point. Thus a fiber bundle is needed to cover a larger fraction of the focal point, however, with a loss due to the packing fraction of the circular fibers.

As it was considered the best choice for the application, a quartz core optical fiber from Thorlabs of 1 mm diameter and low attenuation in the UV-vis range was chosen for the concentrator (Thorlabs BFH48-1000). While keeping costs down by not getting the optical fiber customized, the 1 mm diameter was the largest commercially available. Additionally, it had a numerical aperture of 0.48, which implies that it allowed the coupling of light of a semi-angle as large as 28.7°. A schematic drawing of the fiber is shown in Figure 3.2a. Consequently, this aperture was larger than the one of the lens, which was important to ensure efficient light coupling. The diameter of the focal point of the lens was theoretically 4.7 mm. Since this diameter exceeded the diameter of commercially off-the-shelf optical fibers, a bundle of 7 fibers arranged with one central fiber surrounded by 6 other fibers was used. By this, a 22% of the light intensity was lost due to the packing fraction, as compared to a single hypothetical 3 mm optical fiber. By only absorbing a circular region of 3 mm by the fibers in the 4.7mm circular focal point of the lens, a large tolerance was obtained for the tracking. The focal point may thus theoretically move 1 mm from the center of the focal point before any intensity variations were expected. To increase the buffer region around the fibers, they were displaced slightly in the focal point of the lens to increase tracking stability.

The spectral transmissivity of the optical fibers varied in the UV-vis from 90 %/m (300 nm), to values exceeding 99% in the range of 400 to 800 nm, which is the range relevant to PSC (Figure 3.2b. Consequently, the light transmission through the fiber induced a decreased UV content as compared to the solar spectrum.

The optical fibers were obtained as long fiber on a reel. 7 fibers were cut, each of 15 m of length. Extensive polishing was needed to get smooth surfaces at the fiber ends to ensure efficient light coupling. A polishing machine was used to ease the polishing process in conjunction with commercial optical fiber polishing sheets (Thorlabs LGF03P, LGF1P, LGF3P, and LGF5P). The quality of the polishing of the fibers was frequently controlled with an optical microscopy. When an acceptable level of surface smoothness was obtained, the fibers were mounted in the focal point of the lens. To allow for precise adjustment of the fiber position, the fiber ends were fixed in a hole in a plate, which was in turn mounted on a manual XY stage (Thorlabs T12XZ). In Figure 3.3b the lens is seen to focus light into the optical fiber bundle, for which the position is adjusted by the XY stage. A chassis was constructed of

Rexroth profiles and mounted on the existing solar tracker and a lid was obtained to keep out rain, falling leaves etc. (Figure 3.3a).

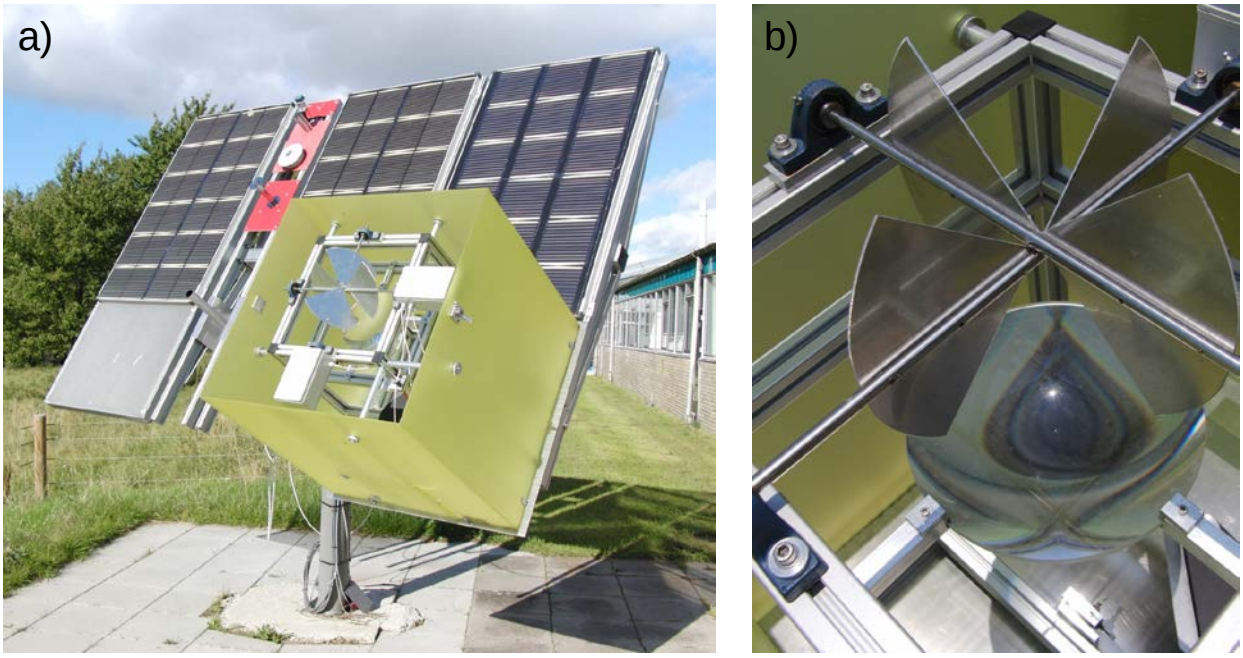

Figure 3.3. a) The lens based solar concentrator mounted on an existing solar tracker. b) Detail photo of the lens focusing light into the optical fibers

An iris system was needed to adjust the light intensity impinging on the lens. A conventional camera-type lens where several shutter blades generate an approximately circular opening of varying diameter is not applicable to lens based solar concentration; Due to the refractive nature of the lens, spherical aberrations are present implying that the focal point is prolonged in space using a camera-style shutter. To overcome this effect, the pizza style iris can be used: it consists of two butterfly-like shutter blades mounted on perpendicular axes of rotation. The optical transmission of the iris is controlled by the angle of the blades. When fully closed, the light can be completely cancelled, while when fully open, the light is hindered by the coverage of the axes of rotation. However, the advantage is that the relative distribution between the light transmitted at the outer and the inner part of the iris is kept constant, and consequently effects of spherical aberrations are handled. For the lens based solar concentrator, two iris plates were constructed in 2 mm aluminum, with a diameter of 34 cm, thus slightly exceeding the diameter of the lens (Figure 3.3b). These were in turn fixed by welding onto two 10 mm aluminum pipes. Two ball bearings were used to fix the axes to the top of the Rexroth chassis. The rotation was

mediated by two geared DC motors ensuring slow rotation. End stops were applied to the rotation angle of completely opened and closed iris positions. The DC motors were driven simultaneously implying that the two iris blades were never out of sync. A controller unit in the lab allowed for remote control of the iris. In Figure 3.3b the pizza iris can be seen above the lens at full opening. Effectively, the iris allowed for complete cancellation of the coupled light. However, due to the gear ratio, the speed of rotation was fairly slow and a quicker shutter mechanism was needed for practical operation of the setup in the laboratory. A drop-shaped 2 mm aluminum plate was fixed to a rotary solenoid (RS components 343-329). The shutter was mounted between the lens and the optical fibers to decrease the area needed for the shutter plate. The rotary solenoid was driven at 24 VDC as opposed to the nominal 12 VDC since a large torque was needed when the rotation was in the vertical plane.

During experimental work in the laboratory, an optical table was used to fix the optical fiber bundle as well as polymer samples and solar cells. Figure 3.4 shows how light exiting the fiber bundle illuminates a polymer sample as well as a solar cell mounted in a sample holder. With this setup a maximum power of 2.0 W can be achieved from the 7 fibers. This implies a local light intensity of approximately 450 suns at each fiber end. However, since the light is highly diverging at the exit of the fiber, no spatially homogeneous light distribution is obtained, and thus such a high efficiency is only found in close proximity to the fiber end. Experimental work up to 200 suns on polymer samples by degradation of circular areas of 3 mm diameter was however routinely made with the setup, for which the sample was kept in a distance from a single fiber of 1-2 mm.

For studies of solar cells, a good control of intensity was needed to evaluate the PSC key cell parameters (*PCE*, V_{oc}, J_{sc} and *FF*) as a function of light concentration. Consequently, a homogeneous spatial light distribution was needed up to 1x1 cm, which was the size of the largest solar cells routinely processed in the laboratory. A means of homogenizing the light is by application of a kaleidoscope at the end of the fiber bundle, as shown in Figure 3.4b. Kaleidoscopes, or light pipes, are used for this purpose with great success. These are pipes of quartz glass of different shapes, i.e. cylinders and tapered pipes. When light impinges on the top of a kaleidoscope at an angle θ_{air} to the air-glass normal, Snell's law describes the angle of refraction θ_{air} relative to the interface normal by

$$\theta_{glass} = \sin^{-1}\left(\frac{n_{air}\sin\theta_{air}}{n_{glass}}\right),$$

where n_{air} and n_{glass} is the refractive index of air and glass respectively. After the first refraction, the light reaches one of the sides of the kaleidoscope (glass-air interface). When θ_{glass} increases from 0°,

θ_{air} also increases. However, at some point, θ_{air} reaches 90° and no light is transmitted across the glass-air interface. At this angle called the critical angle θ_c, and for higher angles, no transmission occurs and all light is reflected, and a phenomenon called *total internal reflection* takes place. Since $n_{air} = 1$ and $n_{glass} \cong 1.50$, at the glass-air boundary θ_c equals 41.8°. This allows light to tunnel loss-less through a kaleidoscope with no losses for each reflection, which would otherwise be the case for mirror based reflection. Finally, the bottom of the kaleidoscope is encountered, and due to the right angle between the side and the bottom of the kaleidoscope, $\theta_{glass} < \theta_c$ and light is transmitted into the air.

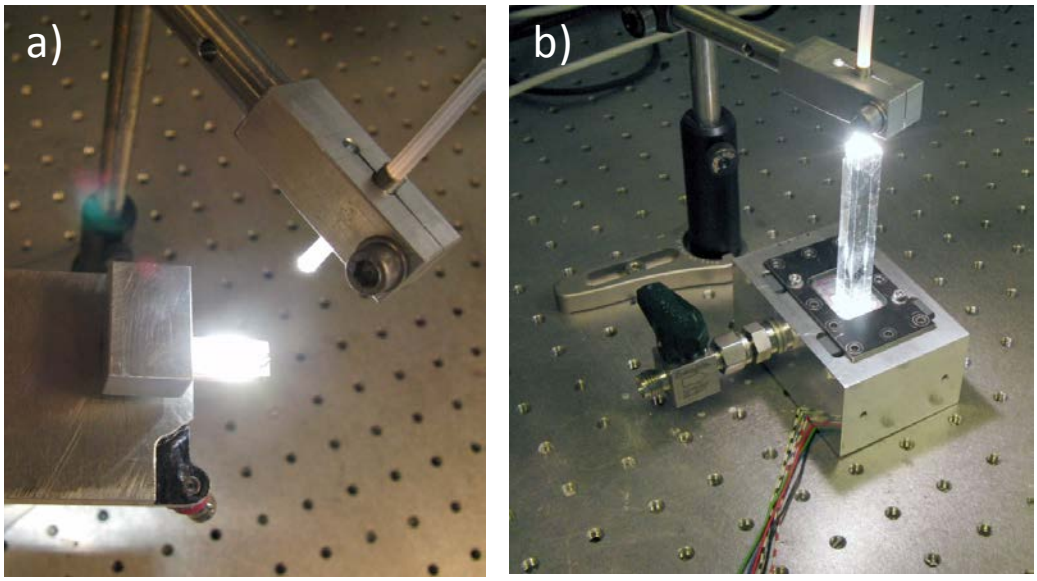

Figure 3.4. a) The light is focused into a bundle of optical fibers. (b) Light from the fiber bundle degrades a sample mounted in a atmospheric chamber through a kaleidoscope

Kaleidoscopes were obtained from Quartz Plus with a bottom area of 1 x 1 cm^2 and with a height of 10 cm shaped as square prisms. A kaleidoscope was positioned between the fiber bundle and the sample (Figure 3.4b). Ray tracing of similar kaleidoscopes of light originating from a single fiber onto a 3 cm high kaleidoscope was made with the software Opticad for an optical fiber of NA = 0.66. This demonstrated a good spatial homogeneity of the light where variations of less than 5 % along the x-axis was found[15] An example of 25 rays in the kaleidoscope is shown in Figure 3.5. The kaleidoscope used in this work was 10 cm while the optical fibers had an optical aperture of 0.48, which overall provided a very high spatial

homogeneity. The overall effect of is kaleidoscope was that the spatial information on the input side is lost on the output side and thus a spatially homogeneous light distribution is obtained.

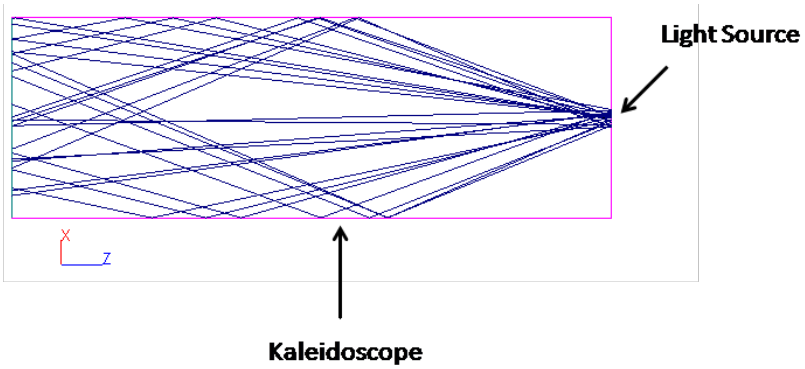

Figure 3.5. Ray tracing of a 3 mm kaleidoscope illuminated by an optical fiber of NA 0.66

The spectrum of the outgoing light resembles AM1.5 and still appears white. However, as a consequence of the refractive nature of the BK7 lens, a UV cut-off at approx. 320 nm is introduced. Furthermore, the spectral variations of the transmissivity of the optical fiber introduce further distortions of the light spectrum. However, overall the light was found to resemble the actual AM1.5G spectrum well.

During practical work, problems were encountered due to inferior precision of solar tracker. The tracker moved in large steps and thus the light coupling was partly lost for each step. Additionally, the concentrator setup was not mounted in its center of gravity and thus both the concentrator as well as the tracker profiles were under significant tension. The effect of this was that the concentrator was not aligned orthogonal to the solar tracker, and consequently the light impinging on the lens was not at normal incidence. The fiber position thus had to be adjusted to allow for coupling at this oblique light incidence. The effect was that as the tracker position changed over time, a different compensation of the focal point was needed. The overall effect was that every 15 minutes, the position of the optical fibers had to be readjusted to ensure optimal light coupling. This was a major problem during practical use of the setup, but for initial studies with concentrated sunlight, the performance of the setup was considered acceptable.

3.3 Reflective light concentration

Sunlight concentration by reflection is a more sophisticated approach by which some of the flaws encountered with the refractive concentration are solved. By using reflections the light does not pass any material, which has several advantages: Conventional glass lenses are normally not produced in large sizes due to practical manufacturing problems, while mirrors can be made in very large dimensions. Additionally, the spectral reflectivity can be very flat for metallic mirrors within the UV-visible spectrum, whereas the transmission from glass will significantly change the light spectrum. Standard BK7 lenses allow transmission of light from 320 nm to 2.5 µm, thus removing a large part of the solar spectrum. Materials such as aluminum allow reflection of light from 200 nm to 5 µm thus preserving a larger part of the solar spectrum. Finally, the effect of aberrations on the system is smaller for the reflective systems. A normal spherical lens suffers from spherical aberration by which light impinging on the periphery of the lens does not focus in the same point as light impinging on the center. While spherical aberrations are complex, to circumvent in the case of lenses, mirrors are easily fabricated in the only mirror type that does not suffer from spherical aberration, the *parabolic mirror*[13]. The effect of spherical aberration on refractive concentrating systems is the loss of light intensity since the focal point is prolonged in space from the different focal points throughout the radius of the lens. Chromatic aberration is another aberration that occurs in lenses, where the different wavelengths do not have the same focal length. This is due to the dispersion of the refractive index, which changes over the UV-visible light spectrum. However, since light does not propagate through the bulk of a mirror, but is reflected from the surface, only the law of reflection applies ($\theta_{in} = \theta_{out}$) to refractive concentration systems and consequently, the refractive index of the material does not affect the outgoing angle.

Feuerman *et al.*[16] suggested a parabolic-mirror-based light concentrating system, which has been widely applied to research of CPV. It is a Cassegrain reflective system where a parabolic mirror reflects sunlight onto a planar mirror from which the light is coupled into an optical fiber, as shown in Figure 3.6a. Normal irradiation is needed in order couple the light, and therefore the system has to be mounted on a solar tracker. High precision of the solar tracking is needed since minor deviations from normal incidence result in the focus moving outside the optical fibers with an associated decrease of coupled light intensity.

As a part of the conducted work during this PhD, a reflective solar concentrator was constructed with inspiration from the above described Cassegrain reflective system. At the Department of Solar Energy

and Environmental Physics, Ben Gurion University of the Negev, a solar concentrator with a parabolic dish of 184 mm is routinely used for CPV. During the first month of this PhD, work was conducted using this setup. Due to the potential of concentrated light as identified in this work, plans were made to construct a similar setup at DTU to allow for research activities in this field. The setup had to fulfill two important criteria: Most importantly, the source of concentrated sunlight had to be stable and thus a high precision tracking system was needed. Commercial trackers for concentrated photovoltaics were available; however, these were all very large and expensive, see e.g. amonix.com. Additionally, these large trackers are to be fixed into the ground, and are thus sensitive to shielding from buildings and trees. An alternative solution was to construct the tracking system in-house, by which the dimensions and the weight could be kept to a minimum. Being an engineering challenge, this system should be able to withstand the temperature variations of Danish weather, and thus issues such as corrosion, condensation, snow and wind had to be addressed. An illustration of the principle of operation and a photo of the final setup are given in Figure 3.6. A discussion of each element of the setup and the rationales behind each design and construction step are given below.

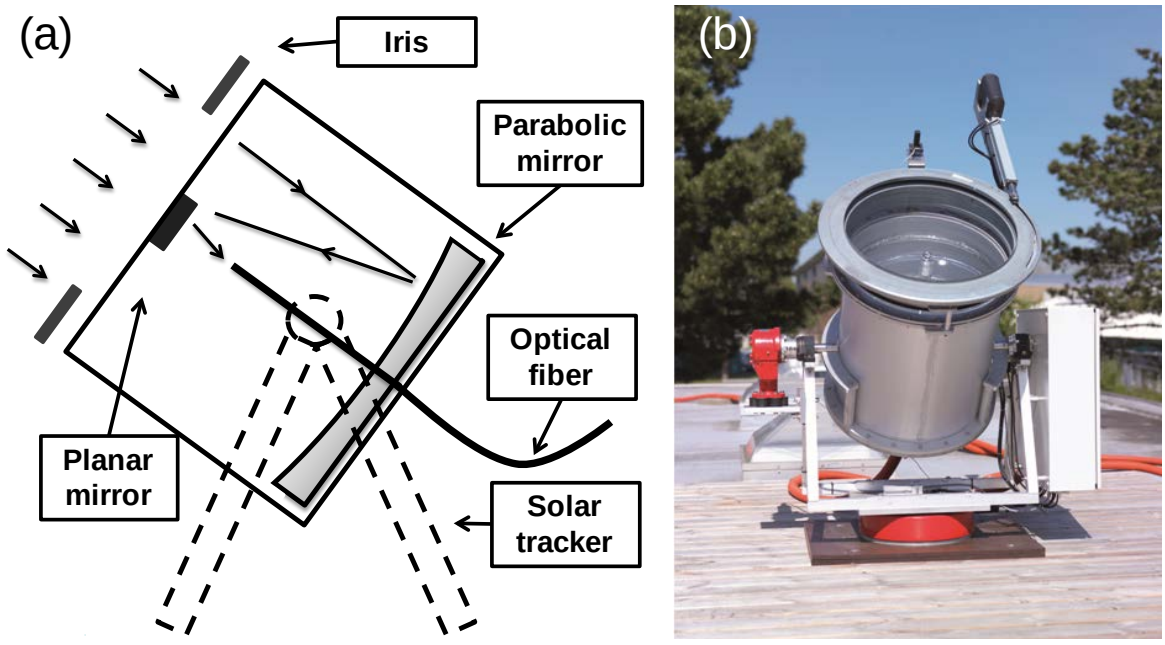

Figure 3.6. (a) The principle behind the reflective light concentration by which a parabolic mirror focuses light onto a small flat mirror focusing light into an optical fiber bundle. (b) A photo of the final roof-mounted setup at DTU under operation.

The core of the entire concentrator is the reflective mirror. The reflector chosen was a 600 mm diameter diamond turned solid aluminum parabola obtained from LT-ultra, Germany (www.lt-ultra.com). This large size was chosen to obtain a high intensity. No protective coating was applied since the size of the parabola exceeded the capacity of the vacuum deposition chamber at the company. However, if the parabola was not directly exposed to water, the company estimated an expected lifetime of 10 years before excessive oxidation would have decreased the reflectivity significantly.

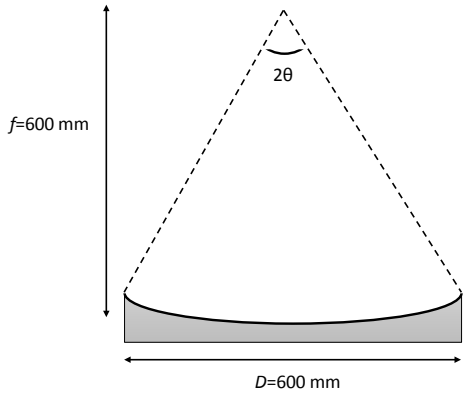

Figure 3.7. Schematic illustration of the parabolic aluminum mirror and its dimensions

The parabola was designed with a focal length of 600 mm (Figure 3.7). For a parabola, the angle of the light in the focal point θ can be related to the dish diameter *D* and the focal length *f* by[13]

$$\tan\left(\frac{\theta}{2}\right) = \frac{D}{4f}.$$

Consequently, the angles of incidence of the most extreme rays reflected by the mirror meet in the focal point with a half-angle of 28.1° and thus a numerical aperture of 0.47. With a 600 mm focal length, the associated diameter of the focal point by is 5.6 mm.

In the following, a description of the different parts and the assembly of the concentrator are given. All part names are given in italic when first mentioned. On the CD attached to the thesis, technical drawings of all parts can be found, where all dimensions needed for reproduction are given. All parts were constructed in aluminum and no protective coating was applied. An explosion plot of the focusing part of the setup is shown in Figure 3.8, which displays the shape and location of each part within the setup. The chassis of the concentrator was a 630 mm high *barrel* made of 2 mm thick aluminum and designed with a diameter that fitted tightly around the mirror. On both the top and the bottom of the barrel, a 20 mm ring had been fixed (*top barrel ring* and *bottom barrel ring*), which was used for assembling other

parts to the barrel. The parabolic mirror was mounted on a 705 mm circular *mirror mounting plate* of 20 mm thickness through 8 M12 threads in the bottom of the parabolic mirror. The mirror plate was in turn fixed to the bottom barrel ring with bolts through 20 holes of 8 mm diameter.

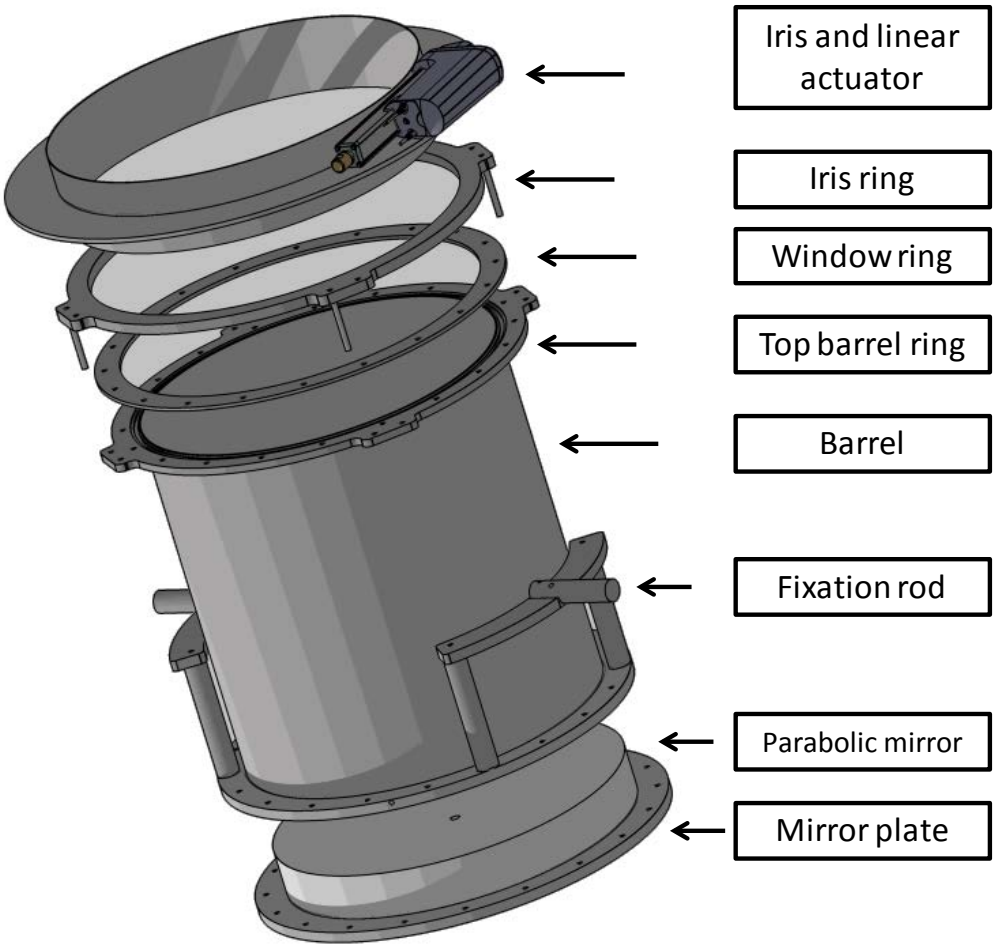

Figure 3.8. CAD explosion plot of the main components of the reflective solar concentrator

The top barrel ring was designed with an o-ring recess. A circular float glass window (Ø 630 mm, thickness 6 mm - not shown) was mounted on top of the top barrel ring and fastened to the top barrel by an another ring (*window ring*) that was pressed against the window to allow for a proper o-ring seal. The focused light from the parabolic mirror was reflected into the fibers by a planar aluminum mirror, which was fixed to the glass plate (Edmund Optics NT47-113, diameter 5.4 mm). The function of the window was both to provide the point of fixation for the planar mirror as well as making the entire barrel air tight, to exclude humidity, snow, rain etc.

To control the intensity of light impinging on the parabolic mirror, an iris was needed. A pizza iris as used for the lens based concentrator was considered. However, since the parabolic mirror does not suffer from spherical aberrations, a simpler “camera-style” iris could be used, where several blades are placed in plane and form an approximate circular aperture. However, due to the large dimensions of the setup, conventional suppliers of optical components did not retail any suitable iris. However, the Danish ventilation company Lindab (www.lindab.dk) retailed irises for ventilation shafts made of aluminum that could thus also be used in outdoor conditions. A DIRU 630 iris was used as the iris for the concentrator (Crude illustration on Figure 3.8). While not being a zero-aperture iris, it could be adjusted from 100% to approx. 20% opening by sliding a lever. To obtain remote control of the iris opening, a linear actuator was needed. For this, a LA36 linear actuator from Linak was obtained (www.linak.dk). It was fitted with moveable hardware end-stops, which ensured that the arm could only move within the range of the iris.

To allow for concentration of light, normal light incidence was needed, and thus the barrel and the focusing optics had to track the sun. On each side of the barrel, a *fixation rod* was mounted, which allowed for the barrel to be fixed to a solar tracker. The inclination of the barrel was to be adjusted by turning the fixation rods. Consequently, due to the mass of the barrel and the focusing optics exceeding 100 kg, the fixation rods had to be placed in the vertical center of gravity to keep the stresses on the fixation rods to a minimum. In the CAD program Autodesk Inventor, all parts displayed in Figure 3.8 were assembled and the mass of each part was estimated. The software allowed for the calculation of the overall center of gravity. Hereby, the height of the pillars supporting the fixation rods was adjusted to place the concentrator in the center of gravity to minimize the stresses on the rods.

A high-precision, custom made tracker was needed for the tracking of the concentrator, since no commercially viable solutions were available. It had to feature 3D tracking of the sun, and thus have two axes of rotation. A typical solution is to use a horizontal slewing drive for the rotation. For the inclination, commercial solar trackers are mainly based on either linear actuators (linak.dk, solfocus.com) or a vertical slewing drive (wattsun.com, degerenergie.de, patriotsolargroup.com). The simplest solution for our setup appeared to be a slewing drive driven inclination, which could be mounted directly on the fixation rod of barrel. The two slewing drives had to allow for a high precision tracking of both axes to allow for a stable coupling of the light into the optical fibers. For high precision tracking, a high gear ratio between the motor and the final axis movement was needed. A general property of slewing drives is that the rotation is intrinsically a gear, where a linear rotating shaft turns a

larger gear, and thus they are by nature precision drives. Additionally, the motors driving the drives had to include gears that would increase the precision.

Rotation	Diameter	Torque	Gear ratio	Precision of position	Motor	Motor gear ratio
Rotation	14"	6.5 kNm	85:1	<0.10°	24VDC	234:1
Inclination	3"	0.4 kNm	62:1	< 0.15°	24VDC	234:1

Table 3.1. Central parameters of the two slewing drives used for the concentrator

Two slewing drives were obtained from the company Huafang, China (h-fang.com.ch). A large 14" drive was selected for the rotation (Table 3.1). With an output torque of 6.5 kNm, it was easily able to rotate the entire concentrator system. For the inclination, a smaller 3" drive was chosen with an output torque of 400 kN. Both drives were driven by 24VDC motors with a gear ratio of 234:1. Combined with the gear ratio in the slewing drives, the tracking precision was estimated to less than 0.10° for the rotation and less than 0.15° for the inclination, which was acceptable for the application. The *rack* constructed to hold the concentrator and the focusing optics was based on two triangles supporting two ball bearings (Figure 3.9a). The rack was mounted on an adapter plate that was fixed to the lower slewing drive. The inclination slewing drive was mounted on a plate that was attached to the side of the rack. The barrel with the focusing optics was mounted in the two ball bearings on the tracker and the vertical slewing drive fixed the end of one of the fixation rods (Figure 3.9b).

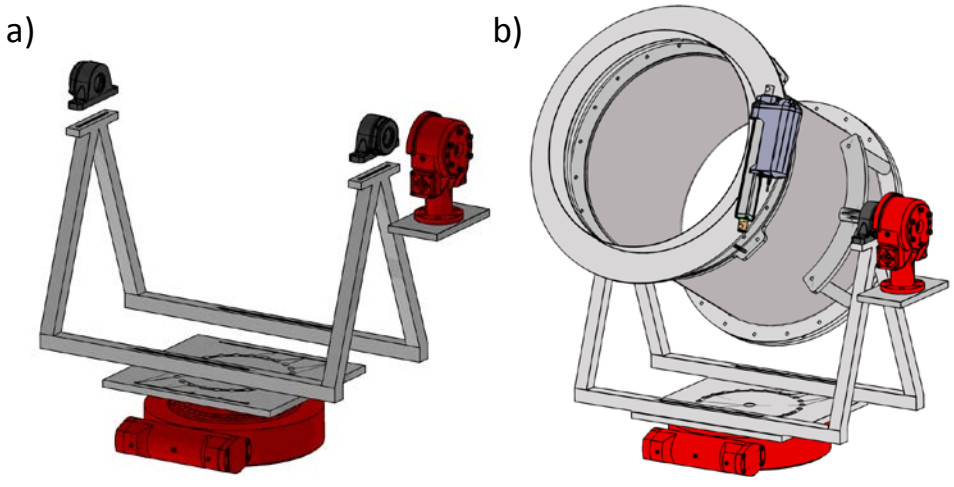

Figure 3.9. a) Explosion plot of the tracker constructed for the solar concentrator. b) CAD assembly of the final concentrator

As in the case of the above described lens based solar concentrator, a bundle of optical fibers were needed to guide light into the lab. The same considerations were made for this application: the fibers had to exhibit a low attenuation in the UV-vis wavelength range. This was specifically important for the reflective concentrator, since a fiber bundle of 35 m was needed since the setup was situated further from the laboratory. Additionally, the numerical aperture of the fiber had to exceed the one of the concentrator of 0.47 to ensure optimal light coupling. The same optical fiber was chosen as used for the lens based concentrator (Thorlabs BFH48-1000). With a numerical aperture of 0.48 and a high transmissivity (Figure 3.2b), this fiber type was an obvious choice.

The focal point diameter of the refractive concentrator was 5.6 mm. The diameter of a fiber bundle consisting of 1 mm fibers with a central fiber surrounded by 6 out fibers would form an approximately circular area of 3 mm diameter was the cladding was stripped. Consequently, only 22 % of the light in the focal point was coupled into the fibers, whereas the remaining light was lost. However, this very large buffer zone for the solar tracking was intended to increase the temporal stability of the output power, which was proven highly important in the case of the lens concentrator. However, the natural consequence of this was that a large fraction of the light was lost. It was contemplated whether an additional 17 fibers should be applied around the outer 6 fibers in the fiber bundle. However, due to the significant cost of these as well as the lower expected stability of these fibers, this idea was not pursued.

The quartz core of the optical fiber was surrounded by a 17.5 µm thick transparent polymer cladding of unknown composition. Finally, a 130 mm thick Tefzel jacket provides chemical and mechanical stability of the fiber (Figure 3.2a). However, the thermal stability of the jacket is low, and is not suitable at temperatures exceeding 150 °C. For this reason, the fibers had to be stripped in both ends, since otherwise the jacket thermally degraded and darkened due to the minor light absorption and the fiber ends. The thermal degradation induced darkening of the jacket thus increasing the material absorption. The overall effect was a complete blackening of the ends and generation of smoke, which severely hindered the coupling of the light. A fiber stripping tool (Thorlabs M44S63) was used to strip approx. 10 cm all fiber ends. However, the polymer cladding was not effectively stripped by this process, which resulted in an opaque appearance of the fibers. The stripped fiber ends were submerged into acetone and gently rubbed with a paper tissue. After repeating this cleaning step several times, the remaining polymer cladding was finally removed.

To hold the bundle of optical fibers together, an aluminum cylinder was constructed in which the fiber ends flushed with the surface of the aluminum cylinder. However, due to the strong generation of heat in the focal point, the aluminum melted and thus an alternative solution was needed. A successful approach was by applying a Teflon ring with a tight fit 10 cm from the focal point on the part where the fiber was no stripped. By this, the fibers only diverged slightly the 10 cm from the ring, and all thermal issues were alleviated.

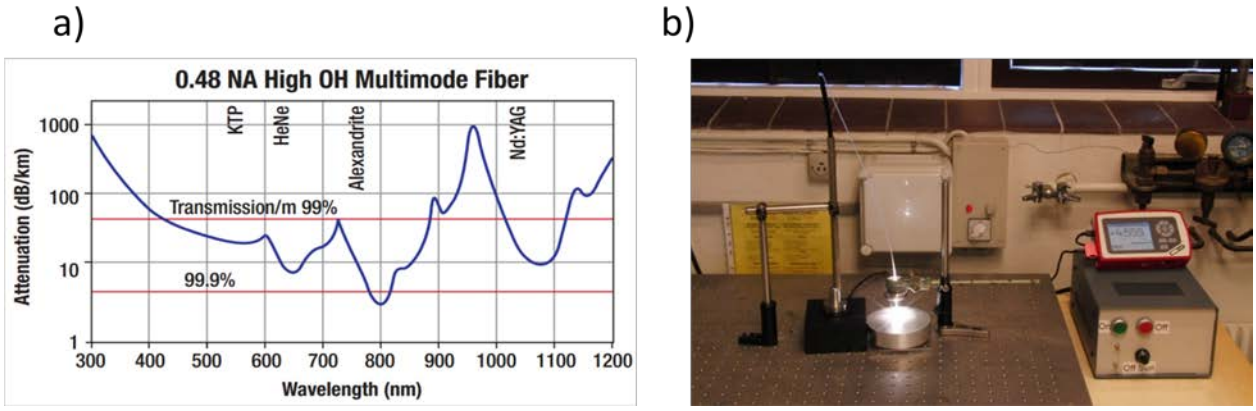

Figure 3.10. a) Irradiance spectrum of the concentrated light obtained from the parabola based solar concentrator compared to AM1.5g. b) Photo of the lab station for the operation of the outdoor concentrator

To perform the actual solar tracking of the concentrator, two alternatives were considered: GPS based tracking and light detector based tracking. GPS based tracking relies on the fact that given the GPS coordinates of the tracking unit, the actual position of the sun on the sky can be precisely determined by computer calculations. By this a very high precision can be achieved. A quotation from a GPS based tracker system was obtained from the company Precision Solar Technologies (www.tapthesun.com). However, due to the complexity of this setup, the price was 3400 USD and a significant delivery time was anticipated. Alternatively, a detector based system is a simple and popular solution to solar tracking. Such a system relies on 4 photodiodes mounted on a plate. A square rod is fixed normal to the plane of the plate. The photodiodes are placed on the bottom plate close to the rod, one diode on each face of the square rod. At any given detector position, the current generated in the photodiodes will be different since the rod will shield some diodes, while others are more exposed. The detector will through an internal chip send signals to the motors to move the two axes of rotation until normal incidence is reached. Compared to GPS based tracking, the tracking is cruder since the detector constantly corrects its position, while the GPS system with its knowledge of the solar position allows for

fewer movements or even one single continuous movement following the sun. A detector based tracking system was by far cheaper (250 USD), and thus a kit including detector and controller was obtained from HelioTrack, USA (www.heliotrack.com). The tracker was mounted on top of the iris ring of the barrel and adjusted accordingly until a constant, good light coupling into the fiber bundle was achieved. The detector is seen in Figure 3.6b as a small black rod on top of the iris. Due to the relatively large focal point of the mirror, the relative crude tracking steps did not introduce any variation of the outgoing light intensity, and thus a detector based tracking system was considered appropriate to application.

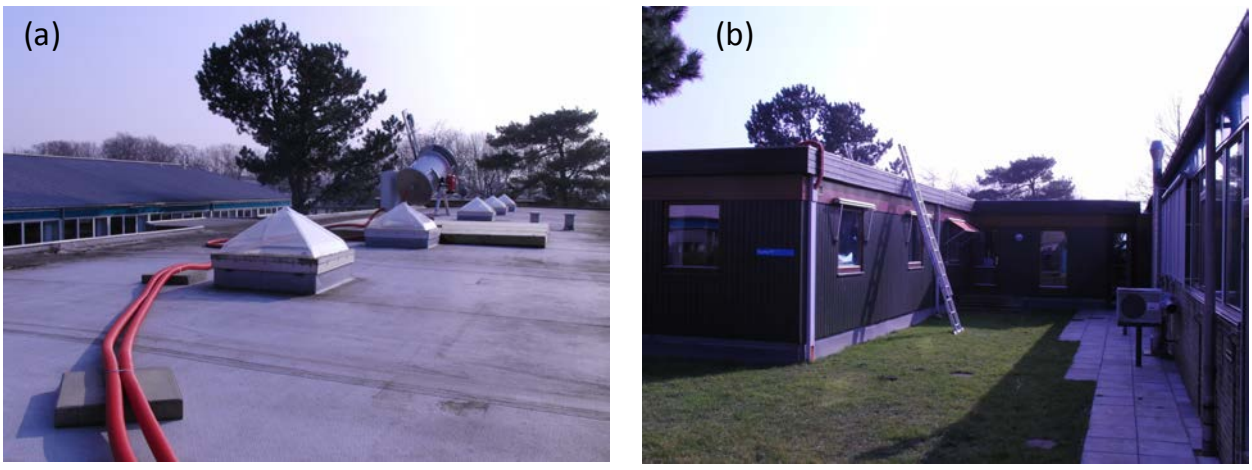

Figure 3.11. a) Photo of the concentrator mounted on a wooden platform on top of a flat-roof office building, where optical fibers and signal cables are guided in the red tubes. b) Photo of the office bulding (left) and the laboratory (right) where the optical fibers and the power and signal cables were guided underground.

The concentrator was mounted on top of an office building with a flat roof (Figure 3.11a). A 3.5 x 3.5 m wooden platform was constructed to distribute the mass of the entire system of around 200 kg to a larger area. The optical fiber bundle and the power and signal cables were guided 35 mm into the lab in two separate tubes. The laboratory is located in a separate building, and consequently between the office and the laboratory building, the cables were dug 70 cm down into the ground to introduce a minimum of visual disturbance to the surroundings as well as to ensure that they were kept in a safe, permanent location (Figure 3.11b).

The fiber bundle was guided through the outer wall into the laboratory and fixed to the wall. The length of the optical fiber bundle in the lab was approx. 3 m. The experimental working station for the setup consisted of a breadboard into which the fiber bundle was fixed by conventional breadboard

components (Figure 3.10b). A controller unit is seen to the right of the bread board. From this the iris opening could be adjusted manually. Additionally, the tracker PCB had a shutter feature by which the tracker drove off the sun for a designated number of seconds. Hereby, the incoming power was practically cancelled, which was important when manually handling of the fibers and the experimental setup was needed due to the intense light coming from the fiber during normal operation. Finally the controller allowed for stopping and starting the solar tracking by the red and the green button, respectively.

The maximum power output with an open iris was 12 W as measured with a thermopile with all the fibers in close contact to the absorber material. Assuming that all fibers emit the same intensity, the power density at each fiber opening (0.785 mm^2) is approx. 2150 suns. This demonstrates the extremely high power density that can be obtained locally and the potential within several scientific fields, where not only high light intensity, but also the associated possible high light-induced temperature for absorbing materials can be highly interesting.

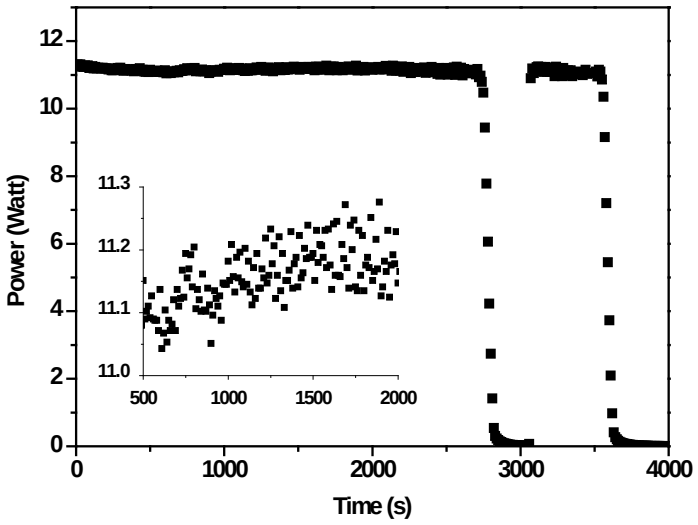

Figure 3.12. Stability of the intensity output of the outdoor concentrator and demonstration of the shutter

The power stability during solar tracking at sunny period was studied by recording the power recorded for every 10 seconds with a thermopile (Figure 3.12). The power is observed to be highly constant around 11 W. To demonstrate the shutter, it was applied twice during this shown power monitoring plot at 2800 and 3600 seconds. Within seconds, the light intensity was effectively cancelled. However, as a

consequence of the time delay of the thermopile due to the nature of the thermopile measurement, a full power decrease is observed over approx. 60 seconds. The inset shows the variations in the power in the range of 500 to 2000 seconds with increased contrast. Fluctuations in the range of 0.1 W and thus approx. 1 % were observed due to the solar tracking. The system was designed with the optical fiber area being smaller than the focal point of the parabola to provide tolerance during the tracking. Within the focal point of the parabola, the light intensity can be regarded as being constant[13]a, while outside, the intensity falls off rapidly. If the focal point of the parabola moved outside the fiber bundle, a significant intensity decrease would be expected. Consequently, the minor intensity fluctuations observed are ascribed to the slightly different efficiency of the light coupling with the angle of incidence of the light impinging on the fibers. Additionally, intrinsic to sunlight concentration, the light intensity varies not only as a function of clouds, air particles etc., but also as a function of the inclination of the sun, and thus the time of the day. The high contrast power plot shows that the average of the intensity band increases slowly from 11.1 to 11.2 W during the 1500 seconds. The data was recorded at 11.00 AM un a sunny day in April 2012, and thus the slow increase is the mere effect of an increased solar intensity impinging on the earth due to a increasing inclination of the sun.

3.4 Concentrated solar simulation

Sunlight can be concentrated by optical systems to obtain very high solar concentrations; however, several problems pertain to this approach. The sun is an inherently limited light source in many parts of the world. Even in the sunniest parts of the world, the sun is only present in the day time, limiting the availability of sunlight to around 50% of the hours of the day. Almost all regions of the world experience cloudy weather during which solar concentration is impossible. Furthermore, a high content of contaminations etc. in the atmosphere can scatter the light and thus only diffuse light impinges on the earth, thus rendering solar concentration impossible. Another issue is the instability of the sun, both spectrally and intensity wise. The solar spectrum changes as a function of the content of molecular species, humidity, dust and the inclination of the sun. Thus, during a day at a specific position, the solar spectrum is observed to vary over time. While minor intensity variations can be compensated for by constantly monitoring the intensity and incorporating this in the experimental conditions, the spectral changes are complicated to handle. Additionally, instability of the light intensity due to the solar tracking precision is inherent to all solar-tracking-based concentration setups. Concentration setups are

constructed in a way that the tolerance of concentration is high enough to allow for the incremental tracking steps performed by the solar tracking system. As described above, this is done in a fiber-based concentration system by making the focal point diameter larger than the fiber diameter allowing for the focal point to move slightly in the fiber plane without losing intensity of the coupled light. Finally, the concentrating optics always change the spectrum of the incoming light due to reflections, refractions, transmissions, etc. Since different concentration setups utilize different geometries, optical components and coupling mechanisms, the concentrated light spectrum is always highly affected by the concentrating system and does not necessarily resemble the spectrum of the sun closely. The general effect of these issues is that direct comparisons between experimental studies conducted with different concentration setups in different regions of the world are inherently performed with different light spectra. Some applications of CPV may not suffer largely from this, *e.g.* highly stable systems based on IPV, whereas for unstable systems such as PSC this may be a major problem.

A solution to these problems was developed at a part of this PhD work. A high-power concentrated solar simulator was developed, which combined high light intensities with the spectral and intensity stability known from conventional solar simulators. By using light bulbs of types commonly used in indoor solar simulators, the same spectrum used for the laboratory degradations could be obtained at high intensities. This allows for direct comparisons between experimental work conducted at 1 sun and at concentrated light. A further advantage is that identical setups in different laboratories produce identical light intensities as well as light spectra, enabling a direct comparison of high light intensity degradation studies between laboratories.

Figure 3.13a shows a schematic drawing of the principle behind the constructed concentrated solar simulator. The system relies on the concentration of light from a 1200-W hydrargyrum medium-arc iodide (HMI) light bulb (Osram 1200/SE) by a rhodium-coated elliptic reflector obtained from Optiforms, USA (www.optiforms.com). Using an elliptical reflector, the light from the light source is reflected by the reflector and focused into another point, by which a very high light intensity can be obtained. By using reflective optics the advantages from the above-described *reflective solar concentration* are utilized. The type of light bulb was chosen since it has been reported to provide a degradation environment that highly resembles outdoor degradations in terms of PSC operational lifetimes[17].

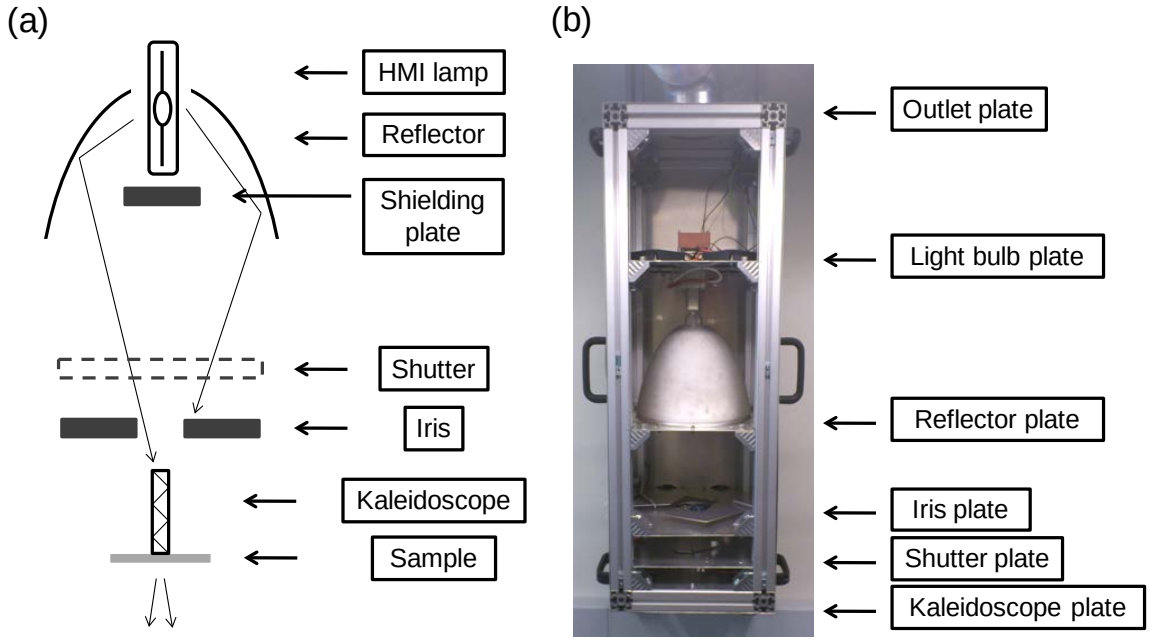

Figure 3.13. (a) Schematic drawing of the principle behind the concentrated solar simulator based on reflection by an elliptical reflector of a high-power HMI lamp. (b) Photograph of the concentrating solar simulator at DTU with the front removed. The names of the different mounting plates have been indicated.

A photograph of the setup is shown in Figure 3.13b. This is a wall-mounted system where the kaleidoscope is placed in the bottom of the chassis (not visible). All parts were before production and assembly designed in AutoCad Inventor 2011. The width of the total system is 34 cm and the height is 100 cm. The frame of the system is based on Rexroth profiles, which allowed for easy construction and assembly of parts. All optical components are mounted on vertical mounting plates, which are fixed onto the main frame. The *light bulb plate* holds a 7 kV igniter needed to induce a spark in the lamp to light the light bulb (Schiederwerk, Germany, model 18-7). Additionally, four fans ventilate the air in the setup. Air is mainly sucked in from the bottom of the setup and removed from the laboratory by the outlet in the *outlet plate,* which also served at a top plate of the chassis. By this, cooling of the light bulb and the embedded electronics is ensured. Furthermore, due to the low UV-cutoff of the lamp (280 nm), ozone is generated. If the ventilation is not on, the ozone can easily be sensed in the laboratory, and thus efficient removal of the ozone is important to the experimenter. On the bottom side of the *light bulb plate*, the socket for the light bulb is mounted (Osram socket G-38) in which the light bulb is placed. The light bulb is inserted in the socket and by tensing a screw on each pin, a tight grip on the pin was

obtained implying that the light bulb was securely fixed even when facing down. The lamp was powered by an external custom made power supply based on an electronic ballast from Schiederwerk (PVG, 12-12 AC SL).

The rhodium coated reflector is mounted on the *reflector plate* and the light bulb was inserted into the reflector opening. A reflector had been chosen with a small opening that allowed for the bulb to be inserted, while not losing too much light intensity. The *reflector plate* was adjustable in height to allow for alignment of the bulb and the reflector to improve the coupling of the light.

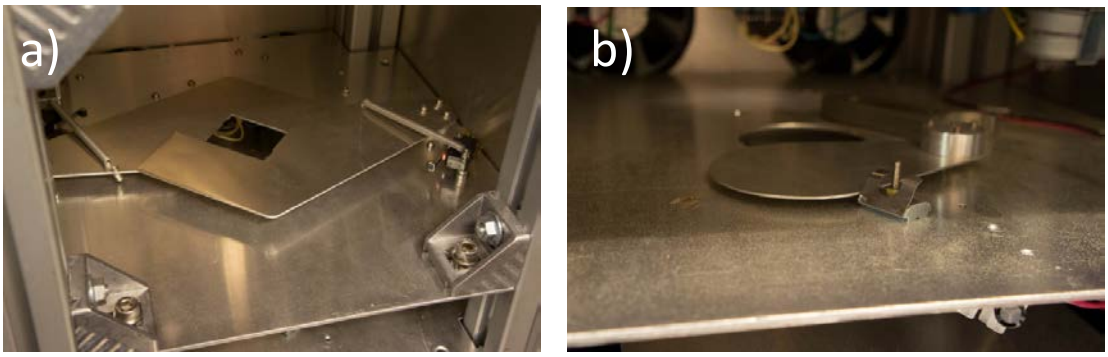

Figure 3.14. a) The iris used for controlling the light intensity of the indoor concentrator. b) The shutter used for flash measurements

A mounting plate was constructed with a 10 cm circular whole and two iris plates by which the light intensity could be controlled (Figure 3.14a). Initially, a zero aperture iris from Thorlabs (Thorlabs D37SZ) was used as the iris. However, it did not withstand the high light power and tougher solution was needed. Consequently, two identical 2 mm aluminum plates were constructed and fixed on each side of the hole. Through the combination of high reflectivity and high thermal conductivity, these were able to sustain the high energy dose from the light source. They were designed to mimic the circular aperture of the above described zero aperture “camera-type” iris, however with only two iris plates. They were made of a 2 mm aluminum plate in which a cut toward the center at right angle had been made. By this an approximate square was obtained for the different iris opening. To avoid the need of backlashing, springs were mounted between the iris plates and the respective endstops. Two stepper motors (RS components 351-4631) were controlled by a Netduino IO-card (Netduino.com) through two stepper motor drivers (RS components 240-7920). For each iris plate, an endstop determined the home position of the iris at which the light was allowed to pass the iris freely. The Netduino IO-card was interfaced and

powered by a USB port from the operator PC. The stepper motors were powered by an external 12 V power supply. All electronics were placed on the lower side of the mounting plate to avoid exposure to the high intensity light.

Below the iris, a shutter was mounted on the *shutter plate.* This was based on a rotary solenoid (RS components 343-329) onto which a 2 mm thick aluminum disc was fixed of a size that allowed for a total cancellation of the light (Figure 3.14a). Hereby, the light could be completely shut in approx. 1 second, and thus faster than in the case of shutting the light with the iris. This was important since a strict control of the exposure time of samples is important to material degradations.

Below the shutter plate, the light from the bulb was focused. However, due to the circular shape of the bulb and the distortion from the optical elements, the intensity distribution within this circle was not constant. Ideally, a completely homogenous spatial intensity distribution was the optimal output from the concentrator, and thus a light homogenizer was needed. For this, a quartz kaleidoscope was used, as in the case of the lens based concentrator. A 10 x 10 x 100 mm kaleidoscope obtained from Quartz Plus was used. The kaleidoscope was mounted in the center of the *kaleidoscope plate* which also served as the bottom plate of the chassis. Most light impinging on the kaleidoscope would bounce a few times during its pass and thus a homogenizing effect is achieved. However, light coming directly from the bulb was found to reduce the homogeneity of the concentrator output since only none or few bounces occurred during the light pass. To filter away the direct radiation, an aluminum shielding plate was mounted in the center of the concentrator below the reflector as shown in Figure 3.13b. By this, highly homogenous spatial distributions were achieved at the kaleidoscope output for all light concentrations.

Within the exit of the kaleidoscope 1 x 1 cm^2 area, a power of 16 W could be achieved, which amounts to an intensity 160 suns. Thus it exceeds the intensity of the lens based concentrator by a factor of 10 and is on the level of the mirror based concentrator.

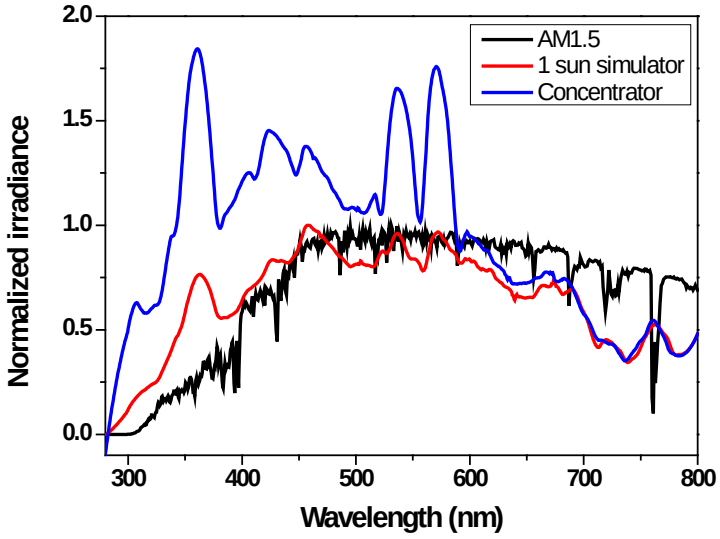

Figure 3.15. Normalized irradiance of the theoretical AM1.5 spectrum, a standard 1 sun simulator and the concentrator operated at 5 suns

At 5 suns, the spectrum is seen to resemble the one of the conventional 1 sun solar simulators routinely used at the laboratory (Figure 3.15). However, a in the range of 300 – 500 nm, the spectrum of the concentrator is relatively higher in irradiance that the solar simulators. The discrepancy is attributed the difference in reflector types where the concentrator used a rhodium reflector while the reflector material of the Steuernagel solar simulator is unknown.

An important aspect of the instrument is the precision of the light intensity when adjusted by the iris. To study this precisely, a thermopile (Thorlabs S314C) with a digital read-out and a PC interface (Thorlabs PM100D) was used to measure the intensities at all iris openings. However, care had to be taken to obtain valid intensity read-outs. A thermopile consists of a junction of two different materials. Due to the Seebeck effect, a voltage difference is generated if a temperature difference is established between the two materials. The voltage difference between two materials *A* and *B* can be expressed by

$$\Delta V = S_{AB}(T)\Delta T,$$

where S_{AB} is the relative Seebeck coefficient for the junction and ΔT is the junction temperature difference[18]. The thermopile used in this work consisted of an absorber which was illuminated, and the reference material, which was in thermal contact with a heat sink on the bottom of the thermopile.

When performing practical measurements, great care had to be taken to avoid excessive heating of the heat sink, by which the intensity read-out was otherwise under-estimated. To handle this issue, pauses in the range of 20-60 seconds were needed between measurements where the thermopile was kept in the dark, to ensure a thermal equilibrium between the two junction materials. To establish a correlation between the iris opening and the outgoing light intensity, several measurements were made at each iris position and the associated intensities were recorded. All iris openings were measured, but in a random pattern where an algorithm chose random iris openings until several measurements had been recorded for each iris opening. The intensity of the outgoing light was found to be constant in the range of 0-26% iris opening and increased until 90% after which the iris plates allowed for unhindered light passage (Figure 3.16a). Within this range, a clear evolution of intensity with iris opening was found. Deviation from the expected tendency was however observed, e.g. at 73 % opening where noise is observed. These observations were found consistently and were attributed to the non-perfect shape of the iris plates and non-perfect precision of the stepper motors at selected angles. Intensities as low at 0.5 suns can be precisely obtained and thus a large interval of intensities were available.

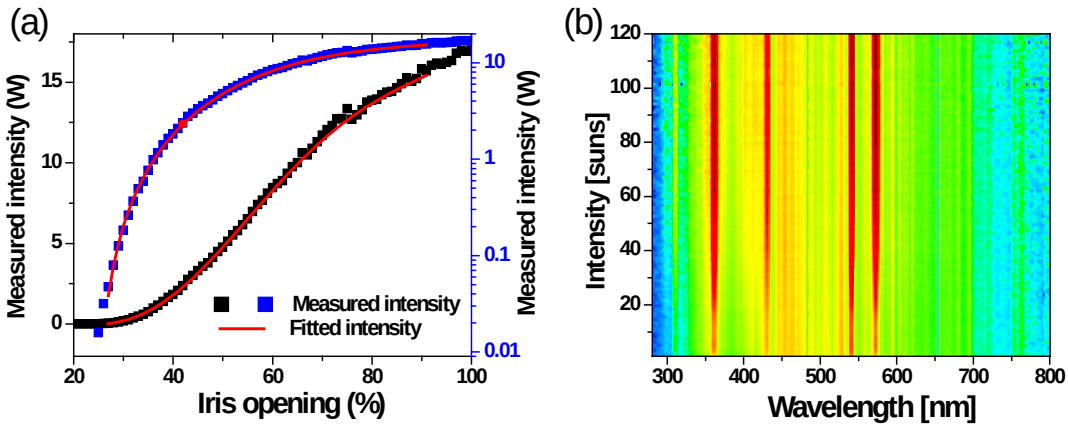

Figure 3.16. a) Relation between iris opening and measured and fitted intensities as used for the general intensity calibration. b) The spectrum of the outgoing light as a function of solar intensity

The intensity correlation was fitted with two polynomials above and below 40 % iris opening to allow for a good fit of the light intensities. This calibration curve was used for the software to adjust the iris position to a given intensity.

Compared to the examples given above of refractive and reflective solar concentrators, the power from the concentrated solar simulator outperformed the above-described refractive concentrator and was comparable to the 600-mm reflective solar concentrator. However, upscaling of the system is possible since HMI lamps are readily available up to 18 kW and thus much higher intensities were reachable.
The stability of light intensity at a fixed iris opening was found to be identical to the stability normally observed for conventional HMI lamp-based solar simulators, namely around 5%. A spatially homogeneous light distribution at the end of the kaleidoscope was obtained from a complete iris opening at 160 suns down to 10 suns. Below this intensity, the iris blocked almost all of the light and only a very small part of the kaleidoscope was illuminated introducing a larger degree of inhomogeneity. The light spectrum was found to be invariant at different iris openings (Figure 3.16b). Overall, the high versatility of this concentrating method showed how many of the flaws of using solar concentration for CPV research were alleviated. A price estimation of the complete setup including lamp power supply was in the range of 2000 US$, which considering the advantages to sunlight concentration is highly competitive relative to solar concentration setups. However, it is important to emphasize the significant time must be invested in the actual construction and calibration of the setup. Concentrating solar simulation thus appears highly interesting due to its large potential combined with low cost.

3.5 Conclusion

Research on concentrated light has a steep learning curve since commercial light concentration setups are built for standard power generation and not with the flexibility and versatility needed for research. In this chapter three different concentration setups have been described. They all differ in collector type and level of sophistication. However, these setups can be used as guidelines or inspiration for future constructions of concentrators. The most versatile setup is the concentrated solar simulator, since it can be used in sun-poor regions and has high inherent intensity stability. Additionally, the low price of all the components, estimated to be below 2000 US$, allows a low-cost alternative to the often more costly solar concentration setups, and thus this setup can advantageously serve as an entrance for different research groups to light concentration. However, significant work has to be directed at the development of the mechanical parts and the electronics and PC control, since no commercial modules are available.

References

1. Frischknecht, F., Gunzer, M. & Shorte, S.L. Retrospective: Birth of the cool - imaging and microbiology from Ibn al-Haytham to Jean Comandon. *Biotech. J.* **4**, 787-90 (2009).

2. Uluç, K., Kujoth, G.C. & Başkaya, M.K. Operating microscopes: past, present, and future. *Neurosurgical focus* **27**, E4 (2009).

3. Mythbusters. at <http://mythbustersresults.com/episode46>

4. Andersen, G. *The Telescope: Its History, Technology, and Future*. (Princeton University Press: 2003).

5. Chemisana, D. Building Integrated Concentrating Photovoltaics: A review. *Renew. Sustain. Energy Rev.* **15**, 603-611 (2011).

6. Uematsu, T., Yazawa, Y., Joge, T. & Kokunai, S. Fabrication and characterization of a flat-plate static-concentrator photovoltaic module. *Sol. Energy Mater. Sol. Cells* **67**, 425-434 (2001).

7. Fraidenraich, N. Design procedure of V-trough cavities for photovoltaic systems. *Prog. Photovoltaics: Res. Appl.* **6**, 43-54 (1998).

8. Weber, K.J., Everett, V., Deenapanray, P.N.K., Franklin, E. & Blakers, a. W. Modeling of static concentrator modules incorporating lambertian or v-groove rear reflectors. *Sol. Energy Mater. Sol. Cells* **90**, 1741-1749 (2006).

9. Zanesco, I. & Lorenzo, E. Optimisation of an asymmetric static concentrator: the PEC-44D. *Prog. Photovoltaics: Res. Appl.* **10**, 361-376 (2002).

10. Luque, A. & Andreev, V. *Concentrator Photovoltaics*. (Springer: Berlin Heidelberg, 2007).

11. Korech, O., Hirsch, B., Katz, E. a. & Gordon, J.M. High-flux characterization of ultrasmall multijunction concentrator solar cells. *Appl. Phys. Lett.* **91**, 064101 (2007).

12. Katz, E.A., Gordon, J.M., Tassew, W. & Feuermann, D. Photovoltaic characterization of concentrator solar cells by localized irradiation. *J. Appl. Phys.* **100**, 044514 (2006).

13. Rabl, A.R.I. *Active Solar Collectors and Their Applications*. *New York* (Oxford University Press: New York Oxford, 1985).

14. Tromholt, T., Manceau, M., Helgesen, M., Carlé, J.E. & Krebs, F.C. Degradation of semiconducting polymers by concentrated sunlight. *Sol. Energy Mater. Sol. Cells* **95**, 1308-1314 (2010).

15. Tromholt, T., Katz, E. a., Hirsch, B., Vossier, A. & Krebs, F.C. Effects of concentrated sunlight on organic photovoltaics. *Appl. Phys. Lett.* **96**, 073501 (2010).

16. Feuermann, D. Solar Fiber-Optic Mini-Dishes: a New Approach To the Efficient Collection of Sunlight. *Solar Energy* **65**, 159-170 (1999).

17. Gevorgyan, S.A. *et al.* An inter-laboratory stability study of roll-to-roll coated flexible polymer solar modules. *Sol. Energy Mater. Sol. Cells* **95**, 1398-1416 (2011).

18. Mikalski, L., Eckersdorf, K., Kucharski, J. & McGee, J. *Temperature measurements*. (Wiley: 2001).

4 Accelerated Polymer Degradation

Research in development of novel polymers for PSC is highly focused on obtaining high PCE, since this quantity is central to the commercial potential of a given polymer. However, the evaluation of the stability of the polymers has not been given the same extensive focus. The reason for this is partly that no standard stability tests have been suggested, and therefore no easily available method can be routinely applied to novel polymers. A solution to this was proposed in Section 2.6, where a method to assess photochemical stabilities of high statistical significance was presented. The intention is that stability testing becomes a routine tool by which novel polymers relevant to PSC presented in scientific publications are not only described by their associated PCE, but also routinely by their photochemical stability. With the increasing stability of conjugated polymers, the time frame of stability assessment of novel polymers is increasing. The timeframe may in ambient conditions for thick samples exceeds weeks or months[1]. However, a future stronger focus on polymer material may even push the time frame to several years. While the PCE assessment is quickly performed, stability assessment is expected to become even more cumbersome introducing a bottleneck to the polymer research.

An obvious solution to this practical problem is accelerated degradation. Under conventional degradation conditions the degradation parameters have been chosen as a tradeoff between mimicking outdoor conditions and still being practically possible with artificial light sources. Thus, degradations are normally performed in the ambient, with associated laboratory levels of ozone, at ambient temperatures with light intensities calibrated to 1 sun. However, it is well-known that the material stability highly depends on each of the above mentioned parameters. Consequently, the timeframe of stability assessments can be highly reduced by increasing the contribution from aggressive environmental factors. This is a conventional approach to general material testing of e.g. ceramics and composites, where additional aggressive conditions such as tensile stress tests etc. allow for an accelerated material stability assessment[2,3].

Degradation mechanisms responsible for the degradation of PSC are generally of different natures: diffusion of water, oxygen into the cell, photochemical degradation, interface diffusion and mixing, and

evolution of active layer morphology are dominant mechanisms, which all differ highly in nature. Consequently, the response of PSC to concentrated light is complex since not only photon flux, but also temperature is increased of the cell. However, if only the photo-active polymer is studied, the range of degradation mechanisms is heavily reduced to only photodegradation[4]. Degradation of single polymers is normally ascribed to three different kinds of mechanisms: photolysis, photooxidation, and thermolysis, which are induced by light, light and oxygen, and heat, respectively. Each of the type of mechanisms comprises several chemical reactions that are specific to the polymer. PPV and P3HT are the most extensively studied polymers, and the dominant of each of the three types of degradation mechanisms have been studied in detail[5–7]. The contribution of the three different kinds of degradation mechanisms highly depends on the degradation parameters subjected to the polymer. The degradation rates of photolysis mechanisms, which are the mechanisms induced by only light, are several orders of magnitude lower than the degradation rate of photo-oxidation in the ambient[7]. Consequently, to study photolysis, degradation studies are normally performed in N_2 chambers or even in closed glass ampoules, where oxygen free conditions can be passively kept for years[5]. The contribution of thermolysis has been shown to be negligible at room temperatures, and thus studies of this mechanism are normally performed above 100°C[6]. If this were done in ambient atmosphere, the effect of photo-oxidation would be highly dominant, and to induce only thermolytic degradation, oxygen free conditions are applied.

4.1 Approaches to accelerated degradation

In terms of photochemical stability of conjugated polymers, no systematic studies have been made on the effect of different aggressive environmental conditions on different polymers. Few studies have presented the response of a single polymer, typically regio-regular P3HT, to selected aggressive conditions[8,9]. However, without knowledge about the response of different polymers, the general implications of different environmental factors remain inconclusive. For PSC, the situation is similar, where the response to accelerated conditions of only P3HT:PC_{60}BM cells have been reported. This field thus lacks general comparative studies of the implication of accelerated degradation on both the single polymers as well as for PSC. To give an overview of the present sporadic knowledge in the field, results on the two most studies conditions used for accelerated degradation are presented: atmosphere and temperature. A third aggressive condition is concentrated light, which has been a strong focus of this PhD work.

4.1.1 Acceleration by Atmosphere

The photochemical stability of polymers varies with atmospheric conditions such e.g. humidity, ozone level, and the composition of the atmosphere as described in Section 2.5. The acceleration of different polymers by increasing an aggressive condition has not been studied in detail for different polymers. However, the response is not expected to be identical for different polymers. Manceau *et al.* performed degradation of P3HT films both in the ambient as well in sealed quartz capsules to study the contribution from O_2 induced degradation (photo-oxidation) and O_2-free degradation (photolysis)[5] at room temperature.

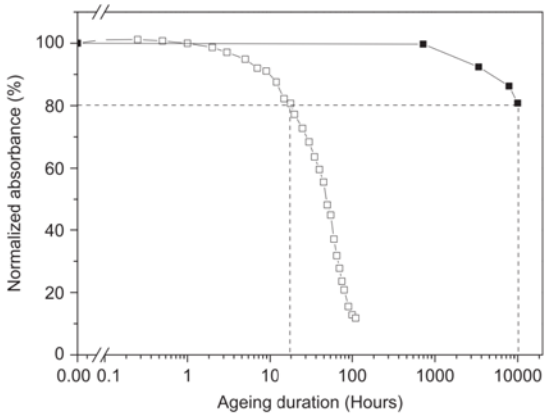

Figure 4.1. Degradation of regio-regular P3HT in the ambient (open squares) and in N_2 (closed squares)[5]

The absorption was observed to decrease until T80 after 20 h in the case of the ambient degradation, while the same degradation state was 10000 h in the case of N_2 degradation (Figure 4.1) and consequently stabilization by a factor of 500 was found. The effect of optical density has not been controlled implying that the P3HT stabilities may originate from different optical densities. The same paper reports that in terms of photolysis, P3HT exhibits 25 times higher stability than MEH-PPV. This value corresponds well with the difference by a factor of 30 that was observed during this PhD work, where the effect of thickness was handled[1]. While the above described observations are made under N_2, similar studies under increasing partial O_2 pressure can be performed by which destabilization is expected.

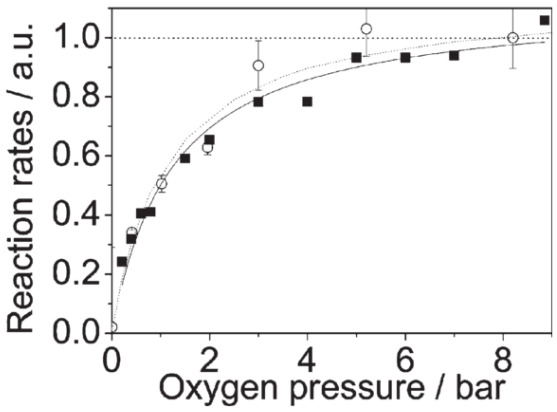

Figure 4.2. Reactive rate of P3HT as a function of oxygen pressure as determined from UV-vis (black squares) and FTIR (white circles)[9]

Hintz et al. studied the relative reaction rate of regio-regular P3HT in oxygen atmosphere from 0.5 to 8 bar (Figure 4.2). The reaction rate is observed to increase logarithmically by a factor of four when the pressure is increased from 0.1 to 8 bar. Consequently, oxygen pressure can be used as an acceleration parameter to reduce the time frame of polymer degradations. However, the oxygen response of other polymers is unknown and the foundation for making direct comparisons is not clear. Additionally, this acceleration parameter does not reflect the actual environment where the polymer is intended to operate in a PSC, where significantly lower levels of oxygen are present.

4.1.2 Acceleration by Temperature

The degradation of PSC is complex since many different types of degradation mechanisms contribute to the overall degradation. Increasing temperature increases these mechanisms to different extents, and thus the acceleration is highly material dependent, which introduces significant variations in acceleration with increasing temperature (See Section 2.5.3 for further information). Since the typical degradation mechanisms in PSC are thermally activated, increasing the temperature under operation accelerates the degradation kinetics[4]. The typically applied model is the Arrhenius model where the degradation rate can be expressed by

$$k_{deg} = A\, e^{\left(\frac{-E_a}{k_B T}\right)},$$

where T is the absolute temperature, k_B is Boltzmann's constant, E_a is a material dependent activation energy, and A is a reaction dependent constant. Under the assumption that only a single thermally

activated process is present, an acceleration factor can be expressed as the ratio between the two individual degradation rates at the temperatures T_1 and T_2 by

$$K = \frac{k_{deg}(T_1)}{k_{deg}(T_2)} = \exp\left[\frac{E_A}{k_B}\left(\frac{1}{T_1} - \frac{1}{T_2}\right)\right].$$

This model has been applied to different types of PSC, of which the first report was on MDMO-PPV[10]. Solar cells were degraded at different temperatures in the range of 20 – 105°C and the degradation rates were evaluated and normalized to the degradation rate at 20°C (Figure 4.3)

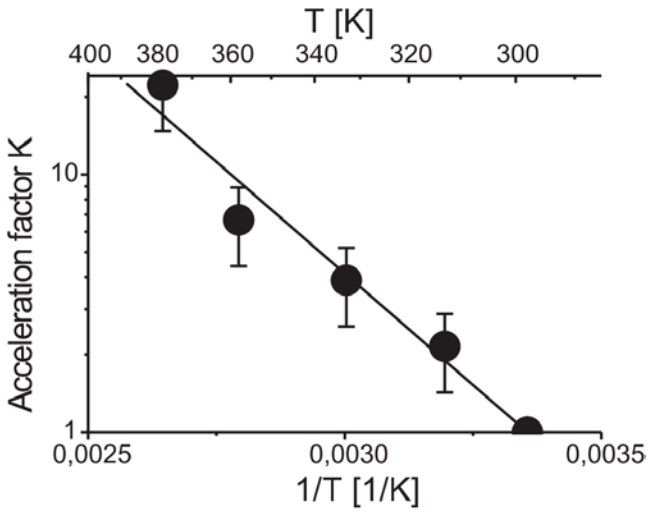

Figure 4.3. Temperature evolution of acceleration factor for the MDMO-PPV:PCBM cells evaluated from the I_{sc} degradation rates[10]

A clear linear tendency was observed with (1/*T*) as expected from the expression for the acceleration factor. Fitting the points linearly provides the activation energy E_a, which was estimated to be 300 – 350 meV. Thermally induced acceleration has consequently been used as a practical tool to increase degradation rates. Debettignies et al. performed degradation studies of P3HT:PC_{60}BM cells at 60°C where a T_{60} for the PCE was reached after 200 h. Compared to 25°C degradation temperature, an acceleration factor of 4.45 was evaluated with activation energy of 350 meV. Consequently, T_{60} at ambient temperatures was estimated to be 1000 h. However, due to the competing nature of a multitude of different degradation mechanisms, the precision of the estimated 25°C lifetime is devious. Indeed, Gevorgyan showed the complexity of the approach by evaluating acceleration factors in N_2 and in O_2 of P3HT:PC_{60}BM cells[11]. Due to the intrinsic variation of PCE performance within a batch of cells,

significant variations in acceleration factor was observed, and no precise energy activation energy could be deduced.

By studying only the stability of polymers exposed to the air by photochemical stability studies, the range of degradation mechanisms responsible for the polymer degradation is highly reduced. Polymer degradation is not associated with complex hysteresis effects and non-linear responses as observed for PSC[4]. The focus of photochemical stability studies is almost entirely on photooxidation processes. Other less dominant mechanisms include thermolysis and photolysis. Manceau et al. showed that complete thermolysis of P3HT took place on a time scale of 10,000 hours, while photooxidation was on the order of 100 hours at ambient temperature[6]. Consequently, in terms of material stabilities, only the photo oxidative contribution needs to be considered under standard degradation conditions. Additionally, the factor of 500 between photolysis and photooxidation shows that practically, photooxidation accounts for all observed degradation at standard conditions. This allows for a more straight-forward acceleration of degradation rates, since the overall degradation can be handled as a single mechanism with an associated activation energy. Photochemical destabilization is, however, highly temperature dependent [9]. Hintz et al. showed that the degradation rate was increased by a factor of 20 of regio-regular P3HT when degradation temperatures were increased from 25°C to 120°C (See Section 2.6.3). This strong temperature acceleration was accurately described by an Arrhenius model, and an activation energy of 276 meV kJ was obtained. Consequently, thermooxidation is a good choice for accelerated polymer degradation. However, the response for different polymers is unknown, and possible deviations between different polymers would complicate direct comparisons. When the temperature is increased, the oxygen diffusion rate increases, and thus the polymer is attacked at a higher rate. As both thermolysis and thermooxidation processes can be considered negligible at below 100 °C, only photooxidation rates are increased, and thus the degradation chemistry is conserved. This makes thermooxidation a good degradation mechanism to accelerate. However, an upper limit of approximately 140 °C applies to this approach above which thermolytic reactions induce polymer decomposition.

4.1.3 Acceleration by Light

Light had before this PhD work not been employed as an acceleration parameter to PSC on a larger scale due to the practical problems concerning obtaining high intensities from artificial light sources as well as

from the sun. However, this approach is promising since not only the light intensity, but also the temperature is increased, thus both increasing the rate of photolysis and photooxidation. Stability studies of polymers deposited on glass are normally performed in the ambient where a high O_2 concentration availability prevails. However, this introduces an increased O_2 induced degradation relative to expected conditions for the polymer in a solar cell for which the active layer is shielded by organic layers and an electrode. However, using concentrated light, the relative contribution of photooxidation decreases with light intensity since the O_2 consumption is highly increased[6]. Conventionally, obtaining high intensity light sources may not be straight forward, and thus most studies of accelerated degradation apply standard solar simulators where the samples are placed closer to the light source to increase light intensity. A greater part of the focus in this PhD work has been on the development of dedicated concentrated light setups, where light intensities exceeding 2000 suns were obtained as described in details in Chapter 3.

With a constant temperature and no limitation of oxygen, it is expected that doubling the photon flux implies a two-fold increase of the degradation rate. Consequently, with the possibility of increasing light intensities to thousands of suns, very high acceleration factors may be obtained. Recently, photochemical stability of P3HT was evaluated from 0.1 to 1.2 suns (Figure 4.4)[9]. This showed a clear linear evolution of degradation rate with intensity where degradation rates increased by a factor of 150.

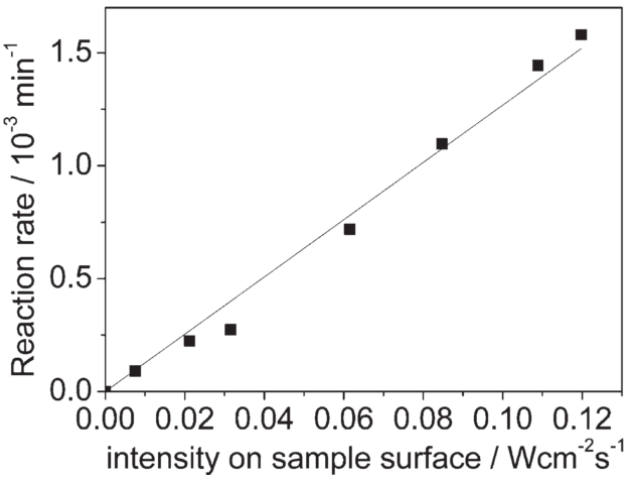

Figure 4.4. Degradation rate as a function of increasing light intensity for regio-regular P3HT[9]

Additionally, when the degradation rates were normalized to the photon flux, an almost constant value for this *photon effectiveness,* i.e. the degradation event per photon, was obtained. This showed that at

low light intensities, photochemical stability testing can be accelerated by light with no significant complication from high temperatures. The extent of the regime of constant photon effectiveness has not been studied, and any upper limit has not been established. However, if the photon effectiveness is constant at even high light intensities, this open up for accelerated degradation by concentrated light where 1 sun degradation rates can be precisely evaluated from be product of the light intensity and the associated degradation rate.

At the initial stages of this PhD work, no studies had reported the response of polymer stability to concentrated light, i.e. solar intensities above 1 sun. However, the potential of this approach is high, since acceleration factors of hundreds or even thousands may be possible.

4.2 Polymer degradation by concentrated sunlight

No commercial light sources are able to provide higher intensities than up to a few suns. To obtain higher light intensities, construction of fully customized light concentration setups was necessary, as described in Chapter 3. A lens based concentrator was constructed in the initial stages of this PhD to allow for quickly studying the polymer response to concentrated light. This work resulted in the article: *T. Tromholt et al.: Degradation of semiconducting polymers by concentrated sunlight. Solar Energy Materials and Solar Cells, 95, p. 1308-1314* and can be found in Appendix 3. The main goals of the paper and the associated conclusions are discussed in the following. The intention was to perform photochemical degradations of well-studied polymers with the solar concentrator to consider whether this approach is viable an approach to accelerated polymer degradation.

4.2.1 Practical sample and degradation considerations

The lens based solar concentrator guides light indoor through a bundle of optical fibers with a high numerical aperture, and thus diverging light exits the fiber (Figure 4.5a). If collimating lenses were not applied, the light intensity falls off quickly at the fiber exit, and thus samples have be placed in close proximity to the fibers. Additionally, a fixed geometry was needed during all degradations to ensure constant illumination intensity. Polymers were spin coated on 5 x 10 x 1 mm KBr substrates, which were successively sandwiched between two 0.5 mm aluminum plates (Figure 4.5b) that were held together by a screw. The top plate was constructed with a 1 mm circular hole, while a 5 mm hole was made in the

lower plate. Illumination of the samples was through top plate. By only studying the degradation of the central 1 mm part of the polymer film, a higher degree of homogeneity was obtained from the fibers. The samples were inserted into a sample holder mounted on an optical rod into an optical table (Figure 4.5c). The sample holder fixed the sample tightly by a spring mechanism, and samples could thus only be removed when the spring was released by pressing the top mechanism above the sample.

Between different degradation experiments, the light intensity was monitored with a power meter. However, the spatial resolution of the power meter was very low since only the total light intensity was measured. To measure the local intensity that illuminated the sample through the 1 mm top sample plate, a photodiode was used (Figure 4.5d - Hamamatzu S5971). A circular area of 1.2 mm diameter was probed by the photodiode, and thus the detection area was close to the illumination area of the sample. The photodiode and the sample aperture were positioned with the same radial distance to the center of rotation of the sample holder. Additionally, the sample holder was constructed with two end stops that ensured that only *light position and photodiode position* could be selected.

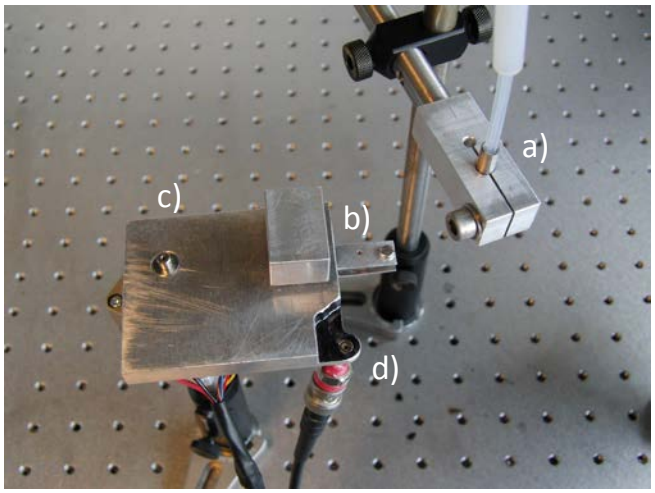

Figure 4.5. Experimental setup used for degradation of polymer samples with concentrated sunlight where a) fiber end, b) sample, c) sample holder, and d) reference photodiode is shown

For the degradation experiment, clear skies were needed to allow for uninterrupted degradation time with constant intensity. The optical fibers were positioned in the *photodiode position* and the light intensity was recorded. With the sample mounted in the sample holder, the sample holder was changed manually to *light position* where degradation was allowed to run. Monitoring the degradation was performed applying the principle described in Section 2.2 where the *total number of absorbed photons*

were evaluated during the degradation of the samples. Samples were moved to a bench top UVvis Shimatzu spectrometer were the absorption spectra were recorded, after which a new degradation step was performed. In the case of cloudy weather conditions, the degradation experiment could be paused, and continued when sunshine was available again. The maximum power output from the setup was 1.8 W, which corresponds to 18 suns on 1 cm^2. However, in the center of fiber bundle, 200 suns were achieved, which was the practical upper limit of degradation intensity.

Initial development of an automated setup was made by mounting the sample holder on a stepper motor, which by computer control would time the light exposures precisely. An optical fiber probe based spectrometer combined with a halogen light source was constructed to allow for automated absorption measurements. While a functioning automatic setup was constructed, no extensive experimental work was carried out with this setup since more sophisticated solar concentrators were developed with higher reliability and intensity.

4.2.2 Differences between 1 sun and concentrated light degradation

When degradation criteria are changed, generally the contribution to the overall degradation is expected to change. Consequently, the dominant degradation mechanisms may be different at 1 sun and at concentrated light. When polymers are degraded at 1 sun, the degradation temperature is slightly above ambient, where the actual temperature depends on the enclosure of the samples etc. However, degradation by concentrated sunlight may possible increase the temperature of the polymer significantly. Thermolysis is not expected to contribute significantly below 100°C[6], and thus only acceleration of photooxidation is expected. Consequently, the degradation kinetics and chemistry is expected to be identical for both degradation types.

The gradual decrease of absorbance of the regio-regular MEH-PPV was studied at both 1 sun and at 100 suns. The 1 sun degradations were performed with a Steuernagel KHS 575 solar simulator, with a spectrum resembling a AM1.5G, while the spectrum of the lens had a lower UV part due to the fraction of the light through the lens. Evolution of *number of absorbed photons* N_{photon} in the UVvis range was monitored as described in Section 2.2. The decrease of N_{photon} depends on the nature of the degradation mechanism and the temperature during the degradation. Higher temperature implies a steeper decay, and thus higher degradation rate, while a variation in the slope may indicate a variation in temperature during the degradation. The degradations performed in this study at 1 sun and at 100 suns showed in

both cases initial linear decays followed by a plateau after which no further degradation was observed (Figure 3 in Appendix 3). If a high temperature had developed in the polymer during accelerated light, during the degradation where the absorption gradually decreases, the temperature would be expected to fall off gradually, implying a nonlinear decay of N_{photon}. As this was not the case, this suggests that the sample temperature was constant during degradation. Furthermore, the typical UVvis blueshift during the degradation was found to be similar in both the case of 1 sun and 100 suns, indicating identical degradation mechanisms (Figure 4 in Appendix 3). However, since UVvis spectroscopy does not provide chemical information, IR spectroscopy was performed on the sample during the degradation for 1 sun and 100 suns degradation of MEH-PPV (Figure 5 and 6 in Appendix 3). Typical degradation products were observed for 1 sun degradation, where e.g. decrease of alkyl, ethers and exocyclic double bonds were found, while different bands in the carbonyl domain evolved at 1800 – 1650 cm^{-1}. An extensive list of vibrational modes in IR spectroscopy can be found in Table 2.1 and 2.2. Comparing the IR spectra during the degradation to the ones of the 100 sun degradation, they were found to be indistinguishable. This suggests that MEH-PPV degradation is governed by the same mechanisms at 1 sun and at 100 sun, and that effects of e.g. thermolysis are negligible. Consequently, concentrated light is a promising acceleration parameter for degradation since the degradation chemistry is conserved at high light intensities. Since two different light sources were used for the 1 sun and concentrated light degradations, the photon effectiveness is expected to by highly influenced by this effect. A higher UV content in the solar simulator is expected to increase photon effectiveness and thus reduce the photon effectiveness. Oppositely, concentrated light degradation may introduce a higher sample temperature during degradation, which would increase the photon effectiveness at concentrated light.

To understand the degradation conditions, the gradual loss of absorption can be studied (Figure 3 in Appendix 3). The evolution of the absorption during the degradation is clearly linear at 1 sun, which is common for almost all photochemically studied polymers[8]. The constant slope implies that the degradation rate is constant during the degradation and that the degradation conditions are also constant. During concentrated light exposure, if the temperature were increased as a function of excessive light absorption and limited thermalisation during light exposure, a higher degradation rate would result. However, as the material bleaches, the temperature would decrease by which the degradation rate also decrease. This would be reflected in the absorption evolution as an initial high slope followed by a gradual decrease of the slope until the slope of the 1 sun degradation is reached. As the absorption evolution during degradation is found to be clearly linear during 100 sun degradation, it

can be concluded that the temperature is kept constant during the entire degradation i.e. that the temperature is not increased significantly above ambient levels.

The constancy of the photon effectiveness was also extracted from the absorption evolutions in Figure 3. While a complete degradation at 1 sun took place within 100 min, the time frame at 100 suns was only 2 min, and consequently acceleration by a factor of 50 was observed. Photon effectiveness is thus only 50 % of the value 1 sun. The reason for the lower effectiveness can either be a lower concentration of reactive species and / or the stronger UV content in the 1 sun spectrum. The only species being consumed during photodegradation is oxygen and consequently, a limitation of oxygen as its consumption is increased by a factor of 100 would imply an increased contribution from thermolysis and photolysis. However, as described above, IR spectroscopy showed identical chemistry during degradation of the 1 sun and 100 sun degraded samples, and the origin of the lower photon effectiveness can thus only be ascribed the lower UV content in the concentrated light.

4.2.3 Acceleration of degradation with increasing light intensity

Degradation of polymers at increasing light intensities is expected to induce increasing degradation rates. If the temperature is kept constant and oxygen availability is unlimited, photon effectiveness is expected to be constant at different light intensities. Degradation of MEH-PPV at increasing solar intensities resulted in increasing degradation rates where the decrease of N_{photon} was linear in all cases allowing for precise evaluation of degradation rates from the slopes of the decay curves. Consequently, a full degradation of MEH-PPV took less than 2 minutes (Figure 7 in Appendix 3). The acceleration factor of the degradation was evaluated as the ratio between the accelerated and the 1 sun degradation rate. For MEH-PPV and P3HT, the acceleration factor was found to increase linearly within the entire intensity range (Figure 8 in Appendix 3). While the absolute values of the acceleration factors were not precise due to the difference in the concentrated and the reference spectra, the increase of acceleration factor with light concentration is interesting. For P3HT, twice the light intensity resulted in twice the acceleration factor. Consequently, the photon effectiveness is constant up to 200 suns. If the degradation temperature were significantly increased, an exponential increase of acceleration factor with light intensity was expected, and the linear increase thus indicates that the temperature has been kept approximately constant. This is a positive result in terms of the applicability of concentrated light to organic photovoltaics, since non-linear effects at high light intensities are not observed, which significantly eases the practical use of concentrated light as an acceleration parameter.

4.2.4 Response to accelerated light of 5 different polymers

The perspective of concentrated light as an acceleration parameter is to use the method to novel material to obtain a rapid estimation of the material stability at 1 sun degradation conditions. Ideally, degradation rates of different polymers are accelerated to the same extent. However, the degradation mechanisms, temperature evolution, and the kinetics vary for different polymers, and thus the same acceleration factor is not expected for different polymers. Finally, since the reference and the concentrated light spectrum were not identical, the differences in absorption of the different polymers introduce variations in acceleration factors. Finally, as this experimental work was performed, no guidelines were available as to how to handle the effect of thickness on the photochemical stability. Consequently, all polymer samples were spin coated with resulting peak absorbances in the range of 0.5 – 1.0, which implies variation in acceleration factors by up to a factor of 2^1.

5 different polymers with different chemical groups, band gaps, and stabilities were degraded (Figure 1 in Appendix 3) at 100 suns and in the solar simulator at 1 sun and the acceleration factors were evaluated (Table 2 in Appendix 3). All polymers were observed to degrade linearly in terms of N_{photon} and thus degradation rates were easily obtained from the respective slopes. Acceleration factors were found to vary within the range of 19 to 55. No correlation between the stability of each material and the acceleration factor was found. Theoretically, an acceleration factor of 100 was expected assuming the constant photon effectiveness. However, due to the reduced UV content of the concentrated light spectrum, rather low acceleration factors were expected. It was concluded that the bias in acceleration factor was an effect of the above mentioned effects of light spectra. The range therefore demonstrates the practical range of acceleration factors obtained when no extensive measures are taken to allow high validity comparisons. However, the relative variation by a factor of 2.5 is acceptable when concentrated light is used as a tool for rapid estimation of polymer stability.

In conclusion, concentrated light is an efficient tool to decrease the time frame of stability evaluation. Since this approach provides a setting for rapid estimation of material stability, it will allow polymer chemists to routinely evaluate the stability of novel materials, which will pave the way for development of future highly stable polymers for PSC. However, the concentration setup used in the above described study has major flaws, which have to be circumvented to obtain higher validity of the acceleration factors etc. The same reference spectrum should be used as for the concentrated light to remove the effect of different absorbances of the materials. Furthermore, the peak absorbance (thickness) of the samples should be adjusted to the same absorbance, since this approach was proven as the best basis

for comparing polymer stabilities[1]. However, the results describe a proof-of-concept of a promising method by which the stability of PSC can be highly increased.

4.3 Polymer degradation by concentrated solar simulation

The refractive light concentrator as described Section 3.2 was a quick solution to obtaining concentrated light. With this setup, interesting degradation results were obtained that provided a proof-of-concept of concentrated light as an accelerated degradation parameter. On the practical level, the setup suffered from an intrinsic instability in the intensity of the coupled light, which implied that the position of the optical fibers should be re-focused every 15 minutes, since the position of the focal point drifted. Finally, the handling of the samples was highly manual since between each degradation step of a single sample, the sample had to be moved to a UVvis spectrometer for absorption measurements. A solution to these problems is simulated light concentration, where an artificial light source is used as a light source to degrade samples. Hereby, the concentrated light is constantly available, and a constant intensity can be obtained from the light source. If such as setup is equipped with a fiber based UVvis spectrometer, a high capacity degradation setup can be constructed, where several samples were degraded, and where the manual handling is kept at a minimum. A concentrated solar simulator was constructed during this PhD work as described in Section 3.4. With the setup, light intensities between 0.1 and 150 suns could be freely chosen, and the light could be quickly turned off by a shutter. A sample exchanger with a capacity of 8 samples allowed for degradation of several degradation points and thus statistically sound data could be obtained. Additionally, the light spectrum of the concentrator was identical to the one of the solar simulators, which is important if absolute acceleration factors are to be evaluated. Additionally, a sample exchanger was constructed with a capacity of 7 substrates of 50 x 25 mm dimensions (Figure 4.6). A rotation stage from Thorlabs (PRM1Z8E) was used to rotate the samples between the kaleidoscope for illumination and an UVvis transmission probe (Avantes AvaSpec3648 spectrometer and AvaLight-DHc Deuterium halogen light source). A fixed mask was mounted 1 mm above the sample exchanger with a circular aperture of 3 mm in the concentrated light position and another 3 mm aperture in the UVvis probe position. This ensured a fixed geometry of the degradation areas on the samples by which a higher precision of the evaluated degradation rates were obtained. Since samples where only moved by a rotation state, the radius from the rotation center to the degradation points was fixed. The radius was selected so that 8 degradation points fitted on the glass slide on the outer periphery of the substrate as demonstrated in Figure 2.11a. The exchanger was

mounted on a drawer that could be pulled from the kaleidoscope position for easy sample replacement. Programming of the setup was performed with the software shown in Figure 2.12. Each degradation points was associated with the same information as in the case of 1 sun degradations, i.e. *Sample name, hole number, substrate number, elapsed time,* and *light*, which in this case determined the light intensity during degradation.

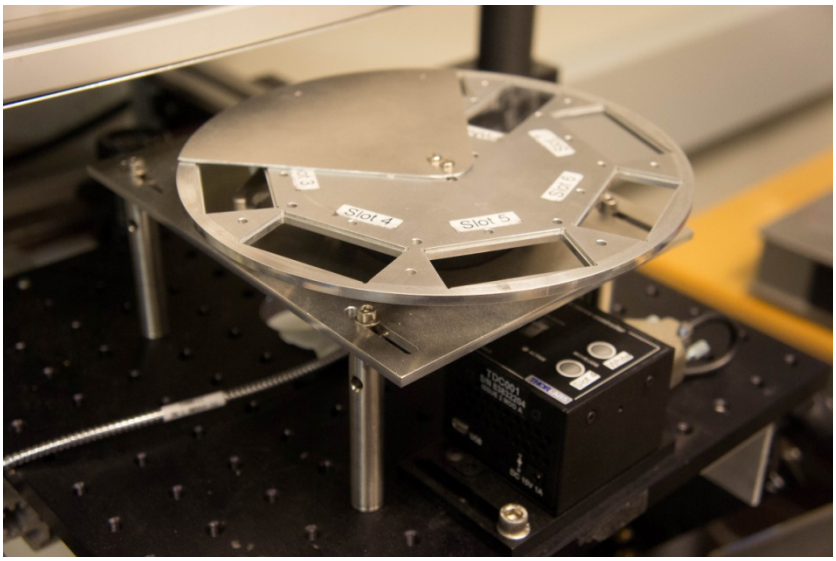

Figure 4.6. Sample exchanger for the indoor concentrator

With this setup, a highly statistically sound analysis of the response of P3HT to concentrated light was made and submitted to *Advanced Energy Materials* as a communication article: M. Madsen, T. Tromholt, K. Norrman & F. C. Krebs: *Concentrated light for accelerated photo degradation of polymer materials*[12]. The manuscript can be found in the Appendix 4. The goals of this work were to establish a quantitative understanding of how P3HT responses to concentrated light and whether the photon effectiveness was constant for different light intensities. Additionally, we wanted to study how the degradation mechanisms and the kinetics are affected by concentrated light, both by the light intensity as well as by the temperature. Regio-regular P3HT was degraded at 50, 100, and 150 suns, and the evaluated degradation rates were compared to 1 sun degradation rates. The light spectrum was kept constant for all light intensities and only the intensity was varied. Linear decay of the N_{photon} was observed for all polymers observed at 1 sun in this PhD work. However, in the case of concentrated light degradation, the slope was observed to be very high in the initial part of the degradation, after which a

gradual decrease of the slope was observed (Figure 2 in Appendix 4). Additionally, when comparing the degradation as a function of the dose on the polymer, the higher light intensities introduced a *dose-corrected acceleration*, i.e. the photon effectiveness had increased. Photo-oxidation, which is the process responsible of the UVvis absorption loss in the ambient is well documented[6]. With the previously described accelerated degradation of polymers with the lens based solar concentrator, the same degradation chemistry was observed by IR spectroscopy for a single sample thickness. However, the response of polymers to high light intensities is not described for different polymer thicknesses. While photo-oxidation is mediated by oxygen diffusion to the polymers, at high light intensities, oxygen diffusion limitations may be experienced, which would decrease the photon effectiveness. To study this, a large number of samples of 10 to 110 nm thicknesses were degraded at 1, 50, 100, and 150 suns and their dose-corrected degradation rates evaluated (Figure 4.7 – In supporting material of submitted manuscript).

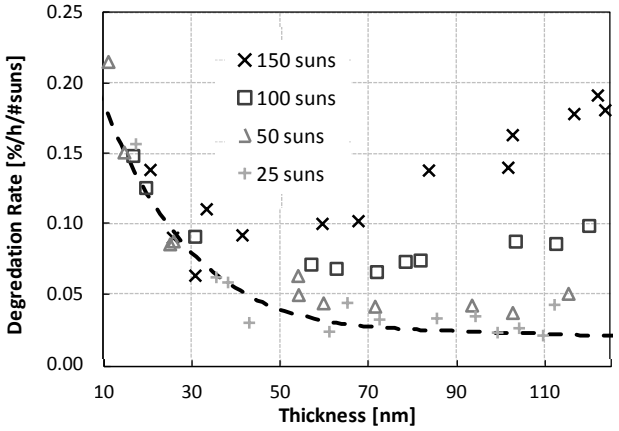

Figure 4.7. Dose corrected degradation rates for different light concentrations and thicknesses. 1 sun degradation rates are indicated by the dashed line[12]

While the 1 sun degradation rates (dashed line) were found to decrease as expected with film thickness, the degradation rates at concentrated light increased with increasing film thickness as well as increasing light intensity. If photon effectiveness were constant for all light intensities, all points should lie on the 1 sun line, and thus a mechanism increasing the degradation rate was introduced. The dose-corrected acceleration factor was evaluated for all the thicknesses and light intensities, expressed as the ratio between *dose-corrected degradation rates* at concentrated light and at 1 sun (Figure 3 in Appendix 4). A linear increase of the dose-corrected acceleration was observed for all light intensities, and the slope of these correlations increased with light intensity.

One of the most critical changes between the 1 sun and concentrated sun degradation is the increase of temperature during the degradation. When the polymers as deposited on 1 mm glass substrates were illuminated with high intensity light, the absorption introduces a temperature increase. Since thicker films absorb more light, the temperature increase is expected with film thickness, as well as with light intensity. However, the specific temperature is not straightforward to measure with e.g. a thermocouple since its absorption differs from the one of the polymers. A simple model was for establishing the temperature of a 100 nm P3HT sample, where the incoming light, the radiative loss, and the thermal loss from the glass substrates were incorporated, which yielded a temperature of 65°C for 150 suns. Since no instant thermalisation between the polymer and the glass is expected, this value was seen as a lower limit of the temperature. A practical measure to establishing the temperature was made, where a glass|P3HT (50 nm)|Ag sample was prepared, which through the metal reflection would have an approximate 100 nm path length of the light in the polymer. The sample was illuminated through the glass and a thermocouple was placed on the back side of the sample in thermal contact with the Ag while being shielded by the light. Hereby, a temperature of 175°C was measured at 150 suns. Since the metal is a non-perfect mirror, the obtained temperature was considered an upper limit of the actual temperature. Hintz et al. have studied the temperature response of the degradation rate of P3HT and modeled the behavior with an Arrhenius model as described in Section 4.1.2 to establish an activation energy of 276 meV. Applying this activation energy to the dose-corrected acceleration factor of 8, an equilibrium temperature of 100 °C is obtained. As this value lies within the above described upper and lower temperature limits, this suggests that the temperature can account for the increased photon effectiveness.

Photo-oxidation is known to be highly temperature accelerated since the oxygen diffusion, which is the rate limiting factor is highly temperature dependent. However, only negligible thermal effects are expected in oxygen free conditions, where photolysis is responsible for the degradation. While the thermal energy $k_B T$ is in the order of 250 – 300 meV, the photon energies range from 1 to 4.5 eV, and increases in thermal energy do practically not change the rate of photolysis above 1 sun. While dose-corrected degradation rates of P3HT in ambient are expected to vary with light intensities, dose-corrected degradation rates in nitrogen atmosphere are expected to be constant. We degraded P3HT at 1, 50, 100, and 150 suns in ambient and nitrogen and saw the splitting in the ambient as expected with higher intensity implying faster degradation (Figure 4 in Appendix 4). However, the samples degraded in nitrogen did not demonstrate any deviation for the different light intensities. This demonstrates at the dose-corrected acceleration factor can be fully ascribed thermal effects by which the rate of photo-

oxidation increases with temperature. The implication of this is that the degradation mechanisms governing the degradation at 1 sun are identical to the mechanisms at 150 suns, which is a great advantage in terms of applying concentrated light as an acceleration parameter to polymers. As a verification of unchanged degradation chemistry at different light intensities, the blueshift observed for the P3HT absorption was studied by evaluating the degradation state of the polymer for which the absorption peak shifts to 480 nm (Figure 5 in Appendix 4).

The heating of the samples during degradation at concentrated light was significant since no active ventilation was applied to the setup. It was thus anticipated that by applying an air stream onto the sample to constantly replace the air, the temperature increases could be considerable decreased. A stream of ambient temperature air (25 L/min) from a dry air pump was directed directly onto the surface of the samples. Since only ventilation was applied and no cooling, the temperature during degradation was never below ambient, and thus a very high flow rate could be applied to minimize any thermal effects. To allow free access of the air onto the polymer surface, the samples had to be turned upside-down implying that the concentrated light passed the glass before hitting the samples. The effect of this illumination geometry is that a 4 % reflection loss is encountered at the air-glass interface, as well as a slightly reduced intensity due to the larger distance to the light exit (1 mm increased distance from the substrate thickness). Finally, the interface between glass and the polymer was subjected to the highest light intensity, while at the polymer surface, the intensity had decreased from the polymer absorption. This may lead to different kinetics since reactive species have to penetrate the film thickness to reach the most illuminated buried glass-polymer interface. However, effectively, the impact of changing the illumination direction was negligible as the degradation rates were conserved. When applying the dry air stream, the degradation rates were, however, found to change significantly (Figure 6 in Appendix 4). The overall effect was that for all light intensities and thicknesses, the otherwise thermally accelerated rates all attained the same dose-corrected degradation rates as in the case of the 1 sun degradations. The implication of this is that the degradation rate is highly deterministic, as it only depends on the number of photons impinging on the sample if the temperature is kept constant. Consequently, 1 sun degradation rates can be precisely evaluated from the 150 sun degradation rates, by which the time frame of stability evaluations can be significantly reduced. This will probe detrimental to development of novel highly photo stable polymers needed for PSC of commercial interest.

4.4 Conclusion

Polymer degradation can be accelerated by a multitude of different conditions to increase the degradation rates. While e.g. thermal degradation has been found accelerate degradation by a factor of 20, this degradation condition accelerates a non-dominant degradation mechanism in the operating PSC. Concentrated light accelerates the dominant degradation mechanism photo oxidation, and is thus a superior acceleration condition. Additionally, very high acceleration factors have been observed with concentrated light. With relatively simple light concentrators such as the presented lens based solar concentrator, 200 suns were applied to the samples by which acceleration factors in excess of 100 were observed. Furthermore, the highly quantitative degradation study of P3HT performed with the indoor concentrator resulted in acceleration factors of 1200 relative to 1 sun. This demonstrates the high potential of significantly reducing the time frame of stability evaluations, assuming that the thermal response of the polymer is understood. If the P3HT samples were kept at ambient temperature during concentrated light degradation, constant photon effectiveness was observed for all light intensities. This implies that at 150 suns, the degradation rate is accelerated by a factor of 150. Consequently, evaluations of 1 sun degradation rates can be precisely obtained from concentrated light studies. Concentrated light will thus provide a means of obtaining rapid stability evaluation of novel polymer materials, and consequently, it is anticipated that photochemical stability data can be just as frequently reported as the PCE of the associated PSC when novel semiconducting polymers are presented.

References

1. Tromholt, T., Madsen, M.V., Carlé, J.E., Helgesen, M. & Krebs, F.C. Photochemical stability of conjugated polymers , electron acceptors and blends for polymer solar cells resolved in terms of film thickness and absorbance. *J. Mater. Chem.* (2012).

2. So, K. *et al.* Accelerated degradation and improved bone-bonding ability of hydroxyapatite ceramics by the addition of glass. *Biomaterials* **27**, 4738-44 (2006).

3. Stark, N.M. & Matuana, L.M. Surface chemistry and mechanical property changes of wood-flour/high-density-polyethylene composites after accelerated weathering. *J. Appl. Polym. Science* **94**, 2263-2273 (2004).

4. Jørgensen, M., Norrman, K. & Krebs, F.C. Stability/degradation of polymer solar cells. *Sol. Energy Mater. Sol. Cells* **92**, 686-714 (2008).

5. Manceau, M. *et al.* Effects of long-term UV–visible light irradiation in the absence of oxygen on P3HT and P3HT:PCBM blend. *Sol. Energy Mater. Sol. Cells* **94**, 1572-1577 (2010).

6. Manceau, M., Rivaton, A., Gardette, J.-L., Guillerez, S. & Lemaître, N. The mechanism of photo- and thermooxidation of poly(3-hexylthiophene) (P3HT) reconsidered. *Polym. Degrad. Stab.* **94**, 898-907 (2009).

7. Rivaton, A. *et al.* Light-induced degradation of the active layer of polymer-based solar cells. *Polym. Degrad. Stab.* **95**, 278-284 (2010).

8. Manceau, M. *et al.* Photochemical stability of π-conjugated polymers for polymer solar cells: a rule of thumb. *J. Mater. Chem.* **21**, 4132-4141 (2011).

9. Hintz, H. *et al.* Photodegradation of P3HT−A Systematic Study of Environmental Factors. *Chem. Mater.* 145-154 (2010).doi:10.1021/cm102373k

10. Schuller, S., Schilinsky, P., Hauch, J. & Brabec, C.J. Determination of the degradation constant of bulk heterojunction solar cells by accelerated lifetime measurements. *Appl. Phys. A-Mater.* **79**, 37-40 (2004).

11. Gevorgyan, S.A., Jørgensen, M. & Krebs, F.C. A setup for studying stability and degradation of polymer solar cells. *Sol. Energy Mater. Sol. Cells* **92**, 736-745 (2008).

12. Madsen, M.V., Tromholt, T., Norrman, K. & Krebs, F.C. Concentrated light for accelerated photo degradation of polymer materials. *Submitted to Advanced Energy Materials* (2012).

5 Polymer Solar Cell Response to Concentrated Light

Electrical studies of PSC at different light intensities have conventionally been used to assess physical phenomena such as recombination pathways and efficiency limiting mechanisms. Furthermore, since the operation of PSC is partially driven by thermally activated electron transport, the different mechanisms dominate to different extents at different temperatures, and thus by changing temperature and light concentration, important conclusions about the physics of PSC have been drawn[1]. Different studies have reported the response of PSC below 1 sun, where conventional solar simulators have been used. However, PSC have not previously been extensively studied with concentrated light due to the lack of commercial light concentration setups. Consequently, only phenomena observable at low light intensities have been reported, while the high intensity regime above 1 sun remains unstudied.

5.1 Key cell parameters below 1 sun

Riedel et al. studied the key cell parameters of PPV:$PC_{60}BM$ solar cells in the range of 0.06 – 1 suns at increasing temperatures between 125 and 320 K to study the recombination mechanisms in the cells[1]. If the exciton generation rate is considered independent of the photon flux, and no mobility problems nor recombination occur, a linear evolution of J_{sc} and the light intensity C_{light} is expected. However, this study found J_{sc} to follow the expression $J_{sc} = C_{light}^{\alpha}$, where α was fitted to 0.85 and 0.92 at 125 and 320 K, respectively (Figure 5.1a). This exponent holds information about the nature of the recombination, where an exponent of 0.5 describes bi-molecular recombination, while for pure monomolecular recombination a value of 1.0 is expected. The found values thus showed that up to 1 sun, monomolecular recombination was dominant, and that the dominance increased with temperature.

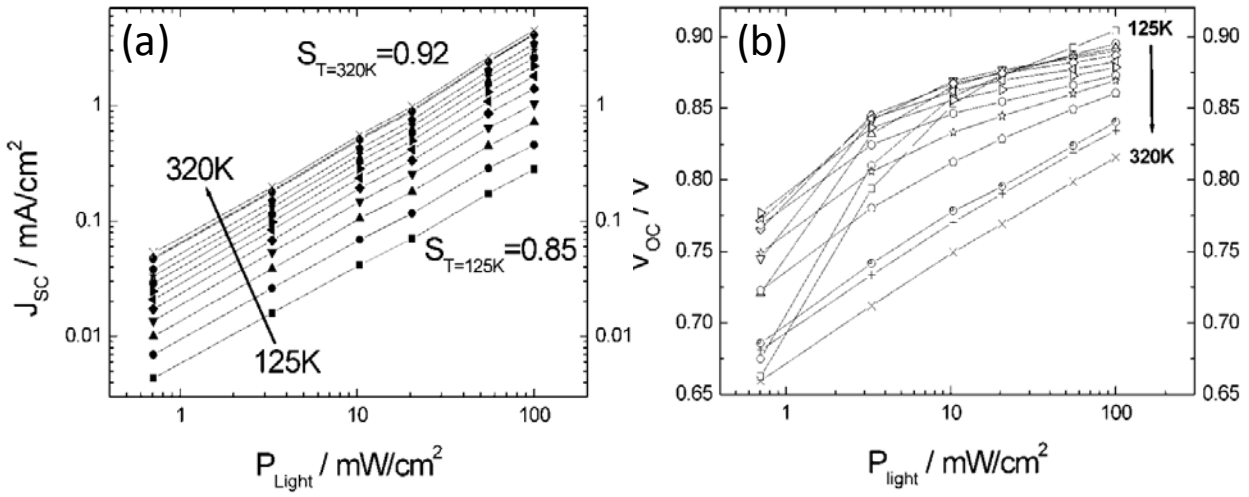

Figure 5.1. Evolution of a) Jsc and b) Voc with light intensity at different temperatures[1]

As discussed in Section 1.4, a diode description is normally used to describe a conventional p-n junction solar cell where the current density under illumination J_L is expressed by

$$J_L = J_s\left(e^{qV/nk_BT} - 1\right) - J_{ph},$$

where J_{ph} is the photocurrent, *q* is the elementary charge, *n* is the ideality factor, *V* is the bias, *T* is the absolute temperature, k_B is the Boltzmann constant, and J_s is the reverse bias saturation current density. J_L cancels at V_{oc}, which thus can be expressed as

$$V_{oc} = \left(\frac{nkT}{q}\right)\ln\left(\frac{J_{sc}}{J_s} + 1\right) \approx \left(\frac{nkT}{q}\right)\ln(J_{sc}) = \left(\frac{nkT}{q}\right)\ln(C),$$

where J_{sc} is the short circuit current density and *C* is the light concentration (See Chapter 1 for further discussion)[2]. Since J_s can be considered independent of and J_{sc} was found to scale almost linearly with light intensity, V_{oc} is expected to increase with the logarithm of *C*. Indeed this was shown above 200 K where the V_{oc} was observed to increase from 0.66 V to 0.83 V at 0.06 suns and 1 sun, respectively (Figure 5.1b). The *FF* was found to decrease slightly throughout the light intensity range, which was also observed for the PCE (not shown). This general picture was ascribed to the decreasing parallel resistance at higher light intensities as observed from the IV curves.

A similar study by Koster et al. studied the key cell parameters in the same light intensity range[2]. They reported similar results with V_{oc} increasing logarithmically with the light intensity with a slope in the range of k_BT/q. Hybrid solar cells based on P3HT and nanocrystalline zinc oxide (ZnO) nanoparticles were

also studied as a function of increasing solar intensity from 1 down to 0.0001 suns[3]. The J_{sc} was found to increase sub-linearly with an exponent of 0.9, while an approximate logarithmic correlation of V_{oc} was found. Since the exponent is constant during the entire light intensity range, no mobility problems hinder charge extraction, and the losses are thus attributed to primarily mono-molecular recombination.

5.2 Key cell parameters with concentrated light

Only a single study discussed the behavior of organic solar cells above 1 sun. Xue et al. reported the key cell parameters of 0.0075 cm^2 copper phthalocyanine : C60 small molecular solar cell in the range of 0.01 to 12 suns[4]. The light intensity was varied with neutral density filters. While the solar simulator is not discussed in detail, it is anticipated that a conventional solar simulator was used, fitted with an extra reflector to increase light intensity. The J_{sc} was found to correlate with light intensity with an exponent of 1.01 (Figure 5.2a) indicating that no recombination or mobility issues arise at 12 suns. However, the low active area of the cell implies that only very low currents are generated thus reducing the contribution from series resistance, which may allow for a linear J_{sc} evolution up to 12 suns.

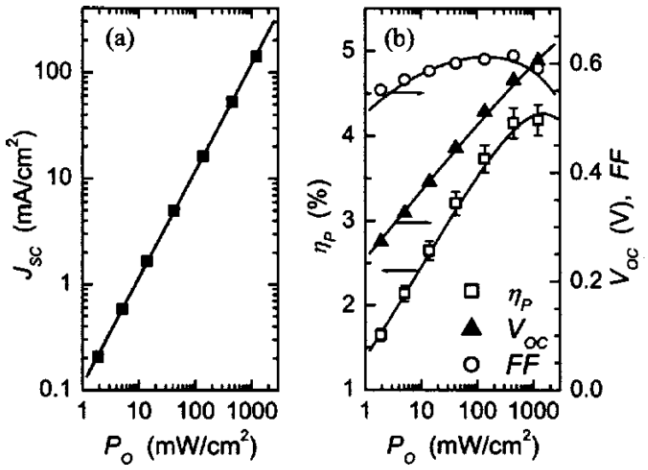

Figure 5.2. Evolution of (a) J_{sc} and b) V_{oc}, *PCE*, and *FF* with light intensity of a copper phthalocyanine : C60 small molecule solar cell[4]

As expected, the V_{oc} was found to increase logarithmically with light intensity throughout the entire intensity range. Additionally, evolution of the FF and PCE were reported (Figure 5.2b). The FF increased slowly until around 8 suns after which it decayed slowly. At short circuit conditions, the strong internal

field allows for efficient exciton disassociation and no mobility problems are experienced. However, the FF is obtained when the cell is under an external load and the internal field is weaker. Consequently, resistances arise in the cell when the current is high and when the internal field is low above 8 suns. This implies that while the exciton and free charge generation rate remain constant, increased recombination within the percolation paths in the acceptor and donor materials decreases the cell performance. This effect was reflected in the PCE, which increased from 1.5 % to 4.2 % up to 5 suns after which the PCE decreased slowly. This large variation in cell performance demonstrates the strong variation with cell performance at different light intensities. Cell performances can thus artificially be boosted as demonstrated here, where the 1 sun performance was only 3.75 % and a relative performance increase of 12 % was achieved by increasing light intensity to 8 suns. Solar cells of 0.02, 0.04, and 0.06 cm^2 were also studied to study the effect of increased series resistance at higher active area. Going from 1 to 2.3 suns, the FF was found to decrease from 61 % to 58 % for the 0.006 cm^2 cell, which shows that even very small cells suffer from charge extraction issues at low light intensities. Consequently, PCE is found to vary clearly with both solar concentration and cell size, which is often used to boost the performance of cells reported in the literature.

Generally, no studies of PSC report the key cell parameters above 1 sun. Consequently, many of the factors limiting the cell performance have not been addressed, which is possible with concentrated light. Additionally, the effect of series resistance of the PSC can advantageously be studied with concentrated light, since high current densities allow for a increased dominance of this effect. Within this highly novel field, many new aspects of PSC can thus be addressed, which made a focus of this PhD work on this very field obvious an obvious choice.

5.3 Polymer solar cell response to concentrated light

The initial part of this PhD work involved an external research stay at the Department of Solar Energy and Environmental Physics at the Ben-Gurion University of the Negev, Sede Boker, Israel. The intention of this stay was to get acquainted with solar concentration as well as answering a basic question: how do the key cell parameters evolve at concentrated solar intensities and what can be deduced from this. The results of this work were published in the article *Tromholt, T., Katz, E. A., Hirsch, B., Vossier, A., & Krebs, F. C. Effects of concentrated sunlight on organic photovoltaics. Applied Physics Letters, 96(7), 073501, 2010* and can be found in the Appendix 5[5]. A large number of cells of 1 x 1 cm active area were

prepared in advance and brought to Israel. Only inverted cells were studied since these are known to have higher stability than normal geometry cells. This was important since significant handling and storage in the ambient during experimental work was expected. Consequently, PSC with a layer stack of glass|ITO|ZnO|P3HT:PC_{60}BM|PEDOT:PSS|Ag|encapsulation were studied. A solar simulator resembling the reflective solar concentrator presented in Section 3.3 provided the concentrated light. The setup guided the light into the laboratory through a single 1.5 mm diameter optical fiber and onto a 30 x 10 x 10 mm kaleidoscope to homogenize the light spatially. The cells were studied from 0.1 to 25 suns and the key cell parameters were studied. The cells were measured with flash illumination, where illumination was kept to less than 1 second per light intensity in order to minimize the degradation etc. induced by the light and temperature. The cells were mounted on a heat sink to keep thermal effects to a minimum.

Increasing the solar intensity from 0.1 to 30 suns, the J_{sc} was found to increase linearly until around 10 suns after which sublinear evolution was observed (Figure 2a in Appendix 5). Below 10 suns, J_{sc} could be fitted with the conventional power law with α values in the range of 0.91 – 0.96 in accordance with the values discussed above from other reports. Above 10 suns, high currents increase the dominance of the series resistance thus introducing additional losses. Likewise, V_{oc} was found to increase with the logarithm of the solar intensity in accordance to expectations (Figure 2b in Appendix 5). However, above 10 suns, decreasing V_{oc} was observed. This can be directly attributed to the heating of the sample, which is known to decrease V_{oc}[1]. As discussed in Section 1.4, a MIM model can be used to describe the V_{oc} as originating from the difference in the work function of the two electrodes and thus the built-in field. However, the electrochemical potential within the photoactive layer is also known to affect the V_{oc}, and a strong correlation of V_{oc} with the difference in the LUMO level of the acceptor and the HOMO level of the donor[6]. V_{oc} of PSC has been reported to approach E_g/q, which is expected to be the theoretical maximum limit for a given material combination. When the thermal energy increases, the energy levels are believe to change implying a change in V_{oc} [6]. The V_{oc} could be fitted to the logarithm of the J_{sc} in accordance with the diode equation (Section 5.1) yielding a slope in the range of kT/q, with diode ideality factors n in the range of 1.21 - 1.27. The *FF* was observed to increase slowly up to 1 sun after which a strong decrease was observed and at 20 suns, a reduction by 50 % relative to the peak value was observed (Inset in Figure 2c in Appendix 5). Likewise, the PCE increased slowly up to 1 sun and at 30 suns only a third of the 1 sun performance remained (Figure 2c in Appendix 5). The initial increase can be directly associated with the increase of V_{oc}, while at higher light intensities, the decrease of *FF* forced the PCE curve down as resistance increased. However, even at 10 suns, 75 % of the peak PCE remained

and consequently, PSC may be an option for low concentration static light concentrators if issues with stability are handled.

5.4 Stability of polymer solar cells under concentrated light

One of the promising potentials of concentrated light is as a means of accelerating PSC degradation to reduce the timeframe of stability testing. This was successfully demonstrated in Chapter 4 for single polymers, where an indoor concentrator provided constant degradation per incoming photon from 1 to 150 suns. Consequently, concentrated light was found to be a highly useable method to accelerate polymer degradation. However the PSC, being composed of several different layers, constitutes a highly complex system, where a multitude of degradation mechanisms contribute to the overall degradation[7]. Since no systematic studies of PSC response to concentrated sunlight have been reported, no knowledge of the stability of PSC under concentrated light is available. Consequently, this topic was given significant attention during this PhD work in collaboration with co-workers in Israel. A final observation in the above described article reporting the key cell parameters, the performance at 1 sun before and after exposures to concentrated light for pristine cells for 3 hours at 1 sun, 55 suns / 30°C, and 58 suns / 55°C (Figure 3 in Appendix 5). The 1 sun degradation induced a decrease of J_{sc} of around 20 %, which was expected given the encapsulation applied to the cells, while the V_{oc} was conserved. The 55 suns / 30°C degradation reduced the J_{sc} by almost a factor of 2 and the V_{oc} decreased from the standard 0.57 V to 0.5 V. Finally, the 58 suns / 55°C degradation introduced even more degradation of the J_{sc} while the V_{oc} went down to 0.23 V.

These observations could not be readily explained and thus a larger study of the stability of PSC to concentrated light was carried out at DTU. The refractive solar concentrator presented in Section 3.2 was used for this study, where PSC of the same layer sequence as discussed above were studied. The results of this work were published as Tromholt, T., Manor, A., Katz, E. A., & Krebs, F. C. *Reversible degradation of inverted organic solar cells by concentrated sunlight.* Nanotechnology, 22, 225401, 2011 and found be found in Appendix 6[8]. The key cell parameters were measured from 1 to 18 suns before and after exposure to 5 suns during 30 minutes. After the degradation, the V_{oc} was observed to attain much lower values, and at 1 sun, V_{oc} was only 0.1 V (Figure 1 in Appendix 6). However, increasing light intensity showed that the V_{oc} had almost been restored at 18 suns. In contradiction to this, the J_{sc} was observed to remain unchanged during the entire light intensity range. This shows that the exciton

generation rate remained constant, and the loss of performance could be related to the charge extraction process. The overall effect was that the PCE decreased from 1.3 % to 0.2 % at 1 sun after light exposure, and thus appeared completely degraded. After a period of 30 minutes where the cells were stored in the dark, the key cell parameters were again recorded. After this period, the cell had almost completely restored its key cell parameters to the pristine values, and a PCE of 0.75 % was reached.

Localization of the observed transient state was important in order to understand it. When the cell is under short circuit conditions, a strong internal field forces the charges toward the electrodes. Consequently, the sensitivity of this part of the IV curve to minor variation in the different layers is expected to be low. However, while the external load increases as the voltage reaches maximum power point (*MPP*) and open circuit (OC), the external load approximately outbalances the internal field and thus variations in layer properties are much more clearly reflected in the overall IV characteristics. Since the J_{sc} did not change, the photon absorption and electron charge transfer were not impeded by the transient state. Thus the photoactive layer appears not to be affected by the transient state. The influence of the transient state decreases with light intensity and almost cancels at 20 suns. Trap formation would be expected to imply a super linear evolution of J_{sc} with light intensity and cancel at high intensity since charge extraction efficiency increases as the traps are filled. However, since no super linearities are observed, trap formation as the reason of the transient state can be ruled out.

The IV curve of PSC in the dark is central to understand the rectification properties of the diode. Dark IV curves as recorded for the three states showed that the rectification before concentrated light exposure was lost and that the cell almost became an ohmic conductor. After the 30 min rest, the rectification properties were almost completely recovered. The reason for the partial recovery of the key cell parameters is that at higher light intensities, a strong J_{sc} forces down the IV curve (Figure 4 in Appendix 7). Hereby, the impact on the *FF* and V_{oc} is less pronounced leading to the partial recovery. However, irreversible degradation to the cells is evident as the key cell parameters are not completely restored. However, this can be ascribed to the conventional degradation of encapsulated inverted PSC when the light intensity and illumination time are considered.

The lack of rectification turned focus to the electron and hole transport layers, ZnO and PEDOT:PSS, respectively. If the electron and hole transport layers lost their charge selective properties and became ohmic, a significant reduction in rectification would be expected. The high photonic flux during concentrated light exposure passes the glass substrate, traverses the ZnO layer, and is almost completely absorbed by the photoactive layer. Finally, the fraction of light that passes this layer is

absorbed or transmitted by the PEDOT:PSS layer. ZnO has been demonstrated to be highly UV sensitive in terms of electrical properties. Verbakel et al. showed that for ZnO|PEDOT:PSS diodes, a clear transition from diode to ohmic behavior was induced by UV exposure[9]. Furthermore, 10 min air exposure was found to restore the rectification properties. The explanation for the transient behavior of ZnO was that normally, O_2^- adsorbs on the surface of the ZnO particles (Figure 3 in Appendix 6). UV illumination generates an electron-hole pair, and the hole combines with the adsorbed O_2^- neutralizing it by which it desorbs. Hereby, ohmic ZnO is generated, since now both holes and electrons are mobile. These observations clearly resemble the ones observed for the solar cells. Indeed, illumination of the cells with only UV light also induced the effect, and consequently it was concluded that the ohmic switching of the ZnO was the origin of the transient state. These results demonstrate that complex responses from PSC may arise when exposed to concentrated light. Consequently, applying concentrated light as an acceleration parameter is not straight-forward, and the response of each layer to concentrated light should be understood for this acceleration parameter to be practically useful.

In another study made in collaboration with coworkers in Israel, the switching effect was further studied with electrical biases. This lead to the publication: Manor, B. A., Katz, E. A., Tromholt, T., & Krebs, F. C. Electrical and photo-induced degradation of ZnO layers in organic in organic photovoltaics. *Advanced Energy Materials*, *1*(5), 836-843 (2011) that can be found in Appendix 7[10]. In the paper presenting the switching mechanisms of ZnO, both UV illumination as well as a strong positive bias were shown to induce the transient effect. The reason for this is that both for optical excitation and forward bias, holes are introduced in the materials, which can combine with the adsorbed O_2^- leading to its desorption and therefore the shunting (Figure 5 in Appendix 7). This behavior was indeed verified on PSC identical in structure to the previously studied cells, where the same effect as observed for extensive illumination with concentrated light was achieved with a forward bias at 10 V for 2 seconds (Figure 6 in Appendix 7). Furthermore, the gradual recovery over time as observed before could be achieved by a rapid – 20 V bias for 2 seconds. Even pristine cells exhibited significant shunting, which could be removed by reverse bias treatment by which the performance was increased (Figure 7a in Appendix 7). However, the reverse bias treatment also decreased the overall ZnO conductivity as observed from the dark curves before and after reverse bias. In the injection regime a significant decrease of current was observed after reverse bias. However, 5 minutes of 1 sun illumination restored the injection regime. With a better dark IV curve, the rectification was improved with the direct implication that the V_{oc} was found to achieve higher values below 1 sun (Figure 7b in Appendix 7).

5.5 Effect of size on polymer solar cells under concentrated light

The applications of concentrated light on PSC is not only an degradation acceleration condition, but also as a means of studying physical phenomena that are less dominant at standard light intensities. As a part of this PhD, further work was focused on the response of concentrated light, namely on the electrical response to cells of different active areas. This work was published as: Manor, A., Katz, E. A., Tromholt, T., Hirsch, B., & Krebs, F. C. Origin of size effect on efficiency of organic photovoltaics. *Journal of Applied Physics*, *109* (7), 074508 (2011) and can be found in Appendix 8[11].

When highly performing hero cells are reported in the literature, the active area of the cell is normally kept to a minimum. Both experimental as well as theoretical work on this topic can be found in the literature[12]. The general conclusion is that the loss of performance observed with increasing active area is due to the power dissipation on the overall cell series resistance and in particular the low sheet resistivity of the transparent electrode ITO. The resistive loss per unit area can be expressed by

$$P_R = \frac{R_S}{A} I_{\max}^2 = R_s A J_{\max}^2, \tag{3}$$

where *A* is the cell area, R_S is the series resistance, and I_{max} and J_{max} are the current and the current density in the MPP, respectively. From this expression is can be seen that the contribution from R_S scales with the cell active area. Larger cells are more affected by resistive loss, and hero cells are consequently reported as cells with active areas well below 1 cm^2. Additionally, the resistive losses increase with the square of the current density. Since the general expression $J_{sc} = G \cdot C_{light}^{\alpha}$ has been found to generally valid, an almost square dependence of the resistive losses with light concentration is expected. Concentrated light thus provides a highly suitable approach for probing resistive losses.

Quadratic inverted P3HT:PC_{60}BM solar cells of 4 mm^2, 25 mm^2, and 1 cm^2 active area were studied from 0.3 to 75 suns. The geometry was designed in order to provide high *FF* by implying a short transport path of the charges on the ITO to minimize the effect of losses not external to the actual cell (Figure 1 in Appendix 8). Dark IV curves of the three sizes of cells showed that in the injection region, the larger cells are severely limited by series resistance, which will impact on cell performance for *FF* and V_{oc} (Figure 2 in Appendix 8). The key cell parameters were found to be highly affected by the cell size. The V_{oc} was found to be slightly higher for the smaller cell, which was believed to be a result of series resistance. J_{sc} displayed a more significant variation with cell area, where at 20 suns, the J_{sc} of the 0.04 cm^2 cell exceeded the 1 cm^2 cell by more than a factor of 2. The evolution of J_{sc} was clearly dividable into two

regions, approximately below and above 5 suns. Below, the α exponent in the J_{sc} expression was close to 1 while above 5 suns, a value of 0.82 was found for the 0.04 cm^2 while only 0.66 for the 1 cm^2 cell. Finally, the *FF* and the *PCE* of the cells showed that higher values are obtained for smaller cells as expected. Furthermore, the rapid decay of performance observed at 1 cm^2 starting around 2 suns was moved to 10 suns for the 0.04 cm^2 cells. This demonstrates that PSC may be considerable for low-cost stationary solar concentration since the performance is practically conserved below 10 suns. Additionally, the results show the in-deterministic nature of the PCE of PSC where the size and light intensity significantly changes the PCE. To allow for direct comparisons of reports of PCE in the literature, the light intensity and the active area should ideally be identical for all compared cells to obtain sound conclusions about the PSC performance.

To understand the reason for the higher *FF* of cells of decreasing area, the photocurrent J_{ph} is introduced. The J_{ph} describes the actual current originating from the absorbed photons and is thus the difference between the white and the dark IV curve, i.e. $J_{\mathrm{ph}} = J_{\mathrm{light}} - J_{\mathrm{dark}}$. While the J_{light} exceeds the J_{dark} at moderate biases, above the V_{oc} the two curves normally coincide and the photocurrent cancels, for which the voltage is referred to as the compensation voltage V_0. The photocurrent is normally plotted against the effective internal voltage $V_{eff} = (V_0 - V)$. In the case of IPV, the excited electron is free to move around the materials due to high mobility, while due to the excitonic nature of PSC, the generation of free charge carriers is preceded by the dissociation of excitons between electron donors and acceptors[13]. As this is a highly voltage dependent process, the same applies to the photocurrent[14]. Typically, the photocurrent increases with the effective field until saturation occurs at a point where all generated charges are extracted. If a high effective field is needed to extract all charges, the photocurrent is effectively lower at the MPP, and consequently *FF* is reduced[15]. In the above described paper, we studied the effect of the size of the PSC on the photocurrent evolution at 1, 5 and 10 suns to see if this could explain the reduced *FF* for larger cell sizes (Figure 6 in Appendix 8). At 1 sun, the photocurrent evolution with effective field was found to be almost identical for different cell areas. The saturation photo currents were also highly similar, and consequently, no effect of photocurrent was found to influence the *FF* at 1 sun. However, differences in the photocurrents were found at 5 and 10 suns, both in terms of the saturation photocurrent as well as the onset of the saturation. The larger cell clearly attains a lower photocurrent in the entire effective field range. Additionally, the MPP as indicated by the circles is found at lower effective fields for the smaller cells, but still at a higher photocurrent. As the photocurrent does not fall of as rapidly for the smaller cells, the IV curve does not decrease as much

from short circuit to MPP introducing in increase in *FF*. Additionally, the decrease of J_{sc} with increasing cell size can be observed from the data. As the photocurrent decreases with cell size in the saturation regime, the overall J_{sc} decreases. The reason for this behavior is however not explained from this data.

The charge extraction is known to depend on the effective field. At short circuit conditions, the strongest internal field is experiences and all free charges are expected to be extracted. While the effective field decreases over MPP to open circuit, charge extraction efficiency decreases. We studied the photocurrent evolution with light intensity at short circuit, MPP, and open circuit for all three cell sizes and found significant variations in charge extraction efficiency (Figure 7 in Appendix 8). At short circuit, in the range of 1 to 15 suns, a linear evolution is observed for the 0.04 cm^2 cell, while increasingly sublinear correlations are found for the larger cells. At a short circuit conditions, primarily series resistance should decrease the J_{sc}, while increasing cell size should not introduce any variations. Moving to the MMP (Figure 7b in Appendix 8) and open circuit (Figure 7c in Appendix 8) the tendency of sublinearity is further increased even for the 0.04 cm^2 cell. Additionally, the importance of size is increased at open circuit, where the largest cell suffers severely attaining an almost constant photocurrent from 5 to 15 suns.

A commonly known effect of increasing cell size is the larger path of the charges on the relatively low conductivity transparent electrode ITO. When an external bias is applied to a PSC, a constant voltage difference is normally assumed throughout the active area of the PSC. However, the voltage drop as experienced by the electrons during the pass introduces a net voltage difference for different parts of the cell, and the effect is a *distributed series resistance*[16] (Figure 8 in Appendix 8). When the cell is e.g. at MPP, this is only the average state of the cell, and some parts are below and some above MPP. As the photocurrent is highly voltage dependent, some parts will generate higher currents and some lower, and simultaneously the IV curve from each sub part of the cell will be at different positions in their diode equations (with e.g. diode opening at high forward bias). The overall effect is a decrease of *FF* and loss of cell performance.

5.6 Conclusion

The performance of PSC was found to highly depend on the light intensity, where the PCE generally increased until 1-3 suns after which a strong decrease was observed. The initial increase was explained by the logarithmic increase of V_{oc} with light intensity, while the PCE decrease was ascribed to the

increased contribution of series resistance as currents increased. In terms of stability, no straight-forward relationship between light intensity, exposure time and cell response can be established after exposure to concentrated light. Strong deterioration of cell performance was observed where the V_{oc} almost cancelled, and after 30 minutes of keeping the cell in the dark, the cell performance had almost recovered. This was explained by the shunting of the ZnO layer by UV illumination. Consequently, care has to be taken when interpreting the stability of PSC under concentrated light and relating this to its 1 sun stability. Finally, characterization of PSC of different active areas demonstrated the possibility of concentrated light to increase the dominance of resistive losses, which is interesting to material characterization. Hereby, the increase of PCE with decreasing active area was explained by a distributed series resistance model of the ITO by which the effective internal field varied over the active area.

References

1. Riedel, I. *et al.* Effect of Temperature and Illumination on the Electrical Characteristics of Polymer–Fullerene Bulk-Heterojunction Solar Cells. *Adv. Funct. Mater.* **14**, 38-44 (2004).

2. Koster, L.J. a., Mihailetchi, V.D., Ramaker, R. & Blom, P.W.M. Light intensity dependence of open-circuit voltage of polymer:fullerene solar cells. *Appl. Phys. Lett.* **86**, 123509 (2005).

3. Beek, W.J.E., Wienk, M.M. & Janssen, R. a. J. Hybrid Solar Cells from Regioregular Polythiophene and ZnO Nanoparticles. *Adv. Funct. Mater.* **16**, 1112-1116 (2006).

4. Xue, J., Uchida, S., Rand, B.P. & Forrest, S.R. 4.2% Efficient Organic Photovoltaic Cells With Low Series Resistances. *Appl. Phys. Lett.* **84**, 3013 (2004).

5. Tromholt, T., Katz, E.A., Hirsch, B., Vossier, A. & Krebs, F.C. Effects of concentrated sunlight on organic photovoltaics. *Appl. Phys. Lett.* **96**, 073501 (2010).

6. Vandewal, K., Tvingstedt, K., Gadisa, A., Inganäs, O. & Manca, J.V. On the origin of the open-circuit voltage of polymer-fullerene solar cells. *Nature Mater.* **8**, 904-9 (2009).

7. Jørgensen, M., Norrman, K. & Krebs, F.C. Stability/degradation of polymer solar cells. *Sol. Energy Mater. Sol. Cells* **92**, 686-714 (2008).

8. Tromholt, T., Manor, A., Katz, E. a & Krebs, F.C. Reversible degradation of inverted organic solar cells by concentrated sunlight. *Nanotechnology* **22**, 225401 (2011).

9. Verbakel, F., Meskers, S.C.J. & Janssen, R. a. J. Electronic memory effects in diodes from a zinc oxide nanoparticle-polystyrene hybrid material. *Appl. Phys. Lett.* **89**, 102103 (2006).

10. Manor, B.A., Katz, E.A., Tromholt, T. & Krebs, F.C. Electrical and photo-induced degradation of ZnO layers in organic in organic photovoltaics. *Adv. Energy Mater.* **1**, 836-843 (2011).

11. Manor, A., Katz, E. a., Tromholt, T., Hirsch, B. & Krebs, F.C. Origin of size effect on efficiency of organic photovoltaics. *J. Appl. Phys.* **109**, 074508 (2011).

12. Choi, S., Potscavage, W.J. & Kippelen, B. Area-scaling of organic solar cells. *J. Appl. Phys.* **106**, 054507 (2009).

13. Gregg, B. A. & Hanna, M.C. Comparing organic to inorganic photovoltaic cells: Theory, experiment, and simulation. *J. Appl. Phys.* **93**, 3605 (2003).

14. Koster, L., Smits, E., Mihailetchi, V. & Blom, P. Device model for the operation of polymer/fullerene bulk heterojunction solar cells. *Phys. Rev. B* **72**, 1-9 (2005).

15. Gupta, D., Mukhopadhyay, S. & Narayan, K.S. Fill factor in organic solar cells. *Sol. Energy Mater. Sol. Cells* **94**, 1309-1313 (2010).

16. Pandey, A., Size effect on organic optoelectronics devices: Example of photovoltaic cell efficiency. *Phys. Lett. A* **372**, 1333-1336 (2008).

6 Conclusion and Outlook

This thesis presents results on the use of concentrated light as well as standard illumination on conjugated polymers and on polymer solar cells. A fully automatic degradation setup was constructed, that allowed for degrading 22 different polymer thin films in parallel, alleviating the normal need for extensive manual handling. Hereby, extensive photochemical stability testing was conducted which validated and matured the technique. Guidelines on how to perform comparative photochemical stability studies were established. Exponential stability increases with film thickness were observed, and the most central guideline of the technique was found to be that comparisons of different polymer types are made for films of the same optical density. With the established guide lines, a high precision of the evaluated stabilities was obtained. Extensive stability studies of different polymers, electron acceptors and blends were conducted. An important result was that for a given stability ranking of polymers, the same ranking was found for the associated polymer blends thus alleviating the need for studying both the polymers and the blends for novel materials. With the automated degradation setup and the validation of photochemical testing as a technique, stability testing is expected to become a routine characterization when novel polymeric materials are reported.

Three different light concentration setups were developed of which two concentrated light sunlight, while the third concentrator was a concentrated solar simulator. With these setups, in excess of 2000 solar intensities could be obtained locally by concentration of sunlight. With the availability of concentrated light, the response of polymers was extensively studied. Since the timeframe of polymer degradation may exceed months, and in the future maybe years, a bottleneck develops between polymer development and stability testing. Acceleration degradation is an obvious solution, and applying light as an acceleration parameter is the most promising acceleration condition as hundreds of solar intensities can be applied without significantly changing the degradation chemistry. Polymer degradation up to 200 suns was conducted in this work for which the photon effectiveness was found to be constant. Consequently, the degradation rate relative to 1 sun degradation is accelerated by exactly a factor of 200, and the 1 sun stability can thus be precisely evaluated.

Polymer solar cells were subjected to concentrated light up to 100 solar intensities by which several interesting observations were made. The cell efficiency increased from 0 to approximately 3 suns after which the efficiency slowly increased. The V_{oc} was found to increase logarithmically with light intensity within the entire light intensity range if thermal effects were minimized. In terms of cell stability, a strong decrease of performance was observed after concentrated light exposure. This effect was ascribed to the switching of the ZnO to a conductive state by which cell rectification was lost. As the switching was not energetically favorable, ZnO rectification was restored after storage in the dark, and consequently cell performance was also restored. Concentrated light is interesting in terms of cell characterization since, due to the high intensity, the dominance of series resistance is augmented relatively to 1 sun degradation. This allows for focusing on this mechanism of the cell while other mechanisms are less dominant. Studies of cells of different active areas indeed demonstrated the strong contribution of series resistance when current densities are high. Smaller cells were superior in handling the currents even up to 100 suns. The origin of the resistance was found to be the series resistance of the ITO, which is a limiting factor to polymer solar cells.

Photochemical stability testing holds a large potential as material stabilities can be obtained. With a fully automated stability testing setup, the otherwise laborious work associated with stability testing is avoided. With the validation and guidelines established in this work, photochemical stability testing is expected to become a routine characterization when novel polymers are presented. Additionally, concentrated light is expected to become a tool for polymer stability evaluation as it provides an acceleration condition that can, in theory, reduce the timescale of stability evaluation by orders of magnitudes if samples are kept at ambient temperature during illumination by effective heat dissipation. With stability being an easily obtained property of a given polymer, development of highly photostable polymers becomes much more transparent and focus, which is detrimental in context of developing polymer solar cells with years of stability.

7 Appendix

7.1 List of publications

Peer reviewed papers

2009

1. Tromholt, T., Gevorgyan, S. A., Jørgensen, M., Krebs, F. C., & Sylvester-Hvid, K. O. (2009). Thermocleavable materials for polymer solar cells with high open circuit voltage-a comparative study. *ACS Applied Materials & Interfaces*, *1*(12), 2768-77. **(Not discussed in thesis)**

2010

2. Tromholt, T., Katz, E. A., Hirsch, B., Vossier, A., & Krebs, F. C. (2010). Effects of concentrated sunlight on organic photovoltaics. *Applied Physics Letters*, *96*(7), 073501. doi:10.1063/1.3298742 **(Appendix 5 – page 135-175)**

3. Krebs, F. C., Tromholt, T., & Jørgensen, M. (2010). Upscaling of polymer solar cell fabrication using full roll-to-roll processing. *Nanoscale*, *2*(6), 873-86. **(Not discussed in thesis)**

4. Tromholt, T., Manceau, M., Helgesen, M., Carlé, J. E., & Krebs, F. C. (2010). Degradation of semiconducting polymers by concentrated sunlight. *Solar Energy Materials and Solar Cells*, *95*, 1308-1314. **(Appendix 3 – page 160-166)**

2011

5. Tromholt, T., Manor, A., Katz, E. A., & Krebs, F. C. (2011). Reversible degradation of inverted organic solar cells by concentrated sunlight. *Nanotechnology*, *22*(22), 225401. **(Appendix 6 – page 176 - 181)**

6. Manor, A., Katz, E. A., Tromholt, T., Hirsch, B., & Krebs, F. C. (2011). Origin of size effect on efficiency of organic photovoltaics. *Journal of Applied Physics*, *109*(7), 074508. **(Appendix 8 – page 190 - 198)**
7. Madsen, M. V., Sylvester-hvid, K. O., Dastmalchi, B., Hingerl, K., Norrman, K., Tromholt, T., Manceau, M., et al. (2011). Ellipsometry as a Nondestructive Depth Profiling Tool for Roll-to-Roll Manufactured Flexible Solar Cells. *Journal of Physical Chemistry C*, 10817-10822. **(Not discussed in thesis)**

8. Manor, B. A., Katz, E. A., Tromholt, T., & Krebs, F. C. (2011). Electrical and photo-induced degradation of ZnO layers in organic in organic photovoltaics. *Advanced Energy Materials*, *1*(5), 836-843. **(Appendix 7 – page 182 - 189)**

9. Helgesen, M., Madsen, M. V., Andreasen, B., Tromholt, T., Andreasen, J. W., & Krebs, F. C. (2011). Thermally reactive Thiazolo[5,4-d]thiazole based copolymers for high photochemical stability in polymer solar cells. *Polymer Chemistry*, *2*, 2536-2542. **(Not discussed in thesis)**

10. Sylvester-Hvid, K. O., Tromholt, T., Jørgensen, M., Krebs, F. C., Zimmermann, K., & Liehr, A. (2011). Non-destructive lateral mapping of the thickness of the photoactive layer in polymer based solar cells. *Progress in Photovoltaics: Research and applications*. **(Not discussed in thesis)**

11. Nan, Y.-X., Hu, X.-L., Larsen-Olsen, T. T., Andreasen, B., Tromholt, T., Andreasen, J. W., Tanenbaum, D. M., et al. (2011). Generation of native polythiophene/PCBM composite nanoparticles via the combination of ultrasonic micronization of droplets and thermocleaving from aqueous dispersion. *Nanotechnology*, *22*(47), 475301. **(Not discussed in thesis)**

12. Jørgensen, M., Norrman, K., Gevorgyan, S. A., Tromholt, T., Andreasen, B., & Krebs, F. C. (2011). Stability of Polymer Solar Cells. *Advanced Materials*, *24*(5), 580-612. **(Not discussed in thesis)**

2012

13. Manor, A., Katz, E. A., Tromholt, T., & Krebs, F. C. (2012). Enhancing functionality of ZnO hole blocking layer in organic photovoltaics. *Solar Energy Materials and Solar Cells*, *98*, 491-493. **(Not discussed in thesis)**

14. Tromholt, T., Madsen, M. V., Carlé, J. E., Helgesen, M., & Krebs, F. C. (2012). Photochemical stability of conjugated polymers , electron acceptors and blends for polymer solar cells resolved in terms of film thickness and absorbance. *Journal of Materials Chemistry*, *22*, 7592-7601. **(Appendix 1 – page 134 - 143)**

Submitted papers

- Madsen, M., Tromholt, T., Norrman, K. & Krebs, F. C.: Influence of intrinsic polymer and processing parameters on photochemical stability of polymer thin films – a comparative P3HT study submitted to *Journal of Polymer Degradation and Stability* **(Appendix 2 – page 144 - 159)**

- Madsen, M., Tromholt, T., Norrman, K. & Krebs, F. C.: Concentrated light for accelerated photo degradation of polymer materials. Submitted to *Advanced Energy Materials* **(Appendix 4 – page 167 - 171)**
- Carlé, J., Andreassen, B., Tromholt, T., Madsen, M., Jørgensen, M., & Krebs, F. C. Comparative Studies of Photo Chemical Cross-linking Methods for Stabilizing the Bulk Hetero-Junction Morphology in Polymer Solar Cells. *Submitted to Journal of Materials Chemistry* **(Not discussed in thesis)**

Book chapter

- Tromholt, T. (2012) Concentrated Light for Organic Photovoltaics. *Stability and Degradation of Organic and Polymer Solar Cells* **(Not discussed in thesis)**

Popular science

- Larsen-Olsen; T., Dam; H.; Andreasen, B.; Tromholt, T.; Krebs, F. C. (2011). Polymersolceller. *Aspekter af Dansk Kemi i det 20. og 21. århundrede* (pp. 109-118). KemiForlaget **(Not discussed in thesis)**

Appendix 1

Journal of Materials Chemistry

Cite this: *J. Mater. Chem.*, 2012, **22**, 7592

www.rsc.org/materials

PAPER

Photochemical stability of conjugated polymers, electron acceptors and blends for polymer solar cells resolved in terms of film thickness and absorbance†

Thomas Tromholt,* Morten Vesterager Madsen, Jon E. Carlé, Martin Helgesen and Frederik C. Krebs

Received 4th December 2011, Accepted 7th February 2012
DOI: 10.1039/c2jm16340c

Photochemical degradation at 1 sun under AM1.5G illumination was performed on six conjugated polymers and five different electron acceptors. Additionally, the respective polymer:$PC_{60}BM$ and P3HT:electron acceptor blends were studied, and all degradations were resolved in terms of film thickness and absorbance. A fully automated degradation setup allowed for inclusion of in excess of 1000 degradations in this study to enable a discussion of reliability of the technique. Degradation rates were found to increase exponentially with decreasing film absorbance for all materials. The relative stabilities within each material group were found to vary for both the pure polymers and the blends. The stability ranking between the materials of the pure polymers was found to be similar to the ranking for their respective blends, implying that the photochemical stability of a pure polymer is a good measure of its associated blend stability. Different electron acceptors were found to stabilize P3HT decreasingly with decreasing donor–acceptor LUMO–LUMO gap. Destabilization of P3HT was observed in the case of the electron acceptor ICBA. Additionally, the decreased stabilization of P3HT by high LUMO electron acceptors poses a challenge to solar cell encapsulation if these materials are to be of commercial interest. The presented method is generally applicable to all types of organic materials to assess photochemical stabilities. The presented results of conjugated polymers demonstrate that this is a powerful tool for conjugated polymer stability assessment if the results are interpreted correctly.

Introduction

With the increasing attention polymer solar cells (PSCs) are receiving on the basis of potential ease of processing, low cost and light weight,[1–3] solving the stability issue is becoming increasingly urgent. While the efficiency of devices has rapidly risen to exceed 8%,[4] stability is still a major limitation to the technology.[5] A multitude of new polymers have been developed and their performances in PSCs have been studied.[6,7] However, the stability of the polymers is only rarely discussed and therefore their practical potential in actual commercial solar cells is not obvious if they cannot combine high performance with high stability.

A general complication regarding stability assessment of the conjugated polymer in PSCs is the influence of several degradation mechanisms external to the polymer, *e.g.* diffusion of water and oxygen into the cell,[8] hole and electron transport layer degradation,[9,10] morphology and phase changes of the active layer.[11] An alternative method is to focus only on the stability of the polymer itself by degrading only the polymer, either in solution[12] or as thin films.[13,14] By this the photochemical stability of a large number of different material classes has been established.[14] Consequently, this knowledge has been used as a practical guide to direct polymer synthesis and development in the direction of higher stabilities.

Photochemical stability of polymers is normally studied by monitoring the UV-visible photo-bleaching as a function of degradation time.[14] However, the photochemical stability of polymers is known to be highly dependent on several different parameters, *e.g.* oxygen concentration, humidity, temperature, light intensity, film optical density (thickness), UV content, ozone concentration and molecular weight.[13,15] As a result, when making comparative studies of polymer stabilities, many different parameters influence the experimental conditions, which may be outside the control of the experimenter. The majority of the above mentioned parameters are normally approximately constant within an experimental study if not actively changed. Parameters such as the temperature, light spectrum, and light intensity are typically kept constant. Contrary to this, the optical density (thickness) of the sample is more prone to variation and great attention must be given to keep this parameter constant for all samples. Furthermore, the effect of varying optical density (thickness) on material stability has not been studied systematically and therefore the uncertainty introduced by thickness variation is unknown. Degradation of

Risø National Laboratory for Sustainable Energy, Technical University of Denmark, Frederiksborgvej 399, DK-4000 Roskilde, Denmark. E-mail: ttro@risoe.dtu.dk

† Electronic supplementary information (ESI) available. See DOI: 10.1039/c2jm16340c

conjugated polymers in the ambient is highly dominated by the concentration of light and oxygen.[5] In general, due to the limited penetration depth of both light and oxygen, a thick film is expected to be more stable than a thin film. In the literature, examples of this effect can be found by comparison of different P3HT stabilities, where the time frame for a complete degradation with the same light source was found to increase ten-fold when the film absorbance was increased from 0.2 to 0.6‡.[14,16] Additionally, when performing comparative stability studies between different materials, the effect of the optical density (thickness) on the stability for different materials is unknown. The overall effect is that the photochemical stabilities obtained for thin films are not necessarily consistent with the stabilities obtained for thick films.

This study presents a rigorous analysis of the influence of the optical density (thickness) on the photochemical stability of different materials and material combinations relevant to PSCs. However, the presented method is applicable as a stability assessment tool to all types of organic materials. To allow for a thorough analysis of the parameter space, a fully automated degradation setup was constructed. By this a high number of degradation studies could be performed while keeping the workload for the experimenter to a minimum. This study therefore presents in excess of 1000 degradations, providing a sound basis for all conclusions. Six different conjugated polymers were studies as well as five different electron acceptors to establish their individual stabilities and the dependence of these on optical density (thickness). To study the actual chemical context of conjugated polymers in PSCs, the impact of blending P3HT with the five different electron acceptors is studied. This studies the consequence of application of high LUMO level acceptors to PSCs. Finally, the stability of blends consisting of the six studied polymers and $PC_{60}BM$ is assessed. This allows for a general discussion of the correlation between photochemical stability of the single polymers and their associated blends, which is essential for making sound predictions of the stability of different polymers in PSCs.

Experimental

Sample preparation

Six different polymers were studied, which contain different chemical moieties (Fig. 1). 90–94% regio-regular poly[3-hexylthiophene] (P3HT) was obtained from Rieke metals. Synthetic procedures and characterization data for poly[2,3-bis-(3-octyloxyphenyl)quinoxaline-5,8-diyl-*alt*-thiophene-2,5-diyl] (TQ1), regio-random P3HT, and poly[(4,4′-bis(2-ethylhexyl)dithieno[3,2-b:2′,3′-d]silole)-2,6-diyl-*alt*-(2,1,3-benzothiadiazole)-4,7-diyl] (PSBTBT) are documented elsewhere.[17–19] A thermocleavable polymer poly[3-(2-methylhexan-2-yl)-oxy-carbonyldithiophene] allowed for the preparation of solid polythiophene (PT) film from solution[20] by cleaving the polymer on a hot plate in the ambient at 300 °C for 10 seconds after spin coating.[21] Molecular weights for all polymers are given in Table S1†. Photochemical stabilities of all polymers of a single thickness have already been established.[13,14,16,22] All polymers and blends were spin coated on

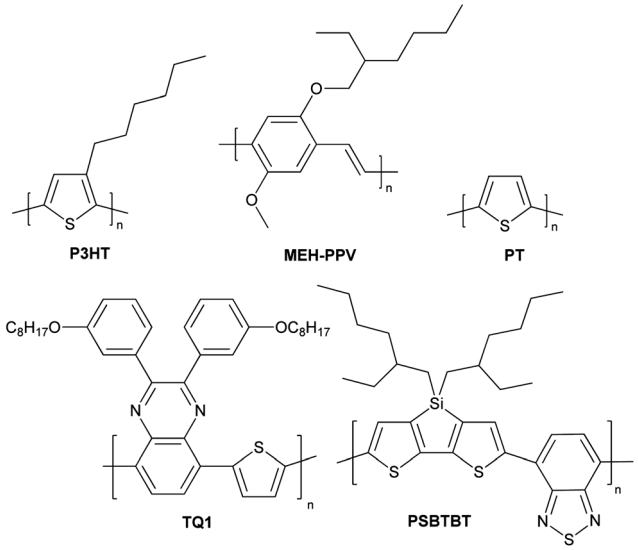

Fig. 1 Schematic illustrations of the polymers studied.

glass substrates from chlorobenzene in the ambient at room temperature in concentrations ranging from 5 to 30 mg mL^{-1} to obtain a wide range of layer thicknesses. Absorbance spectra of all polymers are shown in Fig. S1a†.

Five different electron acceptors were studied of which four are functionalizations of C_{60} Buckminster fullerenes (Fig. 2). Phenyl-[6,6]-C61-butyric acid methyl ester ($PC_{60}BM$), bis$PC_{60}BM$ and $PC_{70}BM$ were obtained from Solenne, C_{60} was obtained from Aldrich, while the indene-C_{60} bis-adduct (ICBA) was obtained from Plextronics. Absorbance spectra of electron acceptors are shown in Fig. S1b†.

Degradation setup

A Steuernagel solar simulator with an Osram 1200 W HMI lamp providing an AM1.5G spectrum was used for all degradations.

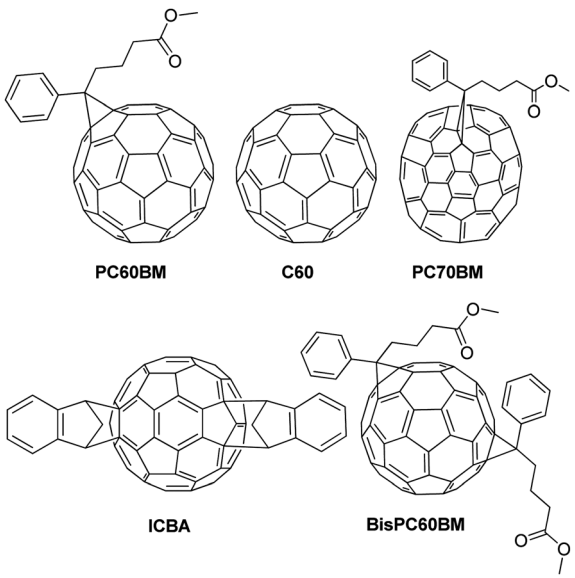

Fig. 2 Schematic illustrations of the studied electron acceptors.

‡ Corrected value in accordance with the article author.

A power meter was used to adjust the solar intensity to 1 kW m^{-2}. The light was not filtered and therefore a UV rich spectrum was obtained with a cut-off at 280 nm (Fig. S2†). All degradations were performed in a laboratory with humidity (20% relative humidity) and thermal control (23 °C room temperature) to ensure a constant degradation environment. The temperature during all degradation experiments of the samples was 32 °C. The ozone generated by the light bulb was removed with a fan, and the samples were thus exposed to the ozone concentration of the laboratory, which was slightly higher than outdoor ozone levels. A fully automated sample exchanger with a capacity of 24 different samples was employed to perform multiple degradations in parallel (Fig. 3A–C). The distance to the center was identical for all samples avoiding effects of spatial inhomogeneities of the illumination. An optical fiber-based CCD spectrometer (Avantes AvaSpec 1024 with a 400 μm quartz fiber) and a halogen/deuterium light source (Avantes AvaLight-DHc) were used to record the absorption spectra in a transmission geometry in the range of 300 to 900 nm at set intervals based on the approach described in ref. 23. By using collimating lenses adjusted normal to the sample, a parallel light probe was obtained by which a circular area of Ø 3 mm was probed. The flowchart in Fig. 3C shows the operation procedure of the degradation setup. During each run 22 samples were mounted in the sample exchanger and eight degradation points were measured on each sample and thus 176 parallel degradations were monitored in parallel to increase the statistic significance. After the recording of the absorbances, the samples were allowed to degrade for a customized interval with no rotation of the exchanger, typically 5 minutes.

Stability evaluation

The degradation rates were extracted from the decrease of the calculated *total number of absorbed photons* (N_{photon}) per second as absorbed by the polymer, when the recorded absorption spectrum is folded with a theoretical AM1.5G solar spectrum as described in ref. 24. 30–500 absorption spectra were recorded for each individual sample point. A strictly linear decrease of N_{photon} was observed for all polymers during the entire degradation. The slope of the decrease of N_{photon} over time allowed for the evaluation of the degradation rate. Only few percent of degradation allowed a precise estimation of the degradation rate due to the high density of recorded absorption spectra. A C# based automated software infrastructure was established to handle the high number of data files generated. This software showed the N_{photon} evolution for all 176 samples as well as the respective absorption spectra. If an erroneous absorption spectrum was recorded, this was clearly observed when processing the data and the data point could thus be dismissed. In total, this study presents in excess of 1000 degradations each including an average of 50 absorption measurements. Invalid data points have been filtered from the data where effects of particles, bad film coverage, inhomogeneous film thickness *etc.* clearly influenced the degradation rates. The reliability of the method is demonstrated by comparison of evaluated degradation rates for P3HT on the same sample, for different samples and different separate experiments, which are all found to strictly follow the same correlation (Fig. 3D).

When neglecting the significant time invested in setting up the apparatus and the time required for its validation, the total operator workload for all the degradation data reported here is

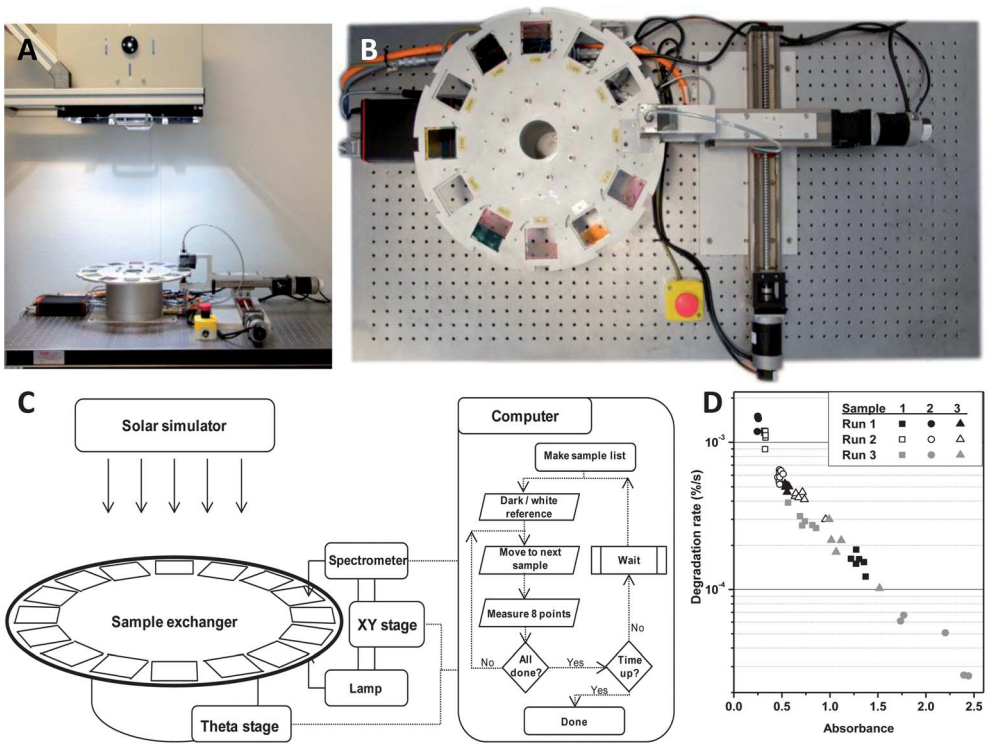

Fig. 3 (A) Side view of the degradation setup. (B) Top view of the sample exchanger. (C) Schematic illustration of the automated degradation setup. A flow chart describes the procedure for the degradations. (D) Absorbance resolved degradation rates for P3HT where data from different samples and different degradation experiments are shown.

estimated to be roughly 4 hours, while a manually operated setup was estimated to a workload of roughly 400 hours, clearly indicating the gain in operator efficiency. Additionally, the precision of the automated setup outperforms any manual handling since measurements are performed with higher frequency, non-interrupted illumination, and with a fixed geometry during the entire degradation as compared to the manual handling where samples are removed from the degradation setup and transported to and from the spectrometer. Finally, in terms of the reliability of the automated setup the timing of the data point acquisition is computer controlled (data are stored with millisecond accuracy), while manual handling involves an attentive operator keeping track of time, introducing a multitude of risks to the data acquisition. We firmly believe that comparative studies on this or larger scales mandatorily require a setup of the complexity described here to enable fast extraction of reliable data.

AFM thickness correlations

A Bruker Neos atomic force microscope (AFM) was used to establish correlations between layer thickness and material absorption for each of the studied materials and material combinations. A minimum of four samples covering a broad thickness range were spin coated. By scratching the sample with a scalpel, AFM measurements across the scratch allowed the determination of film thicknesses with an uncertainty of 5 nm. For all material combinations, linear correlations were found between the peak absorption of the polymer and the thickness. Simulations of the theoretical absorption of the film demonstrate that a linear correlation in the thickness range is indeed expected in accordance with the Lambert–Beers law. Fig. S3† shows an optical simulation in the range of 5 to 200 nm of both P3HT and P3HT:$PC_{60}BM$ demonstrating a clear linear correlation between the polymer peak absorption and the thickness for both the polymer and the blend validating the observed linear AFM correlations. The simulation was based on the refractive index as measured by spectroscopic ellipsometry (Sopra lab GES5E). The refractive index of the P3HT:$PC_{60}BM$ blend was obtained by combination of the refractive indices of the pure phases using an effective media approximation as described in ref. 25.

Results and discussion

Stability of conjugated polymers

In this study six different polymers have been studied (Fig. 1). These have been chosen to cover a wide range of chemical moieties and photochemical stability. Furthermore, all materials are known for their high performance or historical use in PSCs and are therefore highly relevant to the present research. In the discussion of the evaluation of photochemical stabilities of different materials, the basis for comparisons is important. Conventionally, the basis for comparison of different conjugated polymers has been the absorbance peak values in the UV-visible spectrum, where all samples in a comparative study have been adjusted to the same peak absorbance.[14] The absorbance is an easily measurable quantity and intrinsic to the spectroscopic degradation probe. Additionally, it can also be qualitatively estimated by visual inspection of the light attenuation by the film, simplifying sample preparation. Such an *absorbance basis* implies that for a material with low linear attenuation coefficient, a thicker film is needed to achieve the same absorption as for a high linear attenuation coefficient material. The light penetration depth depends on the linear attenuation coefficient, where a low linear attenuation coefficient implies a larger ratio of photons being absorbed deeper into the bulk of the material. To justify an absorbance basis for polymer comparisons, each photon absorbed by the material should thus contribute with equal degradation independent of whether the material is a high or low linear attenuation coefficient material. Since degradation of conjugated polymers in the ambient is governed by oxygen this ideally implies that the oxygen availability is effectively constant within the penetration depth of the light.

Degradation rates of the six polymers are presented in Fig. 4 and resolved in terms of their absorbance. The degradation rate of MEH-PPV is found to exceed the rest of the materials by two orders of magnitude, while the thermocleaved PT is highly stable (Fig. 4). This is in correspondence with the expected stability reported in the literature.[14,22] The absorbance resolved degradation rates additionally show a clear exponential decrease with absorbance for all studied polymers. The degradation rate of regio-regular P3HT is observed to vary from 10^{-3} to 5×10^{-5}% per second with increasing absorbance implying a relative variation of a factor of 20. This observation explains the above described variations of lifetimes of P3HT reported in the literature where degradation rates have been found to range by a factor of 10 for P3HT.[14,16] This clearly demonstrates the high importance of absorbance/film thickness in the discussion of photochemical stabilities of conjugated polymers.

The observed exponential decreases are believed to be an effect of the exponential decay of light into the film. Consequently, an increased degradation in the top layer is expected while the bottom part remains partly shielded. The degradation products in the form of small degradation products, oligomers, *etc.* were found to increase the absorbance in the range of 280–320 nm over the cause of the degradation. This layer may function as a physical barrier toward oxygen or other reactants. Additionally, many other factors come into play such as oxygen solubility, morphology, *etc.* and therefore no simple mechanism for the

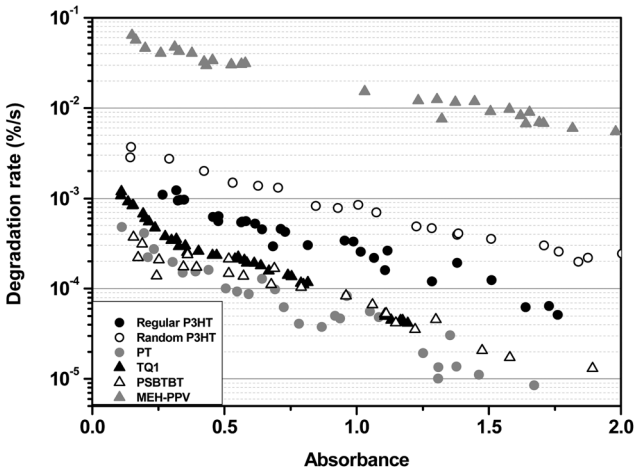

Fig. 4 Absorbance resolved degradation rates for six different polymers.

degradation can be established; see the section *Outlook and Perspectives* for a general discussion on this matter.

Utilizing the absorbance resolved degradation rates, all material stabilities can be evaluated in units of the degradation rates of regio-regular P3HT thus providing a relative stability with regio-regular P3HT as a reference. This unit is advantageously used as a measure of comparative photochemical stabilities of polymers since a reference is needed to compensate for the differences between different degradation setups and environmental factors. All correlations in Fig. 4 were fitted exponentially and their fits divided by the P3HT degradation rate fit to obtain relative stabilities (Fig. 5). Relative stabilities were only evaluated in the range where degradation rates for both the reference and the individual polymer were obtained. Even though not all ranges were covered due to processing difficulties, the strict exponential evolutions observed within the measured ranges are expected to continue if processing were possible. For an ideal basis of comparison for the degradation data, ideally constant relative stabilities for all materials would have been obtained. However, due to the above described assumptions for the absorption basis, constant relative stabilities are not expected. Relative stabilities for all polymers are found to vary within the absorbance range studied with the largest variations being observed for TQ1 where the relative stability increases from 2 to 6 with absorbance. Many parameters are expected to influence the thickness dependent stability of the materials. Specifically, P3HT is known as a highly crystalline material, which may affect the thickness dependence. This effect, in combination with the other issues discussed in the section *Outlook and Perspectives*, may explain the variations.

The slopes of the degradation rate–absorbance (thickness) correlations for the polymers as shown in Fig. 4 are observed to be similar in magnitude and thus the absorption basis seems to provide an acceptable presentation for comparisons of different polymers. The relative stabilities of PT and TQ1 are found to increase slowly with absorbance, while the remaining exhibit a slightly negative slope. This demonstrates that regio-regular P3HT has a degradation rate slope lying in the middle of the remaining polymers and thus serves as a good reference for all

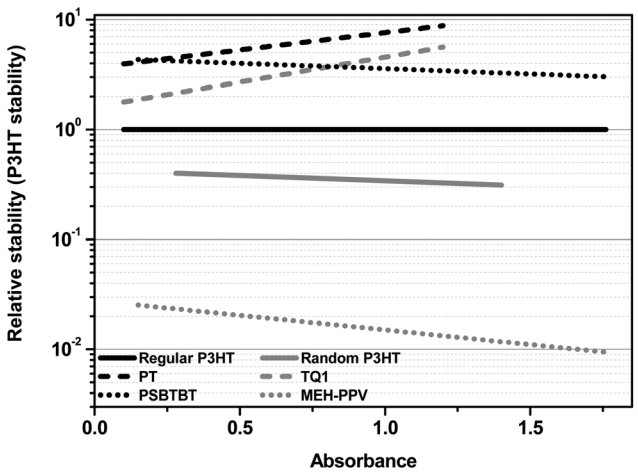

Fig. 5 Absorbance resolved stabilities in units of P3HT stability for the studied polymers.

polymers. The six different polymers have highly different linear attenuation coefficients which may influence the degradation rate slopes. As a result, the film thicknesses for samples with absorbance of 0.6 attain highly different thicknesses as indicated in Table S2†. A PT film would only be 44 nm thick, while a TQ1 film would be 164 nm, as compared to regio-regular P3HT, which would be 101 nm. No pattern was found between the slopes of the relative stabilities and the linear attenuation coefficient and therefore the use of absorption as a basis seems to successfully allow for comparison of polymers with highly different linear attenuation coefficients.

Regio-Random P3HT was found to exhibit relative stabilities of 0.3–0.4 relative to regio-regular P3HT. This is in correspondence with earlier reports on the photochemical stability of regio-regular and regio-random P3HT stating a relative stability of 0.33 for films of 1.8 absorbance.[13] Likewise, photochemical stabilities of TQ1 at 0.2 absorbance[16] and MEH-PPV and PSBTBT at 0.6 absorbance[14] have been established in combination with regio-regular P3HT. These studies showed a relative TQ1 stability of 5, while we observe a relative stability of 2. MEH-PPV and PSBTBT were found to exhibit relative stabilities of 0.010 and 2 while, with our degradation setup, we observed stabilities of 0.019 and 4, respectively. The reason for these deviations could be one of the following: the degradations reported in the literature were performed with a UV filtered light spectrum by which light below 300 nm was removed. The UV responses of different polymers vary with the different functional groups and will thus introduce differences in relative stabilities. The temperature was kept at 85 °C in the earlier studies, which is known to increase degradation rates differently for different polymers.[15] Additionally, the strong decrease of degradation rates with absorbance has not been reported before and therefore this parameter may not have been given much attention. A small variation between the optical densities of two films being compared can lead to large deviations in the observed relative stabilities. Finally, the automated setup presented here is associated with higher precision of the degradation rates due to the large number of degradations carried out, while the degradation rates evaluated from a single sample are associated with significant uncertainty, which may introduce the observed differences. Generally, the absorbance (thickness) is a parameter which introduces large variations in degradation rates. Therefore this parameter must be given extensive attention for future comparative photochemical studies since large uncertainties can easily be introduced and conclusions may be made on a wrong basis. The precision to which the relative stability of a given polymer can be assessed based on a single thickness is found to be rather low due to the variation in relative stability. Only conservative estimations can be made with validity. It is recommended that conclusions on relative stabilities from a single thickness are not resolved in less than factors of five. More precise conclusions demand for degradations of several optical densities and preferably several independent degradation experiments for each optical density as presented in this work. Only then can a more precise conclusion on relative stabilities be made where the effect of absorbance (thickness) is taken into consideration.

An alternative basis for comparison of materials is the film thickness, which is less reported in the literature.[26] For a *thickness basis* to be sensible, the absorption in the bulk should not

introduce degradation. Two different materials with different linear attenuation coefficient would exhibit highly different absorbances if films of identical thicknesses were compared. Thus for this to represent a physically sound model, only the very top part of the material should degrade. This can be understood as the oxygen availability being very limited below the surface, where the bulk of the film will only suffer from negligible photolysis.[27] In this case initially the light only degrades the very top of the film, and gradually the degradation proceeds into the film as the upper parts photobleach.

As for the degradations presented above with an absorbance basis, an analogous analysis can be made by correlation with the material thickness. For each material, linear correlations between the peak absorption value and the film thickness as determined by AFM were established. The parameters for all thickness correlations are given in Table S2† and the individual thickness correlations in Fig. S4 and S5†. This allowed for a direct comparison of polymer degradation rates as a function of the respective film thicknesses (Fig. S6†). Since the thickness correlates linearly with the absorbances, the evolution of degradation rate with film thickness was found to be exponential as in the case of the absorbance basis. Analogous to the absorbance basis all degradation rate correlations were fitted and by division with the degradation rates of regio-regular P3HT, an expression of the relative stability for each polymer compared to regio-regular P3HT was obtained (Fig. 6).

The effect of changing the basis of comparison to a thickness basis changes both the horizontal and vertical positions of the lines. Generally, the variations in the relative stability evolutions are observed to vary to a higher degree than in the case of the absorbance basis, where *e.g.* an order of magnitude of variations is found for PSBTBT and PT. The theoretical absorbances as deduced by AFM thickness correlations for 100 nm films of each polymer show the large deviations in absorption (Table S2†). While regio-regular P3HT lies in the middle of the distribution with an absorbance of 0.59, a similar PT film would have an absorbance of 1.57 and PSBTBT only 0.31. PT and PSBTBT are the extremes in terms of linear attenuation coefficients and these deviations from the linear attenuation coefficient are obviously not handled well by the thickness basis of comparison, where relative stability of PT is found to increase highly with thickness, while the opposite is the case for PSBTBT. Thus it can be concluded that when comparing individual polymers, an absorption basis is considered the best basis of comparison since this allows for comparisons of materials of highly different linear attenuation coefficients.

Stability of electron acceptors

Stability of the single electron acceptors is expected be a function of the oxidation potential and therefore the HOMO level of the acceptor. A high HOMO level is more readily oxidized than a low level, and thus the high HOMO level acceptors are expected to exhibit lower photochemical stabilities. In this discussion the LUMO levels are not considered due to the negligible population relative to the HOMO levels. Photochemical stabilities of electron acceptors were studied in terms of the decrease of their peak absorption in the range of 300–350 nm (Fig. 7). While the solubility of C_{60} in common organic solvents is rather low, functionalization of the fullerene cage may highly increase the solubility.[28] Thus, all acceptors as shown in Fig. 2 were studied in terms of photochemical stability except for C_{60} due to solution processing complications. All acceptors exhibited exponential increases of degradation rates with decreasing absorbance as in the case of single polymers. The stabilities were found to vary by less than a factor of 3, which is significantly lower than the case of the polymers (Fig. 4). $PC_{60}BM$ and $PC_{70}BM$ were found to be approximately three times more stable than the high HOMO acceptors bisPCBM and ICBA, which is in correspondence with their respective HOMO levels.[29]

The electron acceptors were generally found to be more photochemically stable than the polymers, where $PC_{60}BM$ and $PC_{70}BM$ exhibited stabilities one order of magnitude higher than *e.g.* regio-regular P3HT.

Stability of P3HT:electron acceptor blends

The photochemical stability of blends of conjugated polymers and electron acceptors is a topic that has only been briefly discussed in the literature. Rivaton *et al.* evaluated the stabilities of

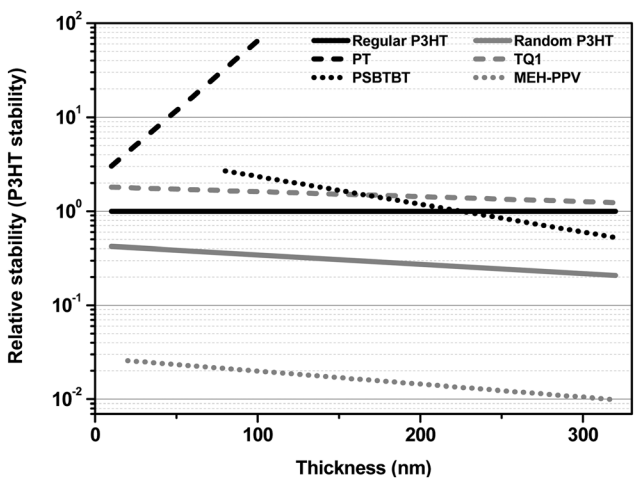

Fig. 6 Thickness resolved degradation rates for different polymers.

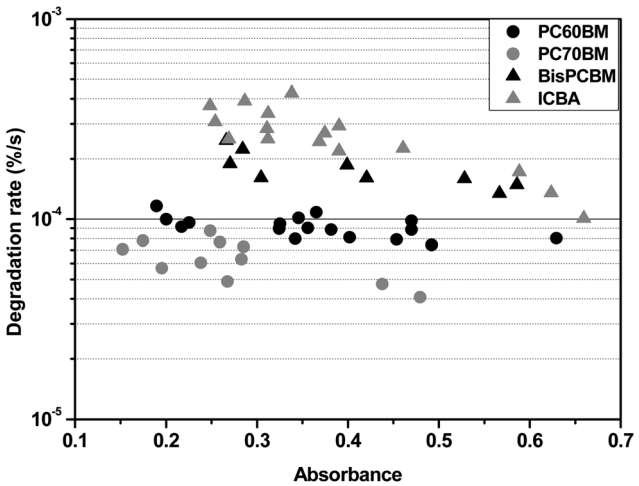

Fig. 7 Absorbance resolved degradation rates of electron acceptors.

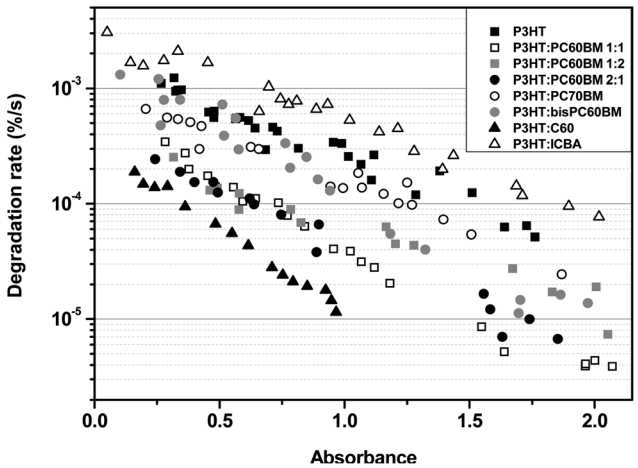

Fig. 8 Absorbance resolved degradation rates for pure regio-regular P3HT blended with different electron acceptors.

regio-regular P3HT and P3HT:$PC_{60}BM$ (1 : 1 ratio) with a thickness basis of comparison, where approximately 200 nm films were compared.[26] In this study a stabilization factor of 8 was found between the polymer and the blend. To make a more thorough comparison of electron acceptors, we have studied five different electron acceptors in conjunction with regio-regular P3HT as well as P3HT:$PC_{60}BM$ in 1 : 1, 1 : 2 and 2 : 1 ratios. Degradation rates were evaluated by integration of the P3HT part of the absorption spectrum (400–600 nm). Degradation of blends generally showed a rapid degradation of the polymer compared to the acceptor as reflected in the respective UV-vis absorption spectra, which is in correspondence with the higher stability of the latter as discussed above.

Degradation rates of all P3HT:electron acceptor combinations as well as pure P3HT compared with an absorbance basis demonstrate a behavior similar to the case for the single polymers and electron acceptors (Fig. 8). All blends show exponential decreases with absorbance (and rather similar slopes on a log scale). Interestingly, the degradation rates are observed to vary with an order of magnitude between the most unstable blend, P3HT:ICBA, and the most stable blend, P3HT:C_{60}. All curves were exponentially fitted and divided by the pure P3HT degradation rate fit to obtain the stabilization of P3HT by incorporation of an electron acceptor (Fig. 9). All relative stability curves were found to increase slightly with absorbance. The reason for this is the steeper slope of the degradation rate correlation with absorbance for P3HT than for the blends. The largest variation in relative stability was observed for P3HT:$PC_{60}BM$ (1 : 1 ratio) where the value increased from 3 to 10 with increasing absorbance. A thickness basis was also applied to the degradation rates (Fig. S7†) and by division of the P3HT degradation rates, the relative stabilities from a thickness basis were evaluated (Fig. S8†). Due to the higher linear attenuation coefficient at the peak absorbance for pure P3HT (approximately 530 nm) when compared to the blends, absorption and thickness bases are expected to provide highly different results. Indeed this is the case for the relative stabilities for the thickness basis, where all relative stabilities are found to decrease with thickness. Generally, larger fluctuations are observed when applying the thickness basis than in the case of the absorbance basis, where *e.g.* for the different blend ratios of P3HT:$PC_{60}BM$ the 2 : 1 ratio displays a significantly higher stability than the 1 : 1 and 1 : 2 ratios, which is counterintuitive. Based on these conclusions, the more suitable basis of comparison of a pure polymer and its respective blends with different electron acceptors is an absorbance basis.

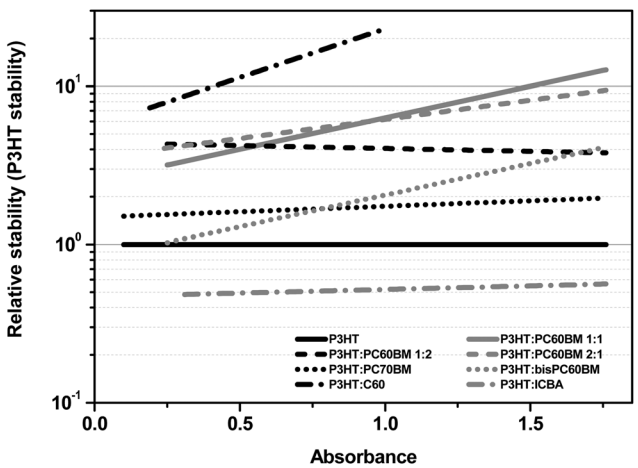

Fig. 9 Absorbance resolved relative stabilities for blends consisting of P3HT and different electrons.

The photochemical stabilities of blends based on a conjugated polymer and different electron acceptors have not been reported in the literature. Nevertheless, significant variations in relative stabilities are observed for the different electron acceptors with C_{60} stabilizing by a factor of approximately 10 while ICBA is observed to destabilize the blend by a factor of 2. The stabilization correlations for the $PC_{60}BM$ blends of different ratios are observed to exhibit intersections in the absorbance range of 0.35–0.8 within which they all exhibit highly similar stabilizations. This is in accordance to expectations, since these blends consist of a highly intimate mixing of the donor and acceptor and therefore no significant variations in acceptor stabilization are expected. However, at higher absorbances, the 1 : 2 blend is less stable, which is counterintuitive since the higher content of $PC_{60}BM$ is expected to induce a higher photochemical stability. Consequently, it appears that sound conclusions on stabilization by electron acceptors should be based on the lower absorbance range (below 0.8). An additional argument for using an absorption basis for the lower absorbance range is that photoactive materials for solar cells are intended to be applied as films that are sufficiently thick to absorb the greater proportion of the incoming light while being sufficiently thin to enable extraction of carriers. For most active layers this equates to film absorptions in this range.

The relative stabilities of the different P3HT:acceptor blends demonstrate the same stability ranking as observed for the pure electron acceptors, however with higher variations. An unstable high HOMO acceptor that degrades significantly within the lifetime of the polymer will decrease the efficiency of the charge transfer of the excited state from the polymer to the acceptor for a given donor–acceptor blend. However, due to the generally higher stabilities of the electron acceptors compared to regio-regular P3HT, this effect is not pronounced. Another effect introduced is the charge transfer efficiency for the different

donor–acceptor blends. It is generally accepted that the excited state of P3HT is efficiently quenched by fullerenes and its derivatives through a charge transfer from the P3HT to the photochemically stable fullerene.[30,31] Extensive attention is directed at developing electron acceptors with lower donor–acceptor LUMO–LUMO gap than for the commonly used $PC_{60}BM$ to increase the open circuit voltage (V_{oc}) of PSC.[32–34] However, the impact of such a decrease in the electron affinity of the acceptor ultimately implies different charge transfer kinetics between the donor and the acceptor. With a higher LUMO level of the acceptor the statistical distribution between excited states on the donor and the acceptor is moved in the direction of the donor. As excited states are prone to photodegradation, the overall effect is a decreased photochemical stability. In the literature there are no reports on the LUMO levels of all the electron acceptors studied in this work. By direct comparison between LUMO levels of the individual electron acceptors, large variations are found, which originate from different cyclic voltammetry setups. An indirect approach to assessment of the LUMO levels is by inspection of the V_{oc} obtained for optimized PSCs applying P3HT and the different electron acceptors.[32] The typical V_{oc} values for regio-regular P3HT and different electron acceptors are (C_{60}) 0.40 V,[35] ($PC_{70}BM$) 0.63 V,[36] ($PC_{60}BM$) 0.65 V,[37] (bisPCBM) 0.73 V,[33] and (ICBA) 0.87.[38] The ranking of the V_{oc} was found to be consistent with individual studies of LUMO levels of typically $PC_{60}BM$ and another fullerene derivative.[33,39,40]

The magnitude of the stabilization of P3HT by the electron acceptor is observed to correlate clearly with the LUMO–LUMO gap in the low absorbance range. A ranking of decreasing stabilization of C_{60}, $PC_{60}BM$, $PC_{70}BM$, bisPCBM, and ICBA is found, which is in clear correspondence with a decreasing LUMO–LUMO gap or increasing V_{oc} of the corresponding PSCs. Only $PC_{60}BM$ and $PC_{70}BM$ do not clearly fulfil this principle since their LUMO–LUMO levels are similar. However, stability of pure $PC_{70}BM$ was found to slightly exceed the one of $PC_{60}BM$, which may explain the deviation from the LUMO–LUMO gap correlation. Additionally, other factors such as morphology and phase segregation may play a role; see the section *Outlook & Perspectives* for further discussion. Overall, this result demonstrates the increasing thermodynamic tendency of increasing the population of excited states on the P3HT relative to the acceptor, thus implying a higher degradation rate. For this reason, the application of ICBA in PSCs to obtain 6.5% efficiency[38] introduces a significant decrease in photochemical stability that in turn will affect the operational device lifetime.

Stability of polymer:$PC_{60}BM$ blends

For each of the studied polymers, their respective blends in a ratio of 1 : 1 with $PC_{60}BM$ were studied. Degradation rates of the decrease of the respective polymer contribution to the UV-visible absorption were evaluated as a function of peak absorbance of the polymer transition (Fig. S9†) and thickness (Fig. S10†). No major differences are observed between the absorbance and the thickness plots, where primarily PT:$PC_{60}BM$ is shifted due to the higher optical density, however to a lesser extent than in the case of the pure polymers due to the $PC_{60}BM$ content. To evaluate the relative stabilities, P3HT:$PC_{60}BM$ is applied as the reference to which remaining blends are compared. The shift of the optically dense PT introduces a difference in relative stability from around 4 with an absorbance basis (Fig. 10) to around 8 with a thickness basis (Fig. S11†), while the low linear attenuation coefficient of blend PSBTBT:$PC_{60}BM$ changes from 3 to 2. This demonstrates the sensitivity of the method toward the basis of comparison where two polymers of similar stability are found to exhibit highly different blend stabilities with the two bases of comparison.

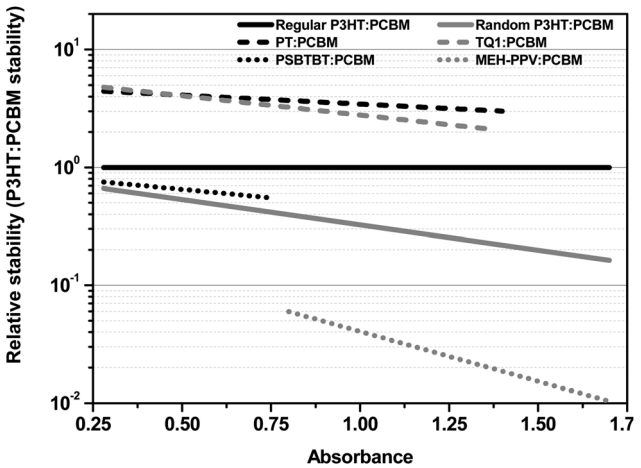

Fig. 10 Absorbance resolved stabilities in units of P3HT:$PC_{60}BM$ stability of blends based on different polymers and $PC_{60}BM$.

The best consistency between the observed polymer and blend relative stabilities is found for the absorbance basis. Additionally, less variation with absorbance/thickness is observed, and thus an absorbance basis is regarded the best basis of comparison for different blends. The relative stabilities of the blends were found to be similar to the case of the single polymers. However PSBTBT demonstrates a deviating behavior, where the material is observed to destabilize by the introduction of $PC_{60}BM$, which is in contradiction to all the other studied polymers. This effect may be attributed to microscopic properties such as morphology,

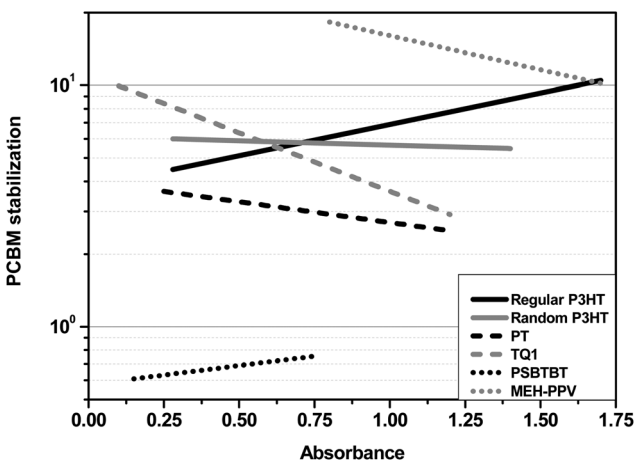

Fig. 11 Absorbance resolved photochemical stabilization of different polymers by introduction of $PC_{60}BM$.

phase segregation, *etc.*, as discussed in the section *Outlook and Perspectives*.

Absorbance resolved $PC_{60}BM$ stabilization of the different polymers was evaluated as the ratio between the degradation rate of the blend and the single polymers (Fig. 11). Fluctuations in the stabilization curves of both positive and negative slopes are observed and both TQ1, regio-regular and regio-random P3HT are observed to intersect around an absorbance of 0.75. However, these results are based on a combination of degradation rates of the single polymers and their respective blends, both of which are affected by uncertainties in the method, and thus their quotient is expected to be further impacted. The general expectation is that a highly unstable material should benefit highly from being blended with $PC_{60}BM$, since each excitation has a large possibility of leading to a degradation event, while for a highly stable material this effect is less pronounced. This is indeed the tendency observed, where the unstable MEH-PPV is highly stabilized by a factor of around 15, while the stable PT is only stabilized by a factor 3. Additionally, PSBTBT is found to destabilize slightly by a factor of 0.3. A destabilization is expected if the polymer is comparable or more photochemically stable than the electron acceptor. This is the case for PSBTBT, where for absorbances above 1, the polymer stability even exceeds the stability of $PC_{60}BM$. For this material combination a charge transfer to $PC_{60}BM$ will induce a larger degradation rate than by keeping the excited electron on the pure polymer. This demonstrates how the photochemical advantage well-known for *e.g.* regio-regular P3HT of blending with $PC_{60}BM$ is found to decrease with more stable polymers, where even destabilizations are introduced.

Outlook and perspectives

This work presents a systematic study of the influence of absorbance and electron acceptor on the photochemical stability of conjugated polymers. It was shown that the relative stabilities of different polymers could only be qualitatively assessed from single thicknesses, since they were found to vary with absorbance. However, attention in the processing was not given to obtain *e.g.* identical morphology, phase segregation, and crystallinity, which are parameters that are expected to influence stability. Photochemical stability testing of polymers appears as a general tool robust enough to establish a stability ranking of the different materials without a specific focus on the control of these parameters. However, in order to understand the mechanisms behind the observed behavior and the variations in relative stabilities with absorbance, detailed studies of several parameters are needed. Parameters that are prone to influence photochemical degradation rates are *e.g.*:

- Morphology
- Kinetics
- Reactant solubility
- Vertical segregation
- Exciton diffusion length

The stability is expected to change as a function of the morphology for both the pure polymers as well as for the blends as a function of solvent, processing method, temperature, humidity, *etc.* Additionally, the impact of these parameters is expected to vary with the material type thus making up a large parameter space. The solubility of the degradation reactant (typically oxygen) and the kinetics of the diffusion of oxygen differ for each material thus influencing the degradation rates for different film thicknesses. Additionally, vertical segregation of P3HT:$PC_{60}BM$ has been observed to vary highly with the processing method and substrate. Finally, the exciton diffusion length may vary for different material systems, which influences the dependence of domain size on photochemical stability. Consequently, obtaining an understanding of the underlying mechanisms demands for further work on *e.g.* regio-regular P3HT where the impact of these above mentioned parameters are studied. Additionally, in order to obtain a higher precision of the relative stabilities of different polymers by photochemical stability testing, a more thorough study of each material and the above described parameters is needed. By this, better estimations of the actual material stabilities can be given thus increasing the precision of the technique.

Conclusions

A novel photochemical stability assessment platform was presented by which degradation of organic materials can be evaluated with high precision. In this work, the technique has been applied to stability studies of electron donors and acceptors relevant to PSC. Photochemical stabilities of six different polymers and 5 different electron acceptors demonstrated a strong increase of degradation rates with film absorbances. This is important for comparative studies where the absorbance has to be kept constant for all materials being studied to provide a basis for valid conclusions on relative stabilities. The validity of estimating a material stability based on a single measurement at a single absorbance is considered doubtful. We believe that only by studying a wide absorbance range for all studied samples can a sound estimation of relative stabilities be obtained. The precision of this estimation was also found to depend on the basis of comparison, where an absorbance basis was considered the best choice for all studied material combinations. Since this model is a simplified version of the real world, uncertainties are introduced into the stability evaluation. Consequently, our conclusion is that only sound relative stabilities are given in no less than factors of five if only a single degradation of each material has been performed. However, with these precautions in mind, photochemical degradation as a stability evaluation tool is found to be a powerful tool to obtain estimates of relative stabilities of conjugated polymers, electron acceptors, and blends relevant to PSCs.

Acknowledgements

This work was supported by the Danish Strategic Research Council (2104-07-0022), EUDP (j. no. 64009-0050) and PV-ERA-NET (project acronym POLYSTAR).

References

1 M. Helgesen, R. Søndergaard and F. C. Krebs, Advanced materials and processes for polymer solar cell devices, *J. Mater. Chem.*, 2010, **20**, 36.
2 G. Dennler, M. C. Scharber and C. J. Brabec, Polymer–fullerene bulk-heterojunction solar cells, *Adv. Mater.*, 2009, **21**, 1323–1338.

3 F. C. Krebs, T. Tromholt and M. Jørgensen, Upscaling of polymer solar cell fabrication using full roll-to-roll processing, *Nanoscale*, 2010, **2**, 873–886.
4 R. F. Service, Outlook brightens for plastic solar cells, *Science News & Analysis*, 2011, **332**, 293.
5 M. Jørgensen, K. Norrman and F. C. Krebs, Stability/degradation of polymer solar cells, *Sol. Energy Mater. Sol. Cells*, 2008, **92**, 686–714.
6 S. Beaupré, P.-L. T. Boudreault and M. Leclerc, Solar-energy production and energy-efficient lighting: photovoltaic devices and white-light-emitting diodes using poly(2,7-fluorene), poly(2,7-carbazole), and poly(2,7-dibenzosilole) derivatives, *Adv. Mater.*, 2010, **22**, E6–E27.
7 P. A. Troshin, *et al.*, Impedance measurements as a simple tool to control the quality of conjugated polymers designed for photovoltaic applications, *Adv. Funct. Mater.*, 2010, **20**, 4351–4357.
8 K. Norrman, M. V. Madsen, S. A. Gevorgyan and F. C. Krebs, Degradation patterns in water and oxygen of an inverted polymer solar cell, *J. Am. Chem. Soc.*, 2010, **132**, 16883–16892.
9 E. Vitoratos, *et al.*, Thermal degradation mechanisms of PEDOT:PSS, *Org. Electron.*, 2009, **10**, 61–66.
10 T. Tromholt, A. Manor, E. A. Katz and F. C. Krebs, Reversible degradation of inverted organic solar cells by concentrated sunlight, *Nanotechnology*, 2011, **22**, 225401.
11 S. Bertho, *et al.*, Effect of temperature on the morphological and photovoltaic stability of bulk heterojunction polymer:fullerene solar cells, *Sol. Energy Mater. Sol. Cells*, 2008, **92**, 753–760.
12 P. J. Goutam, D. K. Singh, P. K. Giri and P. K. Iyer, Enhancing the photostability of poly(3-hexylthiophene) by preparing composites with multiwalled carbon nanotubes, *J. Phys. Chem. B*, 2011, **115**, 919–924.
13 H. Hintz, *et al.*, Photodegradation of P3HT—a systematic study of environmental factors, *Chem. Mater.*, 2010, **23**, 145–154.
14 M. Manceau, *et al.*, Photochemical stability of π-conjugated polymers for polymer solar cells: a rule of thumb, *J. Mater. Chem.*, 2011, **21**, 4132–4141.
15 S. Schuller, P. Schilinsky, J. Hauch and C. J. Brabec, Determination of the degradation constant of bulk heterojunction solar cells by accelerated lifetime measurements, *Appl. Phys. A: Mater. Sci. Process.*, 2004, **79**, 37–40.
16 J. E. Carlé, *et al.*, Fused thiophene/quinoxaline low band gap polymers for photovoltaic's with increased photochemical stability, *Sol. Energy Mater. Sol. Cells*, 2011, **95**, 3222–3226.
17 E. Wang, *et al.*, An easily synthesized blue polymer for high-performance polymer solar cells, *Adv. Mater.*, 2010, **22**, 5240–5244.
18 *Polymer Photovoltaics—A Practical Approach*, Ed. F. C. Krebs, SPIE, Bellingham, 2008.
19 J. Hou, H.-Y. Chen, S. Zhang, G. Li and Y. Yang, Synthesis, characterization, and photovoltaic properties of a low band gap polymer based on silole-containing polythiophenes and 2,1,3-benzothiadiazole, *J. Am. Chem. Soc.*, 2008, **130**, 16144–16145.
20 M. Bjerring, J. S. Nielsen, N. C. Nielsen and F. C. Krebs, Polythiophene by solution processing, *Macromolecules*, 2007, **40**, 6012–6013.
21 T. Tromholt, S. A. Gevorgyan, M. Jørgensen, F. C. Krebs and K. O. Sylvester-Hvid, Thermocleavable materials for polymer solar cells with high open circuit voltage-a comparative study, *ACS Appl. Mater. Interfaces*, 2009, **1**, 2768–2777.
22 M. Manceau, M. Helgesen and F. C. Krebs, Thermo-cleavable polymers: materials with enhanced photochemical stability, *Polym. Degrad. Stab.*, 2010, **95**, 2666–2669.
23 K. O. Sylvester-Hvid, *et al.*, Non-destructive lateral mapping of the thickness of the photoactive layer in polymer based solar cells, *Prog. Photovoltaics*, 2011, DOI: 10.1002/pip.1190.
24 T. Tromholt, M. Manceau, M. Helgesen, J. E. Carlé and F. C. Krebs, Degradation of semiconducting polymers by concentrated sunlight, *Sol. Energy Mater. Sol. Cells*, 2010, **95**, 1308–1314.
25 M. V. Madsen, *et al.*, Ellipsometry as a nondestructive depth profiling tool for roll-to-roll manufactured flexible solar cells, *J. Phys. Chem. C*, 2011, **115**, 10817–10822.
26 A. Rivaton, *et al.*, Light-induced degradation of the active layer of polymer-based solar cells, *Polym. Degrad. Stab.*, 2010, **95**, 278–284.
27 M. Manceau, *et al.*, Effects of long-term UV-visible light irradiation in the absence of oxygen on P3HT and P3HT:PCBM blend, *Sol. Energy Mater. Sol. Cells*, 2010, **94**, 1572–1577.
28 P. A. Troshin, *et al.*, Material solubility-photovoltaic performance relationship in the design of novel fullerene derivatives for bulk heterojunction solar cells, *Adv. Funct. Mater.*, 2009, **19**, 779–788.
29 Y. He, G. Zhao, B. Peng and Y. Li, High-yield synthesis and electrochemical and photovoltaic properties of Indene-C70 bisadduct, *Adv. Funct. Mater.*, 2010, **20**, 3383–3389.
30 M. O. Reese, *et al.*, Photoinduced degradation of polymer and polymer–fullerene active layers: experiment and theory, *Adv. Funct. Mater.*, 2010, **20**, 3476–3483.
31 J. Piris, *et al.*, Photogeneration and ultrafast dynamics of excitons and charges in P3HT/PCBM blends, *J. Phys. Chem. C*, 2009, **113**, 14500–14506.
32 F. B. Kooistra, *et al.*, Increasing the open circuit voltage of bulk-heterojunction solar cells by raising the LUMO level of the acceptor, *Org. Lett.*, 2007, **9**, 551–554.
33 M. Lenes, *et al.*, Fullerene bisadducts for enhanced open-circuit voltages and efficiencies in polymer solar cells, *Adv. Mater.*, 2008, **20**, 2116–2119.
34 Y. He and Y. Li, Fullerene derivative acceptors for high performance polymer solar cells, *Phys. Chem. Chem. Phys.*, 2011, **13**, 1970–1983.
35 I. R. Gearba, C.-Y. Nam, R. Pindak and C. T. Black, Thermal crosslinking of organic semiconducting polythiophene improves transverse hole conductivity, *Appl. Phys. Lett.*, 2009, **95**, 173307.
36 J. Y. Kim, *et al.*, Efficient tandem polymer solar cells fabricated by all-solution processing, *Science*, 2007, **317**, 222–225.
37 M. Reyes-Reyes, K. Kim and D. L. Carroll, High-efficiency photovoltaic devices based on annealed poly(3-hexylthiophene) and 1-(3-methoxycarbonyl)-propyl-1-phenyl-(6,6)C[61] blends, *Appl. Phys. Lett.*, 2005, **87**, 083506.
38 G. Zhao, Y. He and Y. Li, 6.5% Efficiency of polymer solar cells based on poly(3-hexylthiophene) and indene-C(60) bisadduct by device optimization, *Adv. Mater.*, 2010, **22**, 4355–4358.
39 Z.-L. Guan, J. Bok Kim, Y.-L. Loo and A. Kahn, Electronic structure of the poly(3-hexylthiophene):indene-C60 bisadduct bulk heterojunction, *J. Appl. Phys.*, 2011, **110**, 043719.
40 D. Mühlbacher, *et al.*, High photovoltaic performance of a low-bandgap polymer, *Adv. Mater.*, 2006, **18**, 2884–2889.

Elsevier Editorial System(tm) for Polymer Degradation and Stability
Manuscript Draft

Manuscript Number: PDST-D-12-00383

Title: Influence of processing and intrinsic polymer parameters on photochemical stability of polythiophene thin films

Article Type: Research Paper

Keywords: P3HT, photooxidation, organic photovoltaics, photo-chemical stability, degradation

Corresponding Author: Mr. Morten Vesterager Madsen,

Corresponding Author's Institution: DTU

First Author: Morten V Madsen

Order of Authors: Morten V Madsen; Thomas Tromholt; Arvid Böttiger; Jens W Andreasen; Kion Norrman; Frederik C Krebs

Abstract: Intrinsic polymer parameters such as regio-regularity, molecular weight, and crystallinity play an important role when studying polymer stability. 18 different batches of poly-3-hexyl-thiophene (P3HT) were degraded in a solar simulator (AM1.5G, 1000 W/m2) and the degradation kinetics were monitored. The results suggest that the radical reaction responsible for the photodegradation takes place at terminal thiophene rings exposed at points were the conjugation is broken. This proposed mechanism is supported by the fact that stability scales with regio-regularity following the ratio of head-to-tail connected thiophene units. Annealing was found to relax the P3HT films and increase conjugation length and, in turn, increase stability observed as a delayed spectral blueshift caused by photochemical degradation. Crystallinity was found to play a minor role in terms of stability. Oxygen diffusion and light shielding effects were shown to have a negligible effect on the photochemical degradation rate. The results obtained in this work advance the understanding of polymer stability and will help improve the design of materials used for polymer solar cells resulting in longer lifetimes, which will push the technology closer to large-scale applications.

Suggested Reviewers: Agnés Rivaton
agnes.rivaton@univ-bpclermont.fr

Monica Lira-Cantu
monica.lira@cin2.es

Holger Hintz
holger.hintz@uni-tuebingen.de

Matthieu Manceau
matthieu.manceau@cea.fr

Appendix 2

Submission of manuscript to the Polymer Degradation and Stability

I hereby request the manuscript entitled “Influence of processing and intrinsic polymer parameters on photochemical stability of polythiophene thin films” to be published in the Polymer Degradation and Stability. The work presented in the manuscript is within the area of polymer degradation aimed specifically at organic solar cells.

Best regards,

Morten Vesterager Madsen
PhD
Functional Organic Materials
Direct Phone +45 46 77 47 01
Cell +45 22 21 67 47
mves@risoe.dtu.dk

Influence of processing and intrinsic polymer parameters on photochemical stability of polythiophene thin films

Morten V. Madsen*, Thomas Tromholt, Arvid Böttiger, Jens W. Andreasen, Kion Norrman and Frederik C. Krebs

Department of Energy Conversion and Storage, Technical University of Denmark, Frederiksborgvej 399, DK-4000 Roskilde, Denmark

*Email: mves@dtu.dk

Abstract

Intrinsic polymer parameters such as regio-regularity, molecular weight, and crystallinity play an important role when studying polymer stability. 18 different batches of poly-3-hexyl-thiophene (P3HT) were degraded in a solar simulator (AM1.5G, 1000 W/m^2) and the degradation kinetics were monitored. The results suggest that the radical reaction responsible for the photodegradation takes place at terminal thiophene rings exposed at points were the conjugation is broken. This proposed mechanism is supported by the fact that stability scales with regio-regularity following the ratio of head-to-tail connected thiophene units. Annealing was found to relax the P3HT films and increase conjugation length and, in turn, increase stability observed as a delayed spectral blueshift caused by photochemical degradation. Crystallinity was found to play a minor role in terms of stability. Oxygen diffusion and light shielding effects were shown to have a negligible effect on the photochemical degradation rate. The results obtained in this work advance the understanding of polymer stability and will help improve the design of materials used for polymer solar cells resulting in longer lifetimes, which will push the technology closer to large-scale applications.

Keywords

P3HT, photooxidation, organic photovoltaics, photo-chemical stability, degradation

Introduction

The field of polymer solar cells (PSC) is growing fast, manifested in an exponential increase in publications.[1] The technology has reached a point where focus has shifted to application, demonstration and commercialization. The technology combines low cost, flexibility, and fast processability well-suited for large scale production that, in turn, will constitute a strong alternative to energy production. State-of-the-art in terms of efficiency has been reported to have increased to above 10% for small area laboratory devices.[2,3] Large scale production based on roll-to-roll techniques is now possible and production of 10.000 units has been demonstrated.[4] However, limited lifetime of the devices is still an issue and it is thus crucial to be able to both characterize and understand the different degradation mechanisms responsible for the performance deterioration of PSCs. It is well-known

that several aspects affect the final lifetime of the device including stability of the morphology, oxygen, and water diffusion, and polymer photo degradation.[5,6] The exact nature of the degradation mechanisms depends on the specific materials used in the multilayer stack of the solar cell. Consequently, when studying the overall PSC device stability, the actual stability of each layer cannot be deduced. Specifically, the stability of the photo-active layer is highly important since this layer accommodates the free charge carrier generation. Evaluation of the stability of this layer is therefore paramount to overcome the issue of lifetime for PSC. The evaluation of polymer photo-chemical stability using primarily UV-vis spectroscopy is an emerging field as documented by a number of recent reports on comparative studies. Manceau et al. reported a study involving 20 different polymers from which relative stabilities of an extensive range of functional groups were established.[7] In an extensive material screening by Tromholt et al. material stabilities were also resolved in terms of the optical density of the samples. [8] Exponential increases of stability were observed for all materials and it was concluded that identical optical densities are needed when comparing stabilities between different materials.

This paper focuses solely on the intrinsic photo-chemical stability of the well-known conjugated polymer poly-3-hexyl-thiophene (P3HT). Degradation of P3HT is well-documented and can be facilitated by exposure to light and molecular oxygen that destroys the π–conjugation and consequently induces loss of absorption. P3HT is degraded under these conditions in solution as well as a solid (e.g. a film). The consequence of degradation is well-established but the mechanism responsible for it has been subject to discussion. Whereas singlet oxygen is known to be the cause of degradation in solution,[9] the degradation mechanism in the solid state is believed to be different. Manceau et al. have proposed a degradation mechanism based on a radical process beginning from an abstraction of an allylic hydrogen, leading to side-chain and sulfur oxidation.[10,11] This process is responsible for breaking the macromolecular backbone resulting in loss of conjugation and consequent bleaching of the sample. This mechanism occurs under both photo- and thermal oxidation enforcing the notion that singlet oxygen is not the main intermediate in the degradation process. Hintz et al. have conjectured that the polymer is mainly attacked at the terminal thiophene rings under photo-oxidation.[12] The authors concluded this from observing the kinetics of the blueshift in the optical absorption. They observed that the blueshift, indicating loss of conjugation (observed for oligomers with less than 20 thiophene units), is not observed until the end of the degradation of the polymer. Hintz et al. have also demonstrated that a strong increase in photon effectiveness is observed for photo-degradation of P3HT films for decreasing irradiation wavelengths.[13] Changing the illumination wavelength from 554 to 335 nm leads to an increase by a factor of 50 in effectiveness of the P3HT photo-oxidation. This observation supports the radical chain mechanism driven by photo-generation of radicals by the photolysis of precursors absorbing in the UV-region.

The absolute stability of polymers is known to be affected by degradation parameters such as light spectrum, room temperature, ozone level, and humidity. Thus, direct comparisons of absolute stabilities assessed with different degradation setups in different laboratories are not straightforward. To reduce influence of different degradation parameters in photo-chemical stability reports, material stabilities are normally expressed in units of

stability of a reference material of well-known stability, typically P3HT. However, this assumes that P3HT presents an intrinsic, constant stability that is independent of synthesis routes, regio-regularity (RR), molecular weight, molecular weight distribution, crystallinity etc. The overall effect is that the material stabilities expressed in units of P3HT stability as reported in the literature may be associated with significant uncertainty. Furthermore, until now, development of stable conjugated polymers for PSCs has been focused on the stability of the different functional groups used for the synthesis. However, understanding the influence of the above described intrinsic polymer properties on the photo-chemical stability is highly appealing, since this will provide a new set of tools when designing novel materials for PSCs.

In this report we describe the influence of the intrinsic polymer properties on the photo-chemical stability of P3HT. This involves 18 different batches of P3HT from different manufacturers and batches made in house. P3HT polymers with significantly different M_w and RR are studied. The effect of inducing crystallinity by thermal annealing is reported by studying stabilities for different annealing temperatures. Furthermore, the degradation kinetics is studied for films of different thicknesses, which allows for studying the influence of light shielding and oxygen availability in the film.

Experimental

Degradation Setup and Data Evaluation

A fully automated, high-throughput photo-chemical degradation setup was used for the degradation of all materials in this study as described elsewhere.[12] The setup utilized a Steuernagel solar simulator with an Osram 1200 W metal halide arc lamp providing an approximate AM1.5G spectrum with an intensity of 1000 W/m^2. The sample exchanger had a capacity of 22 samples and a UV-vis spectroscopic probe based on an optical fiber-based CCD spectrometer (Avantes AvaSpec 1024) and a halogen/deuterium light source (Avantes AvaLight-DHc) are used to measure the evolution in the absorbance of the samples. For this study, the setup was programmed to monitor 28 degradation points per sample. A fully loaded sample exchanger with 22 samples consequently monitors 616 degradation points in parallel. A C# based automated software infrastructure was established to handle the high number of data files. To avoid spectral shielding from the substrate, illumination was always performed from the polymer side.

Degradation rates were extracted from the rate of decrease of the calculated total number of absorbed photons per second as absorbed by the polymer when the recorded absorption spectrum is folded with a theoretical AM1.5G solar spectrum as described in reference 13. We observed that plotting the rate of number of absorbed photons as a function of initial absorption maximum yields a constant value for a broad interval from 0.4 to 1 in absorbance, see Figure 1. The ordinate axis in this plot is dependent on the choice of integration range and therefore the same integration range (400 – 600 nm) has been used for all materials. It was thus possible to run a large number of degradation experiments for different polymers and compare their stablities while the effect of thickness was cancelled. This behaviour has been observed for P3HT, poly(5-methoxy-2-(2-ethyl-hexyloxy)phenylenevinylene] (MEH-PPV), and polythiophene (PT). Normalized degradation rates in all

comparisons are given in units of the stability of the polymer designated R1, see Table 1. Consequently, values below 1 describe polymers more stable than R1 and values above 1 describe polymers less stable.

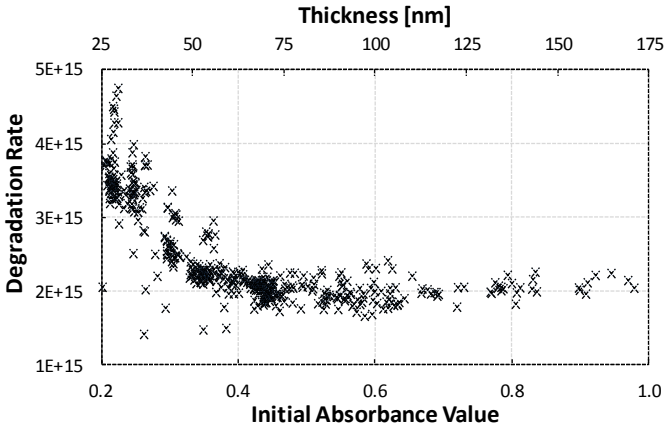

Figure 1. Rate of change in number of absorbed photons as a function of initial absorbance value and thickness.

Using degradation rates based on loss of absorbance directly allows for correlating the degradation state to the number of intact monomer units. The number of monomers scales directly with the absorbance, and thus the degradation state can be written as

$$D_{state} = \frac{N_{Monomer}}{N_{initial}} = \frac{A}{A_{initial}},$$

where $N_{initial}$ is the initial number of monomers, $A_{initial}$ and A is the initial and current absorbance respectively. The number of monomers at a given time during degradation can be expressed by

$$N_{Monomer} = \frac{N_A \rho}{M} t \cdot D_{state},$$

where N_A is Avogadro's number, ρ is the polymer density, M is the molar mass, and t is the film thickness. According to the Lambert-Beer law, the thickness of the film scales with the absorbance. Using the absorption to thickness conversion presented in reference 12 for regio-regular P3HT, the film thickness can be expressed by $t = (A_{\max} - 0.622) \cdot 188.68$ nm, where $A_{\max}$ is the peak absorbance. The density was determined to be $\rho = 1.07\, g/cm^2$ by X-ray reflectometry for polymer R2. The molar mass of the P3HT monomer is $M = 166.3\, g/mol$. The reciprocal rate of monomer loss yields the degradation event interval,

$$\tau = \left(\frac{dN_{Monomer}}{dt} \right)^{-1}.$$

NMR

^{1}H NMR was used to determine the regio-regularity of P3HT in deuterated chloroform solution. For P3HT the regio-regularity is determined as the ratio between the signal at 2.8 ppm, originating from the preferred head-to-tail connected monomers, and the signal at 2.6 ppm being associated with the head-to-head coupled monomers.

X-ray diffraction

X-ray diffraction was used to quantify the crystallinity of annealed films. The position of the P3HT *100* reflection was determined by a specular scan using a dedicated reflectometry setup, with a rotating Cu anode as source, operating at 50 kV, 200 mA. The X-ray beam is monochromatized (λ = 1.5418 Å) and collimated by a 1D multilayer optic and the beam is further collimated by incident and diffracted beam slits.

With a point detector positioned at the diffracted beam angle (2θ) for the *100* reflection, rocking scans were recorded by rotating the sample from incidence angle zero to 2θ. The integrated intensity, less background, was used as a measure of the polymer crystallinity.

Materials

P3HT films were spin-coated on microscopy slides obtained from Menzel from 12 mg/mL chlorobenzene solutions. 18 different batches of P3HT from different manufactures as well as in-house manufactured batches were studied. For each batch the manufacturer, the batch number and an abbreviation have been indicated in Table 1. The regio-regularity was measured by ^{1}H NMR.

Code	**Manufacturer**	**Batch**	**RR**
M1	Merck	EE-97802	94.8%
M2	Merck	EE-99202	94.0%
M3	Merck	EE-101702	95.8%
M4	Merck	EE-99120	93.0%
R1	Rieke Metals	PTL 10-87	91.7%
R2	Rieke Metals	BS19-60A	-
R3	Rieke Metals	BS16-24	92.1%
B1	BASF	GK-2126-108	96.8%
B2	BASF	GK-2566/77	93.7%
B3	BASF	2010_A6-7	94.6%
P1	Plextronics	11-11822	96.0%
P2	Plextronics	P04205	96.0%

P3	Plextronics	PO2122	91.6%
P4	Plextronics	PO4054	95.1%
D1	DTU (in house)	McCullough route, chloroform fraction[15]	96.1%
D2	DTU (in house)	McCullough route, hexane fraction[15]	96.0%
D3	DTU (in house)	Method B, Soxhlet purified[15]	76.2%
D4	DTU (in house)	Method A, Soxhlet purified[15]	76.1%

Table 1. The 18 different samples of P3HT studied. The manufacturers and their batch numbers have been stated as well as the abbreviations used. The regio-regularity has been determined using ^{1}H NMR. R2 was not measured by NMR as the polymer had been depleted.

Results and discussion

Figure 2 shows the relative stabilities expressed as normalized rate of degradation of the 18 different polymers in units of R1, evaluated as described in the experimental section. The polymers are grouped according to manufacturer; D is DTU in-house synthesized batches of P3HT, M are commercial P3HT polymers from Merck, R from Rieke Metals, B from BASF, and P from Plextronics. The complete list of polymers is shown in Table 1. The polymers D3 and D4 are regio-random P3HT polymers, while the rest are regio-regular to different degrees. While all regio-regular P3HT polymers exhibit relative degradation rates close to 1, the regio-random polymers are significantly less stable exceeding relative degradation rates of 2. This is consistent with the work by Hintz *et al.* where an increase in degradation rate by a factor of five was observed, in fair agreement with the factor of three observed on average in this work.[10]

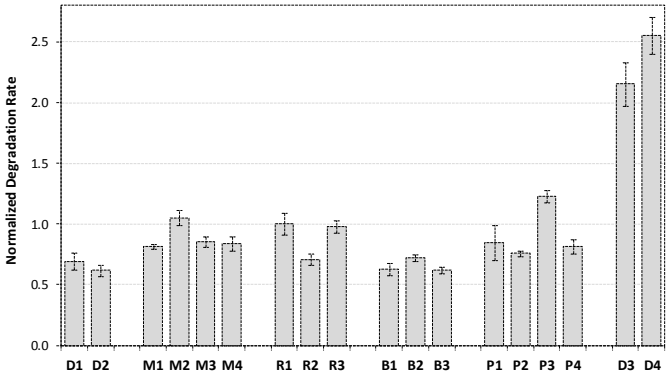

Figure 2 Degradation rates normalized to the value of R1. For each polymer a minimum of three samples with 28 sample points each, were monitored for the full degradation. The error bars indicate the standard deviation.

While the regio-regularity clearly affects the stability of the polymer, the molecular weight seems to have no significant effect, which becomes evident when comparing the polymer D2 that has a particularly low molecular weight (M_n = 2.8 kDa), with the polymer D1 that has a significantly higher molecular weight (M_n = 17.3 kDa). Both polymers have similar regio-regularities close to 96% and clearly have identical degradation rates (Figure 2) if the error bars are considered. This suggests that molecular weight has either no or a negligible influence on the degradation rate. Indeed plotting the normalized degradation rate against the number average molecular weight (not shown) reveals that no correlation is present. It can thus be concluded that the length of the polymer chain is much less important than the conjugation length. However, for very low molecular weights this is probably not true, but is at least valid for polymers with M_n above 2.8 kDa as shown in this work. It therefore seems that the regio-regularity is the major dominating factor on the stability of the polymer.

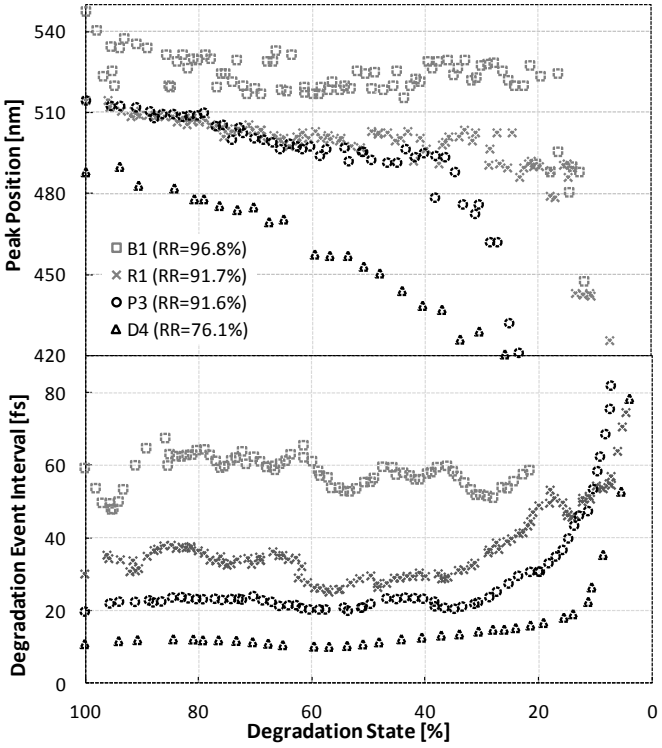

Figure 3. (Top) Absorption peak position as a function of degradation state. (Bottom) Degradation event interval plotted against degradation state. All data is based on polymer films of 140 nm thickness.

Reaction kinetics are indicative of the underlying reaction mechanism determining the rate constants. Figure 3 shows the degradation event interval for selected polymers ranging from a regio-random (D4) to three different degrees of increasing regio-regularity. It is evident that all four polymers follow strict 0^{th} order kinetics for the first 70% of the degradation as the interval is constant. Furthermore, the degradation event interval is observed to increase with regio-regularity. The timescales of photolysis in the absence of oxygen are many orders of magnitude slower than photo-oxidative degradation.[16] Likewise, thermolysis at moderate temperatures (<400

K) is negligible.[11] Both contributions can therefore be neglected in the analysis of the degradation kinetics. The degradation kinetics of the initial part of the degradation is expected to be 0^{th} order assuming that only terminal thiophene rings are attacked during the photo-oxidation. Preferential surface degradation could possibly explain the 0^{th} order kinetics. However, this possibility can be excluded based on the blue-shift dynamics of the polymers, see Figure 3. Observing the regio-regular B1 it is evident that no significant blueshift occurs in the initial parts of the degradation process. This would not be the case if the top layer was preferentially degraded. The hypothesis is that if only terminal thiophene rings are attacked, there should not be a significant blueshift of the spectrum in the initial part of the degradation process. Figure 3 confirms that B1 (RR=96.8%) only exhibits a limited blueshift for the initial 80% of the degradation process. For the regio-random D4 (RR=76.1%) a strong blueshift is observed during the entire degradation process. R1 (RR=91.7%) and P3 (RR=91.6) show stronger blueshift compared to B1. The strong blueshift observed for regio-random P3HT is ascribed to the shorter initial conjugation length of the chain like morphology in the regio-random polymer. Figure 3 shows that the initial peak position for the regio-random D4 at ~490 nm is close to the value at which the regio-regular polymers initiate their quick peak shift, indicating that the conjugation length of D4 is sufficiently short at the initial stage that every monomer contributes strongly to the size of the bandgab and each monomer loss is thus associated with a peak shift. The observation suggests that breaking the regularity induces attack points for the radical reaction, implying that a regio-random polymer is more susceptible to photo-degradation. If true, the stability of the polymer must scale with regio-regularity.

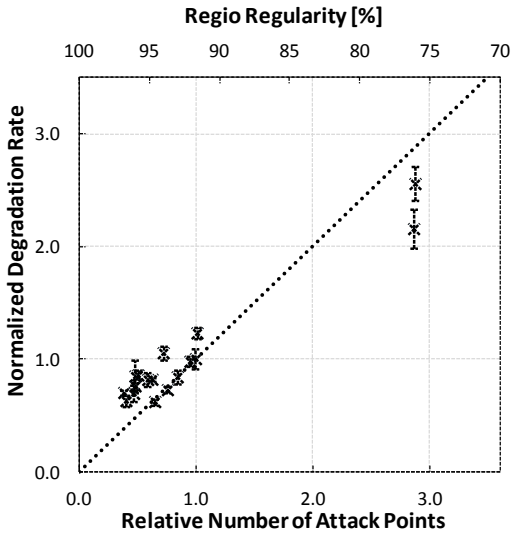

Figure 4. Normalized degradation rate plotted against the calculated relative conjugation length / regio-regularity. The dotted line represents the predicted degradation rate.

Assuming that each breach of regularity introduces two new attack points, it is possible to model the degradation rate as a function of regio-regularity. The relative number of attack points can then be written as

$$N_{ap} = \frac{2(1 - RR_x)}{2(1 - RR_{R1})},$$

where N_{ap} is the number of attack points relative to R1, RR_x is the regio-regularity of the specific polymer, and RR_{R1} is the regio-regularity of R1. Figure 4 shows a plot of the normalized degradation rate as a function of regio-regularity and relative number of attack points. The degradation rate appears to scale with regio-regularity by a linear relationship between regio-regularity and polymer stability. The dotted line in the graph is the theoretical value of degradation rate, calculated from the degradation rate of R1. It is evident that the simple model is capable of explaining the behavior in a convincing manner, suggesting that each breach of regularity induces new attack points that weaken the system. The conjugation length is proportional to the regio-regularity since the conjugation breaks when the polymer is not planar and the π electrons are not in the same plane.

Besides the difference in ratio of head-to-tail connected thiophene units, regio-random and regio-regular P3HT films differ in a more distinct manner. Regio-regular P3HT has been reported to exhibit vanishing intersystem crossing and thereby low triplet yield in contrast to regio-random P3HT.[17] Triplet states are more photochemically active due to their longer lifetime and therefore have been proposed as the cause for the increased degradation rate.[13] It was further implied that the fragmentation of the conjugated π-system in regio-random P3HT takes place on a random basis, while for regio-regular P3HT, terminal thiophene rings are attacked. The results presented in this work, however, demonstrate a strict 0^{th} order degradation rate for both regio-random batches, enforcing the notion that only terminal thiophene rings at points of broken conjugation are attacked. The increase in degradation rate can be explained by an increase in attack points resulting from the lower regularity and the blueshift dynamics is explained by the change in initial conjugation length.

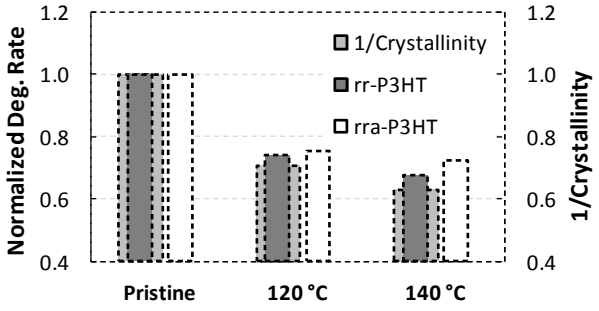

Figure 5. (Left scale) Degradation rate of (dark grey) regio-regular and (white) regio-random P3HT normalized to their respective pristine degradation rates. (Right scale) Reciprocal crystallinity as deduced from X-ray diffraction studies.

Another major difference between regio-regular and regio-random P3HT is that a regio-regular film more readily crystallizes, whereas a regio-random film maintains a more chainlike morphology. Figure 5 shows a plot of the degradation rate superimposed on the reciprocal crystallinity as measured by X-ray diffraction for the regio-

regular polymer R2. As is evident from Figure 5 annealing at 120 °C and 140 °C for one hour was found to induce relative degradation rates of 0.75 and 0.68, respectively, relative to the pristine sample. This indicates that the crystallinity of the sample has affected the stability. While an increase in crystallinity is obtained for regio-regular P3HT, annealing is not expected increase the crystallinity of regio-random P3HT significantly. Indeed, when the regio-random D4 was annealed, no diffraction peaks were observed in the X-ray diffractogram (not shown). This is also consistent with a glass transition temperature of –3 °C reported for regio-random P3HT, indicating that the polymer is indeed amorphous.[18] However, comparable relative stabilizations were observed relative to the regio-regular R2, see Figure 5. Considering that the degradation rate has been shown to scale with the number of kinks in the polymer, it is hypothesized that the main contribution of the annealing step is the relaxation of the polymer leading to an increased conjugation length. Consequently, thermal annealing of P3HT is favorable to the photo-chemical stability. During spin coating the polymers are frozen in a morphology that is not necessarily the lowest energy state. Annealing the films generally relaxes the films, i.e. the chains are stretched and high-energy kinks are avoided. If the annealing effect can be ascribed to an increased conjugation length, a difference in the degradation kinetics as observed in Figure 3 for regio-regularity is expected. This was indeed observed when the regio-regular R1 batch was studied by comparing the pristine polymer to films annealed for two hours at 80 °C and 120 °C. The samples were allowed to cool at a slow rate for 48 hours prior to the degradation experiment. Based on 200 degradation points for each sample type, the degradation state for which the absorption peak reaches 480 nm was 20.85, 18.85, and 17.5% for the pristine, 80 °C and 120 °C annealed samples, respectively. Consequently, annealing the polymer introduces the same delay of the blueshift as observed for higher regio-regular samples. This is in accordance with the hypothesis that the relaxation of the film to a lower energy state increases the conjugation length, which in turn increases film stability.

As a final validation of the hypothesis, the stabilization of the amorphous polymer poly (2-methoxy-5-(2’-ethyl)hexoxy-phenylenevinylene) (MEH-PPV) was assessed as a function of annealing temperature (not shown). For this polymer, stabilization by a factor of 3.5 was observed. The strong stabilization of the MEH-PPV film supports the hypothesis that the relaxation of the polymer is the main contributing factor in the stabilization.

Effect of Thickness on Degradation Kinetics

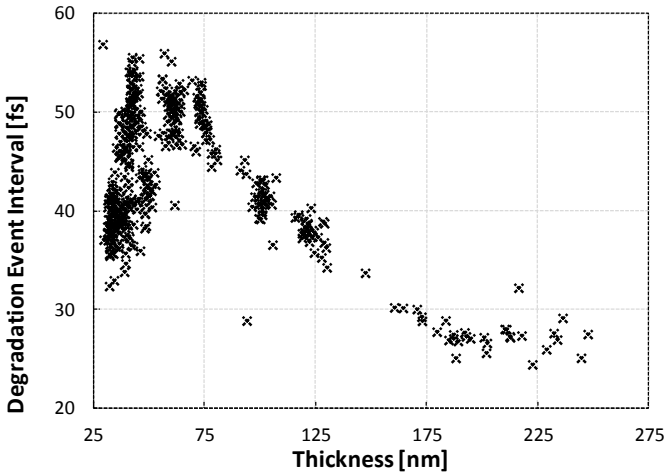

Figure 6. Degradation event interval plotted against the thickness of a film of R1 polymer.

Studying films of different thicknesses gives insight into oxygen availability in the film and effects of light shielding. Assuming that oxygen diffusion is not limited and that light shielding from the top layer of the film is insignificant, the concentration of oxidized thiophene rings is independent of film thickness. No significant spatial reaction gradient is observed in the top 10 nm of a degraded P3HT film, as deduced from angle dependent X-ray photoelectron spectroscopy measurements.[12] This suggests that there is no shielding effect in at least the top layer of the film. Figure 6 shows a plot of degradation event interval against film thickness. It is clear from Figure 6 that a peak is observed around 60 nm. Thin films (below 60 nm) are less stable and very sensitive to changes in film thickness (i.e. steep slope in Figure 6). Thicker films are also less stable manifested in decreasing intervals between degradation events for increasing film thickness, which is close to being a linear correlation between 75 and 175 nm. The decrease in the time between degradation events for thicker films is expected since the thicker film contains a higher number of monomers, and thus more reaction sites. Figure 7 shows the film lifetime plotted against thickness, and it is evident that in the range 125 to 175 nm the film lifetime is constant. The plot is constructed by multiplying the event interval by the initial number of monomers. The existence of a constant lifetime region implies that the degradation takes place in parallel for the entire depth of the film. This means that for this region light shielding is negligible and oxygen is equally available for all depths. For films thicker than 175 nm, either light shielding or lack of oxygen sets the bottom part of the film apart from rest of the film with a lower degradation rate. The event interval is therefore observed to stabilize in this region.

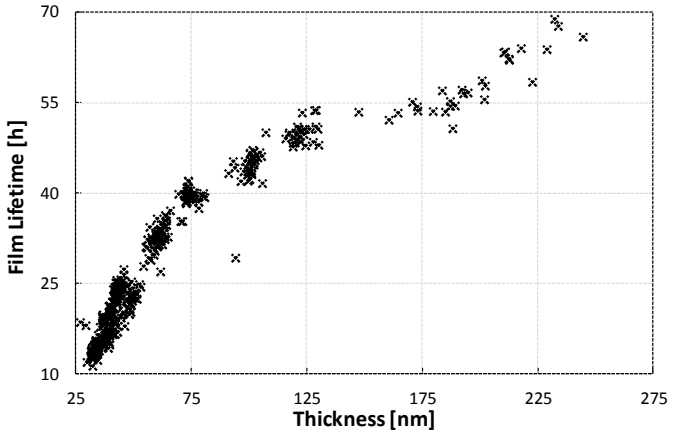

Figure 7. The film lifetime as calculated from the time between degradation events and the initial number of monomers. Thereby the film lifetime is extrapolated from the initial 50% of the degradation.

In Figure 8 the degradation state at which the blueshift reaches 480 nm is plotted. For films in the stable region of 125–175 nm, the blueshift occurs late near the last 20% of the degradation. For films thicker than 175 nm the blueshift appears earlier. This is consistent with the fact that parts of the film degrade later than the top part of the film, thereby extending the degradation. A key point of Figure 8 is the fact that thin films (<75 nm) blueshift rather quickly. This indicates that another mechanism is involved. Ozone has been shown to cause 1^{th} order degradation kinetics and to attack the polymer at random sites.[12] It is conceivable that the relatively high ozone content of the laboratory environment affects the degradation for thin films. This would explain the decrease in degradation interval seen in Figure 6 and also the strong blueshift in Figure 8. However, the kinetics of the degradation remained 0^{th} order. Another likely candidate for the increase in reaction rate is the higher surface to volume ratio. If the reactions are more likely on the surface the rate may easily be different. The polymers in the top layer can be expected to have a higher density of kinks, introducing more attack points for the reaction. This would also explain the fast blueshift observed for thin films.

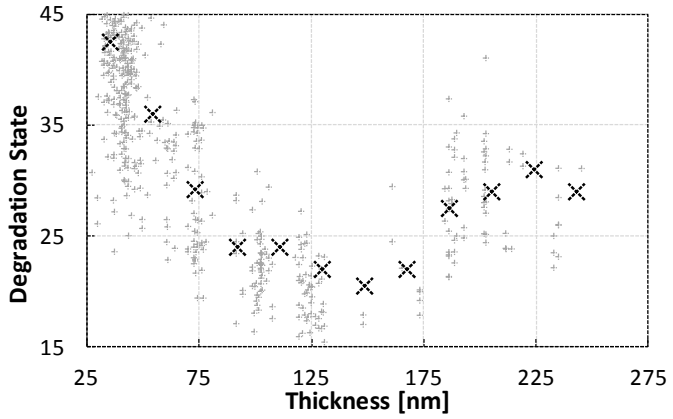

Figure 8. Wavelength shift observed for different thicknesses of P3HT films. The black crosses represent data bins of a width of 40 nm.

Conclusion

18 different batches of P3HT were degraded under simulated sunlight (AM1.5G, 1000 W/m^2) and the respective stabilities were evaluated from the decrease in optical absorption. A highly automated setup allowed for monitoring hundreds of degradation points in parallel to allow for statistically sound investigations of degradation kinetics. It was shown to be evident that the polymer degradation follows strict 0th order degradation kinetics for the initial part of degradation. The typical blueshift of the absorption peak observed during degradation was found to appear later for the more regio-regular films. This indicates that the radical reaction responsible for the photo-degradation attacks terminal thiophene rings exposed at points where the conjugation is broken. Stability was found to increase with regio-regularity following the ratio of head-to-tail connected thiophene units, demonstrating that the polymer is indeed attacked at points of broken conjugation. Annealing relaxes the films and increases conjugation length. This, in turn, increases stability and delays spectral blueshift. For films of different thicknesses, the interval between degradation events is observed to scale linearly with the initial number of thiophene rings for medium thick films (75–175 nm) indicating that oxygen diffusion and light shielding effects have negligible or no effect for medium thickness films.

Acknowledgements

This work was supported by the Danish Strategic Research Council (2104-07-0022), EUDP (j. no. 64009-0050) and PVERA-NET (project acronym POLYSTAR).

References

[1] M. Jørgensen, K. Norrman, S.A. Gevorgyan, T. Tromholt, B. Andreasen, F.C. Krebs, Stability of polymer solar cells, Adv. Mater. 2012;24:580-612.

[2] UCLA, UCLA engineers create tandem polymer solar cells that set record for energy-conversion, Http://newsroom.ucla.edu/portal/ucla/ucla-engineers-create-tandem-polymer-228468.aspx, Accesssed 5/5-2012.

[3] Heliatek, Heliatek sets new record efficiency of 10.7% for its organic tandem cell, Http://www.heliatek.com/?p=1923&lang=en, Accessed 5/5-2012.

[4] F.C. Krebs, J. Fyenbo, D.M. Tanenbaum, S.A. Gevorgyan, R. Andriessen, B. van Remoortere, Y. Galagan, M. Jørgensen, The OE-A OPV demonstrator anno domini 2011, Energy Environ. Sci. 2011;4:4116-4123.

[5] M. Jørgensen, K. Norrman, F.C. Krebs, Stability/degradation of polymer solar cells, Sol. Energy Mater. Sol. Cells. 2008;92:686-714.

[6] K. Norrman, M.V. Madsen, S.A. Gevorgyan, F.C. Krebs, Degradation patterns in water and oxygen of an inverted polymer solar cell, J. Am. Chem. Soc. 2010;132:16883-16892.

[7] M. Manceau, E. Bundgaard, J.E. Carlé, O. Hagemann, M. Helgesen, S. Roar, M. Jørgensen, F. C. Krebs, Photochemical stability of π-conjugated polymers for polymer solar cells a rule of thumb, J. Mater. Chem. 2011;21:4132-4141.

[8] T. Tromholt, M.V. Madsen, J.E. Carlé, M. Helgesen, F.C. Krebs, Photochemical stability of conjugated polymers, electron acceptors and blends for polymer solar cells resolved in terms of film thickness and absorbance, J. Mater. Chem. 2012;22:7592-7601.

[9] M. Koch, R. Nicolaescu, P.V. Kamat, Photodegradation of Polythiophene-Based Polymers : Excited State Properties and Radical, J. Phys. Chem. C. 2009;113:11507-11513.

[10] M. Manceau, A. Rivaton, J.-L. Gardette, Involvement of Singlet Oxygen in the Solid-State Photochemistry of P3HT, Macromol. Rapid Commun. 2008;29:1823-1827.

[11] M. Manceau, A. Rivaton, J.-L. Gardette, S. Guillerez, N. Lemaître, The mechanism of photo- and thermooxidation of poly(3-hexylthiophene) (P3HT) reconsidered, Polym. Degrad. Stab. 2009;94:898-907.

[12] H. Hintz, H. J. Egelhaaf, H. Peisert, T. Chassé, Photo-oxidation and ozonization of poly(3-hexylthiophene) thin films as studied by UV/VIS and photoelectron spectroscopy, Polym. Degrad. Stab. 95 (2010) 818-825.

[13] H. Hintz, H. J. Egelhaaf, L. Lüer, J. Hauch, H. Peisert, T. Chassé, Photodegradation of P3HT−A Systematic Study of Environmental Factors, Chem. Mater. 2010;23:145-154.

[14] T. Tromholt, M. Manceau, M. Helgesen, J.E. Carlé, F.C. Krebs, Degradation of semiconducting polymers by concentrated sunlight, Sol. Energy Mater. Sol. Cells. 2010;95:1308-1314.

[15] F.C. Krebs, Polymer Photovoltaics A Practical Approach, SPIE, 2008.

[16] M. Manceau, S. Chambon, A. Rivaton, J.-L. Gardette, S. Guillerez, N. Lemaître, Effects of long-term UV–visible light irradiation in the absence of oxygen on P3HT and P3HT:PCBM blend, Sol. Energy Mater. Sol. Cells. 2010;94:1572-1577.

[17] O. Korovyanko, R. Österbacka, X. Jiang, Z. Vardeny, R. Janssen, Photoexcitation dynamics in regioregular and regiorandom polythiophene films, Phys. Rev. B: Condens. Matter. 2001;64:235122(1-6).

[18] S. Hugger, R. Thomann, T. Heinzel, T.-A. T., Semicrystalline morphology in thin films of poly(3-hexylthiophene), Colloid. Polym. Sci. 2004;282:932-938.

Solar Energy Materials & Solar Cells 95 (2011) 1308–1314

Contents lists available at ScienceDirect

Solar Energy Materials & Solar Cells

journal homepage: www.elsevier.com/locate/solmat

Degradation of semiconducting polymers by concentrated sunlight

Thomas Tromholt*, Matthieu Manceau, Martin Helgesen, Jon E. Carlé, Frederik C. Krebs

Risø National Laboratory for Sustainable Energy, Technical University of Denmark, Frederiksborgvej 399, DK-4000 Roskilde, Denmark

ARTICLE INFO

Article history:
Received 30 July 2010
Received in revised form
16 September 2010
Accepted 17 September 2010
Available online 8 October 2010

Keywords:
Organic solar cells
Semiconducting polymers
Degradation
Stability
Concentrated sunlight

ABSTRACT

A lens based sunlight concentration setup was used to accelerate the degradation of semiconducting polymers. Sunlight was collected outdoor and focused into an optical fiber bundle allowing for indoor experimental work. Photo-degradation of several polymers was studied by UV–vis absorbance spectroscopy and infra-red spectroscopy. This showed that the degradation rate is significantly increased by increasing illumination intensity. Acceleration factors exceeding 100 compared to standard 1 sun illumination were observed for solar concentration of 200 suns in the case of P3HT. A comparison between infra-red spectra of MEH-PPV degraded at 1 sun intensity and at high solar concentration only showed minor deviations in degradation mechanisms. The acceleration factor was found to vary linearly with the solar concentration. Finally, a comparison of the degradation rates at 1 sun and 100 suns was carried out in a materials study employing five different conjugated polymers relevant to polymer solar cells for which acceleration factors in the range 19–55 were obtained.

1. Introduction

Polymer solar cells (PSCs) have attracted considerable attention over the past decade and great advances have already been achieved in terms of processing, stability and efficiency [1,2]. However, further improvements are still needed within all these areas before large scale commercialization is possible. One of the most challenging points to address is to unite superior device performance, production feasibility and stability in one single conjugated polymer. While a considerable number of semiconducting polymers have been synthesized over the last years – some of them yielding efficiencies in the 5–8% range [3,4] – stability issues have been given only little attention [5,6]. A highly efficient material does not necessarily have a good photochemical stability, which is a prerequisite for stable photovoltaic devices with long operational lifetimes. Therefore, a stability assessment has to be done in conjunction with all efficiency characterizations to assess the practical potential of a novel polymer material.

A natural consequence of the development of more stable polymers is longer periods of time for a sound stability assessment [6]. For this reason a standard stability assessment for relatively stable materials at 1 sun in ambient atmosphere can be very time consuming. Additionally, the number of polymers synthesized for PSCs is increasing rapidly [2,7]. The total effect is a bottleneck between the performance evaluation and the stability evaluation for new semiconducting polymers. The development of a simple, rapid, highly accelerated evaluation method of the polymer stability would highly reduce the impact of this bottleneck. Ideally, with such a method a stability screening of a number of polymers at accelerated conditions should yield the same relative stability as observed at a standard degradation at 1 sun by simulated sunlight.

Different acceleration methods have been utilized to increase the degradation rate, e.g. temperature [8] and atmosphere [9]. With these methods, degradation rates can possibly be increased 20-fold [10] by increasing the rate of certain degradation mechanisms activated by the change in a given physical parameter. Increased illumination intensity has so far not been employed as an acceleration parameter on a larger scale due to the practical problems concerning obtaining high intensities from artificial light sources. Concentration of outdoor sunlight provides a means of obtaining high solar concentrations on small areas. This method is well-known within the field of inorganic solar cells for evaluation of the photovoltaic parameters at high solar concentrations [11]. Within the field of PSCs only a few studies have been made using concentrated sunlight [12]. The use of concentrated sunlight has the potential of accelerating the degradation in combination with temperature and atmosphere control beyond the limits that are given by today's standard.

In this paper we present a sunlight concentrator system, which is used to degrade polymers relevant to PSCs at solar intensities ranging from 1 sun to several hundreds of terrestrial solar intensity. The evolution of the polymer absorbance was recorded during ageing for each polymer. To confirm the viability of this approach, two extensively studied materials, MEH-PPV and P3HT were used as reference materials. These two polymers provide two extremes in terms of stability, with P3HT being much more stable than MEH-PPV. This allows for a study of the

* Corresponding author. Tel.: +45 46 77 54 93; fax: +45 46 77 47 91.
E-mail address: ttro@risoe.dtu.dk (T. Tromholt).

0927-0248/$ - see front matter © 2010 Elsevier B.V. All rights reserved.
doi:10.1016/j.solmat.2010.09.022

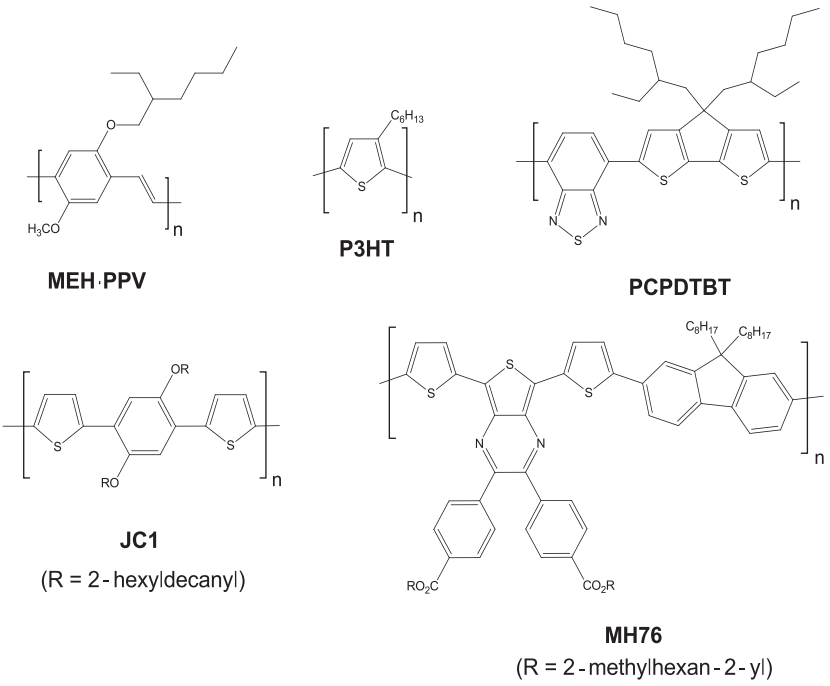

Fig. 1. The chemical structure of the five polymers studied.

photochemical response of processes on two significantly different time scales. Degradation at 1 simulated sun was compared to degradation at high solar concentrations for both polymers allowing for a discussion of the differences between the two degradation setups. Furthermore, three other polymers were studied at 1 simulated sun and at 100 suns and their acceleration factors were compared. The polymers were selected to cover a broad range of chemical structures and stabilities. These were JC1 [13], PCPDTBT [14] and MH76 [15], these two latter being low band gap polymers (Fig. 1). Reported efficiencies are stated in Table S1. All experiments were conducted in ambient air.

2. Experimental

2.1. Sunlight concentration setup

Outdoor sunlight is concentrated by a BK7 plano-convex lens (Ø 32 cm, focal length 50 cm) positioned on a solar tracker into a bundle of 7 optical fibers (length 15 m, core diameter 1 mm), which guide the light to an indoor laboratory. This ensures a controlled experimental environment in terms of humidity and temperature. The illumination intensity was controlled by an adjustable pizza iris positioned above the lens, which through its shape reduces the spectral distortion from spherical aberration. The outdoor concentration setup is shown in Fig. 2a and b, where the iris, the lens and the focal point where light is coupled into the fiber bundle can be seen. The total incoming light intensity was determined with a thermal power sensor. A Hamamatsu S5971 photodiode was used to determine the solar concentration for the part of the light beam that was transmitted by the sample holder. This was done to reduce the influence of flux inhomogeneities within the beam of the fiber bundle. Great care was taken in order to ensure that a constant intensity was impinging on the samples during all degradations. The sample holder had a circular aperture of 2 mm, which can be seen in Fig. 2c together with the fiber bundle and the photodiode. Fig. 2d shows the setup during solar illumination.

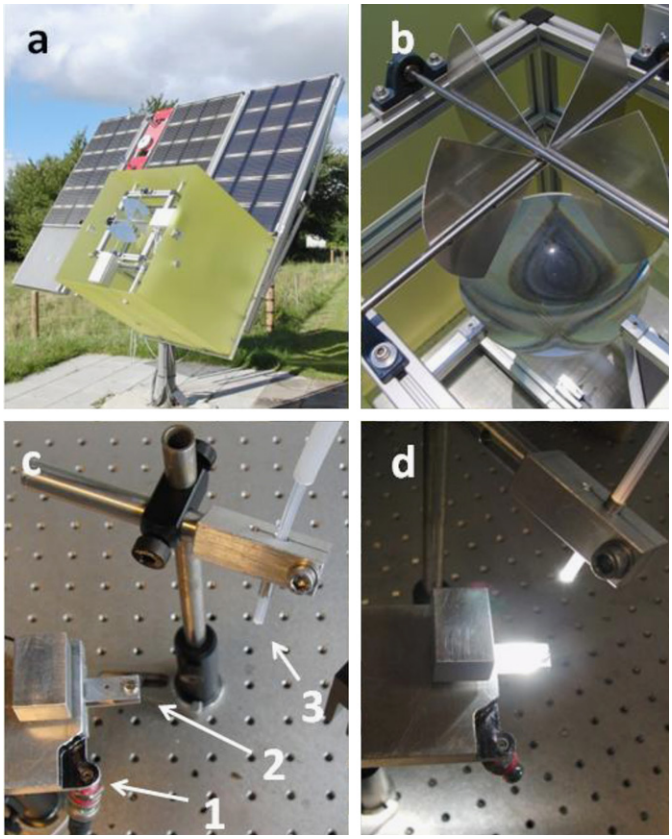

Fig. 2. (a) The solar tracker on which the concentrator system is mounted. (b) The concentrator system consisting of a lens, an optical fiber bundle and an iris to control illumination intensity. (c) Indoor experimental setup showing (1) the photodiode, (2) the sample holder and (3) the fiber bundle. (d) The setup under illumination.

The spectrum of the outdoor and the concentrated light was measured with an Avaspec 2048 spectrometer. The spectrometer was calibrated with an Avantes Avalight-DHS calibration lamp

allowing for precise irradiation measurements. The spectrum of the local outdoor light was found to be very close to the ASTM G173 standard reference for the AM1.5G spectrum [16] (Fig. S1). Additionally, the spectrum of the concentrated sunlight was only slightly red-shifted relative to the outdoor light. For this reason, spectral deviations from direct sunlight are not expected to influence the measurements significantly. The spectral distortions originating from different iris opening angles were found to be negligible, which allows the comparison of degradations at different intensities without correction for spectral variations (Fig. S2).

2.2. Materials and methods

Synthetic procedures and characterization data of all the materials have been described in detail elsewhere [13,15]. Pure polymer samples were spin-coated on KBr plates from chlorobenzene solutions. Samples were then illuminated using (i) a standard solar simulator (KHS 575 from Steuernagel Lichttechnik, AM 1.5 G, 1000 W m^{-2}, 1 sun) and (ii) the solar concentrator (1–200 suns). Periodically the samples were moved from the solar concentrator to the spectrometer where the UV–vis absorbance spectra were recorded to monitor the degradation. Spectra were recorded between 200 and 1100 nm with a UV-1700 spectrometer from Shimadzu.

Infra-red (IR) spectroscopy was conducted with a Spectrum One spectrometer from Perkin Elmer operating in transmission mode (4 cm^{-1} resolution, 32 scans summation).

2.3. Theory

In order to make a quantitative comparison, the total amount of absorbed photons (N^t_{Tot}) was monitored versus ageing time over the absorption peak. For each wavelength, the percentage of the light absorbed was calculated from the absorbance, and then multiplied by the number of incoming photons. The resulting number of absorbed photons was summed over the absorption peak providing the total amount of absorbed photons N^t_{Tot}. This can formally be described as

$$N^t_{Tot} = \sum_{\lambda_1}^{\lambda_2} N_0(\lambda)(1-10^{-A^t(\lambda)}),$$

where $A^t(\lambda)$ is the measured absorbance at a given wavelength λ and time t, and $N_0(\lambda)$ is the incident photonic flux. λ_1 and λ_1 are the limits of the summation, which were chosen to cover the entire absorption peak. For the polymers studied, the absorption was in the UV-vis and the NIR. The summation limits for each polymer is given in Table S2. $A^t(\lambda)$ was directly extracted from the UV–vis absorbance spectra of the sample at the corresponding ageing time, and the photonic flux was taken from the ASTM G173 standard, which was used as the AM1.5G reference spectrum [16]. At the end of the degradation, the quantity of absorbed photons always reached a constant value (N^∞_{Tot}) after which no absorbance evolution followed. This value was always above zero due to the absorption of the KBr substrate. To monitor only the evolution of the degradation of the polymers, N^t_{Tot} was normalized, implying that during the degradation, the normalized number of absorbed photons would go from 100% to 0%. The normalization was applying the expression

$$N^t_{Photons} = \frac{N^t_{Tot} - N^\infty_{Tot}}{N^0_{Tot} - N^\infty_{Tot}}.$$

This implies that initially, $N^0_{Photons} = 100\%$, while after infinite time, at complete degradation, $N^\infty_{Photons} = 0\%$.

3. Results and discussion

3.1. Proof-of-concept of concentrated sunlight for accelerated degradation: MEH-PPV study

3.1.1. Kinetic aspects and reproducibility

The evolution of the degradation as monitored by UV–vis spectroscopy took place on highly different time scales for MEH-PPV samples degraded at 1 simulated sun and 100 suns. For each absorbance measurement $N_{photons}$ was calculated. Fig. 3a shows the behavior of the sample degraded at 1 sun, where a linear decay of $N_{photons}$ is followed by a plateau, after which no further degradation is observed. The value of $N_{photons}$ is set to 0% at this time since a complete degradation of the polymer has taken place. A similar tendency is observed in the case degradation of 100 suns, shown in Fig. 3b. Three different samples have been studied to evaluate the reproducibility of the degradation at a specified solar concentration. All three degradations exhibit the same overall linear decay followed by a plateau, similar to the tendency observed for the 1 sun degradation. This shows that at high concentration, the same degradation behavior is observed as for 1 sun, only on a shorter time scale. Additionally, the reproducibility with the concentration setup was found to be high since only minor variations are observed for the three measurements conducted at constant solar concentration. The degradation rates of the 100 sun degradations are stated in Table 1 together with the acceleration factors. The acceleration factor is calculated from the ratio between the slopes of the linear regions at accelerated and non-accelerated degradation. For the three 100 sun degradation experiments acceleration factors of 44, 51 and 52 were obtained. The deviations in the acceleration factors are believed to be mainly a consequence of minor intensity variations in the illumination intensity introduced by the finite step size of the solar tracker when tracking the sun.

3.1.2. Influence on the degradation mechanism by high solar concentration

Degradation of polymers at high solar concentrations not only introduces a high photon flux, but also an increased temperature.

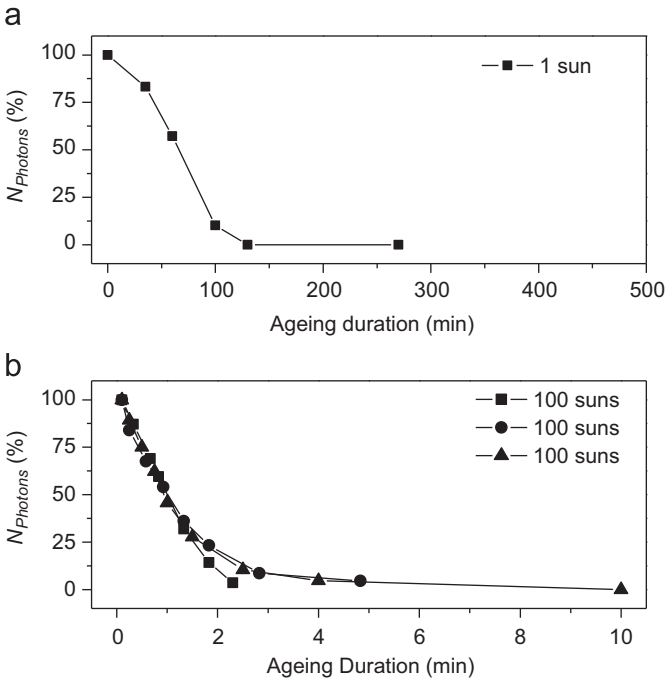

Fig. 3. Evolution of the normalized number of absorbed photons during ageing at (a) 1 sun and (b) 100 suns.

Table 1
Degradation rates and acceleration factors for MEH-PPV and P3HT for solar concentrations ranging from 1 sun to 200 suns.

Sample	Concentration (suns)	Degradation rate (% min^{-1})	Acceleration factor
MEH-PPV	1	0.96	1.0
	5	8	8.4
	25	16	17
	50	25	26
	100	42	44
	100	49	51
	100	50	52
	200	71	74
P3HT	1	0.0082	1.0
	100	0.45	55
	150	0.75	91
	200	0.89	108

This might introduce degradation mechanisms that are not observed at 1 sun degradation. Additionally, the weight between the different well known degradation mechanisms at 1 sun might be different at accelerated conditions. To study the difference between the accelerated and non-accelerated degradation, the evolution of the absorbance during degradation of MEH-PPV at 1 sun in a solar simulator and at 100 suns with concentrated light was compared, as shown in Fig. 4. The general tendency is the same in both cases, with the magnitude of the peak decreasing over time (photo-bleaching). Three pairs of similar degradation states have been indicated in the legend by the respective $N_{photons}$ values, calculated in the range 370–650 nm as indicated by the dashed lines. The peak position for each pair of degradation stages is found to be highly similar for both the sample degraded at 1 sun and 100 suns. This gives the impression that the same degradation reactions are found for both 1 and 100 suns. Due to the lack of chemical sensitivity of UV–vis spectroscopy, IR spectroscopy is used to follow the chemical composition of the polymer during degradation.

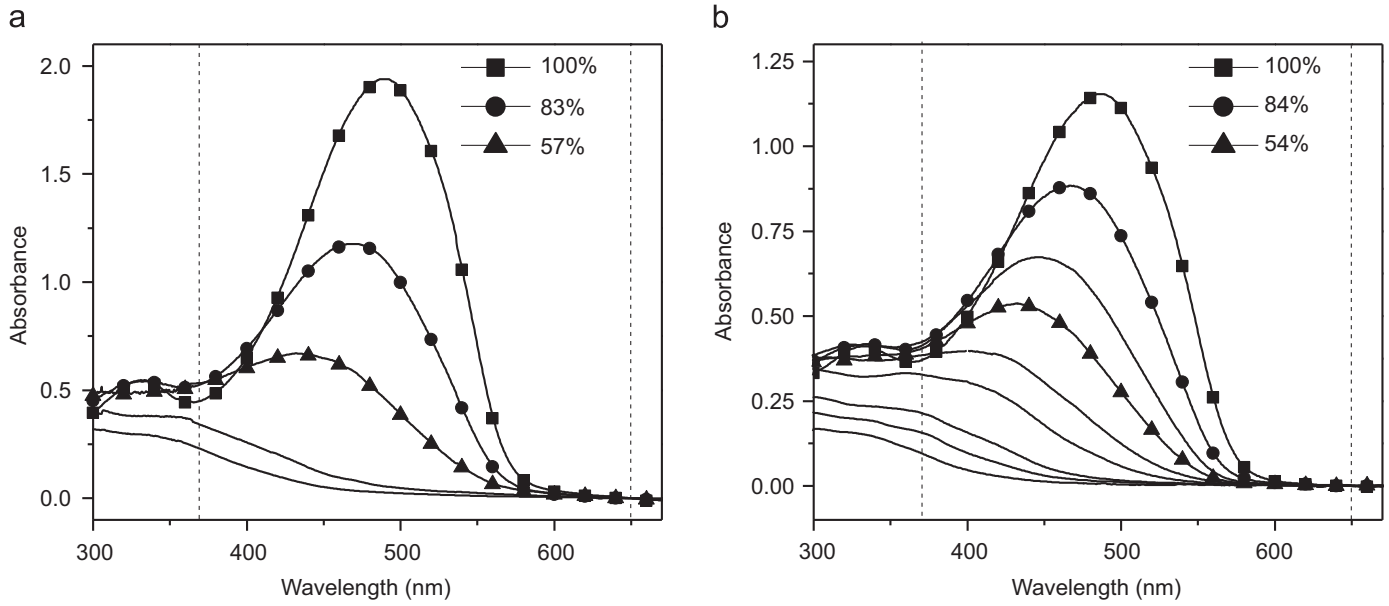

Fig. 4. Evolution of absorbance during ageing of MEH-PPV (a) 1 sun in solar simulator and (b) 100 suns concentrated light. The legends present $N_{photons}$ at different degradation stages.

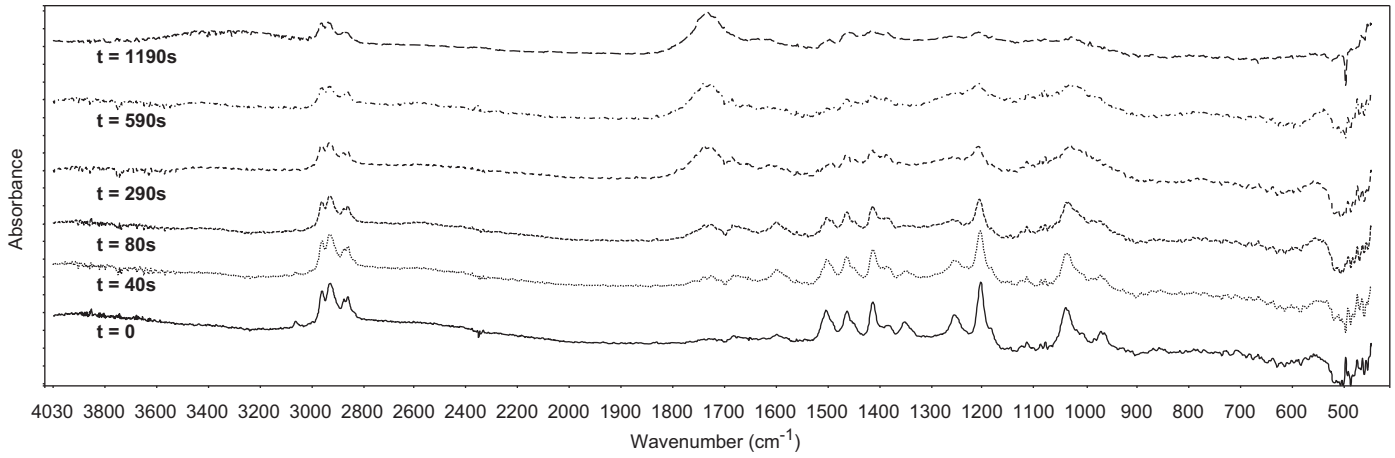

Fig. 5. Evolution of the IR spectra of MEH-PPV during photo-oxidation by concentrated sunlight (100 suns).

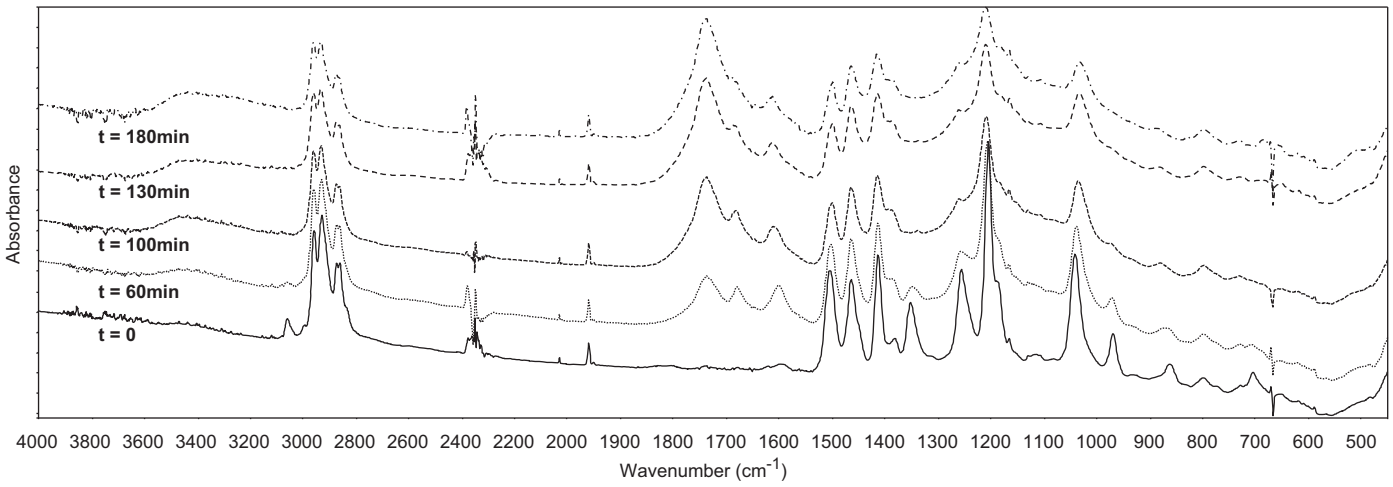

Fig. 6. Evolution of the IR spectra of MEH-PPV during photo-oxidation from a solar simulator (1 sun).

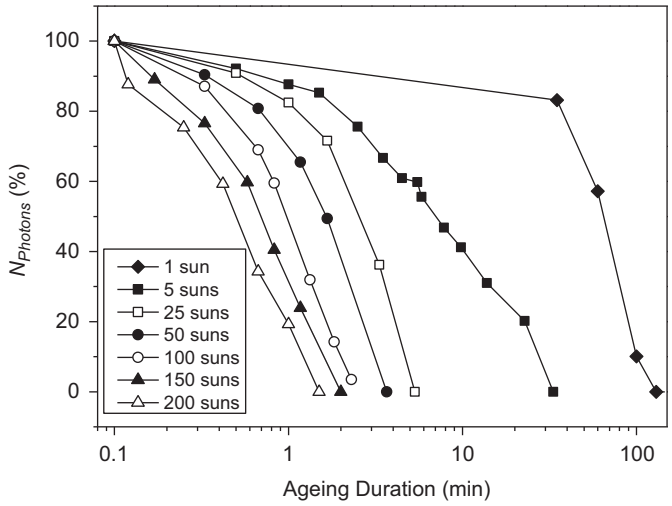

Fig. 7. Normalized number of absorbed photons during ageing of MEH-PPV for different solar concentrations.

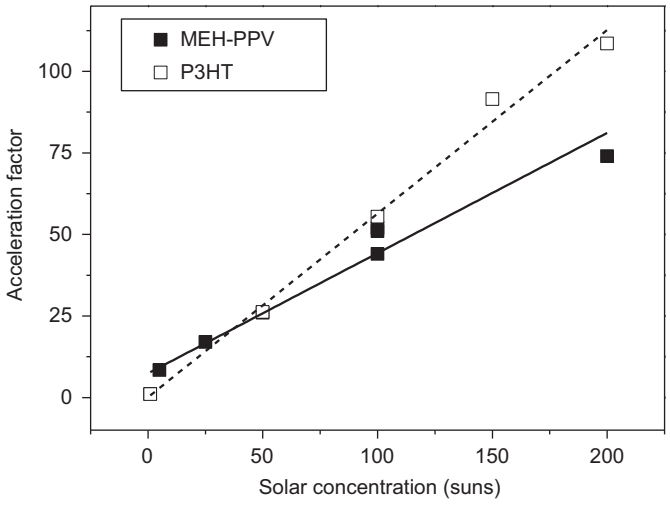

Fig. 8. Acceleration factors for MEH-PPV and P3HT at different solar concentrations. The dashed line is a linear fit of P3HT while the solid line is a linear fit of MEH-PPV.

Results obtained under concentrated sunlight (Fig. 5) were compared to the data obtained for a sample photo-degraded under 1 simulated sun (Fig. 6). The photochemical behavior of MEH-PPV is anticipated to be almost identical to the extensively studied MDMO-PPV due to their very similar chemical structure [17].

From the IR spectroscopy the most important finding is that very similar modifications are observed during the degradations for the two different ageing setups (Figs. 5 and 6). In both cases one can first notice a gradual loss of several functions characteristic for the pristine polymer: alkyl (ν_{C-H} between 3000 and 2850 cm^{-1}), ethers (ν_{C-O} around 1350 and 1255 cm^{-1}) and exocyclic double bonds (δ_{C-H} around 970 cm^{-1}).

In parallel, two different absorption bands developed in the carbonyl domain (1800–1650 cm^{-1}). The first one is located at 1735 cm^{-1} and its intensity increases all along the experiment. This band progressively overlaps the second signal located at 1680 cm^{-1}. In the same region, one can also notice the appearance of a band around 1600 cm^{-1}. In the case of MDMO-PPV the formation of this band has been ascribed to changes in the aromatic ring substitution [17]. As the same bands appeared both under simulated and concentrated sunlight, this indicates that identical degradation products were formed. This suggests that the MEH-PPV degradation mechanisms remain very similar for degradation at high concentration relative to 1 simulated sun.

3.2. Intensity dependent degradation

3.2.1. MEH-PPV

The degradation response to different solar concentrations was studied to get information about the intensity dependent degradation behavior as well as the acceleration factors. Solar concentrations in the range 1–200 suns were used for the degradation. All degradations exhibited tendencies highly resembling the ones observed for 1 sun and 100 suns degradations. Fig. 7 shows the evolution of $N_{photons}$ at different solar concentrations plotted versus the logarithm of the ageing duration. For each curve the plateau reached after total degradation has been omitted in the representation to clarify the figure. There is a clear tendency that higher solar concentrations yield a higher degradation rate. Table 1 shows the acceleration factors for all conducted MEH-PPV degradations. At 200 suns an acceleration factor of 74 was attained, meaning that a full degradation of the sample could be conducted in approximately 1 min.

3.2.2. P3HT

P3HT was studied in the same way as for MEH-PPV at different solar concentrations. Due to its higher photochemical stability compared to MEH-PPV, the photochemical response of much slower degradation mechanisms could be studied. Solar concentrations at 1,

Table 2
Degradation rates for 1 sun and 100 sun degradation and the resulting acceleration factors for 5 different polymers.

Sample	Concentration (suns)	Degradation rate under 1 sun (% min^{-1})	Degradation rate under 100 suns (% min^{-1})	Acceleration factor
MEH-PPV	100	0.96	42	44
P3HT		0.0082	0.45	55
JC1		0.011	0.25	24
PCPDTBT		0.0049	0.093	19
MH76		0.086	2.1	25

100, 150 and 200 suns were used for the degradation. The tendency was similar for 1 sun and high concentration degradation. A linear decay followed by a plateau after the full degradation of the polymer was observed in all cases, as in the case of MEH-PPV (Fig. S3). This proves that both low and high rate degradation mechanisms can be speeded up by concentrated sunlight without changing the overall tendency of the degradation.

The degradation rates and the respective acceleration factors are shown in Table 1 for both MEH-PPV and P3HT. In the case of MEH-PPV, an acceleration factor of 74 was obtained in the case of 200 suns, whereas an acceleration factor of 108 was obtained at the same concentration for P3HT. The reason for this discrepancy is believed to be a consequence of both uncertainties pertaining to the experimental setup as well as different photochemical responses for the different polymers.

The correlation between the acceleration factors and the light intensity is shown in Fig. 8 for MEH-PPV and P3HT. In the case of MEH-PPV five different intensities were used for degradation. These data points exhibited a linear correlation, as shown by the linear fit. The 1 sun solar simulator point deviates slightly from the general linear fit. The reason for this may be the different temperatures in the two degradation environments that change the rate of the thermally activated degradation mechanisms. The slope of the linear fit for MEH-PPV is 0.37.

Five different concentrations were used for the P3HT degradation. As in the case of MEH-PPV, these points constitute a clear linear correlation. This shows that even for very long illumination times, a high degree of control of the solar concentration is obtained. A linear fit of the P3HT data points resulted in a slope of 0.56. This implies that for P3HT degradation above 35 suns, the acceleration factor is higher than for MEH-PPV at the same solar concentration, while below 35 suns the opposite behavior is the case.

3.3. Accelerated screening of polymer stability

Once the proof-of-concept of the setup was established, it was used to study the photochemical stability of the three other polymers, JC1, MH76 and PCPDTBT under 100 suns. The degradation of these materials was very similar to the degradations observed for MEH-PPV and P3HT implying an initial linear decay of $N_{photons}$ followed by a constant plateau, at which no further degradation was observed (Figs. S4–S6).

Acceleration factors were determined for each polymer (Table 2). Acceleration factors were very dependent on the polymer nature as values from 19 to 55 were obtained. This could seem rather surprising as all the experiments were realized under the same intensity (100 suns). It should however be recalled that for a given accelerated ageing test, all the polymers behave differently, especially when their chemical structures are very different [18].

At accelerated degradation the polymer stability ranking remained almost identical to the case of non-accelerated degradation. From the lowest to the highest photochemical stability this ranking was as follows: MEH < PPV < MH76 < P3HT < JC1 < PCPDTBT. The reason for the discrepancy in the ranking of JC1 and P3HT is due to different photochemical responses to high solar concentration. Since JC1 and P3HT present almost identical stabilities at 1 simulated sun, only a minor deviation in acceleration factors results in a different stability ranking at high solar concentration. It is thus evidenced that this degradation method can effectively be used to qualitatively evaluate polymer photochemical stability and determine the polymer potential for organic solar cells from a photochemical stability point of view.

3.4. Perspectives of concentrated sunlight for polymer degradation

The use of concentrated sunlight within the field of organic photovoltaics is at present rather undiscovered. However, it is believed to have a large potential in many different aspects of organic solar cell research. In this paper degradation of semiconducting polymers was accelerated up to 100 fold by concentrated sunlight, without altering the chemistry significantly from degradation at 1 simulated sun. This is a proof-of-concept of this method that allows for stability assessment of semiconducting polymers on a highly accelerated time scale. However, concentrated sunlight is also promising within the field of physical characterization of organic solar cells. Light induced processes can be highly favored, which allows for characterization of solar cells in an environment not yet studied. By this approach, knowledge about e.g. recombination effects and the diode properties of the device can be obtained [12]. This may allow for a better understanding of the underlying physical processes within the separate materials constituting the organic solar cells, as well as the entire solar cell.

4. Conclusion

A lens based solar concentrator has been presented and used to study the photochemical stability of five different conjugated polymers. The UV–vis absorbance evolution was monitored to follow the polymer degradation. Samples were exposed to intensities up to 200 suns and their absorbance evolutions were compared to samples degraded with a conventional solar simulator (AM 1.5G, 1 sun). A strong increase in the degradation rate was systematically observed at high intensities while the degradation mechanisms were shown to remain very similar to non-accelerated degradation. Acceleration factors exceeding 100 were obtained for P3HT. At 100 suns degradation acceleration factors in the range 19–55 were found for five different polymers, which is a result of different photochemical responses for the different chemical moieties. The method provides a highly accelerated qualitative stability evaluation where an estimate of the material stability can be obtained within a short period of time.

Acknowledgements

We thank Kristian Larsen and Torben Kjær for constructing the mechanical setup employed in this study. This work was supported by the Danish Strategic Research Council (DSF 2104-05-0052 and 2104-07-0022), EUDP (j. nr. 64009-0050) and PV-ERA-NET (project acronym POLYSTAR).

Appendix A. Supplementary material

Supplementary data associated with this article can be found in the online version at doi:10.1016/j.solmat.2010.09.022.

References

[1] G. Dennler, M.C. Scharber, C.J. Brabec, Polymer-fullerene bulk-heterojunction solar cells, Adv. Mater. 21 (13) (2009) 1323–1338.

[2] M. Helgesen, R. Søndergaard, F.C. Krebs, Advanced materials and processes for polymer solar cell devices, J. Mater. Chem. 20 (1) (2010) 36–60.

[3] H.-Y. Chen, J. Hou, S. Zhang, Y. Liang, G. Yang, Y. Yang, L. Yu, Y. Wu, G. Li, Polymer solar cells with enhanced open-circuit voltage and efficiency, Nat. Photonics 3 (11) (2009) 649–653.

[4] S.H. Park, A. Roy, S. Beaupré, S. Cho, N. Coates, J.S. Moon, D. Moses, M. Leclerc, K. Lee, A.J. Heeger, Bulk heterojunction solar cells with internal quantum efficiency approaching 100%, Nat. Photonics 3 (5) (2009) 297–303.

[5] M. Jørgensen, K. Norrman, F.C. Krebs, Stability/degradation of polymer solar cells, Sol. Energy Mater. Sol. Cells 92 (7) (2008) 686–714.

[6] F.C. Krebs, K. Norrman, Analysis of the failure mechanism for a stable organic photovoltaic during 10000 h of testing, Prog. Photovol. Res. Appl. 15 (8) (2007) 697–712.

[7] S. Beaupré, P.-L.T. Boudreault, M. Leclerc, Solar-energy production and energy-efficient lighting: photovoltaic devices and white-light-emitting diodes using poly(2,7-fluorene), poly(2,7-carbazole), and poly(2,7-dibenzosilole) derivatives, Adv. Mater. 22 (8) (2010) E6–27.

[8] S.A. Gevorgyan, M. Jørgensen, F.C. Krebs, A setup for studying stability and degradation of polymer solar cells, Sol. Energy Mater. Sol. Cells 92 (7) (2008) 736–745.

[9] J. Philippart, C. Sinturel, J.-L. Gardette, Influence of light intensity on the photooxidation of polypropylene, Polym. Degrad. Stab. 58 (3) (1997) 261–268.

[10] S. Schuller, P. Schilinsky, J. Hauch, C. Brabec, Determination of the degradation constant of bulk heterojunction solar cells by accelerated lifetime measurements, Appl. Phys. A: Mater. Sci. Process 79 (1) (2004) 37–40.

[11] E. Katz, J. Gordon, D. Feuermann, Effects of ultra-high flux and intensity distribution in multi-junction solar cells, Prog. Photovol. Res. Appl. 14 (4) (2006) 297–303.

[12] T. Tromholt, E.A. Katz, B. Hirsch, A. Vossier, F.C. Krebs, Effects of concentrated sunlight on organic photovoltaics, Appl. Phys. Lett. 96 (7) (2010) 073501.

[13] J.E. Carlé, J.W. Andreasen, M. Jørgensen, F.C. Krebs, Low band gap polymers based on 1,4-dialkoxybenzene, thiophene, bithiophene donors and the benzothiadiazole acceptor, Sol. Energy Mater. Sol. Cells 94 (5) (2010) 774–780.

[14] J. Peet, J.Y. Kim, N.E. Coates, W.L. Ma, D. Moses, A.J. Heeger, G.C. Bazan, Efficiency enhancement in low-bandgap polymer solar cells by processing with alkane dithiols, Nat. Mater. 6 (7) (2007) 497–500.

[15] M. Helgesen, F.C. Krebs, Photovoltaic performance of polymers based on dithienylthienopyrazines bearing thermocleavable benzoate esters, Macromolecules 43 (3) (2010) 1253–1260.

[16] NREL ASTM G173 reference AM1.5G solar spectrum. 〈http://rredc.nrel.gov/solar/spectra/am1.5/astmg173/astmg173.html〉.

[17] S. Chambon, A. Rivaton, J.-L. Gardette, M. Firon, L. Lutsen, Aging of a donor conjugated polymer: photochemical studies of the degradation of poly [2-methoxy-5-(3′,7′-dimethyloctyloxy)-1,4-phenylenevinylene], Polym. Degrad. Stab. 45 (2) (2007) 317–331.

[18] R. Fisher, W. Ketola, Accelerated weathering test design and data analysis, in: S. Halim Hamid (Ed.), Handbook of Polymer Degradation, second ed., CRC Press2000, pp. 645–668 (Chapter 17).

Appendix 4

Concentrated light for accelerated photo degradation of polymer materials

Journal:	*Journal of the American Chemical Society*
Manuscript ID:	Draft
Manuscript Type:	Communication
Date Submitted by the Author:	n/a
Complete List of Authors:	Madsen, Morten; Technical University of Denmark, Department of Energy Conversion and Storage Tromholt, Thomas; Technical University of Denmark, Department of Energy Conversion and Storage Norrman, Kion; Technical University of Denmark, Department of Energy Conversion and Storage Krebs, Frederik; Technical University of Denmark, Department of Energy Conversion and Storage

Appendix 4

Concentrated light for accelerated photo degradation of polymer materials

Morten V. Madsen*, Thomas Tromholt, Kion Norrman, and Frederik C. Krebs

Department of Energy Conversion and Storage, Technical University of Denmark, DK-4000 Roskilde, Denmark

KEYWORDS Concentrated light, P3HT, Photo oxidation, organic photovoltaics, degradation

Supporting Information Placeholder

ABSTRACT: Concentrated light is an attractive method for accelerating the degradation process of polymer materials. At intensities corresponding to 50, 100 and 150 suns (1 sun = 0.1 W/cm^2) the photo oxidation of poly-3-hexyl-thiophene (P3HT) has been studied using a novel concentrator setup. It was demonstrated that concentrated light can be used to perform photochemical degradation of polymer solar cell (PSC) materials with acceleration factors up to 1,200. The degradation rates of the polymer materials under high concentration (up to 150 suns) was shown to follow the same reaction mechanism as for 1 sun conditions. With proper cooling the photon efficiency in regards to photo degradation is constant for all concentrations (1–150 suns) and oxygen diffusion rates is not a limiting factor. Induced heating of the samples at high intensities, however, accelerates degradation that exhibits an Arrhenius behavior. Photolysis at 50 and 150 suns have been conducted and shown to be unaffected by temperature as the thermal activation is related to oxygen diffusion. This clearly demonstrates that concentrated light for accelerated polymer degradation can be a practical approach for polymer stability evaluation, and enable rapid routine studies of even very air-stable polymers, which is a valuable tool for the development of commercial PSC.

The field of polymer solar cells (PSCs) is maturing fast manifested in an ever increasing number of publications covering the subject. Over the last decade, reported efficiencies have risen to exceed 10%, and several companies have entered the field.[1,2] While efficiencies and production scalability are high interest areas, the Achilles' heel of polymer solar cells has long remained the operational lifetime of the devices. When organic matter is illuminated, the materials react via photochemical and photolytic processes, making it essential to utilize materials where the yield and rate of photochemical degradation is minimized. Outdoor tests of PSCs with lifetime exceeding one year have been demonstrated[3] and materials such as polythiophene (PT) have been shown to have degradation rates of 0.029% / h under ambient 1 sun conditions[4]. With this level of stability, fast material screening under accelerated conditions is an appealing prospect. Acceleration methods utilizing atmosphere and temperature control have been used to increase degradation rates by a factor of 20.[5] It has been demonstrated that increasing the temperature accelerates the degradation according to the Arrhenius equation for both PSCs and single polymer layers.[5,6] Concentrated light is another novel direct acceleration condition, which accelerates the rate of photo oxidation of the polymer. Due to the multitude of degradation mechanisms that are accelerated by concentrated light, the PSC response to concentrated light is complex,[7] and even effects such as reversible degradation have been observed.[8] For the simplified system of pure polymer in the ambient, accelerated degradation has been performed up to 200 suns.[9] This study demonstrated that degradation of polymers can serve as a standard tool for rapid polymer stability evaluation. However, the validity of using concentrated light to accelerate the degradation process still remains to be studied.

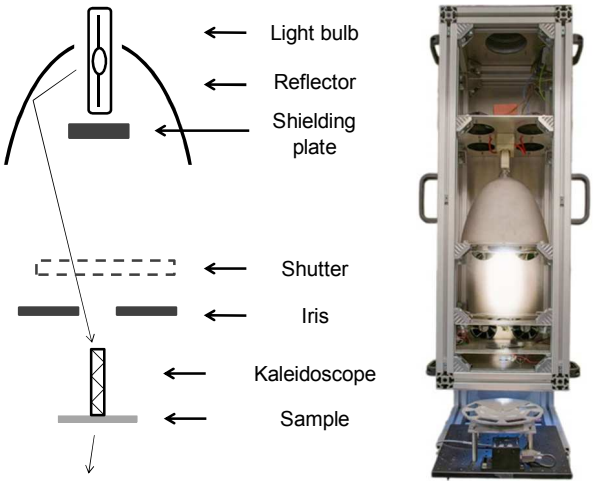

Figure 1. Schematic representation and photo of the concentrator setup.

This paper focuses on the use of concentrated light as a deterministic method of polymer degradation. For this, films of pure regio-regular poly-(3-hexyl-thiophene) (P3HT) were studied and their degradation rates compared. A novel fully automated lamp-based light concentrator (Figure 1) was constructed to allow for precise evaluation of degradation rates at high light intensities ranging from 0.1 to 150 suns. The evaluated degradation rates were, in turn, compared to the degradation rates of 1 sun degradation, with equivalent light spectra at all intensities. The degradation state is deduced by monitoring the changes in the optical spectrum of the sample during the illumination.[4] The artificial solar concentrator had the advantage of long term stability and precision in comparison with solar collector setups.[9] Automated sample exchangers were employed to ensure that no errors were introduced when

Appendix 4

handling samples. The full details of the experiments and the setups are provided in the Supporting Information.

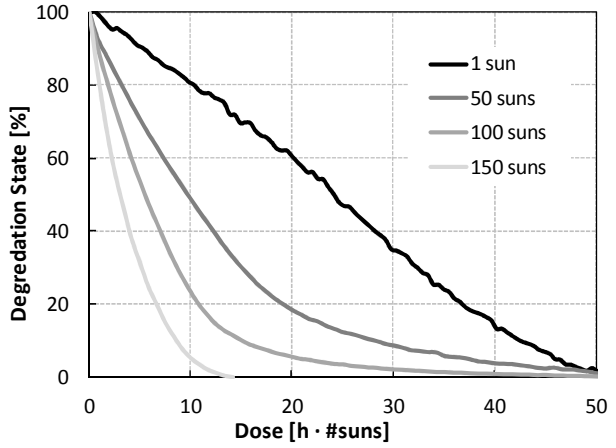

Figure 2. Degradation state *versus* dose for 110 nm P3HT films performed at 1, 50, 100, and 150 suns.

Degradation of P3HT films at 1 sun is a well described phenomenon, known to proceed *via* a mechanism based on a radical process initiated by an abstraction of an allylic hydrogen, leading to side-chain and sulfur oxidation.[10,11] This process is responsible for breaking the macromolecular backbone resulting in loss of conjugation and consequent bleaching of the sample. It has been demonstrated that the P3HT polymer is attacked at terminal thiophene rings at points of broken conjugation, and that degradation is both thickness and regioregularity dependent.[4,12] A strong increase in photon effectiveness is observed for photo degradation of P3HT films for decreasing irradiation wavelengths, and it has been demonstrated that oxygen diffusion is not a rate limiting factor under 1 sun conditions.[6] For concentrated light conditions it is unknown if this remains true. Concentrated light might introduce degradation mechanisms that are not observed at 1 sun, which could change the degradation rates. The thermal equilibrium of the sample is expected to change with intensity convoluting the degradation rates. A single study by Tromholt *et al.* reports accelerated photochemical degradation by concentrated sunlight. They observed an acceleration factor of 55 for P3HT by comparing the degradation rate at 1 sun (0.1 W/cm^2) and at 100 suns (10 W/cm^2).[9] This suggests that at 100 suns, each photon has roughly half the effectiveness that a photon has at 1 sun. The spectrum at 1 sun in that particular work was an artificial light source, while the 100 sun spectrum was natural sunlight focused through a concentrating lens setup. The spectra thus had vastly different UV content and a decrease in photon effectiveness was consequently expected. The question, however, remains: are the photons equally destructive at all intensities or do some higher order degradation mechanisms become prevalent at higher intensities. The gradual decrease of absorbance during degradation of P3HT is linear in the initial part of the degradation process at 1 sun.[6] In Figure 2 the black line represents degradation of a 110 nm P3HT film at 1 sun. The degree of degradation is observed to increase linearly with dose and is completely degraded after roughly 50 hours in agreement with the literature.[4] For concentrated light at 50, 100, and 150 suns, the dose-corrected degradation rate is observed to be higher as shown in Figure 2. Furthermore, the linearity is observed to be lost for concentrated light conditions. The degradation rate is decelerating with time, making it impossible to establish a single degradation rate for polymers degraded under concentrated light. The dose-corrected degradation rates, expressed as degradation rate per solar intensity, for concentrated conditions, have been determined for the initial 10 percent of the degradation process and compared (Figure S1). The dose-corrected acceleration factor, calculated by the ratio of the dose-corrected concentrated degradation rates and the corresponding value for 1 sun, is shown in Figure 3 for degradations at 50, 100, and 150 suns for film thicknesses between10 and 115 nm. The degradation rate corresponding to 1 sun, depicted as the dashed line in Figure 3, represents a polynomial fit of 526 separate degradation experiments covering the entire film thickness range with an r-squared value of 0.93. The dose-corrected acceleration factor of 8 observed for 150 suns at the largest film thickness indicates an absolute acceleration factor of 1,200, which is the highest acceleration factor reported in literature. It is evident that increasing light intensity implies increasing dose-corrected degradation rates when compared to the 1 sun data. Additionally, the effect is observed to increase with film thickness, suggesting that the photon effectiveness increases with higher light intensities and film thicknesses.

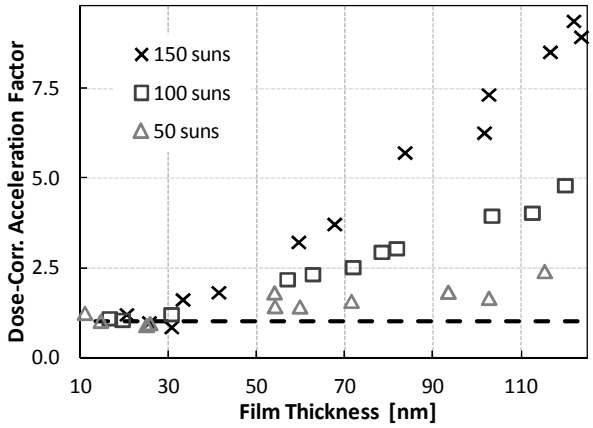

Figure 3. Dose-corrected acceleration factors for films degraded at 50, 100, and 150 suns as a function of film thickness.

The concentrated light will induce a temperature increase in the material, and we thus hypothesize that the rise in effectiveness observed in our data is purely a consequence of the induced temperature increase during experiments. The extent of the induced temperature increase depends on the absorption of the sample, and thus the hypothesis explains the decelerating degradation rates observed in Figure 2. It was technically not possible to measure the temperature in the material during light exposure, so an estimate was done based on a simple approximation. By assuming that the temperature can be modeled by the absorbed energy Q_{in}, a radiative loss, and a loss associated with the thermal conductivity through the glass, the steady state can be written as $Q_{rl} + Q_{TC} = Q_{in} + Q_0$, where Q_{rl} is the radiative loss given as $Q_{rl} = 2\sigma e T^4 a$, $Q_0 = 2\sigma e T_0^4 a$ is the room temperature energy, and $Q_{TC} = ka\left|dT/dx\right|$ is the thermal conductivity. The emissivity is set to $e = 0.92$ equal to the emissivity for glass, and in the interval given for poly-vinyl-chloride. The room temperature energy is set to $T_0 = 30°C$. For the thermal conductivity it is assumed that the glass is coupled to a perfect heat reservoir, the glass has a thickness of

Appendix 4

1 mm, and a thermal conductivity of $k = 0.8$. The area a is given by the area of the incoming light. The input energy is calculated as the number of photons absorbed at each wavelength ($A(\lambda)$) multiplied by the energy at that given wavelength ($E(\lambda)$) by $Q_{in} = \sum \left[A(\lambda) \overline{N} \cdot E(\lambda) \right]$. The absorption is measured for each thickness and the number of photons is calculated from the spectrum of the light source. By solving the equation for each thickness, it is possible to calculate the temperature (Figure S2). For a film of 100 nm, a temperature of 65 °C is predicted for 150 suns. It is important to emphasize that this temperature will be a lower limit estimate since the model assumes an instant thermalisation between the polymer and the glass substrate. Furthermore, the model assumes that the substrate is coupled to a perfect heat reservoir.

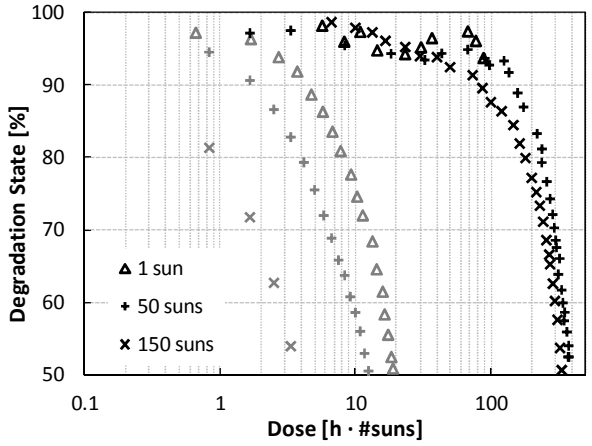

Figure 4. Degradation of P3HT in nitrogen atmosphere (black markers) and degradation in ambient atmosphere (grey markers).

In an attempt to obtain an experimental value for the temperature, a glass /polymer / silver sample with a thickness of 50 nm was constructed by evaporating silver on a P3HT covered glass substrate. By illuminating the sample from the glass side, the temperature could be measured by coupling a thermocouple to the silver layer, thereby avoiding the temperature increase due to the absorption of the thermocouple. At 150 suns a temperature of 175 °C was measured. Since the reflection from the silver interface is not perfect, the silver will induce a temperature increase by itself, so the measured value can be considered as an upper limit for the temperature of the polymer. As the light passes the film twice, the effective thickness is 100 nm. Consequently, a film with a thickness of 100 nm will have a temperature in the range between 65 °C and 175 °C.

Assuming that the temperature dependence of the reaction can be described by an Arrhenius model, it is possible to model the temperature based on the observed acceleration factor. The acceleration observed during degradation at two different temperatures *T'* and *T* can be described by

$$K = B e^{\frac{E_A}{R}T'} \Big/ B e^{\frac{E_A}{R}T} = e^{\frac{E_A}{R}\left(\frac{1}{T} - \frac{1}{T'}\right)},$$

where R is the gas constant, E_A is the activation energy, and B is the pre-factor. The activation energy for P3HT has been reported by Hintz *et al.* to be $E_A = 26.5kJ$ and thereby it is possible to calculate the temperature of the material for a given acceleration factor (Figure S2).[6] The temperature for a film of 100 nm is thus predicted to be 100 °C at 150 suns, which is within the established upper and lower limit.

The hypothesis implies that materials with different activation energies will yield different acceleration factors. In order to investigate this further, polythiophene (PT) with an activation energy of $E_A = 16.0kJ$ was tested.[13] It is assumed that the temperature of PT is equal to the temperature of P3HT at equal absorption level since the absorption spectrum of P3HT and PT are similar. At an optical density of 0.5, PT is predicted to have a dose-corrected acceleration factor of 2.2. The experimentally determined dose-corrected acceleration factor for PT was 2.0 in fair agreement with the prediction. This implies that the degradation rate based on concentrated light is deterministic given the sample temperature and the activation energy.

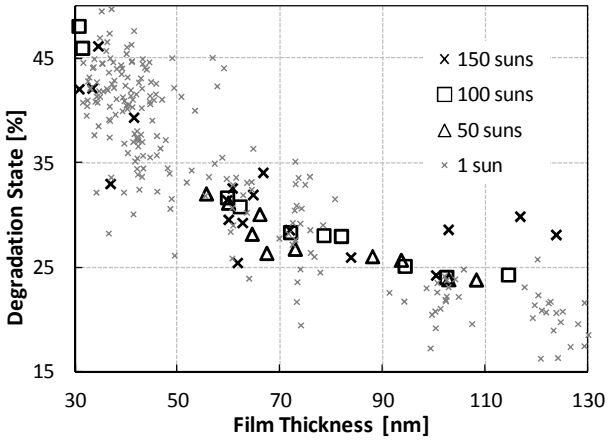

Figure 5. Degradation state for which the film absorbance has shifted to 480 nm as observed for different thicknesses of P3HT films and at different light intensities.

The thermal activation is expected only for samples where photo oxidation is dominant. The increased energy associated with the temperature increase is insignificant in comparison to the energy of the light. At 100 °C, the thermal energy equates to 32 meV, which is significantly lower than the photon energy (1 - 4.5 eV). Figure 4 shows the degradation of six samples under ambient and nitrogen atmospheres. It is evident that the photolysis of P3HT is not thermally activated as the degradation at 1 sun, 50 suns, and 150 suns overlap in degradation time. Reference 11 has documented that thermo oxidation takes place on a time scale of 10,000 hours while photo oxidation takes place in the time frame of 100 hours. It thus follows that for all practical purposes thermal activation only occurs when oxygen is present. Under ambient atmosphere, acceleration is observed for increasing intensity. The sample exposed to 1 sun and a nitrogen atmosphere was stopped at 96% of the initial absorbance. In order to degrade the 1 sun sample to 50 percent, a timeframe of 1 month was needed, far exceeding the capacity of nitrogen available. This study represents the first degradation experiment described in the literature where P3HT under photolysis has reached T50.

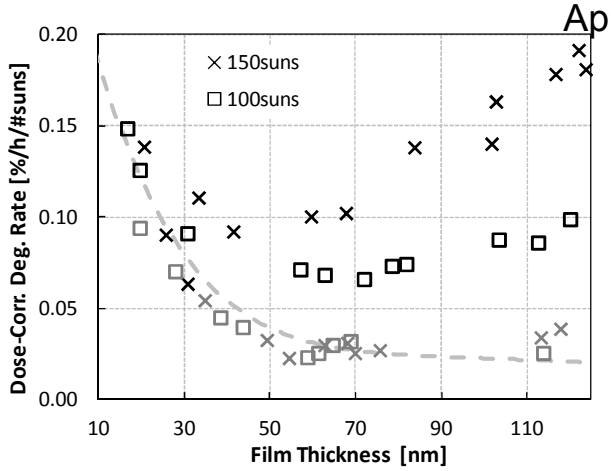

Figure 6. Dose-corrected degradation rates for cooled (grey markers) and non-cooled samples (black markers).

The hypothesis of thermal activation as the only major contributing factor to the dose-corrected acceleration factor also implies that the reaction mechanism remains unchanged. This is in agreement with the findings described in reference 9 where IR spectra of degraded polymers were compared at 1 sun and 100 suns for poly-(phenylene-vinylene) (PPV). Figure 5 shows a plot describing the evolution of the peak shift in the optical absorption spectrum for 1 sun and concentrated light. The values represent the degradation state at which the absorption peak has shifted from the initial value to 480 nm. It is clearly evident that the peak shift occurs at the same degradation state for all light concentrations. This supports the fact that the reaction mechanics remain unchanged for all intensities.

In an attempt to prevent heating of the samples, an air ventilation setup was installed. The samples were continuously ventilated by a dry air flow at a flow rate of 25 liters per minute at ambient temperature directed at the polymer surface, effectively cooling the samples. As is evident from Figure 6 the degradation rates from the cooled samples overlay the 1 sun degradation rates. It was further observed that the degradation rates exhibited a linear behavior with dose, suggesting that no temperature change took place. The fact that the temperature influence can be eliminated by effective cooling proves the hypothesis of thermal activation and demonstrates that the degradation mechanism remains constant for all intensities between 1 and 150 suns. This also implies that concentrated light can be used to determine the degradation rates for polymer films with proper cooling, leading to the opportunity of using concentrated light as a rapid evaluation tool in the pursuit of stable materials.

By studying degradation rates at different light intensities of conjugated polymers, it has been clearly established that the degradation rate scales linearly with light intensity. Any observed deviations from this behavior can be ascribed to an induced temperature increase leading to a thermal acceleration factor. The degradation mechanism and kinetic have been demonstrated to remain unchanged in the range between 1 and 150 suns, and oxygen diffusion rates are not a limiting factor, even at 150 suns. This documents that the photon effectiveness towards degradation is fundamentally independent of the light intensity for films of P3HT. If the temperature of the sample and activation energy is known, it is possible to compensate for the temperature induced acceleration and use concentrated studies deterministically. This can lead to extremely high acceleration factors, and an acceleration factor of 1,200 has been reported in this paper for P3HT. Photolysis has been shown to be unaffected by temperature and degradation experiments have been performed to T50 at 50 and 150 suns. Concentrated light for accelerated polymer degradation thus constitutes a practical approach by which the time frame of polymer stability evaluation can be severely reduced and the 1 sun stability can be precisely calculated. This allows for rapid, routine stability studies of even very air-stable polymers, which will prove valuable to the development of commercial PSCs with stability exceeding years.

ASSOCIATED CONTENT

Supporting Information. Complete experimental procedures, setup documentation, and supporting data.

AUTHOR INFORMATION

Corresponding Author

*mves@dtu.dk

ACKNOWLEDGMENT

This work was supported by the Danish Strategic Research Council (2104-07-0022), EUDP (j. no. 64009-0050) and PVERA-NET (project acronym POLYSTAR). The authors would like to express gratitude to Kristian Larsen valuable in building the solar concentrator, the sample exchanger robot, and the atmosphere chambers.

REFERENCES

(1) UCLA http://newsroom.ucla.edu/portal/ucla/ucla-engineers-create-tandem-polymer-228468.aspx, accesssed 5/5-12 **2012**.
(2) Heliatek http://www.heliatek.com/?p=1923&lang=en, accessed 5/5-12 **2012**.
(3) Hauch, J. A.; Schilinsky, P.; Choulis, S. A.; Childers, R.; Biele, M.; Brabec, C. J. Sol. Energy Mater. Sol. Cells **2008**, 92, 727-731.
(4) Tromholt, T.; Madsen, M. V.; Carlé, J. E.; Helgesen, M.; Krebs, F. C. J. Mater. Chem. **2012**, 22, 7592-7601.
(5) Schuller, S.; Schilinsky, P.; Hauch, J.; Brabec, C. J. Appl. Phys. A-Mater. **2004**, 79, 37-40.
(6) Hintz, H.; Egelhaaf, H.-J.; Lu□er, L.; Hauch, J.; Peisert, H.; Chassé, T. Chem. Mater. **2010**, 23, 145-154.
(7) Tromholt, T.; Katz, E. A.; Hirsch, B.; Vossier, A.; Krebs, F. C. Appl. Phys. Lett. **2010**, 96, 073501.
(8) Tromholt, T.; Manor, A.; Katz, E. A.; Krebs, F. C. Nanotechnology **2011**, 22, 225401.
(9) Tromholt, T.; Manceau, M.; Helgesen, M.; Carlé, J. E.; Krebs, F. C. Sol. Energy Mater. Sol. Cells **2010**, 95, 1308-1314.
(10) Manceau, M.; Rivaton, A.; Gardette, J.-L. Macromol. Rapid Commun. **2008**, 29, 1823-1827.
(11) Manceau, M.; Rivaton, A.; Gardette, J.-L.; Guillerez, S.; Lemaître, N. Polym. Degrad. Stab. **2009**, 94, 898-907.
(12) Hintz, H.; Egelhaaf, H.-J.; Peisert, H.; Chassé, T. Polym. Degrad. Stab. **2010**, 95, 818-825.
(13) Otero, T. F.; Santos, F. Electrochim. Acta **2008**, 53, 3166-3174.

Appendix 4

TOC graphic:

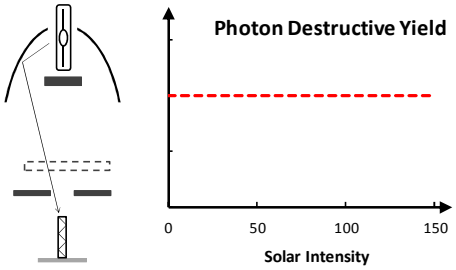

APPLIED PHYSICS LETTERS **96**, 073501 (2010)

Effects of concentrated sunlight on organic photovoltaics

Thomas Tromholt,[1] Eugene A. Katz,[2,3,a)] Baruch Hirsch,[2] Alexis Vossier,[2] and Frederik C. Krebs[1]

[1]*Risø National Laboratory for Sustainable Energy, Technical University of Denmark, Frederiksborgvej 399, DK-4000 Roskilde, Denmark*

[2]*Department of Solar Energy and Environmental Physics, J. Blaustein Institutes for Desert Research, Ben-Gurion University of the Negev, Sede Boker Campus, Midreshet Sede Boker 84990, Israel*

[3]*The Ilse Katz Institute for Nanoscale Science and Technology, Ben-Gurion University of the Negev, Beersheva 84105, Israel*

(Received 8 October 2009; accepted 1 January 2010; published online 16 February 2010)

We report the effects of concentrated sunlight on key photovoltaic parameters and stability of organic photovoltaics (OPV). Sunlight collected and concentrated outdoors was focused into an optical fiber and delivered onto a 1 cm^2 bulk-heterojunction cell. Sunlight concentration C was varied gradually from 0.2 to 27 suns. Power conversion efficiency exhibited slow increase with C that was followed by saturation around 2% at $C=0.5-2.5$ suns and subsequent strong reduction. Possible OPV applications in stationary solar concentrators ($C \leq 2$ suns) are discussed. Finally, experiments at $C=55-58$ suns demonstrated potential of our approach for accelerated studies of light induced mechanisms in the OPV degradation. © *2010 American Institute of Physics*. [doi:10.1063/1.3298742]

Organic photovoltaics (OPV) has been suggested as a low-cost, lightweight, flexible alternative to inorganic photovoltaics. In particular, intense research is directed toward the development of OPV with a bulk heterojunction (BHJ) between donor-type conjugated polymers and acceptor-type fullerenes [e.g., poly(3-hexylthiophene) (P3HT)] and fullerene derivative, phenyl-C61-butyric acid methylester (PCBM).[1]

OPV is known to suffer from significant degradation upon simultaneous exposure to sunlight and air (oxygen and water vapor).[2,3] A typical operational lifetime of encapsulated OPV under full solar illumination (1 sun $=100$ mW/cm^2) has for a long period of time been in the range of only days or weeks.[4] Recently long-term-stable BHJ cells have been developed.[3,5–7] This achievement opens various possibilities in OPV investigations (e.g., round robin test)[8] and development of practical applications. On the other hand, it raises problems, e.g., need for relevant accelerated tests of operational life-time.

We suggest that stable OPV can be used with low-cost stationary concentrators of sunlight working in the low concentration regime (<3 suns).[9] To check this hypothesis effects of sunlight concentration on the OPV efficiency and stability should be investigated. Here we report experimental exploitation of concentrated sunlight for such study using fiber-optic/mini-dish concentrator[10–12] [Figs. 1(a) and 1(b)]. We also demonstrate that our experimental approach can be used for accelerated tests of the OPV degradation.

The BHJ OPV devices were prepared in the ambient at Risø DTU, using a fully roll-to-roll compatible solar cell device preparation.[8,13] Commercially available indium tin oxide (ITO) glass substrates with a sheet resistivity of $5-8\ \Omega^{-1}$ were sonicated in isopropanol followed by washing in demineralized water. Layers of ZnO nanoparticles photoactive P3HT:PCBM and poly(3,4-ethylenedioxythiophene): polystyrene sulfonate (PEDOT:PSS) were then subsequently spin-coated. The layered architecture of the device was thus glass|ITO|ZnO|P3HT:PCBM|PEDOT:PSS|Ag [Fig. 1(c)]. The photoactive area is defined by the 1×1 cm^2 overlap between the ITO and the Ag electrodes. The samples were encapsulated by applying an adhesive plastic foil on the Ag electrode. During illumination, the cells were masked to ensure that only 1 cm^2 active area contributed to the photocurrent.

Prior to the transportation to Sede Boker, Israel, the current-voltage (I-V) characterization was performed with a Steuernagel Solarkonstant KHS575 solar simulator (100 mW/cm^2, AM1.5G, 25 °C).

Power conversion efficiency η was calculated as

$$\eta = P_m/P_{in} = I_{sc}V_{oc}FF/P_{in} \quad (1)$$

where I_{sc} and V_{oc} and FF denote short-circuit current, open-circuit voltage and fill factor, respectively. P_m and P_{in} are the

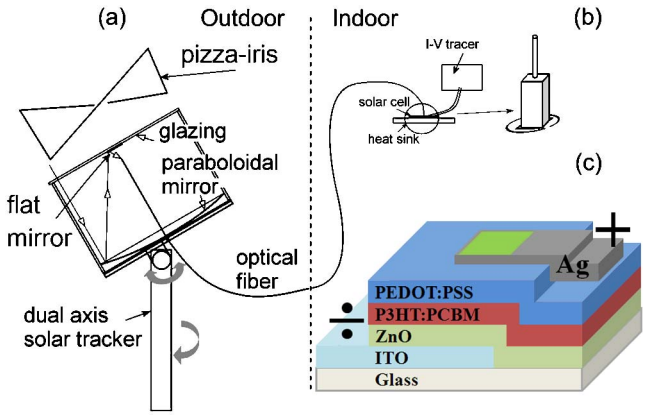

FIG. 1. (Color online) (a) Minidish dual-axis tracking solar concentrator (20 cm in diameter). Solar radiation is concentrated outdoors into the tip of a highly transmitting optical fiber which guides the concentrated sunlight indoors onto the solar cell being tested. (b) Uniform cell irradiation via a kaleidoscope. (c) The layer sequence of the inverted P3HT:PCBM BHJ cell (through-glass illumination). The solar cell area is defined as the overlap between the ITO and the Ag electrodes.

a)Author to whom correspondence should be addressed. Electronic mail: keugene@bgu.ac.il.

TABLE I. Fitting parameters for four studied solar cells. G and α are the fitting parameters describing a power law relation between I_{sc} and P_{in} [Eq. (3)]. n is the diode ideality factor calculated by evaluating the semilogarithmic fit of the V_{oc} data according to Eq. (2). G, α, and n were calculated for $C \leq 10$ suns.

Solar cell	R_s (Ω)	G	α	n
A	4.06	40.83	0.96	1.27
B	2.71	44.18	0.92	1.23
C	4.12	53.33	0.95	1.22
D	5.57	55.49	0.91	1.21

maximum electrical power output and incident light power.

The cell series resistance R_s was calculated from the reciprocal slope of the I-V curve at high applied voltage ($V=1$ V).

Four different solar cells with $\eta \sim 2\%$ and $FF \sim (0.55-0.6)$, indicating low R_s (Table I), were delivered to Sede Boker for a study with concentrated sunlight.

In Sede Boker, sunlight collected and concentrated outdoors was focused into a transmissive (quartz-core) optical fiber of 1 mm in diameter and then delivered indoors onto the solar cell being tested [Fig. 1(a)].[10–12] Flux uniformity was achieved with a 3 cm long square cross-section kaleidoscope, matching the size of the cell, placed between distal fiber tip and cell [Fig. 1(b)].

Measurements were limited to clear-sky periods, two hours around solar noon. The light spectrum on the cell was nearly invariant and close to the AM1.5.[8,14,15] Concentration of sunlight delivered to the cell (C) was varied gradually from 0.2 to 27 suns with a pizza-slice iris [Fig. 1(a)], and measured pyrometrically. I-V measurements were made with opening a shutter above the iris and illuminating the cell during I-V tracing only (<3 sec) to avoid excessive degradation and temperature variations.

In addition, the cells were subjected to a long-term (3 h) illumination at $C=55-58$ suns in order to study effect of high concentration on OPV degradation.

For conventional inorganic solar cell, I_{sc} is known to depend linearly on C. Meanwhile, V_{oc} increases logarithmically with I_{sc} and C

$$V_{oc} \approx (nkT/q)\ln(I_{sc}/I_o) = (nkT/q)\ln(C) + \text{const}, \quad (2)$$

where n and I_o denote the diode quality factor and the reverse saturation current, correspondingly.

Semilog plots of η as a function of C should exhibit linear behavior in the lower flux regime, with a slope proportional the effective thermal voltage nkT/q (from the contribution of V_{oc}). These plots should also feature (a) a nonlinear decrease at sufficiently high flux due to R_s dissipation, and (b) a maximum that reflects this tradeoff. So the flux level at which η peaks is governed by R_s. In recent generations of inorganic concentrator cells, η is maximized at hundreds of suns and higher.[11,12]

Figure 2 summarizes our data for I_{sc}, V_{oc}, FF, and η as functions of sunlight concentration.

For OPV the intensity dependence of the photovoltaic parameters is still under discussion. To the best of our knowledge, for BHJ OPV it was studied only for $C \leq 1$ sun.[16,17] C_{60}/copper phthalocyanine (CuPc) bilayer cells were characterized up to 12 suns of simulated illumination).[18][174]

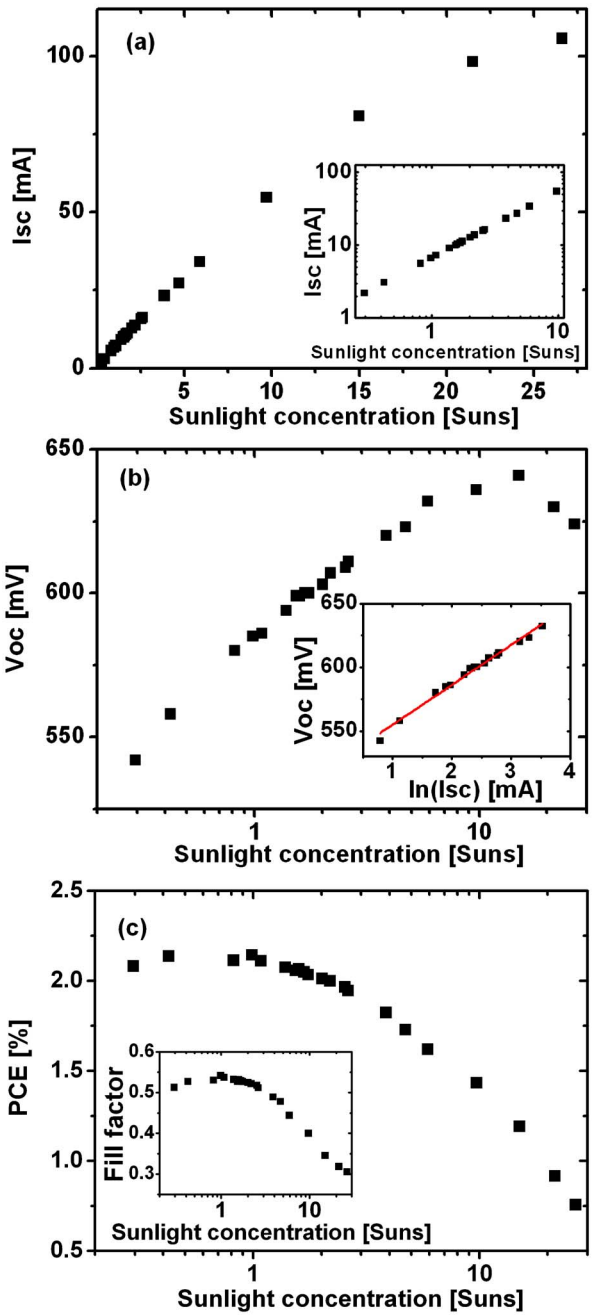

FIG. 2. Effect of sunlight concentration on I_{sc} (a), V_{oc} (b) η, (c) and FF [inset in (c)] of BHJ cell. Insets in (a) and (b) show the linear dependence of $\log I_{sc}$ on $\log C$ and the linear correlation between V_{oc} and $\ln I_{sc}$, respectively.

In general, I_{sc} of OPV can increase with C according to a power law

$$I_{sc} = G \times P_{in}^{\alpha}. \quad (3)$$

The deviation of α from 1 is attributed to a bimolecular recombination of photogenerated carriers (for dominant bimolecular recombination $\alpha=0.5$).[16] For $C \leq 10$ suns I_{sc} of our cells was found to increase with C according to Eq. (3) [inset in Fig. 2(a)] with α very near to 1 (0.91–0.96 in Table I). This is consistent with the published characteristics of highly efficient BHJ OPV obtained for $C=0-1$ sun.[16] For $10 < C \leq 27$ suns, a sublinear behavior of I_{sc} is in evidence [Fig. 2(a)] that can be explained either by the increased influence of the bimolecular recombination or by effect of nonideal uniformity of illumination (see below).

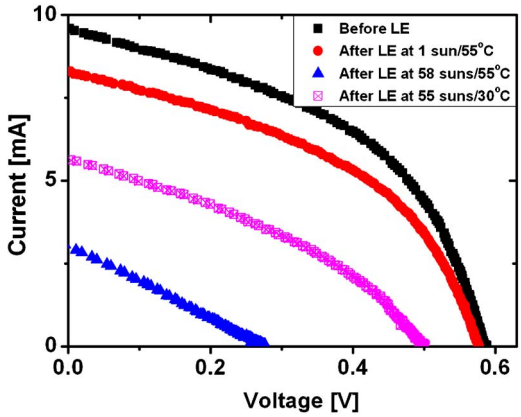

FIG. 3. (Color online) *I-V* curves measured before and after 3 hours of light exposure (LE) at: various *C* and temperature.

For $C \leq 10$ suns, V_{oc} increases logarithmically with I_{sc} [inset in Fig. 2(b)] with a slope approximately equal to kT/q ($n=1.21-1.27$ in Table I) that was theoretically predicted for OPV.[17] Decrease in V_{oc} in h flux regime ($C=10-27$ suns) indicates BHJ overheating by concentrated sunlight (the thermocouple placed on the cell backside revealed a constant temperature $T=27-29$ °C for $C<10$ suns and T increased for $C>10$ suns).

FF [inset in Fig. 2(c)] exhibits slow increase with *C* in low flux regime reaching a maximum of ~0.55 at $C \approx 1$ sun. For 1 sun $< C \leq 2$ suns, *FF* is almost independent on *C* and then starts to roll off (down to ≈0.3 at $C=27$ suns).

η shows a predictable slight increase followed by a saturation region with η around 2% (at $C=0.5-2.5$ suns) and strong reduction at high *C*. Existence of the pronounced saturation regime is very important for OPV applications in stationary solar concentrators (at $C \leq 2$ suns)[8] and benefit of possible bifacial architecture of OPV devices.[13]

Use of OPV at $C>1$ raised challenges for the cell stability at these illumination levels and technology optimization to minimize R_s. The latter can move the efficiency peak toward high sunlight concentration. The C_{60}/CuPc cells with a small area (from 0.007 to 0.06 cm^2) and optimized R_s were demonstrated to reach the maximum η at 4–12 suns.[18] R_s is known to increase with the cell area for both inorganic cells[12] and OPV[18] that should result in the reduction in concentration for the peak η. Recently[12] it was demonstrated that η of 1 mm^2 III-V semiconductor concentrator cells is maximized at ~1000 suns while for a 1 cm^2 cell of the same nominal architecture it peaked at ~350 suns.

At $C=10-27$ suns the observed η behavior [Fig. 2(c)] is controlled by a strong *FF* reduction due to R_s dissipation [inset in Fig. 2(c)]. Indeed *FF* rolls off from ~0.4 at $C=10$ suns down to ~0.3 at 27 suns. These low *FF* values together with possible nonideal uniformity of the illumination[19] can cause the observed sublinear behavior of I_{sc} [Fig. 2(a)].[11]

Figure 3 shows 1 sun outdoor *I-V* measurements of 3 similar cells (with initial $\eta \approx 2\%$) before and after 3 h of light exposure at various *C* and temperatures. Details of our outdoor measurements are described elsewhere.[8,14,15]

Exposure of the first cell under 1 sun was performed outdoor at $T=50$ °C. Both *FF* and V_{oc} were found to decrease slightly (by ~2% of their initial value) while I_{sc} exhibited more pronounced degradation, by ~20%.

For the high *C* experiments the cells were mounted on a 6 mm thick copper heat sink and exposed indoor with the setup shown in Fig. 1. Exposure of the second cell by $C=58$ suns resulted in $T=55$ °C and caused significant degradation: both V_{oc} and I_{sc} degraded by ~50% while *FF* reached its minimum value of 0.25.

Water cooling of the heat sink allowed to keep the third-cell $T=30$ °C during the illumination by similar light concentration. The degradation was considerably slower than that revealed in the high *C*/high *T* experiment.

In summary, using the fiber-optic/mini-dish solar concentrator, we studied the effect of sunlight concentration on the key parameters of 1 cm^2 P3HT:PCBM BHJ cells. *C* was varied gradually from 0.2 to 27 suns. For $C \leq 10$ suns I_{sc} was found to increase with *C* almost linearly while V_{oc} increased logarithmically with I_{sc}. Decrease in V_{oc} at $C=10-27$ suns was attributed to the BHJ heating by concentrated sunlight. Both *FF* and the efficiency η exhibit slow increase in low flux regime that was followed by a saturation region (η saturated around 2% at $C=0.5-2.5$ suns) and subsequent strong reduction due to R_s dissipation. Existence of the saturation regime is very important for possible OPV applications in stationary solar concentrators ($C \leq 2$ suns). Finally, the preliminary long-term experiments at high *C* (55–58 suns) and various temperatures proved that our setup can be used for accelerated tests of the OPV operational lifetime. Furthermore, one can propose a research strategy for future detailed experiments that may select light induced mechanisms in the OPV degradation from those (like interface diffusion, etc.)[5,6] controlled by the cell temperature.

[1] C. J. Brabec, N. S. Sariciftci, and J. C. Hummelen, Adv. Funct. Mater. **11**, 15 (2001).
[2] M. Jørgensen, K. Norrman, and F. C. Krebs, Sol. Energy Mater. Sol. Cells **92**, 686 (2008).
[3] *Organic Photovoltaics: A Practical Approach*, edited by F. C. Krebs (SPIE, Bellingham, 2008).
[4] F. C. Krebs, J. Alstrup, H. Spangaard, K. Larsen, and E. Kold, Sol. Energy Mater. Sol. Cells **83**, 293 (2004).
[5] J. A. Hauch, P. Schilinsky, S. A. Choulis, R. Childers, M. Bielea, and C. J. Brabec, Sol. Energy Mater. Sol. Cells **92**, 727 (2008).
[6] F. C. Krebs and K. Norrman, Prog. Photovoltaics **15**, 697 (2007).
[7] B. Zimmermann, U. Würfel, and M. Niggemann, Sol. Energy Mater. Sol. Cells **93**, 491 (2009).
[8] F. C. Krebs *et al.*, Sol. Energy Mater. Sol. Cells **93**, 1968 (2009).
[9] T. Uematsu, Y. Yazawa, T. Joge, and S. Kokunai, Sol. Energy Mater. Sol. Cells **67**, 425 (2001).
[10] J. M. Gordon, E. A. Katz, D. Feuermann, and M. Huleihil, Appl. Phys. Lett. **84**, 3642 (2004).
[11] E. A. Katz, J. M. Gordon, W. Tassew, and D. Feuermann, J. Appl. Phys. **100**, 044514 (2006).
[12] O. Korech, B. Hirsch, E. A. Katz, and J. M. Gordon, Appl. Phys. Lett. **91**, 064101 (2007).
[13] F. C. Krebs, S. A. Gevorgyan, and J. Alstrup, J. Mater. Chem. **19**, 5442 (2009).
[14] E. A. Katz, D. Faiman, S. M. Tuladhar, J. M. Kroon, M. M. Wienk, T. Fromherz, F. Padinger, C. J. Brabec, and N. S. Sariciftci, J. Appl. Phys. **90**, 5343 (2001).
[15] E. A. Katz, S. Gevorgyan, M. S. Orynbayev, and F. C. Krebs, Eur. Phys. J.: Appl. Phys. **36**, 307 (2006).
[16] J. K. J. van Duren, X. Yang, J. Loos, C. W. T. Bulle-Lieuwma, A. B. Sieval, J. C. Hummelen, and R. A. Janssen, Adv. Funct. Mater. **14**, 425 (2004).
[17] L. J. A. Koster, V. D. Mihailetchi, R. Ramaker, and P. W. M. Blom, Appl. Phys. Lett. **86**, 123509 (2005).
[18] J. Xue, S. Uchida, B. P. Rand, and S. R. Forrest, Appl. Phys. Lett. **84**, 3013 (2004).
[19] See supplementary material at http://dx.doi.org/10.1063/1.3298742 for description of the ray tracing in our optical system.

IOP PUBLISHING NANOTECHNOLOGY

Nanotechnology **22** (2011) 225401 (6pp) doi:10.1088/0957-4484/22/22/225401

Reversible degradation of inverted organic solar cells by concentrated sunlight

Thomas Tromholt[1,4], **Assaf Manor**[2], **Eugene A Katz**[2,3] **and Frederik C Krebs**[1]

[1] Risø National Laboratory for Sustainable Energy, Technical University of Denmark, Frederiksborgvej 399, DK-4000 Roskilde, Denmark
[2] Department of Solar Energy and Environmental Physics, J Blaustein Institutes for Desert Research, Ben-Gurion University of the Negev, Sede Boker Campus 84990, Israel
[3] The Ilse Katz Institute for Nanoscale Science and Technology, Ben-Gurion University of the Negev, Beersheva 84105, Israel

E-mail: ttro@risoe.dtu.dk

Received 7 January 2011, in final form 10 February 2011
Published 1 April 2011
Online at stacks.iop.org/Nano/22/225401

Abstract

Concentrated sunlight was used to study the performance response of inverted P3HT:PCBM organic solar cells after exposure to high intensity sunlight. Correlations of efficiency as a function of solar intensity were established in the range of 0.5–15 suns at three different stages: for a pristine cell, after 30 min exposure at 5 suns and after 30 min of rest in the dark. High intensity exposure introduced a major performance decrease for all solar intensities, followed by a partial recovery of the lost performance over time: at 1 sun only 6% of the initial performance was conserved after the high intensity exposure, while after rest the performance had recovered to 60% of the initial value. The timescale of the recovery effect was studied by monitoring the cell performance at 1 sun after high intensity exposure. This showed that cell performance was almost completely restored after 180 min. The transient state is believed to be a result of the breakdown of the diode behaviour of the ZnO electron transport layer by O_2 desorption, increasing the hole conductivity. These results imply that accelerated degradation of organic solar cells by concentrated sunlight is not a straightforward process, and care has to be taken to allow for a sound accelerated lifetime assessment based on concentrated sunlight.

S Online supplementary data available from stacks.iop.org/Nano/22/225401/mmedia

(Some figures in this article are in colour only in the electronic version)

1. Introduction

Polymer solar cells (PSCs) have attracted attention over the past decade due to the potential of low cost, flexibility and large scale production [1, 2]. However, the technology is at the present stage not mature for full scale energy production. One of the challenging points is the development of a photoactive polymer that unites high efficiency, stability and processability in a single material. Efficiency has been given the highest attention due to its intuitive importance to solar cells, where efficiencies in excess of 8% have been reached [3]. The stability of the photoactive polymers has been subjected to less focus. A reason for this is the lack of a rapid stability assessment. The efficiency assessment can be made within seconds whereas the timescale for the stability assessment may be of the order of months or years. This is a hindrance to the research, since the stability evaluation of materials postpones the time frame of the entire development [4].

A solution to this is the application of accelerated degradation conditions. The introduction of various aggressive conditions can increase the degradation rate relative to conventional degradation at 1 simulated sun and thus decrease the time frame of the stability assessment. A prerequisite for such an approach is that the accelerated degradation rate can be related to the standard condition degradation rate by a well known acceleration factor. Heat is the conventional approach, by which acceleration factors in excess of 20 are reachable [5]. A novel approach is based on concentrated sunlight, where the

[4] Author to whom any correspondence should be addressed.

impact of a high photonic flux combined with the associated heating further increases the stress on the cells. Preliminary studies of operating PSCs have demonstrated this, where rapid decreases of J_{sc}, FF and especially V_{oc} were observed after high intensity exposure [6]. However, the temporal evolution of PSC performance has so far not been studied in detail in this context. Our recent study describes the accelerated degradation of single layers of various polymers for PSCs by concentrated sunlight, probed by the evolution of the light absorption decrease during degradation [7]. This study showed a highly predictable evolution of the degradation, conserving the chemistry observed at 1 simulated sun even at high illumination intensities. In particular, acceleration factors exceeding 100 were obtainable for P3HT relative to 1 simulated sun degradation—a level not obtainable by the application of only heat during the degradation. However, the performance response of PSC devices operating at high concentration should be more complicated and less predictable due to the increased complexity of the system. Different performance hysteresis effects have been reported in the literature for PSCs. An example is the performance recovery effect, where lost cell performance after 1 sun illumination was partly recovered after overnight dark storage [8]. However, the opposite effect has been observed where light soaking is needed to reach maximum performance [9, 10]. This shows the intricate sensitivity of the electrical performance of PSCs to even minor changes within the operating device.

High intensity exposure is believed to introduce significant permanent as well as transient (metastable) states. Correlations of efficiencies as a function of illumination intensity have been studied in detail for inorganic solar cells [11]. Due to the stability of inorganic solar cells, the state of the cells does not change significantly from high intensity illumination. Peak efficiencies have been shown to be in the range of several hundreds of suns, whereas in the case of PSCs, the efficiency was found to peak at 1–3 suns [6]. However, only pristine PSCs have been studied, while performance evolution over time at high light intensities has not been addressed.

This paper describes the initial results obtained for PSC performance response to high intensity light illumination. The key solar cell parameters (V_{oc}, J_{sc}, FF and efficiency) as a function of illumination intensity are studied before and after high intensity exposure for pristine PSCs. This provides information about the possible electrical changes which may be introduced, and allows for a discussion of the feasibility of applying high intensity light exposure for accelerated testing.

The timescale of the processes has been studied by following the key cell parameter evolution after high intensity exposure. This gives an understanding of the kinetics involved, and provides a basis for further investigation of the underlying physical mechanisms.

2. Experimental details

2.1. Materials and methods

1 cm × 1 cm inverted bulk heterojunction PSC devices were prepared in the ambient using a fully roll-to-roll compatible solar cell device preparation [12]. A schematic layout of the cell structure is shown in [6]. Commercially available ITO glass substrates with a sheet resistivity of 5–8 Ω/Square were sonicated in isopropanol followed by washing in demineralized water. Layers of ZnO, photoactive P3HT:PCBM and poly(3,4-ethylenedioxythiophene):polystyrene sulfonate (PEDOT:PSS) were then subsequently spin-coated. The ZnO layer was prepared as previously reported, with a concentration of 45 mg ml^{-1} ZnO nanoparticles in acetone stabilized with 10% (w/v) methoxyethoxyacetic acid, forming a 100 nm fully covering layer [9]. An Ag top electrode was evaporated by thermal deposition through a shadow mask, providing the 1 cm × 1 cm geometry of the devices. The complete layer structure was glass|ITO|ZnO|P3HT:PCBM|PEDOT:PSS|Ag. The solar cells were encapsulated by applying an adhesive plastic foil on the Ag electrode.

The solar cells were mounted in a solid aluminium sample holder during all measurements to avoid manual handling during contacting. Two-probe current density–voltage (JV) measurements were recorded with a Keithley 2400 sourcemeter. The sample holder served as a thermal reservoir, keeping the thermal fluctuations to a minimum due to prominent heat dissipation. During longer exposures to high intensity light, all cells were kept in open circuit.

2.2. Sunlight concentration setup

A lens based concentration setup was used to obtain high intensity sunlight, as described in our previous work [7]. Outdoor sunlight was concentrated by a BK7 plano-convex lens (⌀ 32 cm, focal length 50 cm) into a bundle of seven optical fibres (length 15 m, core diameter 1 mm), which guided the light to an indoor laboratory. A glass kaleidoscope was used to homogenize the light output from the fibre bundle, providing a homogeneous spatial light intensity throughout the cell active area. The concentrated solar spectrum was found to resemble the AM1.5G solar spectrum well, differing only by a reduced UV contribution, as shown in figure S1 (available at stacks.iop.org/Nano/22/225401/mmedia). The illumination intensity was controlled by an adjustable pizza iris positioned above the lens, which kept spectral distortions from spherical aberrations at different opening angles to a minimum (figure S2 available at stacks.iop.org/Nano/22/225401/mmedia). An energy output of 1.8 W was obtainable from the setup, implying a maximum of 18 suns (1 sun = 0.1 W cm^{-2}) on the 1 cm^2 active area. The light intensity was monitored by a Thorlabs S314C thermopile between each measurement.

All measurements at 1 sun were performed with simulated sunlight from a KHS 575 solar simulator from Steuernagel Lichttechnik, operating at 1000 W m^{-2}, AM1.5G at 70 °C. The light spectrum is shown in figure S1 (available at stacks.iop.org/Nano/22/225401/mmedia). The incident light intensity of the solar simulator was calibrated with a pyranometer.

Concentrated light JV measurements were performed during clear-sky periods, 4 h around solar noon. The light spectrum on the cell was nearly invariant during this period. Illumination was chopped during the recording of

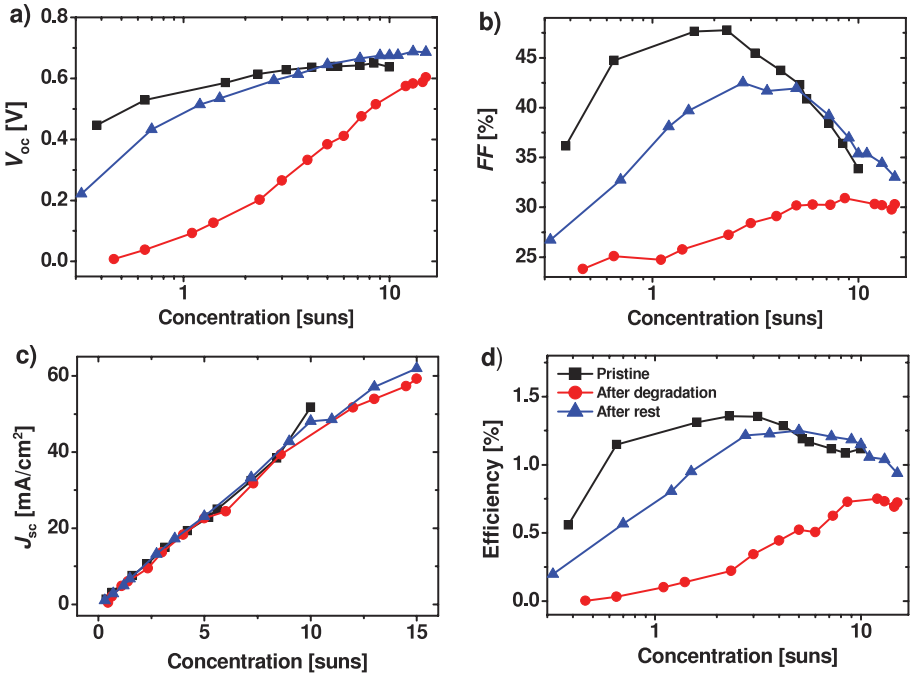

Figure 1. Evolution of the key cell parameters before degradation, right after, and after rest.

the JV curves to reduce the impact of physical changes from higher temperature and photonic flux. JV curves at different illumination intensities were performed from low to high intensity, allowing for measurements under approximate pristine conditions in the low intensity regime.

3. Results and discussion

3.1. Key cell parameter dependence on light intensity

Key cell parameters at different intensities were recorded at three different stages of the cell lifetime: after processing, after 30 min exposure of 5 suns, and after 30 min rest in the dark. Figure 1 shows the key cell parameters plotted versus the light concentration. A typical evolution of V_{oc} with intensity is observed for the pristine cell. After degradation the V_{oc} is highly decreased, and a high slope is observed. 30 min rest introduces an almost complete recovery of the V_{oc} where only 10% loss relative to the pristine sample is observed.

The pristine cell shows a typical FF evolution with an increase from 0 to 1–3 suns followed by a decrease due to the higher contribution of series resistance for high light intensities [6]. The high intensity exposure greatly decreases the FF to 25–30%. This shows that the diode behaviour of the solar cells is completely lost by the high intensity exposure, and thus the solar cell performs as a photoactive resistor. 30 min rest restores the FF partly in the low intensity regime, while above 5 suns complete recovery is observed.

Figure 1 shows the J_{sc}, where a strong linearity for all three states is observed for all solar intensities. This shows that the introduced transient state does not influence the charge extraction properties at high internal electric field within the cell. Additionally, the linearity shows a complete monomolecular nature of recombination in all three states [6].

The overall efficiency of the device shown in figure 1 shows peak efficiency for the pristine cell around 3 suns, but with a relatively stable plateau in the range of 0.5–10 suns. High intensity exposure implies an efficiency decrease, where only 6% of the initial efficiency is conserved at 1 sun, and the cell appears completely degraded. However, at higher illumination intensities performance is found to increase, indicating that the cell is only in a transient degraded state. 30 min rest recovers the efficiency partly, where 60% efficiency at 1 sun is obtained relative to the pristine cell. This general evolution was characteristic for all measured cells (>10). At above 5 suns the performance is even observed to have been increased after the 30 min rest. The high intensity illumination increases the cell temperature, which anneals the active layer. This is known to increase the crystallinity and thus lower the cell series resistance. The effect of this is pronounced at high illumination levels, where large carrier concentrations increase the series resistance contribution to the cell performance. As a result, the annealing side effect of the high intensity illumination increases the cell performance at higher illumination levels.

The general impression is that the transient state affects the device efficiency by decreasing the V_{oc} and FF, which are electrical parameters recorded at a low internal field. On the contrary, the J_{sc} is unchanged, implying that the generation of charges is not changed by the high intensity exposure, since no losses are observed at high internal field. To understand the mechanisms introducing the observed electrical behaviour, the effect has to be localized in the cell. Illumination takes place through the glass substrate (UV cut-off 280 nm), implying that

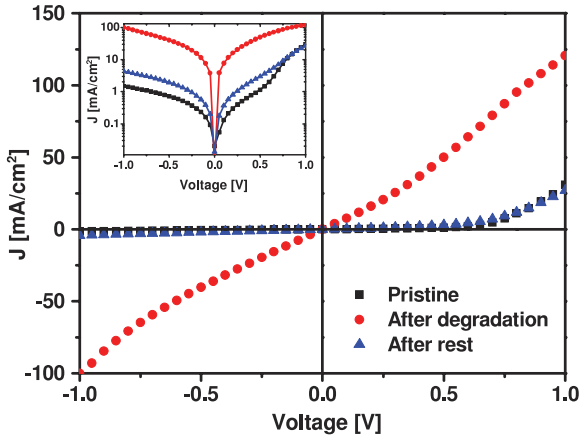

Figure 2. Dark current JV curves for the three different states of the cell. The inset shows the dark log J–V curve with logarithmic J_{sc}.

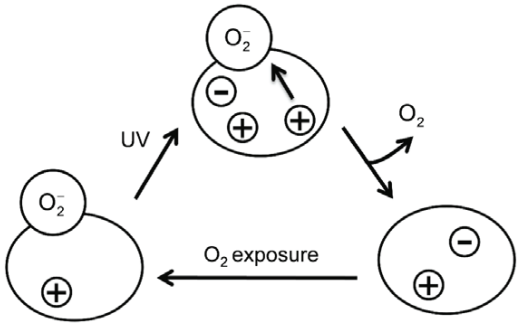

Figure 3. The mechanism proposed by Verbakel *et al*, by which adsorbed oxygen on the ZnO is desorbed by UV illumination, generating free charges. Successive oxygen exposure re-adsorbs the oxygen on the ZnO, thus recovering the rectification properties.

the UV part of the spectrum is absorbed by the ZnO layer (absorption: 280–370 nm, figure S3 available at stacks.iop.org/Nano/22/225401/mmedia) and the visible part is absorbed by the active layer, while the PEDOT remains rather shielded from the light. A side effect of the high intensity exposure is general heating of the entire solar cell. However, a transient state as described here has never been observed for heated solar cells of the type studied in this work, and thus heating is not expected to be the reason for the observed behaviour. Additionally, continuous illumination at 1 sun did not introduce the transient state, implying that the observed effect is a direct consequence of the high illumination intensity. Thus the physical location of the effect is expected to be either the ZnO or the photoactive layer, which are the layers exposed to the high intensity illumination.

As for the photoactive layer, an obvious degradation mechanism from high intensity sunlight is photobleaching, for which the rate is increased at higher illumination intensities [7]. However, the recovery effect cannot be explained from this.

For the data presented here, the transient state is dominant in the low illumination intensity regime—a behaviour expected for trap dominant recombination. Correlations between V_{oc} and the logarithm of the J_{sc} have been studied, since they hold information about the dominant recombination mechanisms. A slope in the range of kT/q was found for dominant bimolecular recombination, where k is Boltzmann's constant, T is the temperature and q is the elementary charge [13]. Experimental work and modelling of trap dominant operation of organic solar cells by the introduction of traps in the PCBM acceptor showed higher correlation factors of the order of several kT/q [14, 15]. For the data presented here the slopes are found to be 2.44, 8.3 and $2.76kT/q$ before, right after high intensity exposure, and after 30 min rest, respectively. However, trap generation would imply a superlinear evolution of the J_{sc} with illumination intensity, since at high illumination intensity trap filling would decrease the trapping contribution to the device performance. However, as J_{sc} varies linearly with illumination intensity in the data presented here, trap generation cannot explain the transient state.

The dark JV response of solar cells has been associated with the light JV behaviour at V_{oc} due to identical loss mechanisms [16]. This makes dark JV analysis interesting since the transient state is most dominant for V_{oc}. Observations of the dark curves should be reflected in the V_{oc} and partly in the FF, which are the key parameters that govern the efficiency of the solar cell in the transient state. Dark curves recorded for the three different states of the cell are presented in figure 2. The behaviour is clearly changed during the high intensity exposure. In the transient state, the conductivity is increased by an order of magnitude in forward bias. Additionally, the pristine IV curve is asymmetric, while after the high intensity exposure the asymmetry is broken and the diode collapses (see inset). However, 30 min rest results in a partial recovery of the rectification properties.

The electron transport layer ZnO used in the solar cells studied here has been studied before and after UV exposure of ZnO-PEDOT:PSS diodes by Verbakel *et al*, and showed a clear transition from a diode to ohmic behaviour [17]. Furthermore, a recovery effect was observed for the material, where 10 min air exposure would restore the rectifying properties. This was explained by desorption of O_2 from the ZnO acting as electron traps by UV induced photogenerated holes, followed by successive re-adsorption of the O_2 on the ZnO, as shown in figure 3. JV analysis of the solar cells showed a similar behaviour of the ZnO, as observed for the dark curves of the solar cells, where both the transition to Ohmic, high conductivity as well as recovery are observed. The consequence of the collapse of the diode is a lowering of V_{oc} and FF. This can be explained from the dark current, for which a very low parallel resistance is observed: the large degree of shunting in the transient state implies significant injection into the solar cell even at low voltages. Increasing the solar intensity increases the photocurrent $J_{ph}(V) = J_{light}(V) - J_{dark}(V)$, which forces the JV curve down relative to the dark curve in figure 2. The overall effect is a strong increase of V_{oc} with increasing solar intensity when J_{ph} increases, and thus the relative effect of the shunting decreases at high intensity. Likewise a clear decrease of the FF is observed after high intensity exposure, where the FF of 25% illustrates the complete collapse of the diode, and thus effectively the solar

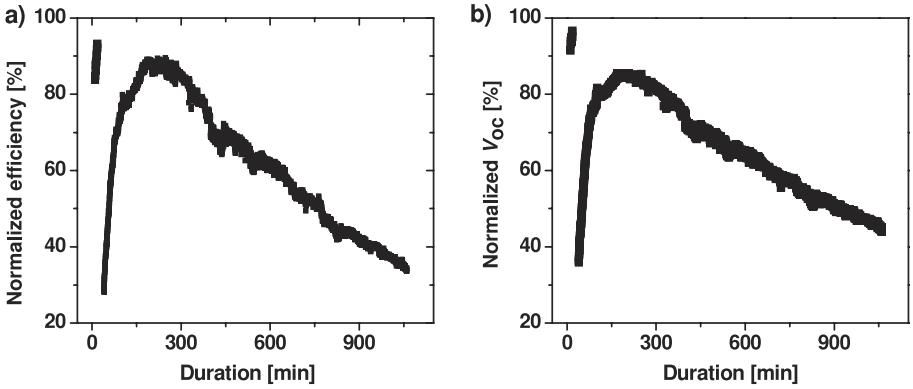

Figure 4. Evolution of (a) normalized efficiency and (b) normalized V_{oc}, measured at 1 sun before and after a 30 min illumination at 5 suns (not shown), which introduced an abrupt decrease of the parameters shown.

cell only works as a photoactive resistor. At high intensities, the FF is observed to increase with light intensity. One possible explanation for this is that the generation of highly conductive channels by the high intensity exposure is current density dependent. They can thus be viewed as a resistor that can be varied by increasing the current density, i.e. the shunting of ZnO by the hole conduction paths. At higher current densities the shunt hole conductivity is outweighed by electron conduction in ZnO, and when they no longer balance rectification gradually sets in (with an associated increase in fill factor).

3.2. Time series

The recovery effect from the ZnO induced transient state was studied over time to establish the time frame of its creation and relaxation. A solar simulator was used to study the cell at 1 sun before and after subjection to concentrated sunlight. A general pattern was observed: illumination at a high intensity would rapidly decrease the performance at 1 sun, after which a slow recovery would take place. Figure 4(a) shows a typical evolution of the efficiency over time before and after high intensity exposure: during the time 0 to 20 min at 1 sun illumination, the cell is observed to recover from a prior high illumination period, by which efficiency increases. 15 min illumination of 7 suns introduces a rapid decrease in efficiency (not shown). Further 1 sun illumination shows that the efficiency decreases to approximately 25% relative to the former value. The recovery effect starts immediately, and after 150 min a local maximum efficiency value is attained, almost at the efficiency level prior to the high intensity exposure. After the local performance peak, actual degradation of the cell is observed.

During the degradation, the evolution of the efficiency was mainly controlled by V_{oc} and FF. Figure 4(b) shows the evolution of the V_{oc}, for which the tendency highly resembles that observed for the efficiency. Initially the V_{oc} is slowly increasing after a high intensity illumination. After the high intensity exposure, the V_{oc} decreased significantly, reduced by 60% compared to before the exposure, followed by a recovery of the V_{oc} over time. The effect of increased temperature from the high light intensity cannot explain the significant V_{oc} decrease, since the steady state temperature after the high intensity exposure was reached within seconds. Thus the V_{oc} reduction can only be ascribed to the high intensity exposure. This fact fits the suggested explanation that the ZnO should introduce the transient state. Even at 1 sun UV photoactivation of the active layer is expected; however this effect may be negligible compared to other dominant recombination mechanisms. The timescale of the recovery was of the order of 2 h, which is close to the timescale of the recovery effect observed for the ZnO conductivity [17]. This is further evidence of the ZnO contribution to cell performance.

The transient effects introduced by high intensity exposure demonstrate the complexity of relating performance of solar cells at high solar intensity to 1 sun reference degradation studies. The response to high intensity light for each material has to be known to understand the overall device performance at accelerated conditions. However, if the solar cell materials are well described, high concentration sunlight can be utilized to perform accelerated degradation studies, thus allowing for a rapid stability assessment of solar cell performance.

Finally, in terms of application of inverted PSCs in commercial concentrator setup, only minor efficiency losses are observed at high intensity (>10 suns) for solar cells in the photoactivated state. This implies that less care has to be taken to avoid the photoinduced reversible transitions as observed for ZnO, while other parameters such as durability to high light intensity are of higher importance.

4. Conclusion

Inverted P3HT:PCBM solar cells were studied in terms of their key cell parameters as a function of light intensity before and after 5 suns exposure for 30 min. Performance at 1 sun of the cell after high intensity exposure was found to be 6% of the initial value as a result of significant decreases of V_{oc} and FF. 30 min rest in the dark almost restored the cell performance, indicating that a transient state was generated, while the individual materials and interfaces remained mostly intact. Dark JV curve analysis showed extensive shunting and increased conductivity of the cell after high intensity exposure,

which was directly related to the key cell parameters. The introduced transient state was explained by photoactivation of the ZnO electron transport layer by which the rectification properties are lost by desorption of O_2, introducing an increased hole conductivity. Recovery of the cell performance after high intensity exposure was explained by successive re-adsorption of O_2, restoring the cell to its pristine state. These results show that accelerated stability studies with concentrated sunlight introduce effects not observed at 1 sun, and care has to be taken when evaluating the accelerated device performance using concentrated sunlight.

Acknowledgments

This work was performed, in part, in the framework of the 'Largecells' project that received funding from the European Commission's Seventh Framework Programme (FP7/2007-2013) under Grant Agreement No. 261936. TT and FCK acknowledge support by the European Commission through the Seventh Framework Programme under the THEME for ENERGY.2010.2.1-2, development of novel materials, device structures and fabrication methods suitable for thin film solar cells and TCOs including organic photovoltaics.

References

[1] Helgesen M, Sondergaard R and Krebs F C 2010 Advanced materials and processes for polymer solar cell devices *J. Mater. Chem.* **20** 36–60

[2] Dennler G, Scharber M C and Brabec C J 2009 Polymer-fullerene bulk-heterojunction solar cells *Adv. Mater.* **21** 1323–38

[3] Chen H *et al* 2009 Polymer solar cells with enhanced open-circuit voltage and efficiency *Nat. Photon.* **3** 649–53

[4] Krebs F C and Norrman K 2007 Analysis of the failure mechanism for a stable organic photovoltaic during 10 000 h of testing *Prog. Photovol. Res. Appl.* **15** 697–712

[5] Schuller S, Schilinsky P, Hauch J and Brabec C J 2004 Determination of the degradation constant of bulk heterojunction solar cells by accelerated lifetime measurements *Appl. Phys.* A **79** 37–40

[6] Tromholt T, Katz E A, Hirsch B, Vossier A and Krebs F C 2010 Effects of concentrated sunlight on organic photovoltaics *Appl. Phys. Lett.* **96** 073501

[7] Tromholt T, Manceau M, Petersen M H, Carlé J E and Krebs F C 2010 Degradation of semiconducting polymers by concentrated sunlight *Sol. Energy Mater. Sol. Cells* doi:10.1016/j.solmat.2010.09.022

[8] Katz E A, Gevorgyan S, Orynbayev M S and Krebs F C 2006 Out-door testing and long-term stability of plastic solar cells *Eur. Phys. J. Appl. Phys.* **36** 307–11

[9] Lilliedal M R, Medford A J, Madsen M V, Norrman K and Krebs F C 2010 The effect of post-processing treatments on inflection points in current–voltage curves of roll-to-roll processed polymer photovoltaics *Sol. Energy Mater. Sol. Cells* **94** 2018–31

[10] Krebs F C *et al* 2009 A round robin study of flexible large-area roll-to-roll processed polymer solar cell modules *Sol. Energy Mater. Sol. Cells* **93** 1968–77

[11] Korech O, Hirsch B, Katz E A and Gordon J M 2007 High-flux characterization of ultrasmall multijunction concentrator solar cells *Appl. Phys. Lett.* **91** 064101

[12] Krebs F C, Gevorgyan S A and Alstrup J 2009 A roll-to-roll process to flexible polymer solar cells: model studies, manufacture and operational stability studies *J. Mater. Chem.* **19** 5442–51

[13] Xue J, Uchida S, Rand B P and Forrest S R 2004 4.2% efficient organic photovoltaic cells with low series resistances *Appl. Phys. Lett.* **84** 3013

[14] Mandoc M M, Veurman W, Koster L J A, de Boer B and Blom P W M 2007 Origin of the reduced fill factor and photocurrent in MDMO-PPV:PCNEPV all-polymer solar cells *Adv. Funct. Mater.* **17** 2167–73

[15] Mandoc M M, Kooistra F, Hummelen J C, de Boer B and Blom P W M 2007 Effect of traps on the performance of bulk heterojunction organic solar cells *Appl. Phys. Lett.* **91** 263505

[16] Shuttle C G, Maurano A, Hamilton R, O'Regan B, de Mello J C and Durrant J R 2008 Charge extraction analysis of charge carrier densities in a polythiophene/fullerene solar cell: analysis of the origin of the device dark current *Appl. Phys. Lett.* **93** 183501

[17] Verbakel F, Meskers S C J and Janssen R A J 2009 Electronic memory effects in diodes from a zinc oxide nanoparticle–polystyrene hybrid material *Appl. Phys. Lett.* **89** 102103

www.MaterialsViews.com

ADVANCED ENERGY MATERIALS
www.advenergymat.de

Electrical and Photo-Induced Degradation of ZnO Layers in Organic Photovoltaics

Assaf Manor, Eugene A. Katz, Thomas Tromholt, and Frederik C. Krebs*

We present the case of degradation of organic solar cells by sunlight concentrated to a moderate level (~4 suns). This concentration level is not enough for sufficient acceleration of the photobleaching or trap-generation in the photoactive layer and therefore such short treatment (100 minutes) does not affect the short-circuit current of the device. However, a significant degradation of V_{OC} and *FF* has been recorded by measurements of the cell current-voltage curves with a variation of light intensity, for the devices before and after the treatment. The same degradation was found to occur after short application of forward voltage biases in the dark. This kind of degradation is found to be repairable, and could even be prevented by simple electrical treatment (short pulses of the reverse bias). Moreover, even the fresh cells can be improved by the same process. Generation and degeneration of shunts in ZnO hole-blocking layer as underlying physical mechanisms for the cell degradation and restoration, respectively, can explain the results.

1. Introduction

Organic photovoltaics (OPV) has been suggested as a low-cost, lightweight, flexible alternative to inorganic photovoltaics. In particular, intense research is directed towards the development of OPV with a bulk heterojunction (BHJ) between donor-type conjugated polymers and acceptor-type fullerenes (e.g., poly(3-hexylthiophene) (P3HT)) and fullerene derivative, phenyl-C61-butyric acid methylester (PCBM)).[1,2]

The most challenging problem in OPV technology to be solved yet is the development of devices that unite high efficiency, stability and processability. While inorganic solar cells exhibit operational lifetimes in the range of 25 years, a typical operational lifetime of encapsulated OPV under full solar illumination (1 sun = 100 mW/cm^2) has for a long period of time been in the range of only days or weeks.[3] Recently BHJ cells with operational lifetime of 1 year and longer have been developed.[4–7] This achievement opens various possibilities in OPV applications but also raises new problems, e.g. the need for relevant accelerated tests of operational lifetime.

Degradation mechanisms in OPV are complex and include a variety of processes: photo-bleaching of the photoactive layer and trap generation,[8,9] degradation of the hole conducting PEDOT:PSS layer,[10] ion migration from the electrodes and morphological changes of the device,[8] etc. These processes share the same catalysts (exposure of the device to light, heat, water and oxygen) and therefore are almost inseparable. This complicates the task of revealing the responsible process of a specific degradation phenomenon.

Recently we suggested using concentrated sunlight for accelerated study of the degradation of OPV materials[11] and devices.[12] The degradation experiments with single layers of various polymers demonstrated an acceleration of the polymer photo-bleaching, conserving the chemistry observed at 1 sun even at highest illumination intensities. In particular, acceleration factors exceeding 100 were obtained for P3HT illumination by 200 suns (a level not obtainable by conventional heat-assisted acceleration[13]). However, the performance of similar experiments with OPV cells can be more problematic and less predictable due to the increased complexity of the system. Increased light intensity can not only accelerate the degradation processes occurring at 1 sun operation but also stimulate some "hidden" degradation mechanism.

Here, we report an example of this situation by the study of BHJ OPV of *inverted* device architecture under concentrated light of ~4 suns. This concentration level is not enough for sufficient acceleration of the photobleaching or trap-generation in the photoactive layer but it considerably stimulates such "hidden" degradation mechanism as generation of shunts in ZnO hole blocking layer.

Inverted geometry OPV cells have developed to exclude low work function metal electrode that requires evaporation of metal onto the spin-coated organic layers. For large scale OPV processing such as roll-to-roll printing, metal vacuum evaporation is not suitable. Using high work function Ag electrode

A. Manor, Dr. E. A. Katz
Dept. of Solar Energy and Environmental Physics
J. Blaustein Institutes for Desert Research
Ben-Gurion University of the Negev
Sede Boker Campus 84990, Israel
E-mail: keugene@bgu.ac.il
Dr. E. A. Katz
The Ilse Katz Institute for Nanoscale Science and Technology
Ben-Gurion University of the Negev
Beersheva 84105, Israel
T. Tromholt, Dr. F. C. Krebs
Risø National Laboratory for Sustainable Energy
Technical University of Denmark
Frederiksborgvej 399, DK-4000 Roskilde, Denmark

DOI: 10.1002/aenm.201100227

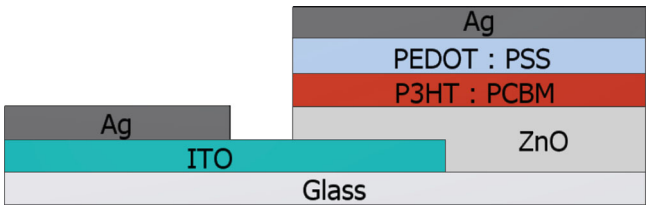

Figure 1. Layer sequence of the inverted P3HT:PCBM BHJ cell (through-glass illumination). The solar cell area is defined as the overlap between the ITO and the Ag electrodes.

solves this problem, since Ag can be applied from solution in printing processes.[14] However, adaptation in the layer sequence of the device had to take place since the high work function Ag could no longer serve as a cathode. This adaptation was successfully demonstrated in the form of "inversion" of the directions of charge extraction in the device. Electrons, which used to be collected by the metal electrode, should be extracted through the transparent ITO cathode, while holes are extracted by the Ag anode. In addition, an electron transport layer (ZnO) should be inserted between the active layer and the cathode in order to prevent the leakage of holes to the cathode. The latter would cause shunts and the decrease in the cells efficiency due to incomplete current extraction.

In this paper, we analyze the OPV degradation phenomenon which is related to the decrease in ZnO functionality, caused by the exposure to UV containing light and/or injected current. We also show this degradation type is reversible and can be repaired by the simple means of reverse–biasing the cell.

2. Results and Discussion

2.1. Effect of the Concentrated Sunlight on the OPV Key Parameters

We studied BHJ OPV cells with the inverted device layered architecture 'glass|ITO|ZnO|P3HT:PCBM|PEDOT:PSS|Ag' (**Figure 1**) and photoactive area of 1 × 1 cm^2 by means of the fiber-optic/mini-dish solar concentrator[15,16] (see also section 4 and Figure S1). Study of OPV using this outdoor/indoor test facility was described in details elsewhere.[12,17]

Figure 2 shows the effect of the cell exposure under concentrated sunlight of ~4 suns for 100 minutes on the light intensity dependence of the cell key parameters.

One cannot observe any change in the short-circuit current density J_{SC} due to the exposure, through all illumination levels (from 0 to 20 suns) (Figure 2a). It certainly means that no degradation of charge generation occurred during the exposure and the active layer was not damaged by photo-bleaching or any other possible degradation processes that we recently demonstrated using highly concentrated sunlight (50–200 suns).[11,12]

Light intensity dependence of open-circuit voltage V_{OC} plotted in a semi-logarithmic scale (Figure 2b) can be divided into two linear regimes. In the first regime (from 0 to ~2 suns), a significant degradation of the V_{OC} values and increase of the slope of the light intensity dependence of V_{OC} due to the exposure are in evidence. The second regime (~2–20 suns) is characterized by the "returning" of the V_{OC} values of the degraded cell to those of the fresh device.

The dependence of the fill factor *FF* (Figure 2d) for the fresh cell is in accordance to that recently observed for OPV of similar device architecture.[12,17] However, this dependence for the degraded device demonstrates a different behavior. Similarly to the V_{OC}, the *FF* dependence for the degraded cell can be divided to two regimes. The first regime (0 – ~3 suns) is characterized by a strong degradation of FF and unusual non-linear increase in FF with light intensity, up to a certain concentration where it meets the fresh cells values and follows them (the second regime: ~3–20 suns). It is clear that the decrease in *FF* values in this regime is not due to the degradation process but is controlled by the same mechanism that limits the fresh cell's *FF* values (mainly series resistance effects[12,17]).

It should be noted that the "turning points" between the two regimes are different for the V_{OC} and *FF*. This is due to the fact that the *FF* follows the maximum power point (*mpp*) voltage, which dependence upon illumination level is different than that of the V_{OC}.[17] This difference will be analyzed below.

Since the power conversion efficiency (*PCE*) can be derived from a product of J_{SC}, V_{OC} and *FF*, its light intensity dependence simply integrate the trends mentioned above. Here, *PCE* values are mainly controlled by the *FF* trend, with the additional effect of the decreased V_{OC} in its first regime. As a result the *PCE* dependence also follows the two-regime behavior which was already mentioned.

2.2. Effect of the Concentrated Sunlight on the Dark Current-Voltage Curves of OPV

The dark current density–voltage (*J–V*) curves are shown in both linear and semi-logarithmic scales in **Figure 3**.

The dark *J–V* curve shows the device response to applied bias without charge photo-generation in the cell, i.e. any measured current is necessarily injected into the active layer of the device through the selective contact barriers. If the device contacts are ideally selective, the current should be very close to zero at biases lower than the voltage threshold of injection. In reality, even for fresh cells, non-perfect selectivity of the contacts as well as defects in the cell structure cause the minor passing of current even for low applied voltages.

The concentrated light exposure significantly magnifies this shunting effect (Figure 3). For the degraded cell, the dark *J–V* in the first voltage range (–0.5 V – +0.5 V) is characteristic for an ohmic-like resistor, implying the formation of effective shunts during the exposure.

The second voltage range (~ +0.5 V – +1 V) is characterized by injection currents for both the fresh and degraded cells. The current values are higher in the degraded cell but it shows an exponentially "weaker" diode behavior: when looking in the semi-log plot (Figure 3b), the curve slope the injection region is clearly smaller for the degraded cell. This means that the junction ideality number *n* is greater for the degraded cell, due to non-recombinative current losses caused by shunts.

Thus, we can already conclude that the concentrated sunlight exposure by 4 suns resulted in the simultaneous degradation

www.MaterialsViews.com

ADVANCED ENERGY MATERIALS
www.advenergymat.de

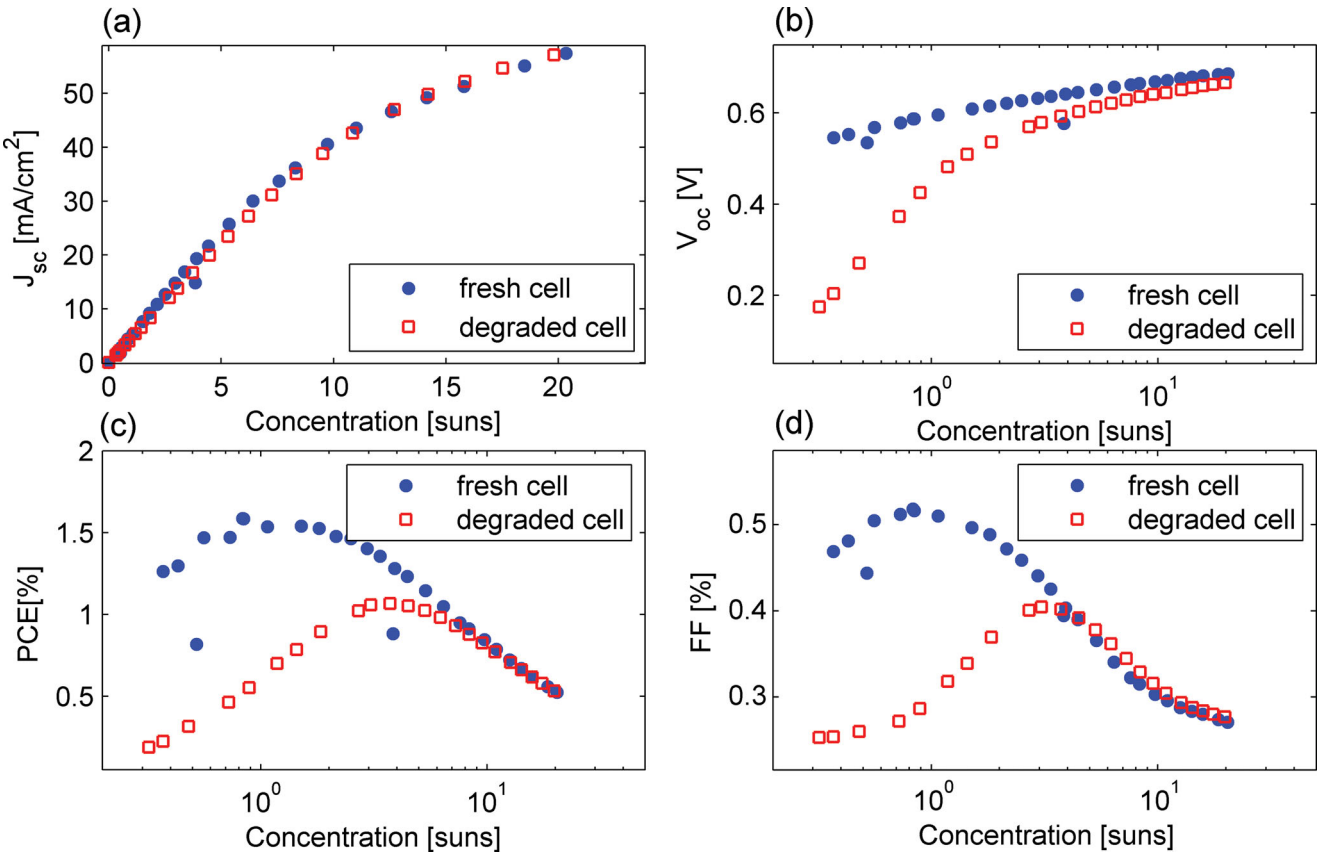

Figure 2. Light intensity dependence of the cell key parameters before and after the cell exposure under concentrated sunlight with intensity of ~4 suns during 100 minutes.

of the V_{OC} and *FF* at low light intensities as well as the dramatic change in the device dark *J–V* curve while no change was observed for the J_{SC}. These finding completely confirmed our recent results for similar cells exposed shortly (30 min) to 5 suns using a lens-based concentration setup.[18] We suggest that all these degradation features can be explained by the same shunting mechanism. Below we will challenge and elaborate this hypothesis.

2.3. Relationship between the Shunting Effect on the Dark Current and V_{OC}/*FF*

Identically to open-circuit condition (where all photo-generated carriers are recombined), the dark current in BHJ OPV cell is controlled by bimolecular recombination at the polymer/fullerene interface,[19] and thus the two cases are of physical equivalence, and should be correlated through the illumination dependence of V_{OC}.

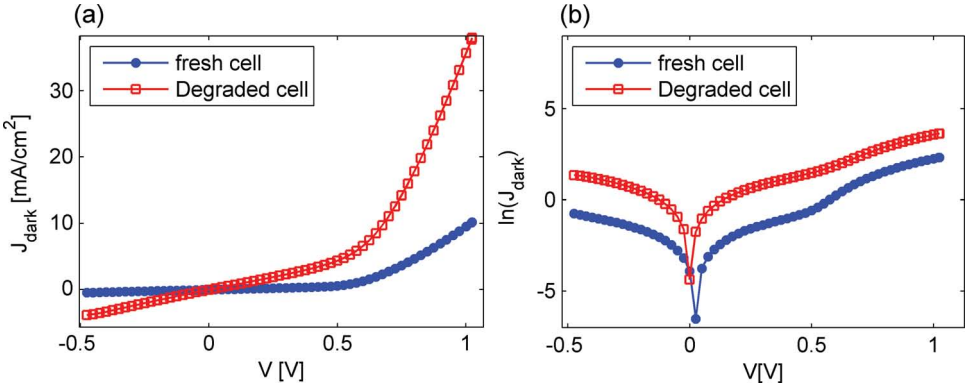

Figure 3. Dark *J–V* curves before and after the cell exposure under concentrated sunlight (4 suns, 100 minutes): (a) linear scale. (b) semi-logarithmic scale.

This is illustrated by the evolution of the cell *J–V* curves with illumination (**Figure 4**). For the fresh device (Figure 4a), V_{OC} values correspond to the injection regime of the dark *J–V* curves ($V > 0.5$ V) where exactly enough recombination current is injected in order to cancel the generated photo-current. The inset presents the light intensity dependence of V_{OC}, which is typical for this kind of BHJ cells.[12] For the degraded cell (Figure 4b), the V_{OC} values for low illumination levels (marked by ellipses) correspond to the "ohmic-resistor" region in the dark *J–V* curve ($V < 0.5$ V).

This correlation between the dark *J–V* curve and the light intensity dependence of V_{OC} *show* that the linear slope of the V_{OC} -log (C) graph in the first regime and the linear slope of the dark *J–V* curve in the corresponding "resistor" regime share the same origin, which is shunting introduced to the cell by the degradation process.

The degradation effect on the V_{OC} behavior in the second regime (high light intensities) and the injection regime of the dark *J–V* curve is also consistent with this picture. The high voltage region in the dark *J–V* curve (0.5 V – 0.7 V) is characterized by a greater ideality number *n* in the degraded cell (already shown by Figures 2b and 3b). This causes the V_{OC} values in high intensity regime to be still lower than those of the fresh cell, and the V_{OC}-intensity slope to be greater. In the highest illumination levels the V_{OC} values are almost comparable, due to the high photocurrent (Figure 2b).

As for the *FF* degradation, shunts can also reduce the voltage in the maximum power point (V_{MPP}), in a similar way to the lowering of the V_{OC}. Since the *FF* depends both on extracted current and voltage, it is clear that shunts play a crucial role in its degradation. Figure S2 in supplementary information shows V_{MPP} and J_{MPP} responses to the degradation. While the J_{MPP} values are almost equal for the fresh and degraded devices, the V_{MPP} voltage shows a behavior that is very similar to the V_{OC} trend. This demonstrates that the *FF* behavior (shown in figure 2c) is controlled by the V_{MPP} degradation caused by the same mechanism as the V_{OC}.

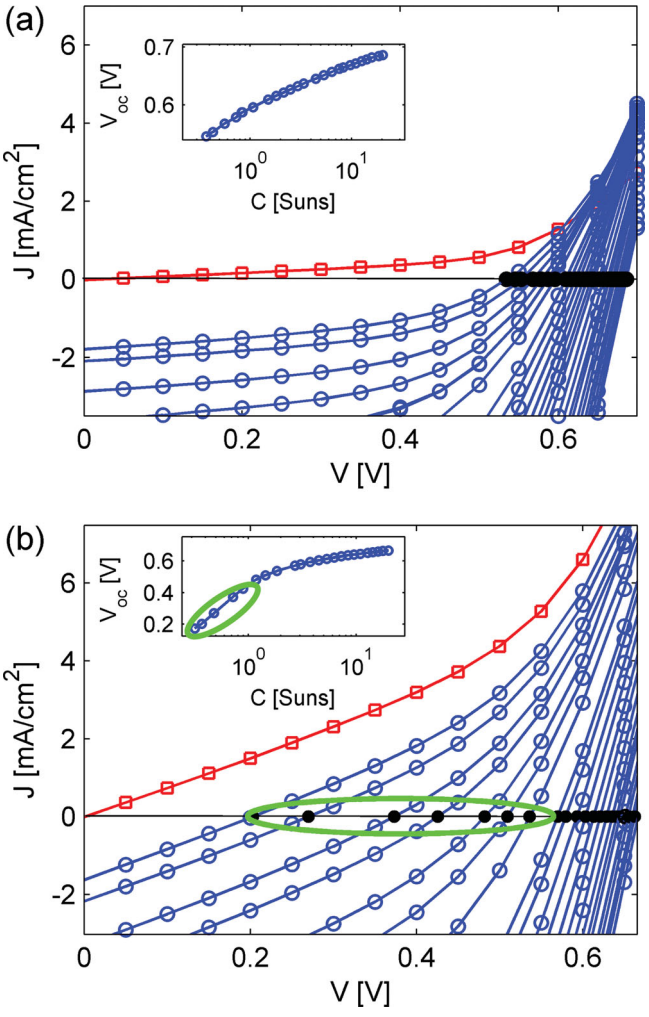

Figure 4. Evolution of the cell *J–V* curves with increasing light intensity. Open squares mark the dark curve, while open circles mark the light *J–V* curves. V_{oc} points are marked by bold circles. Insets show light intensity dependence of V_{oc}. (a) fresh cell; (b) degraded cell. In figure b, the regime of low Voc values is marked by ellipses.

2.4. Possible Mechanism Underlying the Shunting Effect

As mentioned, shunts formed due to the degradation process are responsible for the ohmic behavior of the cell between –0.5 V and 0.5 V. In a simplified way, it can be viewed as a result of a non-functioning blocking layer. In an inverted device, the ZnO layer is introduced in order to prevent collection of holes by the ITO electrode, while the PEDOT layer blocks electrons' drift to the Ag contact. If at least one of those layers becomes non-selective it should result in significant shunt currents that can explain the various degradation effects described above. However, this model has to be carefully elaborated in order to fully explain our experimental observations.

Our explanation for this phenomenon is based on the known facts that (1) surface oxygen impurities behave as strong electron traps in ZnO nanoparticle layers;[20–22] (2) oxygen desorption changes the ZnO electronic properties after UV illumination[21,22] or high forward biasing, while ZnO layer is incorporated in a diode structure.[20] In the latter case a ZnO/PEDOT diode started to exhibit ohmic properties that were attributed to the additional n-type doping of the ZnO layer. The author of ref. 7 suggested that this process can be activated by both UV light and forward biasing (injection of free holes), equivalently. **Figure 5** illustrates this mechanism: once a hole is generated or injected into the ZnO layer, it causes neutral oxygen desorption from the surface of the nanoparticles. The release of oxygen leaves the once-bounded electron free in the ZnO conductivity band. Furthermore, this process should be physically reversible: when its triggering is stopped, ambient oxygen can be re-adsorbed by the surface, while catching a free electron and thus lowering conductivity again. Recently, we reported experimental observation of reversible light-induced degradation (under 5 suns) of inverted BHJ OPV.[18]

The described phenomenon may be relevant in our case since the sunlight concentration increases the amount of UV photons which causes the n-doping of the ZnO layer to a state

www.MaterialsViews.com

ADVANCED ENERGY MATERIALS
www.advenergymat.de

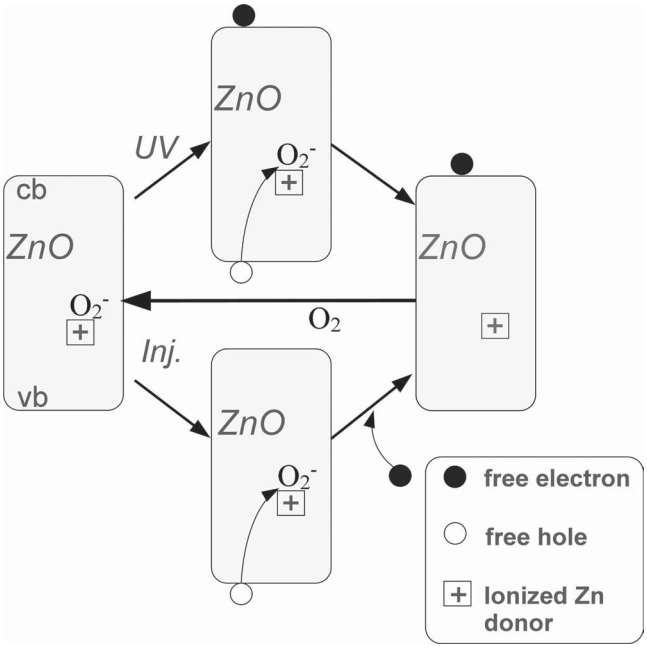

Figure 5. Effect of light induced (upper path) or injection induced (lower path) oxygen desorption on the electronic doping of ZnO nanoparticles. The reversibility of the process is demonstrated by the arrow leading from the final state back to the initial state.

of high conductivity and the formation of shunt channels in the device. (A detailed explanation how the ZnO doping causes nanoscale shunting in the device will be presented in section 2.6). For the verification of this hypothesis, a similar degradation experiment (as described in section 2.1) was repeated with a UV only pass filter (300–400 nm). The observed shunting effect (Figure S3 in supplementary information) confirms our hypothesis.

However, if this mechanism is responsible for our light-induced degradation, similar degradation of our devices should be also triggered by forward voltage biasing. The recovery effect by reverse biasing[20] must be verified for our case as well. Experimental challenging of this suggestion is described in the next section.

2.5. Injection Induced Degradation and Recovery

2.5.1. Forward Bias Injection

In order to reproduce the observed degradation effect with current injection, a cell was connected to moderate forward bias ($V < 1$ V), to pass current of 10 mA for 30 seconds.

Figure 6a depicts the dark *J–V* curve that was recorded after this process, and after 20 minutes of rest in the ambient.

Clearly, we observe shunting effect similar to the one caused by concentrated sunlight. Furthermore, a partial restoration process is shown to take place: after 20 minutes in the ambient, the device almost returns to its original state.

The same trend for V_{OC} degradation as in the case of concentrated sunlight and the partial recovery of V_{OC} are also in evidence (Figure 6b). *FF* behavior (not shown) was also similar to the degradation by sunlight and exhibited reversible character.

In previous experiments[20] holes were injected by a strong (10 V) forward bias. Our finding point out that it can be achieved even with a relatively low (<1 V) applied voltages, due to inherent shunts that exist even in the fresh cell. This point will be explained in more detail in section 2.6.

2.5.2. Reverse Bias Injection and Accelerated Recovery Processes

Figure S4a in supplementary information presents a series of dark *J–V* measurements taken after initial degradation of the cell, demonstrating the relaxation process that occurs in the ambient. This relaxation process is diffusive by nature (oxygen re-adsorption) and therefore reaches some saturation level. In this example, the dark *J–V* was recorded in time intervals of 5–10 minutes, followed by a last measurement after a 180 minute break, for which the cell still has not returned completely to its original state. This experiment demonstrates a relatively long time is needed for the cell restoration (see also Figure 6). Restoration times were found to vary with the severity of cell's shunting, but were always in the order of hours. Furthermore, restoration process should depend on environment atmosphere (i.e., can be accelerated with increasing oxygen pressure, and vice versa[23]).

On the other hand, applying reverse bias on the cell was found to shorten the recovery time by orders of magnitude:

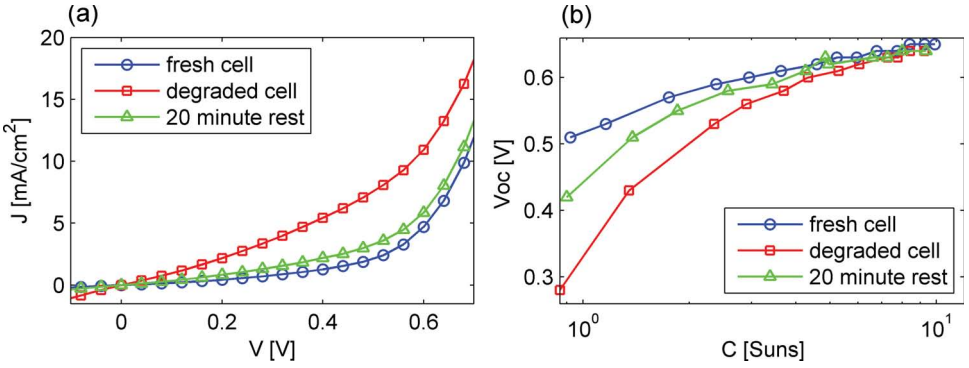

Figure 6. Dark *J–V* curves (a) and the corresponding light intensity of V_{oc} (b) for the fresh, electrically degraded and recovered cell.

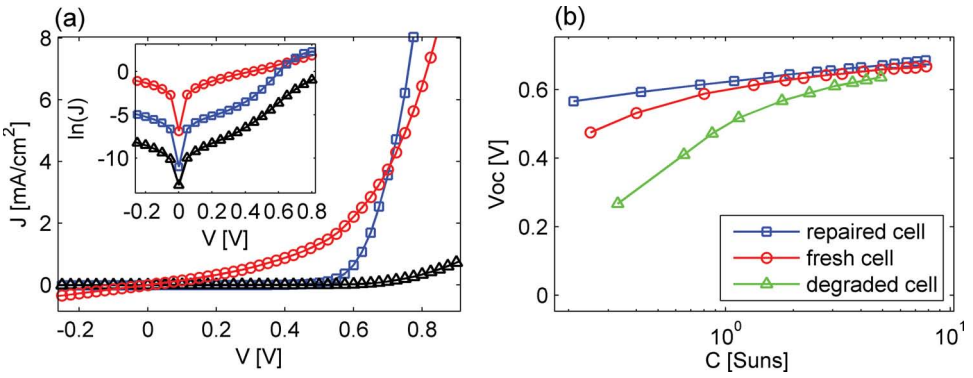

Figure 7. (a) Dark *J–V* curves for the fresh cell (circles), cell treated by 20 V reverse bias for 2 seconds (triangles) and after subsequent illumination by sunlight (1 sun) for 5 minutes (squares). (b) Corresponding light intensity dependence of VOC for the fresh and treated states, with the degraded state for comparison.

typically, applying −1 V for 2 minutes restored the cell to its previous state before degradation (Figure S4b).

Applying the shorter and stronger reverse bias pulses (−20 V for 2 seconds) resulted in even sharper recovery: fresh cells treated this way exhibited almost no initial shunting, although conduction in the injection regime was also sacrificed (**Figure 7**a). This undesirable problem was solved by treating the cell under natural sunlight (1 sun) for 5 minutes, which recovered its injection conductivity while keeping shunting level minimized. This physical process is similar to the one behind the concentrated sunlight degradation, but with a smaller dose of UV photons received by ZnO layer. It resembles recent observations regarding the disappearance of an *J–V* inflection point after light-soaking of the inverted OPV devices.[24]

The dramatic improvement of the cells dark characteristics implies that there should be an improvement of the V_{OC} as well. This is shown in Figure 7b: while the fresh device V_{OC} values tend to drop below 1 sun due to inherent shunts, the "repaired" cell shows almost linear dependence of V_{OC} on log(*C*) and higher V_{OC} values (especially in the low intensity regime) than those of the fresh cell. (V_{OC} values of this cell in its degraded state are presented as well, for comparison).

Thus, the fresh cell's initial shunting (probably originated from local excessive ZnO doping) can be repaired, improving even the *fresh* device performance, especially in low illumination levels where shunting effects are enhanced. In addition, treated cells that showed no shunts were also indifferent to moderate forward biasing since no initial injection of current was possible.

A more comprehensive research of the extent of the improvement in efficiency of the fresh OPV is ongoing in order to determine whether this process could be used as a post production step (to be published elsewhere).

It is important to mention here that the same processes were tested on the normal geometry BHJ OPV cells (without ZnO blocking layer) and no sign of shunting effects was found. This together with all observations presented above strongly support the conclusion that the reported shunting effects and the corresponding reversible degradation of the cell performance originate from the losses in selectivity of the ZnO blocking layer. Physical processes that lead to such losses will be elaborated in the next section.

2.6. Detailed Physical Picture of the Degradation and Recovery Processes

The discussed phenomenon of ZnO doping and de-doping is well known and is relevant for almost every electrical device employing ZnO films, such as solar cells, diodes, transistors, sensors etc.[20–27] However, the analysis reported in the literature is often simplistic and based solely on the change of the ZnO conductivity without referring to the specific device structure. Here, we suggest a physical picture that explains the various observed effects in the context of the inverted geometry BHJ OPV cell.

Figure 8 depicts an approximated energy band diagram of our device in the dark under a forward (Figure 8a) and reverse (Figure 8b) biases, when both ZnO and PEDOT layers are ideally selective.

Under the low forward bias (Figure 8a), there is no recombination of electron-hole pairs in the active layer, since electrons are stopped by the ZnO/active layer barrier. Holes, on the other hand, are blocked by the P3HT:ZnO layer barrier. This demonstrates well the need for hole blocking layer near the cathode. (Same blocking is required under illumination, when holes populate the P3HT valance band and could be collected to the cathode without the existence of hole blocking layer). When reverse bias is applied (Figure 8b), neither holes nor electrons can get through their corresponding blocking layers.

Under UV irradiation the ZnO layer becomes doped by free electrons (Figure 4). For an n-type selective contact, additional doping means better selectivity since the minority carriers' number in the layer drop with the Fermi level rising. In addition, n-type doping of ZnO is required in order to allow good electron transport through the PCBM-ZnO contact. This can be seen well in figure 7a: a short exposure to UV improved the electron injection while keeping shunts minimized. The demonstrated shunting phenomenon is caused *only* by quite a long exposure to *concentrated* sunlight (high UV dose), which causes the extremely high *n* doping of ZnO. At this stage, the electron quasi–Fermi level is very close to the ZnO conduction band, making the tunneling of holes from the adjacent P3HT valance band into the ZnO conduction band possible, causing the observed shunt current in forward bias.

Similar observation has been made in tandem OPV devices, where a recombination layer is needed as a contact between

www.MaterialsViews.com

ADVANCED ENERGY MATERIALS
www.advenergymat.de

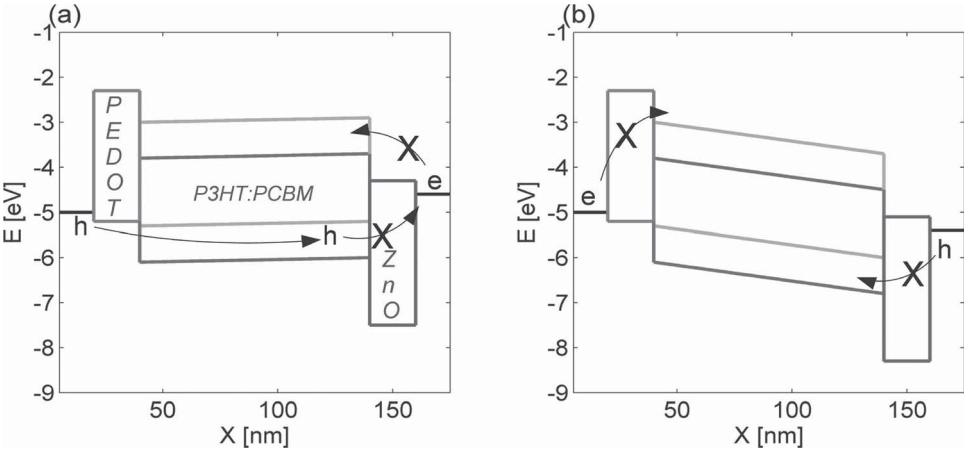

Figure 8. Band–diagram illustration of an inverted geometry BHJ OPV cell in the dark for applied forward bias of 0.4 V (a) and applied reverse bias of –0.4V (b). X marks pathways through which electrons/hole cannot pass.

the two series connected cells (similar function is achieved by means of Esaki tunnel diodes incorporated in inorganic tandem cells[28]). It was shown by Sista et al[29] that upon UV illumination, the TiO_2:PEDOT contact in such a tandem OPV cell can undergo a Schottky-to-ohmic transition. The origin of such a transition is the increase of concentration of free electrons in the TiO_2, which causes the narrowing of the PEDOT:TiO_2 Schottky barrier width (figure 1 in Ref. 29). Such narrowing enables the carrier tunneling through the barrier. An identical observation was also reported by Gilot et al.[30] for ZnO:PEDOT recombination layer in tandem OPV. The similarity between the cases and the fact that P3HT and PEDOT share very close energy levels for holes make us adopt this explanation for our observed shunting phenomena.

The tunneling of holes also explains the current-induced degradation (section 2.5): holes that are injected through the PEDOT to the active layer and can tunnel into the ZnO layer. This facilitates more oxygen desorption and hence more shunting. As already mentioned, this injection-induced degradation was not observed for "repaired" cells which exhibited no shunting, because no initial hole tunneling to the ZnO is possible. This implies that the process suggested above (Section 2.5) may not only improve the initial cell's performance but also "immune" it to injection induced shunting.

The recovery effect in reverse bias is explained by the depletion of the ZnO layer from excess free electrons: in this mode, electrons cannot pass the PEDOT barrier, and hence the excess charge is "drained" via the ITO contact, lowering the ZnO electron quasi–Fermi level back to its intrinsic level. This process is much faster than the regular relaxation process caused by oxygen re-adsorption, and when followed by a subsequent short exposure to UV light, a good selectivity/conductivity behavior of the ZnO layer is reached, enabling the results presented in figure 7b.

3. Conclusions

We studied BHJ OPV cells with inverted layered architecture (glass|ITO|ZnO|P3HT:PCBM|PEDOT:PSS|Ag) under the exposure of concentrated sunlight (~ 4 suns) and injected current. The degradation of both V_{OC} and *FF* was found to lead to significant loss in the efficiency under a wide range of light intensities (mostly at low sunlight flux). The degradation is found to be repairable, and could even be prevented by the suggested post production treatment.

The physical reasons for the degradation and its reversibility are analyzed in detail, in the context of the inverted solar cell geometry. Generation and de-generation of shunts in the ZnO hole blocking layer as underlying physical mechanisms for the cell degradation and restoration, respectively, can explain all observed phenomena.

Our observations are also relevant for ZnO containing plastic roll-to-roll OPV. In these cells, PET barrier layer was shown to block UV light to some extent,[24] but there is still UV transmission in the range 360–400 nm, where the ZnO nanoparticles absorb. Long term stability tests of inverted solar cells have demonstrated a certain degradation of V_{OC}.[31] This V_{OC} decrease could result partially from ZnO layer degradation. (In this case, the corresponding efficiency degradation is enhanced by the accompanied decrease in *FF*). Relatively low degradation of this kind recorded by the outdoor measurements during many days[28] can be explained by ZnO recovery during every night.

For recently suggested concentrated sunlight applications of OPV[12,17] or for possible operation under UV-rich conditions, we expect this degradation process to be superior comparing to the relaxation process. However, the demonstrated opportunity of cells recovery (by short pulses of the reverse bias) may eliminate degradation problems of this kind. Moreover, since even fresh cells were shown to be improved by applying the same process, an overall improvement in average efficiency yield could be realized by implementation of such post production treatment.

4. Experimental Section

Solar cells: BHJ OPV cells of inverted layered architecture (Figure 1) were prepared in the ambient using a fully roll-to-roll compatible solar cell device preparation.[14] Commercially available ITO glass substrates with a sheet resistivity of 5-8 $\Omega\cdot\square^{-1}$ were sonicated in isopropanol

followed by washing in demineralized water. Layers of ZnO nanoparticles, photoactive P3HT:PCBM and poly(3,4-ethylenedioxythiophene): polystyrene sulfonate (PEDOT:PSS) were then subsequently spin-coated. All processing steps were conducted in the ambient. An Ag electrode pattern was deposited by thermal evaporation resulting in 1 cm × 1 cm geometry of the cells. The samples were encapsulated by applying an adhesive plastic foil on the Ag electrode.

The solar cells were mounted in an Al sample holder to ease the physical handling of the samples during the measurements. Additionally, it served as a thermal reservoir, decreasing the heating during the illumination of the cells.

Sun concentrating system: Sunlight collected and concentrated outdoors was focused into a transmissive (quartz-core) optical fiber of 1mm in diameter and then delivered indoors onto the solar cell being tested (FigureS1a in supplementary information). Flux uniformity was achieved with a 3 cm long square cross-section kaleidoscope, matching the size of the cell, placed between distal fiber tip and cell (Figure S1b).

Photovoltaic characterization: Concentration of sunlight delivered to the cell was varied gradually from 0.2 to 20 suns with a pizza-slice iris (Figure S1a), and measured pyrometrically. Light current-voltage *I–V* measurements were made by opening a shutter above the iris and illuminating the cell during *I–V* tracing only (<1 sec) to avoid excessive degradation and temperature variations. Before this testing dark *I–V* curves for every cell were recorded.

I–V curves were recorded with a Keithley 2400 sourcemeter/HP pA meter 4140B.

Light *I–V* measurements were limited to clear-sky periods, two hours around solar noon. The light spectrum on the cell was nearly invariant and close to the AM1.5.[15]

The cell fill factor *FF* and PCE η were calculated as

$$FF = P_m / J_{SC} V_{OC}$$

$$\eta = P_m / P_{in} = J_{SC} V_{OC} FF / P_{in}$$

P_m and P_{in} are the maximum electrical output power density and incident light power density.

Degradation experiments: During the degradation experiment with concentrated sunlight (4 suns, 100 minutes), the cell temperature was controlled by a water cooling of the cell heat sink and kept at level 30–40 °C. Experiments on the electrically induced degradation and recovering were performed at room temperature.

Supporting Information

Supporting Information is available from the Wiley Online Library or from the author.

Acknowledgements

This work was performed, in part, in the framework of the "Largecells" project that received funding from the European Commission's Seventh Framework Programme (FP7/2007-2013) under Grant Agreement No. 261936." T. T. and F.C.K. thank the Danish Strategic Research Council (2104-07-0022) and EUDP (j. nr. 64009-0050) for a financial support.

Received: April 28, 2011
Revised: June 21, 2011
Published online:

[1] M. Helgesen, R. Søndergaard, F. C. Krebs, *J. Mater. Chem.* **2010**, *20*, 36.
[2] G. Dennler, M. C. Scharber, C. J. Brabec, *Adv. Mater.* **2009**, *21*, 1323.
[3] *Organic photovoltaics: a practical approach* (Ed: F. C. Krebs), SPIE Press, Bellingham **2008**.
[4] F. C. Krebs, J. Alstrup, H. Spanggaard, K. Larsen, E. Kold, *Sol. Energy Mater. Sol. Cells* **2004**, *83*, 293.
[5] J. A. Hauch, P. Schilinsky, S. A. Choulis, R. Childers, M. Biele, C. J. Brabec, Sol. *Energy Mater. Sol. Cells* **2008**, *92*, 727.
[6] F. C. Krebs, K. Norrman, *Prog. Photovolt: Res. Appl.* **2007**, *15*, 697.
[7] B. Zimmermann, U. Würfel, M. Niggemann, *Sol. Energy Mater. Sol. Cells* **2009**, *93*, 491.
[8] M. Jørgensen, K. Norrman, F. C. Krebs. *Sol. Energy Mater. Sol. Cells* **2008**, *92*, 686.
[9] M. O. Reese, A. M. Nardes, B. L. Rupert, R. E. Larsen, D. C. Olson, M. T. Lloyd, S. E. Shaheen, D. S. Ginley, G. Rumbles, N. Kopidakis, *Adv. Funct. Mater.* **2010**, *20*, 3476.
[10] K. Kawano, R. Pacios, D. Poplavskyy, J. Nelson, D. D.C Bradley, J. R Durrant, *Sol. Energy Mater. Sol. Cells* **2006**, *90*, 20.
[11] T. Tromholt, M. Manceau, M. Helgesen, J. E. Carlé, F. C. Krebs, *Sol. Energy Mater. Sol. Cells* **2011**, *95*, 5.
[12] T. Tromholt, E. A. Katz, B. Hirsch, A. Vossier, F. C. Krebs, *Appl. Phys. Lett.* **2010**, *96*, 073501.
[13] S. Schuller, P. Schilinsky, J. Hauch, C. J. Brabec, *Appl. Phys. A*, **2004**, *79*, 37.
[14] F. C. Krebs, S. A. Gevorgyan, J. Alstrup, *J. Mater. Chem.* **2009**, *19*, 5442.
[15] J. M. Gordon, E. A. Katz, D. Feuermann, M. Huleihil, *Appl. Phys. Lett.* **2004**, *84*, 3642.
[16] E. A. Katz, J. M. Gordon, W. Tassew, D. Feuermann, *J. Appl. Phys.* **2006**, *100*, 044514.
[17] A. Manor, E. A. Katz, T. Tromholt, B. Hirsch, F. C. Krebs, *J. Appl. Phys.* **2011**, *109*, 074580.
[18] T. Tromholt, A. Manor, E. A. Katz, F. C. Krebs, *Nanotechnology* **2011**, *22*, 225401.
[19] C. G. Shuttle, A. Maurano, R. Hamilton, B. O'Regan, J. C. de Mello, J. R. Durrant, *Appl. Phys. Lett.* **2008**, *93*, 18.
[20] F. Verbakel, S. C. J Meskers, R. A. J. Janssen, *Appl. Phys. Lett.* **2006**, *89*, 102103.
[21] Q. H. Li, T. Gao, Y. G. Wang, T. H. Wang, *Appl. Phys. Lett.* **2005**, *86*, 123117.
[22] H. Kind, H. Yan, B. Messer, M. Law, P. Yang, *Adv. Mater.* **2002**, *14*, 158.
[23] Q. H. Li, T. Gao, Y. G. Wang, T. H. Wang, *Appl. Phys. Lett*, **2005**, *86*, 123117.
[24] M. R. Lilliedal, A. J. Medford, M. V. Madsen, K. Norrman, F. C. Krebs, *Sol. Energy Mater. Solar Cells* **2010**, *94*, 2018.
[25] J. Zhou, Y. Gu, Y. Hu, W. Mai, P. H. Yeh, G. Bao, A. K. Sood, D. L. Polla, Z. L. Wang, *Appl. Phys. Lett.* **2009**, *94*, 191103.
[26] Q. H. Li, Y. X. Liang, Q. Wan, T. H. Wang, *Appl. Phys. Lett.* **2004**, *85*, 26.
[27] W. J. E. Beek, M. M. Wienk, M. Kemerink, X. Yang, R. A. J. Janssen, *J. Phys. Chem. B* **2005**, *109*, 9505–9516.
[28] S. M. Bedair, M. F. Lamorte, J. R. Hauser, *Appl. Phys. Lett.* **1979**, *34*, 38.
[29] S. Sista, M. Park, Z. Hong, Y. Wu, J. Hou, W. L. Kwan, G. Li, Y. Yang, *Adv. Mater.* **2010**, *22*, 380.
[30] J. Gilot, M. M. Wienk, R. A. J. Janssen, *Appl. Phys. Lett*, **2007**, *90*, 143512.
[31] S. A. Gevorgyan, A. J. Medford, E. Bundgaard, S. B. Sapkota, H. Schleiermacher, B. Zimmermann, U. Würfel, A. Chafiq, M. Lira-Cantu, T. Swonke, M. Wagner, C. J. Brabec, O. Haillant, E. Voroshazi, T. Aernouts, R. Steim, J. A. Hauch, A. Elschner, M. Pannone, M. Xiao, A. Langzettel, D. Laird, M. T. Lloyd, T. Rath, E. Maier, G. Trimmel, M. Hermenau, T. Menke, K. Leo, R. Rösch, M. Seeland, H. Hoppe, T. J. Nagle, K. B. Burke, C. J. Fell, D. Vak, T. B. Singh, S. E. Watkins, Y. Galagan, A. Manor, E. A. Katz, T. Kim, K. Kim, P. M. Sommeling, W. J. H. Verhees, S. C. Veenstra, M. Riede, G. M. Christoforo, T. Currier, V. Shrotriya, G. Schwartz, F. C. Krebs, *Sol. Energy Mater. Sol. Cells* **2011**, 1398.

JOURNAL OF APPLIED PHYSICS **109**, 074508 (2011)

Origin of size effect on efficiency of organic photovoltaics

Assaf Manor,[1] Eugene A. Katz,[1,2,a)] Thomas Tromholt,[3] Baruch Hirsch,[1] and Frederik C. Krebs[3]

[1]*Department of Solar Energy and Environmental Physics, J. Blaustein Institutes for Desert Research, Ben-Gurion University of the Negev, Sede Boker Campus 84990, Israel*

[2]*The Ilse Katz Institute for Nanoscale Science and Technology, Ben-Gurion University of the Negev, Beer Sheva 84105, Israel*

[3]*Risø National Laboratory for Sustainable Energy, Technical University of Denmark, Frederiksborgvej 399, DK-4000 Roskilde, Denmark*

(Received 13 November 2010; accepted 17 February 2011; published online 7 April 2011)

It is widely accepted that efficiency of organic solar cells could be limited by their size. However, the published data on this effect are very limited and none of them includes analysis of light intensity dependence of the key cell parameters. We report such analysis for bulk heterojunction solar cells of various sizes and suggest that the origin of both the size and the light intensity effects should include underlying physical mechanisms other than conventional series resistance dissipation. In particular, we conclude that the distributed nature of the ITO resistance and its influence on the voltage dependence of photocurrent and dark current is the key to understanding size limitation of the organic photovoltaics (OPV) efficiency. Practical methods to overcome this limitation as well as the possibility of producing concentrator OPV cells operating under sunlight concentrations *higher* than 10 suns are discussed. © *2011 American Institute of Physics*. [doi:10.1063/1.3567930]

I. INTRODUCTION

Organic photovoltaics (OPV) has been suggested as an alternative to conventional photovoltaics based on inorganic semiconductor solar cells. The major advantages of OPV include their light weight, mechanical flexibility, and processability (OPV cells may be solvent-processed via common low-cost, high-throughput coating and printing techniques enabling the preparation of *large-area,* low-cost devices). In particular, intense research is directed toward the development of OPV with a bulk heterojunction (BHJ) where donor-type conjugated polymers (hole conducting) and acceptor-type (electron conducting) fullerenes [or fullerene derivatives, such as [6,6]-phenyl-C61- butyric acid methyl ester (PCBM)] are mixed to form the photoactive layer.[1–3] The most studied donor/acceptor pair in the BHJ cells is poly(3-hexylthiophene) (P3HT)/PCBM.[4–7]

Upon illumination, light is absorbed by the conjugated polymer resulting in the formation of a neutral and stable excited state (binding energy ~0.5 eV)[8] on the polymer chain. Free carriers can be generated by exciton dissociation at a donor–acceptor interface, leaving the electron on the acceptor (fullerene in this case) and the hole on the conjugated polymer donor. Efficient charge generation requires, therefore, that the donor and acceptor materials form interpenetrating and continuous networks, "phase separated" on the scale of the exciton diffusion length: $\leq$10 nm.[9] Following the exciton dissociation into free carriers, the electrons and holes are conducted through the respective semiconductor moieties (fullerene percolation network for electrons, and conjugated polymer chains for holes) toward the respective electrodes.

Accordingly, the main difference in charge generation in organic and inorganic solar cells lies in the basic properties of the photogenerated excitations. In organic solids, photogenerated excitations (excitons) are strongly bound and do not spontaneously dissociate into separate charges. The immediate consequence is that light absorption does not necessarily lead to the generation of free carriers and photocurrent becomes voltage dependent.[10–15]

Serious progress has been achieved in the improvement of photovoltaic performance of BHJ solar cells: while the best power conversion efficiency (PCE) reported 8 years ago barely reached values higher than 1%,[3] certified efficiencies beyond 6% and even 8%[16] are state of the art today (Table I).

It is widely accepted that OPV efficiency can be limited by the cell area. All of the record efficiencies (Table I) were reported for ultrasmall BHJ OPV cells (with area $\ll 0.4$ cm^2, a low area limit for the PCE measurements suggested in the recent editorial report[24]). However, no systematic attention has been paid on the influence of the OPV cell area (size) on the key photovoltaic parameters of the devices. Experimental[25–27] and modeling[26–29] data on this effect are very limited and most of the published papers attributed the reduction of the OPV performance with increasing area to the power dissipation on the cell series resistance R_s and in particular to the R_s contribution by front electrode of transparent conductive oxide (ITO).

The resistive power losses per unit area P_R is given by

$$P_R = \frac{R_s}{A} I_{\max}^2 = \frac{R_s}{A} (J_{\max} A)^2 = R_s A J_{\max}^2, \qquad (1)$$

a)Author to whom correspondence should be addressed. Electronic mail: keugene@bgu.ac.il.

TABLE I. Record efficiencies for BHJ OPV.

Photoactive layer	Cell area, [cm^2]	I_{SC} (mA cm^2)	V_{OC} (V)	FF	PCE (%)	Ref.
P3HT/PCBM	0.148	9.5	0.63	0.68	5	4
P3HT/PCBM	0.148	11.1	0.61	0.66	5	5
P3HT/PCBM	Not mentioned	11.3	0.64	0.69	5.2	6
P3HT/PCBM	0.19	11.1	0.65	0.54	4.9	7
PSBTBT/PCBM	0.12	12.7	0.68	0.55	5.1	17
PCPDTBT:C_{70}-PCBM	0.17	16.2	0.62	0.55	5.5	18
PTB4/PCBM	0.095	13.0	0.74	0.61	6.1	19
PCDTB: $PC_{70}BM$	0.127	10.593	0.88	0.64	6.0[a]	20
—[b]	0.043	10.321	0.81	0.72	6.0[a]	21
tandem PCDTB:PCBM/P3HT:$PC_{70}BM$ BHJ	0.045	7.8	1.24	0.67	6.5	22
Low band gap polymer[c]/PCBM	0.047	13.3	0.76	0.66	6.8[a]	3
Low band gap polymer[c]/PCBM	0.047			0.71	7.6[a]	23
Low band gap polymer[c]/PCBM	Not mentioned				8.13[a]	16

[a]Certificated by NREL.
[b]Composition of the photoactive layer remains proprietary to Plextronics.
[c]Remains proprietary to Solarmer.

where A is the cell area, R_s is series resistance which in turn can be a function of A, I_{max} and J_{max} are the cell current and current density in the maximum power point.

Equation (1) shows that P_R increases with J_{max}, i.e., with light intensity. Therefore the most powerful tool to investigate the R_s effect on the cell performance is measurement of light intensity dependence of the key photovoltaic parameters of solar cells, especially in the regime of high intensities (i.e., above the light intensity at which the cell efficiency peaks).[30,31] Unfortunately, the authors of Refs. 25–27 measured the cell I–V curves only at one illumination level ($C = 1$ sun $= 100$ mW/cm^2).

For OPV the intensity dependence of the photovoltaic parameters is still under discussion. To the best of our knowledge, for BHJ OPV it was studied only for $C \leq 1$ sun.[13,32,33] Ultrasmall bilayer C_{60}/copper phthalocyanine (CuPc) cells were characterized up to 12 suns of simulated illumination.[34] Recently,[35] we reported an experimental exploitation of concentrated sunlight for such measurements and demonstrated that the PCE of 1 cm^2 P3HT:PCBM BHJ cells peaks at ~ 1 sun.

In the present study we extend our experimental approach on the BHJ cells of various areas (1, 0.25, and 0.04 cm^2). Perusal of the unexpected results we obtained suggests that the origin of both size and light intensity effects should also include other (than conventional R_s dissipation) underlying physical mechanisms. In particular, we conclude that the distributed nature of the ITO resistance and its influence on the voltage dependence of photocurrent (incomplete exciton separation) and dark current is the key to understanding size limitation of the OPV efficiency. This limitation can be fundamental for all kind of excitonic cells[15] employing front ITO or similar transparent electrode.

II. EXPERIMENTAL DETAILS

Using outdoor/indoor test facility based on the fiber-optic/minidish solar concentrator [Figs. 1(a) and 1(b)][30,31,35] we studied BHJ OPV cells of various areas [Fig. 1(c)] layered architecture of "glass|ITO|ZnO|P3HT:PCBM|PEDOT:PSS|Ag" [Fig. 1(d)].

The BHJ OPV devices were prepared in the ambient using a fully roll-to-roll compatible solar cell device preparation.[36] Commercially available ITO glass substrates with a sheet resistivity of 5–8 Ω/Square were sonicated in isopropanol followed by washing in demineralized water. Layers of ZnO nanoparticles, photoactive P3HT:PCBM, and poly(3,4-ethylenedioxythiophene): polystyrene sulfonate (PEDOT:PSS) were then subsequently spin coated. All processing steps were conducted in the ambient. An Ag electrode pattern was deposited by thermal evaporation resulting in the three different geometries of the cells. The samples were encapsulated by applying an adhesive plastic foil on the Ag electrode.

The solar cells were mounted in an Al sample holder to ease the physical handling of the samples during the measurements. Additionally, it served as a thermal reservoir, decreasing the heating during the illumination of the cells.

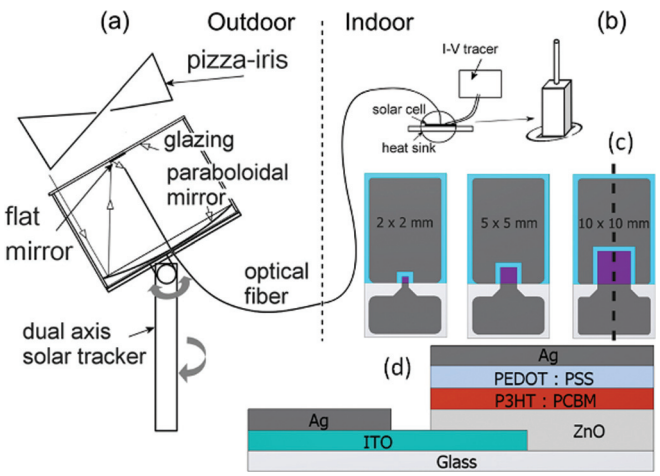

FIG. 1. (Color online) (a) Minidish dual-axis tracking solar concentrator (20 cm in diameter). (b) Uniform cell irradiation via a kaleidoscope. (c) Top view of cells of various areas. (d) The layer sequence of the inverted P3HT:PCBM BHJ cell (through-glass illumination). The solar cell area is defined as the overlap between the ITO and the Ag electrodes.

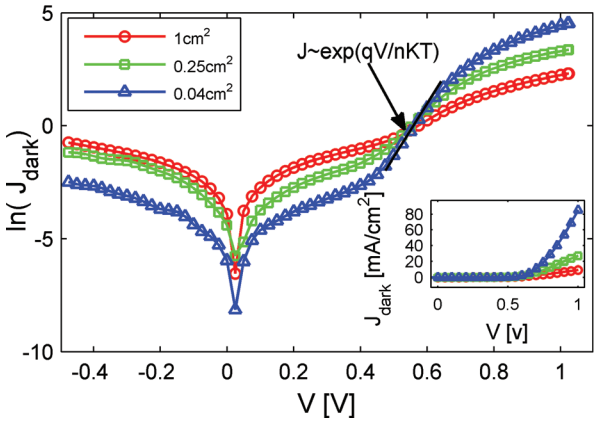

FIG. 2. (Color online) The dark *J–V* curves for three representative cells with various areas in a semilogarithmic scale. Inset shows the same curves in a linear scale.

Sunlight collected and concentrated outdoors was focused into a transmissive (quartz-core) optical fiber of 1mm in diameter and then delivered indoors onto the solar cell being tested [Fig. 1(a)]. Flux uniformity was achieved with a 3 cm long square cross-section kaleidoscope, matching the size of the cell, placed between distal fiber tip and cell [Fig. 1(b)].

Concentration of sunlight delivered to the cell C was varied gradually from 0.2 to 100 suns with a pizza-slice iris [Fig. 1(a)], and measured pyrometrically. Light current–voltage *I–V* measurements were made by opening a shutter above the iris and illuminating the cell during *I–V* tracing only (<1 s) to avoid excessive degradation and temperature variations. Before this testing, dark *I–V* curves for every cell were recorded.

I–V curves were recorded with a Keithley 2400 sourcemeter. Light *I–V* measurements were limited to clear-sky periods, 2 h around solar noon. The light spectrum on the cell was nearly invariant and close to the AM1.5.[37]

The cell fill factor (FF) and PCE η were calculated as

$$FF = Pm/J_{SC}V_{OC}, \tag{2}$$

$$\eta = P_m/P_{in} = J_{SC}V_{OC}FF/Pin, \tag{3}$$

where J_{SC} and V_{OC} denote short-circuit current density and open-circuit voltage, respectively. P_m and P_{in} are the maximum electrical output power density and incident light power density.

III. RESULTS

Thirteen cells with areas of 1, 0.25, and 0.04 cm^2 were investigated. Cells of the same area exhibited similar results. The dark *J–V* curves for three representative cells of various areas are shown in Fig. 2.

Evolution of the *J–V* curves of three representative cells recorded under various C are shown in Figs. S1–S3 in supplementary material.[38]

Figure 3 summarizes our data for J_{SC}, V_{OC}, FF, and η of the representative BHJ cells of various areas as a function of sunlight concentration C.

One can see that the observed trends for all the key parameters of the cells qualitatively reproduce those recently[35] reported for the 1 cm^2 cell of similar device architecture. However, we assumed that for the smaller cells the PCE peak would shift toward higher concentrations due to the corresponding shift of FF (this is the known R_s effect in inorganic PV also manifested in the larger negative slope of FF vs ln C in the high concentration regime). For the inorganic semiconductor concentrator cells, it was demonstrated[31] for example that the PCE of 1 mm^2 cell is maximized at ~1,000 suns while for a 1cm^2 cell of the same nominal architecture it peaks at ~350 suns.

Contrary to this expectation we have observed:

(1) Increase in the short-circuit current *density* with the cell area decrease [this is in evidence for all sunlight

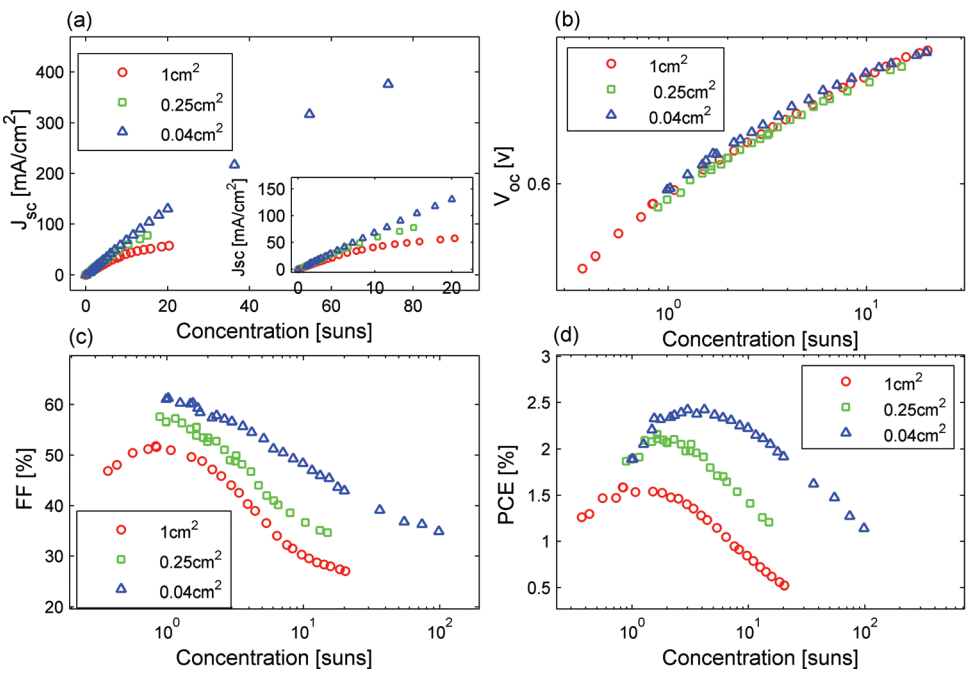

FIG. 3. (Color online) I_{SC} (a), V_{OC} (b), FF (c), and PCE (d) for the representative cells of various areas as a function of sunlight concentration C. Inset in (a) shows zoom-in for low concentrations ($0.2 \leq C \leq 20$ suns).

TABLE II. Analysis of the light intensity dependence of J_{SC} and comparison of diode quality factors n obtained by three different methods: fitting the curves V_{OC} vs $\ln(J_{SC})$; fitting the curves V_{OC} vs $\ln(J_{ph}@V_{OC})$; fitting the dark J–V curves.

Cell area (cm^2)	G_1	α_1	G^a	α_2	α_1:α_2 border (suns)	n (J_{SC})	n ($J_{ph}@V_{OC}$)	n (J_{dark})
1	5.03	0.99	5.33	0.66	4.5	1.5	4.7	4.5
0.25	6.36	1	5.75	0.86	6.53	1.3	3.1	2.5
0.04	6.77	1	9.4	0.82	19.44	1.2	2.4	1.8

[a]Reference 38.

concentrations but the effect amplifies with increased concentration—Fig. 3(a)].

(2) Higher FF values of smaller cells for all light intensities (low and high concentration regimes) but no considerable shift of light intensity of the FF peak value with the area decrease [Fig. 3(c)].

(3) Higher PCE values of smaller cells for all light intensities (low and high concentration regimes) [Fig. 3(d)].

(4) Shift (to higher illumination) of the peak PCE light intensity with the area decrease [Fig. 3(d)]. However, it is probably not due to FF shift (as expected) but due to the enhanced J_{SC} of smaller cells.

The latter is very important, from a practical point of view, for OPV applications in low-cost stationary solar concentrators (at $C \leq 10$ suns).[39] Indeed, PCE of the smallest cell peaks at $C \sim 3$ suns and exhibit similar values at 1 and 10 suns [Fig. 3(d)].

The observed trends point out that the effect of the cell area is mostly controlled by some mechanism other than R_s dissipation. To explain the observed results we will discuss in the following the light intensity dependence for every one of the OPV key parameters (J_{SC}, V_{OC} FF) as well as for the photocurrent and its voltage dependence.

IV. DISCUSSION

A. Light intensity dependence of J_{SC}

It is known that J_{SC} increases linearly with illumination level ($J_{SC} = GP_{in}$) for inorganic PV (Ref. 30) and for OPV in the low illumination regime.[35] For high levels of illumination, the processes of bimolecular recombination[10] and/or space charge limitation[11,12] may be intensified and hence the J_{SC} depends sublinearly on the P_{in} and C:$J_{SC} = G \cdot P_{in}^{\alpha}$, where $\alpha < 1$ [for dominant bimolecular recombination $\alpha = 0.5$ (Ref. 13) and for dominant space charge limitation $\alpha = 0.75$].[11,12]

The values G and α are extracted by:

$$ln(J_{sc}) = ln(G) + \alpha ln(P_{in}). \quad (4)$$

By this purpose we replotted the data shown in Fig. 3(a) in a log–log scale and then subdivided every curve by two parts: linear (α_1 is very close to 1) and sublinear ($\alpha_2 < 1$) (with the curve-fitting coefficient of determination R^2 higher than 0.99 for all extracted parameters).

Table II shows the results of such analysis

One can see that:

(1) G_1 and G_2 values are higher for smaller cells, implying better current extraction (even in the linear regime);

(2) For smaller cells, the linear regime extends further toward higher concentrations (see the column "α_1:α_2 *border*" with the approximate concentration levels (in suns) where the data starts to deviate from linearity).

B. Light intensity dependence of V_{OC}

For a p–n junction solar cell:

$$V_{OC} = (nkT/q)[ln(J_{ph}/J_0 + 1], \quad (5)$$

$$J_{ph} = J_{light} - J_{dark}, \quad (6)$$

where n is a p–n junction quality factor (for an ideal p–n junction cell, $n = 1$), J_{ph} is photocurrent density, J_{light} and J_{dark} are the cell current densities measured under illumination and in the dark, respectively [see Fig. 4(a)].

Since in inorganic PV the voltage-independent J_{ph} is approximately equal to J_{SC} and linearly proportional to c:

$$V_{OC} \approx (nkT/q)ln(J_{SC}/J_0) = (nkT/q)\ln(c) + \text{const}. \quad (7)$$

Figure 5(a) shows light intensity dependence of V_{OC} [shown in Fig. 3(b)] replotted in the scale "V_{OC} vs ln (J_{SC})" in order to extract n values according to Eq. (7). One can see that the data can be linearly fitted and the slopes of the linear fits and the corresponding n values decrease with the cell size decrease. Values of n are summarized in Table II. However,

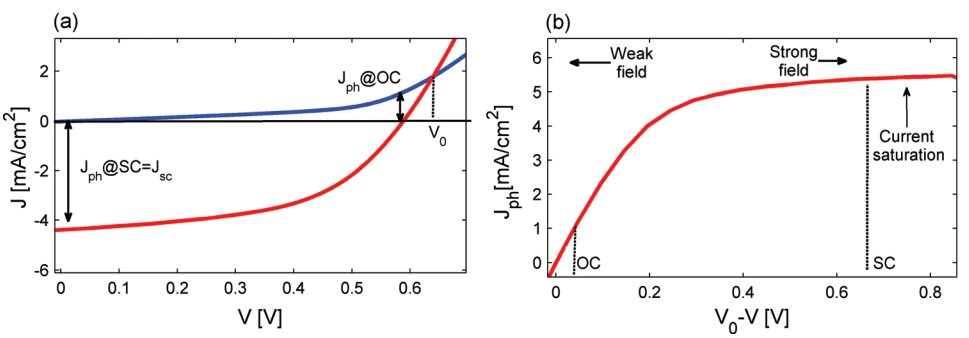

FIG. 4. (Color online) (a) J–V curves of the 1 cm^2 cell measured in the dark and under illumination of 1 sun. It is evident that the $J_{ph} = J_{light} - J_{dark}$ measured at the short-circuit conditions ($J_{ph} \approx J_{SC}$) is much higher that that measured at open circuit ($V_{OC} = 0.59$ V). Compensation voltage V_0 at which $J_{light} = J_{dark}$ is also indicated ($V_0 = 0.64$ V). (b) The same curves replotted as J_{ph} vs $V_{eff} = V_0 - V$. V_{eff} values for open-circuit (OC) and short-circuit (SC) conditions are indicated.

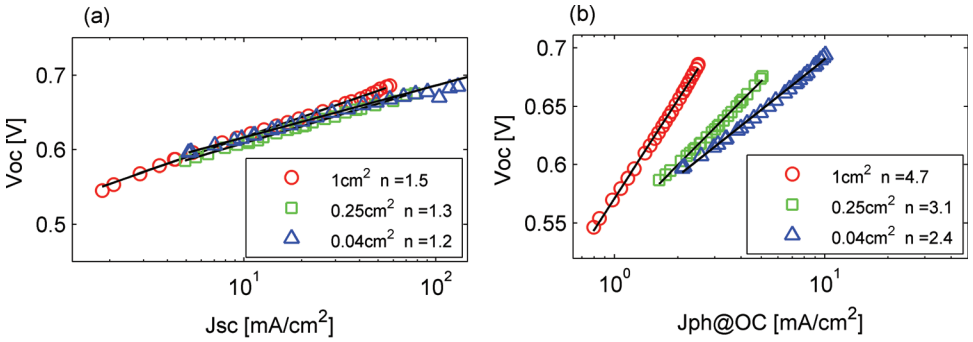

FIG. 5. (Color online) V_{OC} as a function of Ln (J_{SC}) (a) and Ln ($J_{ph}@V_{OC}$) (b).

these n values contradict with those obtained by the treatment of the dark J–V curves of the same cells (Fig. 2).

Forward-biased dark J–V curves are represented by three successive regimes:[40] local leakage current, injection current ($J \propto \exp[qV/nkT]$) and space charge limited current ($J \propto V^{0.5}/d^3$). Thus the semilogarithmic plots of the dark J–V curves (Fig. 2) in the injection current regime ($0.5\ \text{V} < V < 0.7$ V, marked by an arrow in Fig. 2) has a slope of q/nkT. The obtained n values are shown in Table II. One can see that they are considerably higher than those obtained with Eq. (6) and Fig. 5(a).

This contradiction is due to the above-mentioned fact that, because of the excitonic nature of photogeneration in OPV, the photocurrent itself is voltage-dependent.[10–15] It is clearly seen in Fig. 4(a) and will be discussed in detail in the following (Sec. III C). Accordingly, in order to get more accurate n values we suggest using a semilogarithmic plot of V_{OC} and $J_{ph} = J_{light} - J_{dark}$ measured at open-circuit conditions, $J_{ph}@V_{OC}$) [Fig. 5(b), Table II]. This limits our range of interest to the V_{OC} voltage range, and therefore to the corresponding J_{ph} range—which equals exactly $(-J_{dark})$. One can see the better agreement of these data with those obtained by the treatment of the dark $J-V$ curves, as again, smaller cells are characterized by lower n values.

Although a microscopic model for n in BHJ OPV is missing, it is accepted that the ideality factor reflects the "opening behavior" of the diode with the applied voltage with respect to its recombination behavior.[41] It was also proposed for OPV that $n > 2$ could be related to the tunneling effect[42] (where recombination is intensified by tunneling of charge carriers) or due to reduced mobility in disordered materials where Einstein relation is generalized and can differ from its classical form with $n = 1$.[43] Anyway, a change in the ideality factor could be evidence of a different type of mechanism for the recombination losses at the junctions.

C. Light intensity dependence FF: Evolution of the shape J_{ph}–V curves with illumination

Let us discuss now the field (voltage) dependence of J_{ph} as a possible underlying mechanism for the shape deterioration of the J–V curves and, as a result, for the light intensity dependence of FF.

Photogeneration of free charge carriers in OPV is preceded by the dissociation of excitons at the donor–acceptor interface. The formation of free electron and hole pairs is a highly field-dependent process, which is reflected in the strong voltage dependence of J_{ph}. To study this dependence it is widely accepted[10–15] to plot $J_{ph} = J_{light} - J_{dark}$ against the effective applied bias voltage $(V_0 - V)$, where V_0 is the compensation voltage, defined by the voltage at which the $J_{ph} = 0$, i.e., $J_{light} = J_{dark}$ [see Fig. 4(b)].

For example in short circuit (SC), $V = 0$ and the built-in-potential at the junction $V_{eff} = V_0$ [regime of strong field, $V_0 = 0.64$ V in Fig. 4(b)]. In open-circuit (OC), $V_{eff} = V_0 - V_{OC}$ [0.05 V in Fig. 4(b)]. In this regime the built-in-voltage is low and the field across the junction is weak.

Strong voltage dependence of J_{ph} reduces the FF significantly.[44] From the shape of the J_{ph} curve it is possible to characterize the carrier photogeneration and transport in different regimes. Indeed, the behavior of the illuminated J–V response depends on the drift length ($L_D = \mu\tau E$, where μ is the mobility, τ is the lifetime of the charge carriers, and E is the field across the device) of the electrons (e) and holes (h) and the ratio (b) of their drift lengths ($b = \mu_e\tau_e/\mu_h\tau_h$). For balanced transport ($b \sim 1$), J_{ph} varies linearly with V_{eff} at lower voltage regime and at higher voltage (V_{sat}) it saturates to a value $J_{ph} = qGL$, where G is the generation rate, and L is the thickness of the active layer.

Saturation of J_{ph} happens when all generated carriers are extracted. If $V_{sat} > V_0$ [SC at Fig. 4(b)], the charge collection efficiency does not approach 100% even under short-circuit conditions. As V_{sat} moves closer to OC it results in the increasing FF and vice versa.

In case of unbalanced transport ($b < 1$ or $b > 1$), which is also known as "$\mu\tau$-limited" process, carrier accumulation takes place near both contacts, modifying the field. In an extreme case ($b \ll 1$ or $b \gg 1$), the slower charge carrier will accumulate near one of the electrodes to a greater extent, leading to buildup of an internal field. When the field in this region becomes equal to the external applied voltage V, the current becomes "space charge limited" (SCL). $J_{ph} \propto V^{0.5}$ in both SCL and $\mu\tau$-limited cases. However, the J_{ph} varies linearly with G, hence with the intensity of illumination (P_{in} or c) in $\mu\tau$-limited case and shows a three-quarter dependence on G in the SCL case. The square root dependence on voltage limits the maximum possible FF to 42% in the SCL case.[11]

Figure 6 shows the voltage dependence of J_{ph} in a double logarithmic scale for three cells of different areas and three levels of illumination (~1,~5, and ~10 suns).

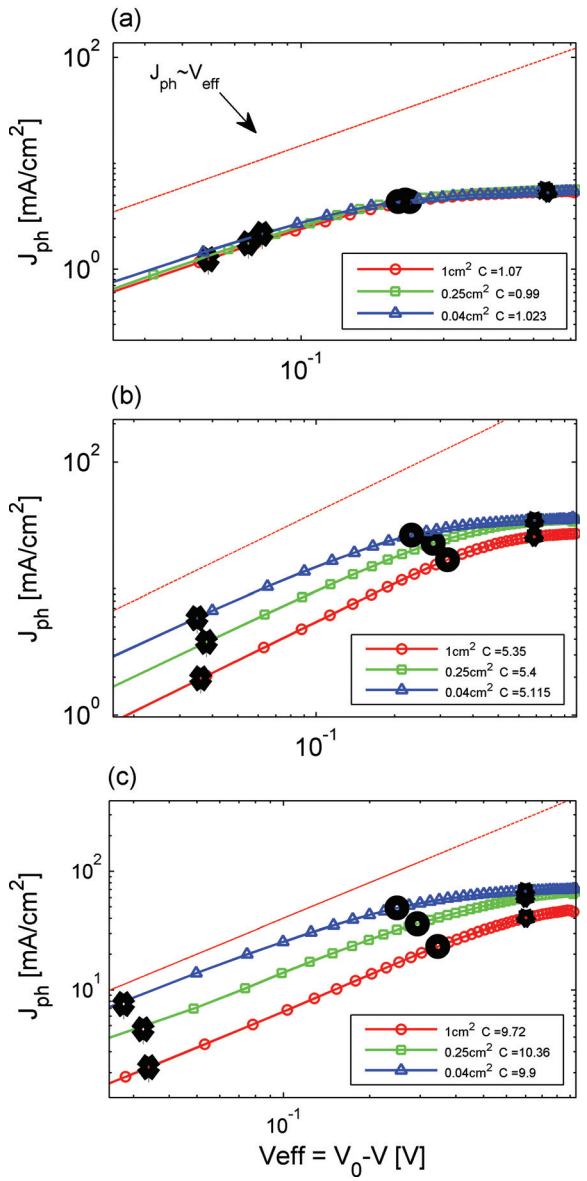

FIG. 6. (Color online) Dependence of J_{ph} on $V_{eff} = V_0 - V$ in a log–log scale for three representative cells with various areas measured under ~1 sun (a), ~5 suns (b), and ~10 suns (c). The line marks the slope of 1 for comparison ($J_{ph} \propto V_{eff}$). Positions of OC, maximum power point (MPP), and SC are indicated by diamonds, circles, and stars, respectively.

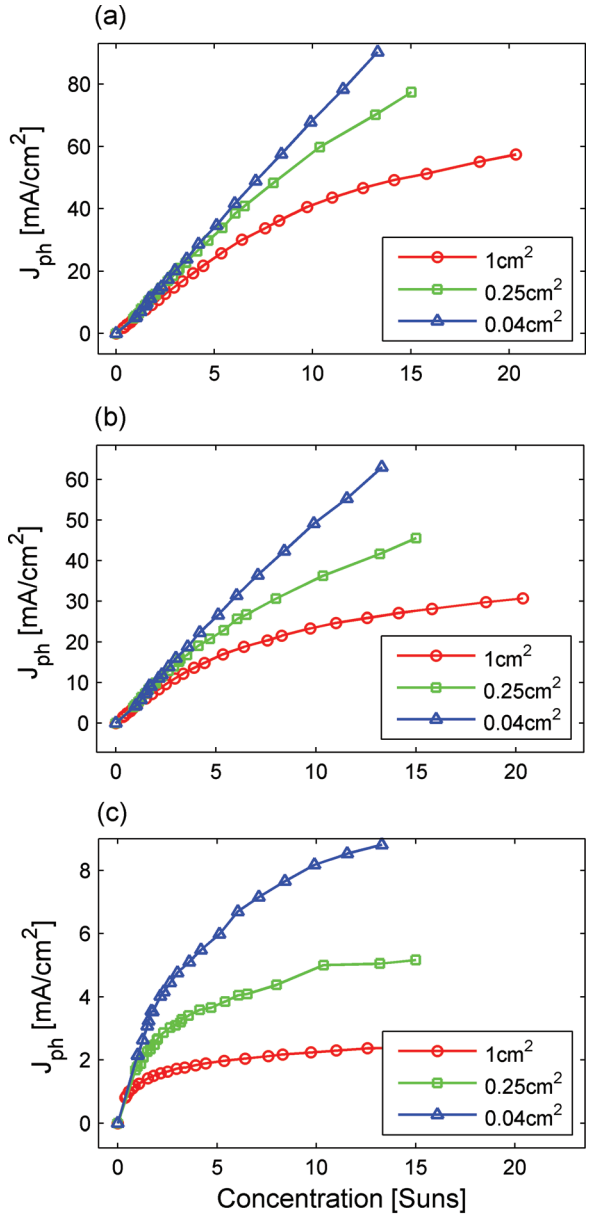

FIG. 7. (Color online) Light intensity dependence of J_{ph} for the cells of various sizes at SC (a), MPP (b), and OC (c).

One can see from Fig. 6(a) that the photocurrent is approximately equal for the three sizes at ~1 sun. The saturation values differ a little but the field dependence is similar, meaning that, at this level of illumination, there is no size effect on the photocurrent. The reduced FF value for the larger cell [Fig. 3(c)] should be controlled by a different mechanism (effect of the dark current for example, see the following).

For higher levels of illumination [Figs. 6(b) and 6(c)] the size effect on the photocurrent is evident: the smallest cell reaches saturation regime at lower V_{eff} than the larger one and the saturation value itself is higher. Such behavior controls both FF (via the location of the MPP on the J_{ph} curve, as will be discussed in Sec. III C) and J_{SC} and can explain the size effect on these parameters at high concentrations.

One can see however, that for all concentrations, all the cells behave linearly in the low field regime (there is no evidence of SCL effect).

Figure 7 shows the irradiance dependence of J_{ph} for the cells of various sizes at SC, MPP, and OC conditions.

One can observe that as V_{eff} decreases (going from SC to OC) the nonlinear behavior starts to be exhibited. The first that enters the nonlinear regime is the largest cell—see behavior for SC and MPP [Figs. 7(a) and 7(b)] while at OC all three cells behave nonlinearly at all concentrations [Fig. 7(c)].

Data shown in Fig. 7(a) are in accordance with the results for J_{SC} [Fig. 3(a)]: for high illumination levels the smaller cell is still in the linear regime of J_{SC}–C, while the larger cells suffer from sublinear behavior.

Thus, we can conclude that the voltage-dependent photocurrent behavior can be responsible for the size effect on

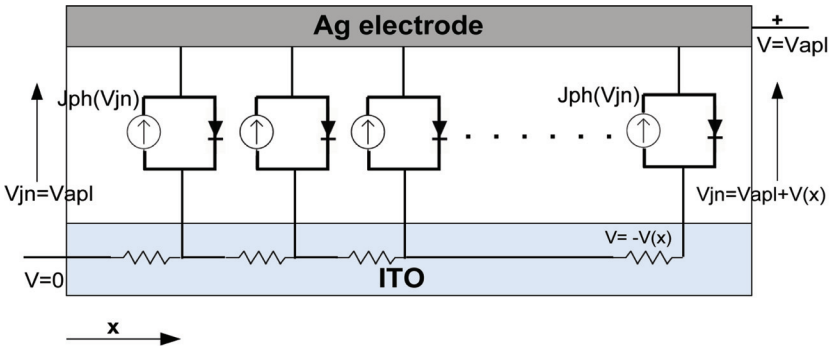

FIG. 8. (Color online) Simplified one-dimensional graphic sketch for a solar cell with distributive series resistance.

both J_{SC} and FF (at least for $C > 1$). However, two questions still remain open:

(1) Why is the voltage dependence of J_{ph} stronger for larger cells?
(2) What controls the effect at low illumination levels ($C \leq 1$)?

To try and answer the second question let us discuss what controls FF at low light intensities.

Figure S4a in supplementary material[38] demonstrates voltage dependence for all three currents (J_{dark}, J_{light} and $J_{ph} = J_{light}$ - J_{dark}) measured at 1 sun. Although J_{ph} for all three cells are similar, the J_{light} curves exhibit differences (that result in the lower FF for the larger area) and this difference is due to the corresponding difference in the J_{dark} curves.

However, for $C > 1$ (the case of 5 and 10 suns are shown in Figs. S4b-c supplementary material[38]) it is evident that the J_{light} curves (i.e. J_{SC}, FF, and the corresponding size effects) are completely controlled by J_{ph} behavior.

D. On the underlying mechanism of the size effect in OPV cells

The observed results can be explained on the basis of a model presenting a distributed series resistance of the ITO front electrode in OPV (Refs. 26 and 45) or any other similar electrodes in which current flows parallel to the cell surface (Fig. 8).

The current density J is not constant along the device because the charges that flow from the side distant to the extracting contact experience more series resistance. Simulations (see Fig. 4 in Ref. 44) show that there is a reduction in current density and increase in voltage across the active layer along the dimension x in Fig. 8.

For each voltage applied to the cell (V_a) there is a voltage drop along the distance from the current-extracting contact (marked by a dash in Fig. 8). This drop causes the increase in voltage across the junction (V_{jn}) and the reduction in the current from the distant parts of the cell, caused by the diodes' opening when V_{jn} increases[45] and by the voltage dependence of J_{ph} (Fig. 6). In other words, even if $V_a = 0$, not all parts of the cell are under SC conditions. Unfortunately, the authors of Ref. 45, assumed in their simulations that photocurrent is voltage independent ($J_{ph} = \text{const}$). Therefore, they only demonstrated a partial effect on FF (current at $V_a > 0$) but did not observe any effect on J_{SC} (constant current for $V_a = 0$ in Fig. 5 in Ref. 45). The effect of cell size on FF via the distributive series resistance is well known for inorganic solar cells. However, in OPV it also influences the voltage-dependent J_{ph} (Figs. 6 and 7). This influence can explain the J_{SC} behavior [Fig. 3(a)] and provide an additional mechanism for FF degradation. Indeed, if the maximum power point is situated considerably below the saturation regime in the J_{ph}–V_{eff} curve [as demonstrated in Figs. 6(b) and 6(c)], voltage difference along the cell's active layer (due to the ITO distributive resistance) causes a large decrease in J_{ph} in the cell areas that are far from the current extracting contact, and, as a result, strong decrease in FF.

The discussed mechanism is dependent on the dimension of the cell (the distance x from the contact). Anyway, the effect should increase for large area cells while the smaller area cells should exhibit better performance.

The phenomenon is fundamental and should take place in any OPV or other excitonic (with voltage-dependent photocurrent) solar cells[15] with ITO front electrode or any other similar transparent electrodes (graphene[46,47] and carbon nanotube electrodes,[48] surface-plasmon enhanced Ag grids,[49] metal nanowire mesh,[50] etc.) in which current flows parallel to the cell surface. The effect intensifies with illumination level. The illumination level at which the effect starts to be a dominant limiting factor for a certain solar cell may depend on the cell area, resistivity of the transparent electrode, electronic properties of the active layer, etc. We suggest also that this effect can be significant even in the case when the ITO electrode contribution to the R_s dissipation of the entire cell is not dominant. However, practical methods to overcome such size limitation and produce efficient large-area OPV cells and modules can be similar to those for reduction of ITO distributive resistance, for example deposition of metal subgrid on the ITO layer.[27,51] Our results also suggest that by using this technological approach one can produce future concentrator OPV cells operating under sunlight concentrations *higher* than 10 suns. The latter of course will raise new challenges for OPV stability at these illumination levels.[35]

It is important to add here, that the suggested loss-mechanism analysis also can be relevant in a situation where J_{ph} is considered to be voltage-independent while recombination losses are charge-density dependent.[52] Whether the

additional loss is originated from voltage dependence of photogeneration or enhanced bimolecular recombination, it should depend on the voltage drop along the device front electrode.

Finally, we suggest that the cell's dark current is also affected by the same mechanism. At forward bias the charge carriers are injected into the device and are recombined in the active layer. When the voltage across the ITO layer is not equal, the most distant locations will experience reduced fields and therefore reduced forward currents, thus lowering the quality of the entire diode. It is manifested in the deterioration of the dark *J–V* curve shape and the effect intensifies with the cell area (as shown in Fig. 2, Table II). Our suggestion is supported by the experimental results on the reduction of electroluminescence intensity with increasing area of ITO transparent electrodes in organic LEDs.[53]

We therefore conclude that the effect of distributed resistance of the transparent electrode can limit the cell FF in high and low illumination regimes in two ways: (1) by the decrease of the photocurrent via its dependence on the applied voltage (high *C*); and (2) by the decrease of the diode quality factor and the corresponding deterioration of the dark *J–V* curve (mainly in lower *C* regime).

V. CONCLUSIONS

1. The *I–V* curves of as-produced OPV cells of various areas (1, 0.25, and 0.04 cm^2) were measured under different sunlight concentrations (from 0.2 to 100 suns) and light intensity dependence of the OPV key parameters (I_{SC}, V_{OC}, FF, PCE) was analyzed.
2. We demonstrated experimentally that increase in the cell area results in:
   (a) decrease in the short-circuit current *density* (this is true for all sunlight concentrations but the effect amplifies with the concentration increase);
   (b) decrease in FF for all light intensities (low and high concentration regimes);
   (c) decrease of the PCE values for all light intensities (low and high concentration regimes) and shift (to higher illumination) of the peak PCE light intensity;
   (d) increase of the diode quality factor *n*
3. All the results can be consistently explained by the voltage dependence of photocurrent J_{ph} (incomplete exciton separation) and the dark current in the presence of significant distributed series resistance of the ITO front electrode or any other similar transparent electrodes in which current flow parallel to the cell surface.
4. The discussed phenomenon is fundamental and should take place in any OPV or other excitonic (with voltage-dependent photocurrent) solar cells with highly resistive transparent electrode. The effect intensifies with the illumination level. The light intensity at which the effect starts to be significant for certain solar cells may depend on the cell area, resistivity of the electrodes, electronic properties of the active layer, etc.
5. The results are important for both a basic understanding of the operation of excitonic solar cells and for the practical purpose of producing efficient large-area OPV cells and modules. The possibility of producing concentrator OPV cells operating under sunlight concentrations is *higher* than 10 suns and is discussed.

ACKNOWLEDGMENTS

This work was performed, in part, in the framework of the "Largecells" project that received funding from the European Commission's Seventh Framework Programme (FP7/2007-2013) under Grant Agreement No. 261936." T.T. and F.C.K. thank the Danish Strategic Research Council (2104-07-0022) and EUDP (j. nr. 64009-0050) for financial support. E.A.K. acknowledges financial support by the FIRST - Focal Initiatives in Science and Technology foundation of the Israel Science Foundation (grant no. 1004/07).

[1]C. J. Brabec, N. S. Sariciftci, and J. C. Hummelen, Adv. Funct. Mater. **11**, 15 (2001).
[2]M. Helgesen, R. Søndergaard, and F. C. Krebs, J. Mater. Chem. **20**, 36 (2010).
[3]C. J. Brabec, S. Gowrisanker, J. J. M. Halls, D. Laird, S. Jia, and S. P. Williams, Adv. Mater. **22**, 3839 (2010).
[4]W. Ma, C. Yang, X. Gong, K. Lee, and A. J. Heeger, Adv. Funct. Mater. **15**, 1617 (2005).
[5]J. Y. Kim, S. H. Kim, H.-H. Lee, K. Lee, W. Ma, X. Gong, and A. J. Heeger, Adv. Mater. **18**, 572 (2006).
[6]M. D. Irwin, D. B. Buchholz, A. W. Hains, R. P. H. Chang, and T. J. Marks, PNAS **105**, 2783 (2008).
[7]M. Reyes-Reyes, K. Kim, and D. L. Carroll, Appl. Phys. Lett. **87**, 083506 (2005).
[8]V. I. Arkhipov and H. Bassler, Phys.Status Solidi A **201**, 1152 (2004).
[9]J. J. M. Halls, K. P. R. H. Friend, S. C. Moratti, and A. B. Holmes, Appl. Phys. Lett. **68**, 3120 (1996).
[10]L. J. A. Koster, V. D. Mihailetchi, and P. W. M. Blom, Appl. Phys. Lett. **88**, 052104 (2006).
[11]V. D. Mihailetchi, J. Wildeman, and P. W. M. Blom, Phys. Rev. Lett. **94**, 126602 (2005).
[12]V. D. Mihailetchi, H. Xie, B. de Boer, L. J. A. Koster, and P. W. M. Blom, Adv. Funct. Mater. **16**, 699 (2006).
[13]J. K. J. van Duren, X. Yang, J. Loos, C. W. T. Bulle-Lieuwma, A. B. Sieval, J. C. Hummelen, and R. A. Janssen, Adv. Funct. Mater. **14**, 425 (2004).
[14]P. W. M. Blom, V. D. Mihailetchi, L. J. A. Koster, and D. E. Markov, Adv. Mater. **19**, 1551 (2007).
[15]B. A. Gregg and M. C. Hanna, J. Appl. Phys. **93**, 3605 (2003).
[16]See http://www.pv-tech.org/news/(last accessed July 2010).
[17]J. Hou, H.-Y. Chen, S. Zhang, G. Li, and Y. Yang, J. Am. Chem. Soc. **130**, 16144 (2008).
[18]J. Peet, J. Y. Kim, N. E. Coates, W. L. Ma, D. Moses, A. J. Heeger, and G. C. Bazan, *Nature Mater.* **6**, 497 (2007).
[19]Y. Liang, D. Feng, Y. Wu, S. Tsai, G. Li, C. Ray, and L. Yu, J. Am. Chem. Soc. **131**, 7792 (2009).
[20]S. H. Park, A. Roy, S. Beaupré, S. Cho, N. Coates, J. S. Moon, D. Moses, M. Leclerc, K. Lee, and A. J. Heeger, *Nat. Photonics* **3**, 297 (2009).
[21]R. Tipnis and D. Laird, "High efficiency solar cells," SPIE Newsroom Website, December 2008, http://spie.org/x31682.xml?ArticleID=x31682 (last accessed December 2008).
[22]J. Y. Kim, K. Lee, N. E. Coates, D. Moses, T.-Q. Nguyen, M. Dante, and A. J. Heeger, Science **317**, 222 (2007).
[23]See http://www.pv-tech.org/news/(last accessed December 2009).
[24]G. P. Smestad, F. C. Krebs, C. M. Lampert, C. G. Granqvist, K. L. Chopra, X. Mathew, and H. Takakura, Sol. Energy Mater. Sol. Cells **92**, 371 (2008).
[25]D. Gupta, M. Bag, and K. S. Narayan, Appl. Phys. Lett. **93**, 163301 (2008).
[26]A. K. Pandey, J. M. Nunzi, B. Ratier, and A. Moliton, Phys. Lett. A **372**, 1333 (2008).
[27]S. Choi, W. J. Potscavage, and B. Kippelen, J. Appl. Phys. **106**, 054507 (2009).

Appendix 8

[28]C. Lungenschmied, G. Dennler, H. Neugebauer, S. N. Sariciftci, M. Glatthaar, T. Meyer, and A. Meyer, Sol. Energy Mater. Sol. Cells **91**, 379 (2007).
[29]J. D. Servaites, S. Yeganeh, T. J. Marks, and M. A. Ratner, Adv. Funct. Mater. **20**, 97 (2010).
[30]E. A. Katz, J. M. Gordon, W. Tassew, and D. Feuermann, J. Appl. Phys. **100**, 044514 (2006).
[31]O. Korech, B. Hirsch, E. A. Katz, and J. M. Gordon, Appl. Phys. Lett. **91**, 064101 (2007).
[32]I. Riedel, J. Parisi, V. Dyakonov, L. Lutsen, D. Vanderzande, and J. C. Humme, Adv. Funct. Mater. **14**, 38 (2004).
[33]L. J. A. Koster, V. D. Mihailetchi, R. Ramaker, and P. W. M. Blom, Appl. Phys. Lett. **86**, 123509 (2005).
[34]J. Xue, S. Uchida, B. P. Rand, and S. R. Forrest, Appl. Phys. Lett. **84**, 3013 (2004).
[35]T. Tromholt, E. A. Katz, B. Hirsch, A. Vossier, and F. C. Krebs Appl. Phys. Lett. **96**, 073501 (2010).
[36]F. C. Krebs, S. A. Gevorgyan, and J. Alstrup, J. Mater. Chem. **19**, 5442 (2009).
[37]J. M. Gordon, E. A. Katz, D. Feuermann, and M. Huleihil, Appl. Phys. Lett. **84**, 3642 (2004).
[38]See supplementary material at http://dx.doi.org/10.1063/1.3567930 for a brief discussion of the material.
[39]T. Uematsu, Y. Yazawa, T. Joge, and S. Kokunai, Sol. Energy Mater. Sol. Cells **67**, 425 (2001).
[40]A. Moliton and J.-M. Nunzi, Polym. Int. **55**, 583 (2006).
[41]C. Waldauf, M. C. Scharber, P. Schilinsky, J. A. Hauch, and C. J. Brabec, J. Appl. Phys. **99**, 104503 (2006).
[42]A. Kumar, R. Devine, C. Mayberry, B. Lei, G. Li, and Y. Yang. Adv. Funct. Mater. **20**, 2729 (2010).
[43]Y. Roichman and N. Tessler, Appl. Phys. Lett. **80**, 1948 (2002).
[44]D. Gupta, S. Mukhopadhyay, and K. S. Narayan, Sol. Energy Mater. Sol. Cells **94**, 1309 (2010).
[45]M. W Denhoff and N. Drolet, Sol. Energy Mater. Sol. Cells **93**, 1499 (2009).
[46]S. S. Li, K.H. Tu, C. C. Lin, C. W. Chen, and M. Chhowalla, ACS Nano **4**, 3169 (2010).
[47]L. G. De Arco, Y. Zhang, C. W. Schlenker, K. Ryu, M. E. Thompson, and C. W. Zhou, ACS Nano. **5**, 2865 (2010).
[48]R. Ulbricht, S. B. Lee, X. M. Jiang, K. Inoue, M. Zhang, S. L. Fang, R. H. Baughman, and A. A. Zakhidov, Energy Mater. Sol. Cells **91**, 416 (2007).
[49]T. H. Reilly III, J. van de Lagemaat, R. C. Tenent, A. J. Morfa, and K. L. Rowlen, Appl. Phys. Lett. **92**, 243304 (2008).
[50]J.-Y. Lee, S. T. Connor, Y. Cui, and P. Peumans, Nano Letters **8**, 689 (2008).
[51]S.-Y. Park, W.-I. Jeong, D.-G. Kim, J.-K. Kim, D. C. Lim, J. H. Kim, J.-J. Kim, and J.-W. Kang, Appl. Phys. Lett. **96**, 173301 (2010).
[52]C. G. Shuttle, R. Hamilton, B. C. O'Regan, J. Nelson, and J. R. Durrant, Proceedings of the National Academy Sciences **107**, 16448 (2010).
[53]C. Pillego, M. Mazzeo, M. Salemo, and G. Gigli, Appl. Phys. Lett. **89**, 103514 (2006).